A flavour of family symmetries in a family of flavour models

Adelhart Toorop, R. de

A flavour of family symmetries in a family of flavour models

Proefschrift

ter verkrijging van
de graad van Doctor aan de Universiteit Leiden,
op gezag van de Rector Magnificus prof. mr. P.F. van der Heijden,
volgens besluit van het College van Promoties
te verdedigen op dinsdag 21 februari 2012
klokke 15.00 uur

door

Reinier de Adelhart Toorop

Geboren te Amsterdam in 1984

Promotiecommissie

Promotor	Prof. dr. Jan-Willem van Holten (Nikhef en Universiteit Leiden)
Co-promotor	Dr. Federica Bazzocchi (SISSA, Trieste, Italië)
Overige leden	Prof. dr. Daniël Boer (Rijksuniversiteit Groningen)
	Dr. Alexey Boyarski (Universiteit Leiden)
	Prof. dr. Eric Eliel (Universiteit Leiden)
	Prof. dr. Ferruccio Feruglio (Universiteit van Padua, Italië)

Het werk beschreven in dit proefschrift is onderdeel van het onderzoeksprogramma van de stichting Fundamenteel Onderzoek der Materie. Deze stichting wordt financiëel ondersteund door de Nederlandse Organisatie voor Wetenschappelijk Onderzoek.

Omslagontwerp Rozan Vroman
Casimir PhD series Delft-Leiden 2012-3
ISBN 978-90-8593-116-4

Contents

List of publications

1. Reinier de Adelhart Toorop, Ferruccio Feruglio and Claudia Hagendorn
   Discrete Flavour Symmetries in Light of T2K
   Phys.Lett. **B703** (2011) 447-451; arXiv:1107.3486 [hep-ph]
   (Chapter 3)

2. Reinier de Adelhart Toorop, Ferruccio Feruglio and Claudia Hagendorn
   Finite modular groups and lepton mixing
   Submitted to Nucl.Phys.B; arXiv:1112.1340
   (Chapter 3)

3. Reinier de Adelhart Toorop, Federica Bazzocchi and Luca Merlo
   The Interplay Between GUT and Flavour Symmetries in a Pati-Salam x S4 Model.
   JHEP **1008** (2010) 001; arXiv:1003.4502 [hep-ph]
   (Chapter 4)

4. Reinier de Adelhart Toorop
   Family physics with S4 and Pati-Salam
   Proceedings of the Erice School of Nuclear Physics 2009
   Prog.Part.Nucl.Phys. **64** (2010) 318-320

5. Reinier de Adelhart Toorop
   The interplay between grand unified and flavour symmetries in a Pati-Salam x S4 model
   Proceedings of Pascos 2010
   J.Phys.Conf.Ser. **259** (2010) 012099; arXiv:1010.3406 [hep-ph]

6. Reinier de Adelhart Toorop, Federica Bazzocchi, Luca Merlo and Alessio Paris
   Constraining Flavour Symmetries At The EW Scale I: The A4 Higgs Potential
   JHEP **1103** (2011) 035; arXiv:1012.1791 [hep-ph]
   (Chapter 5)

7. Reinier de Adelhart Toorop, Federica Bazzocchi, Luca Merlo and Alessio Paris
   Constraining Flavour Symmetries At The EW Scale II: The Fermion Processes
   JHEP **1103** (2011) 040; arXiv:1012.2091 [hep-ph]
   (Chapter 5 and subsection 2.2.5)

8. Reinier de Adelhart Toorop
   Flavour symmetries at the EW scale
   Proceedings of Discrete 2010
   J.Phys.Conf.Ser. **335** (2011) 012030

9. Reinier de Adelhart Toorop, Federica Bazzocchi and Stefano Morisi
   Quark mixing in the discrete dark matter model
   Nucl.Phys.**B 856** (2012) 670; arXiv:1104.5676 [hep-ph]
   (Subsections 5.10.4 and 5.12.4)

Chapter 1

Introduction

Di, coeptis [...]
adspirate meis primaque ab origine mundi
ad mea perpetuum deducite tempora carmen.

Gods, inspire my attempts
and spin out a continuous song
from the first origin of the world into my times.

Ovid [1], Metamorphoses I 2-4.

We live in exciting times. The Large Hadron Collider at CERN is working better than anyone expected; it is collecting data at world-record holding center-of-mass energy and ever growing luminosity (a measure of the number of interactions per unit time). The Tevatron accelerator at Fermilab closed down at the end of the fiscal year 2011. In the last months of its service it worked at top-luminosity to collect as much data as possible before its shut-down. This data is currently being investigated and may contain a treasure of information.

On the neutrino front, the discovery of neutrino oscillations is now a little over ten years old and neutrino physics has entered the precision era. There is hope that in the next decade, all mixing angles, including the only recently measured angle θ_{13}, are known to great precision; that the absolute mass scale and the related hierarchy can be set and that neutrinoless double beta decay may be observed. In September 2011, the OPERA experiment reported superluminal velocities for neutrinos traveling from CERN to Gran Sasso, adding a new mystery to the neutrinos' character.

The oldest light in the universe, the cosmic microwave background, is measured more and more precisely by the WMAP and Planck satellites, thereby delivering a wealth of data also to the particle physics community.

Between all this experimental force, it is up to the theorist community to give frameworks in which the new results can be interpreted. In the first section of this introductory chapter, we describe the Standard Model, that has been the leading theory of particle physics for the last forty years. Still, there are reasons to expect that the Standard Model should be extended. These are described in the next three sections. One of these extensions is the addition of family symmetries (also called flavour symmetries). This is the main topic of this thesis. In this chapter, we also come across the neutrino seesaw, dark matter, supersymmetry and gauge unification, that are other important elements of some chapters of this thesis.

1.1 The Standard Model

The leading theory in particle physics is, with good reason, called the Standard Model (SM). The SM was developed in the 60s and describes all known elementary particles and their interactions with unprecedented precision. The Standard model consists of matter particles, forces and related force carriers and a sector that should give mass to it all, the Higgs sector.

On the matter side, the Standard Model describes quarks and leptons, that are ordered in generations, as shown in figure 1.1. Ordinary matter is made of first generation matter. Atomic nuclei are

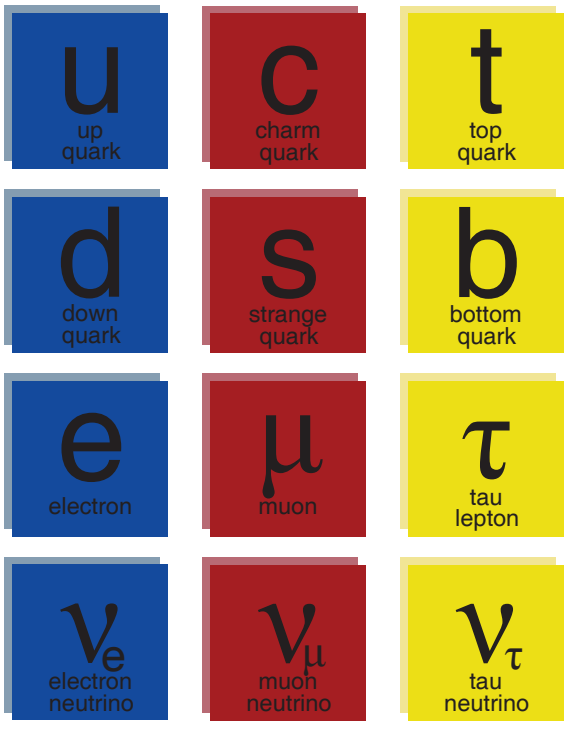

Figure 1.1: *The matter content of the SM.*

ultimately build of up and down quarks: two ups and one down form a proton and two downs and one up form a neutron; a nucleus can be seen as a specific combination of protons and neutrons. Around the nucleus circle the electrons to form an atom. Electrons together with the rarely interacting neutrinos are called leptons. See also figure 1.2.

Experimentalists found that the spectrum of elementary particles is much more interesting than just the first generation particles that are needed to build up atomic matter. In 1936-7, a new particle was discovered. Eventually, it became known as muon and was identified as a heavier brother of the electron. This is remarkable. A priori, there is no reason that a new particle should resemble any 'older' particle, but the muon does. It has all its properties in common with the electron: same electric charge, same spin, also invisible to the strong nuclear force, etcetera. Only the mass is different; for the rest, it is a perfect copy.

It was found that this relationship is not unique to the electron and the muon: all first generation particles have exactly two heavier brothers. Next to the electron and the muon, there is the even heavier tau particle. The down quark is accompanied by a strange and a bottom quark and next to the up quark are a charm and a top quark. Also neutrinos come in three types, generally dubbed electron-, muon- and tau-neutrino.

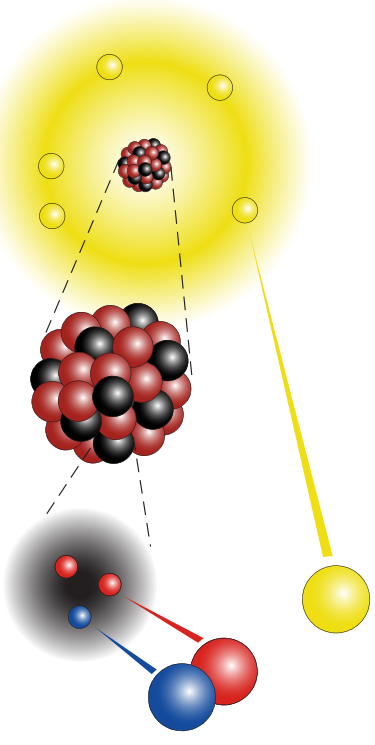

Figure 1.2: *Normal matter is made of atoms, that are on their turn build up from up quarks (blue), down quarks (red) and electrons (yellow)[Schematic view – not to scale]*

The quarks and leptons of the Standard Model interact via exactly three elementary forces. The first one is the strong nuclear force that only works on the particles in the nucleus, the quarks. The other two are called the weak force and the hyperforce and they are together called the electroweak interactions. At 'low' energies, this gives rise to electromagnetism. According to the theory, there is a force carrier (or gauge boson) related to each of these forces. For electromagnetism, this is the well-known photon, or light-quantum. Apart from the photon, the electroweak interactions give rise to W and Z bosons. Gluons, lastly, mediate the strong nuclear force.

A force carrier only couples to a particle that is charged under the appropriate charge. In the language of gauge theory, in which the Standard Model is written, this translates to being in a non-trivial representation of the related gauge group. The relation between the group theory of symmetry groups and the physics of forces and couplings that is behind this is one of the best examples of the power of mathematics in physics.

The interactions of the Standard Model are graphically depicted in figure 1.3. There, it can be seen that also some gauge bosons couple to each other.

The Standard Model as described so far explains all known elementary particles and all their interactions in great detail, but with two important shortcomings: if the above theory were all, all elementary particles would be exactly massless and the electromagnetic force and the weak nuclear force, that combine at higher energies would not separate. Both problems can be solved with the introduction of an extra field to the theory, as explained by Brout, Englert, Guralnik, Hagen, Kibble and Higgs and eventually called after the latter. The Higgs fields can give the required dynamics to break electroweak symmetry and thereby give mass to the W and Z bosons. The quark and lepton masses follow from the so-called Yukawa couplings to the Higgs field, that gives a mass term below the electroweak scale. Addition of more than one Higgs field is in principle possible, but with only one copy we have the most simple complete theory. We refer to this theory as 'the Standard Model' and to theories with more than one Higgs as extensions of it.

The addition of the Higgs fields leads to the prediction of the existence of an extra particle, called the Higgs boson. The Higgs has not been found yet and the search for this particle was one of the main motivations to construct the LHC — although this argument was also used for its predecessor, the large electron-positron collider (LEP). Many physicists believe that the LHC will indeed find the Higgs and this would then 'complete' the Standard Model.

The Standard Model passed many experimental tests over the last decades and it was always able to perfectly fit the experimental outcomes. Still there are reasons to believe that the Standard Model, after the discovery of a single Higgs particle, is not the whole story. The arguments for this claim fall in three groups. Firstly, there are experimental/observational reasons to believe that the Standard Model is incomplete. Interestingly enough, arguments come mostly from cosmological and astrophysical sources. Secondly, there are theoretical reasons to believe that the Standard Model is 'unnatural', meaning that although it can explain many experimental results very well, this requires very special values of the parameters of the theory. Thirdly, the Standard Model fails to give a microscopic theory of gravity. When we study places in the universe like black holes or times like the Big Bang, we need both the physics of the very small and of the very heavy. Unfortunately, the Standard Model of particle physics and the leading theory of gravity, Einstein's general relativity, are not compatible and a new theory of quantum gravity is needed.

We discuss the first two challenges to the Standard Model in some detail in the rest of this chapter, each time suggesting solutions. As we will see, these are often the addition of extra particles and/or symmetries to the Standard Model. The search for a quantum theory of gravity has been the holy grail for high energy physicists for the last decades. Interesting theories, like string theory and loop quantum gravity exist, but a conclusive answer has not yet been given. We do not study quantum gravity in this thesis, although we refer to the scale at which quantum gravity is thought to exist — the Planck scale — quite often.

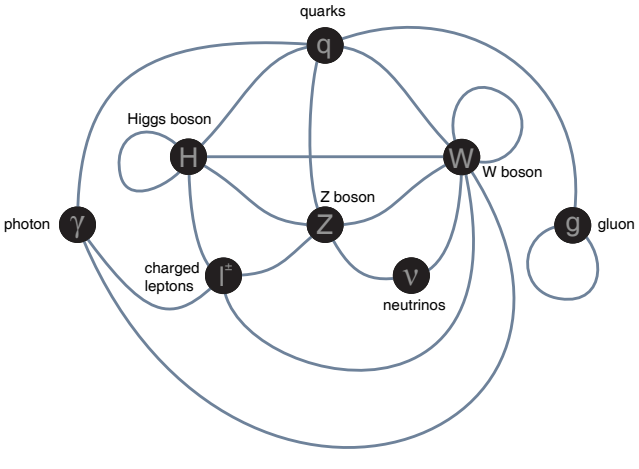

Figure 1.3: *Schematic representation of the interactions of the Standard Model*

1.2 Reasons why the Standard Model is incomplete

The Standard Model has successfully explained a multitude of experimental data, meaning that it well predicted the behaviour of elementary particles in Earthbound colliders. However, particle physics also has a strong connection with astrophysics and cosmology. This shows itself in the fact that the Earth is constantly bombarded with particles from the Sun and many other sources in the sky; it shows itself in the fact that the particle content of the universe steers its fate of contraction or expansion and it shows itself in the fact some of the early phases of the universe, such as inflation and nucleosynthesis can be described extremely well by particle physics.

Indeed, many of the elementary particles were first discovered as elements of the cosmic radiation and detected in bubble and cloud chambers long before they could be recreated and observed in colliders on Earth. However, there are cases where the Standard Model falls short to describe what we observe in the cosmos. We describe neutrino oscillations, dark matter and the baryon asymmetry of the universe in the next sections.

1.2.1 Neutrino Oscillations

The Sun shines very brightly. Indeed, if we could capture the energy it radiates on Earth for just one hour, this would be enough to satisfy humanity's energy consumption for a full year. The energy needed for this enormous amount of radiation is created in the center of the Sun, where protons are fused into helium nuclei in one of the most energetic reactions imaginable. In this process, energy is not only produced in the form of photons, or light, but also as (kinetic) energy of particles called neutrinos, that we have seen above of companions to the charged leptons.

Neutrinos were postulated in 1930 to explain properties of radioactive materials and were eventually observed in 1956. Their name is well-chosen. They are electrically neutral and the Italian suffix -ino refers to something that is small. In particle language, that translates to having a small cross section, a measure of how easily a particle interacts. Above, it was mentioned that neutrinos interact rarely. This is an understatement: if we send a beam of neutrinos through a bar of lead, the bar would have to be *half a lightyear* long in order to let half of the neutrinos interact with it. For comparison, for visible light, this would be only a few atomic distances and even for the most energetic X-rays, it would be a few millimetres. Still, no matter how rarely, neutrinos sometimes do interact with matter. This is key to one of the most outstanding theorist-experimentalist collaborations ever.

We know the amount of radiation that the Sun produces very well and we also know how the origin of this radiation is also the origin of many neutrinos. We can therefore calculate how many neutrinos should reach the Earth every second. If we also know how many, or rather how few, of these interact with a certain detector material, we can predict a detection rate. This was done by Ray Davis and John Bahcall, using an ingenious set up in the old Homestake gold mine. They indeed found evidence for reactions that were initiated by solar neutrinos, but it was a factor three less than they expected. Of course, first their solar model and experimental efficiency were challenged, but eventually the result stood. In 2002, Ray Davis received the Nobel Prize in physics.

Above, it was mentioned that neutrinos, like the other charged leptons and the quarks, come in three 'generations'. The electron-neutrino is defined as the neutrino that reacts together with an electron under the weak nuclear force and analogous for the muon-neutrino and the tau-neutrino. The neutrinos produced in the Sun are of the electron type, as their creation is related to transmutation of normal, first generation matter. The experiment of Davis and Bahcall was only sensitive to electron neutrinos. It could not measure muon- or tau-neutrinos. The conclusion of their experiment is thus that of the electron-neutrinos produced in the Sun, only a third arrives at Earth as an electron-neutrino.

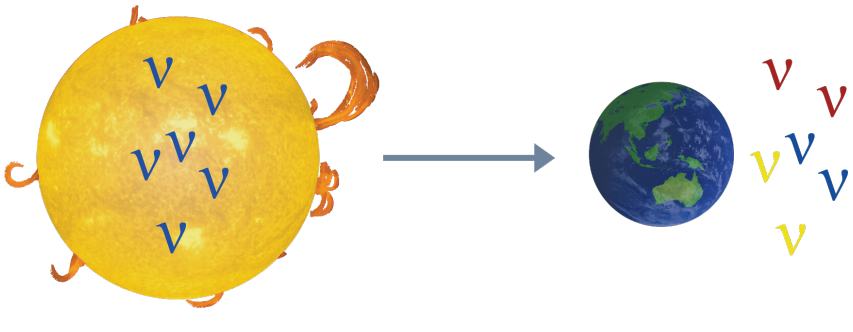

Figure 1.4: *Schematic view of neutrino oscillations. In the centre of the Sun all neutrinos are of the blue electron-type; at Earth all three flavours are equally present.*

Comparable results were obtained using neutrinos that are produced when a cosmic-ray particle collides high in the atmosphere and produces a muon and a muon-neutrino. Also of these muon-neutrinos, only a limited fraction reaches the Earth as a muon-neutrino. Other experiments use neutrinos from nuclear reactors or specific collider processes and they all find the same result: only a limited fraction of the neutrinos produced is observed later as a neutrino of the same species. They also found that it is possible to detect neutrinos of a species that is not the one that is produced.

The above observations can be explained if we assume that neutrinos oscillate. This means that if a neutrino is produced as a neutrino of a certain species, it can become a neutrino of a different species while flying through space.

Neutrino oscillations can be explained using simple techniques from quantum mechanics, but only if one fundamental assumption is satisfied: neutrinos should have mass. In the Standard Model, neutrinos do not have mass. Mass terms in the Standard Model are discussed in more detail in chapter 2. The crucial point is this: in order to obtain a mass from interactions with the (standard) Higgs field, a particle should appear both in 'lefthanded' and 'righthanded' form. Only the lefthanded neutrino interacts via the weak nuclear force and as can be seen in figure 1.3, this is the *only* interaction that neutrinos have. This means that all observations of neutrinos are of those of the lefthanded type. When the Standard Model was constructed, it was deemed enough to include only lefthanded neutrinos and leave out the righthanded neutrinos. An automatic consequence was that neutrinos were supposed to be massless, but that was in good agreement with all experimental data at that time.

As the above discussion suggests, the problem of the massless neutrinos can be solved in a straightforward way. If righthanded neutrinos are added to the theory, the left- and righthanded neutrino can interact with the Higgs field and acquire a mass term. In chapter 2, we will see that this is indeed a possibility. We will also see that the addition of righthanded neutrinos to the theory also gives rise to a different possibility to make neutrinos massive. This mechanism is called the type-I seesaw and it also explains why neutrinos, even if they are massive, are much lighter than all other known particles. We also discuss two other seesaw theories (type-II and III), that give rise to lefthanded neutrino mass without a righthanded neutrino.

In conclusion, the observation of neutrino oscillations proves that the Standard Model is incomplete, as it allows only massless neutrinos that cannot oscillate. There are a number of suggested remedies for this problem and all of them involve beyond the Standard Model physics.

1.2.2 Dark Matter

The Sun accounts for 99.9% of the mass in the solar system. When we look out in the night sky, we see many stars and not much more. It is therefore intuitive to assume that most of the matter in the cosmos is in stars. This turns out to be incorrect. Interstellar and intergalactic gas clouds make up more than three times more mass than there is in stars, but as they barely emit any light, they are much harder to see.

The real surprise comes when we make an energy balance of the universe. Then we see that only about one sixth of all matter in the universe can be in the form of normal atomic matter. The majority of the matter in the universe occurs in the form of 'dark matter'[1]. It is called 'dark' because it does not interact with light in any way; invisible matter would be an even better name.

In terms of the Standard Model, not interacting with light means not coupling to the photon. A glimpse at figure 1.3 shows that there are a few particles that do not couple to the photon. However, the Z- boson, the Higgs boson and combinations of gluons (they cannot occur on their own), are all unstable and decay to particles that do couple to the photon. The only candidates left are the (normal lefthanded) neutrinos, but also these eventually get discarded. This has to do with the fact

[1] An even larger part of the energy content of the universe is in the form of 'dark energy'. It is even more mysterious than dark matter, but we do not discuss it any further in this thesis as it might as well be related to new aspects of gravity as to new aspects of particle physics.

that even if neutrinos have mass, this mass is too low to give them the right dark matter properties. In particular, neutrinos do not cluster enough, behaviour that was observed for the unknown dark matter particles.

We conclude that the Standard Model does not have a credible candidate for the dark matter. Again, the remedy is rather straightforward. Just add *any* particle to the theory that is stable and does not interact with the photon. The problem is that physicists generally don't like the *ad hoc* addition of a particle to the theory. It would be better if the dark matter candidate naturally occurs in a beyond the Standard Model theory. Indeed some of the extensions of the Standard Model discussed in sec 1.3 automatically give a dark matter candidate. In chapter 5, we discuss the appearance of a dark matter candidate after a flavour symmetry gets broken.

1.2.3 Matter-antimatter Asymmetry of the Universe

When we discussed the matter content of the Standard Model at the beginning of this chapter, we left out an important detail. We mentioned that the electron has two brothers, the muon and the tau lepton that are much like it, but only have a different mass. There is actually a particle that looks even more like the electron, called the positron. It has all the properties of the electron, only its charge is exactly the opposite. The electron has charge -e, so the positron has charge $+e$. All particles of the Standard Model have these almost-identical twins and together they are called antimatter. When a particle and its corresponding antiparticle meet, they cannot peacefully coexist. Instead, they annihilate each other in a burst of pure energy.

Now if the Earth were made partly of matter and partly of antimatter, that would be quite inconvenient, as matter-antimatter annihilating explosions would occur with catastrophic consequences. Fortunately, this does not happen outside Dan Brown novels. The Earth is completely made of matter and so is the solar system and most probably the whole observable universe. Obviously, the (observable) universe has a preference to be in a matter state rather than in an antimatter state. Even matter is quite scarcely present in the universe though. If we count the number of matter particles and the number of light particles (photons), the photons win by a factor in the order of a billion.

Now comes the crucial point. There are many reasons to believe that the universe went through a phase of so-called inflation almost directly after the Big Bang. Theory demands that directly after this inflationary era, there were equal amounts of antimatter particles, matter particles and photons. This is clearly not what we observe today: now there are no antimatter particles, few matter particles and many photons.

The annihilation relations referred to above, provide part of the solution. In later stages of the universe, matter and antimatter particles met and annihilated. This certainly explains why there is much more light than matter, but it fails to explain why there is more matter than antimatter or even why there is still any matter at all. Matter and antimatter could have completely annihilated each other until nothing was left of either.

So the story can be this: directly after inflation, there were equal numbers of matter, antimatter and light particles. Then some reactions occurred that slightly shifted the balance. For every billion antimatter particles, there were a billion +1 matter particles (and still about a billion photons). Now the annihilation reactions set in. All billion antimatter particles annihilated with a billion of the matter particles, but a single matter particle survived. This matter particle, however, is dwarfed in a sea of billions of photons. This scenario is schematically represented in figure 1.5.

The crucial question is of course what are the 'some reactions' of the previous paragraph. Clearly, they treat matter and antimatter on different footing. In technical terms, this is called violating charge-parity symmetry, or CP. Actually, there are some reactions in the Standard Model that violate CP and these were very important in the history of particle physics. After the discovery of CP violation in the decay of subatomic particles called kaons in the 1960s, Makoto Kobayashi and Toshihide Maskawa showed in 1973 that the Standard Model can account for this CP violation, but only if there are at least three generations of quarks and leptons. At that time, only two generations

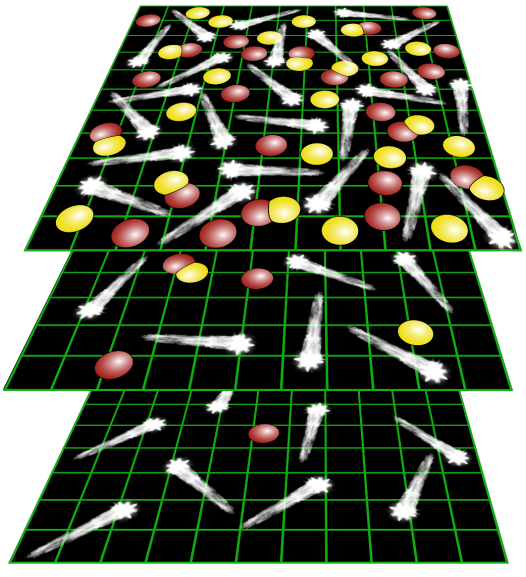

Figure 1.5: *Schematic view of matter (red), antimatter (yellow) and photons (white) at different stages of the history of the universe.*

were observed, so their argument was really the prediction of a third generation. Particles of the third generation were indeed discovered soon thereafter: the tau lepton in 1975 and the bottom quark in 1977, with the top quark and the tau neutrino following in 1995 and 2000. Kobayashi and Maskawa received the Nobel Prize in Physics in 2008.

A detailed analysis of the CP violation in the Standard Model shows however that this is *not enough* to explain the cosmic overabundance of matter over antimatter. To explain this, new physics is needed. The solution to this problem might be related to the solutions of other challenges for the Standard Model. For instance, if the problem of neutrino masses is indeed solved by the introduction of righthanded neutrinos, the physics of these particles in the early universe might give the matter-antimatter asymmetry by a process known as leptogenesis. And if the Standard Model is extended to a supersymmetric Standard Model, there are new ways to generate the asymmetry at the moment when the Higgs field makes the electroweak symmetry break as described above.

1.2.4 Minimal extensions of the Standard Model

From the above sections, it is clear that cosmological observations prove that the Standard Model is incomplete. It should be extended with at least a number of new fields and operators such that it is able to generate neutrino masses; that it has a dark matter candidate and that it can explain that the universe is matter-antimatter asymmetric.

Recently, a very minimal model was proposed by M. Shaposhnikov and collaborators, dubbed the neutrino minimal Standard Model or νMSM [2]. In this model, only three righthanded neutrinos are added to the Standard Model. These open the possibility for (normal) neutrino mass terms. Of the new righthanded neutrinos, one is much lighter than the others and it is stable and can serve as the dark matter. The two others are much heavier and unstable. They decayed early in the universe and did so in a way that shifted the matter-antimatter balance. It is technically very challenging to make these decays generate *enough* asymmetry. A number of points in parameter space have been found however, where the two heaviest neutrinos are almost of identical mass and the balance shift is large enough.

Extensions of the Standard Model like the one by Shaposhnikov *et al* are very appealing from the

point of view of minimality. They explain all the *hard* criticism on the Standard Model, all the points where we are certain that it lags behind. However, it fails to address many *why*-questions. Why are the parameters the way they are. An example is the tiny mass gap between the two heavy righthanded neutrinos. Why is it this small? Only to provide the right amount of matter-antimatter asymmetry? That would be a justification *post hoc*. Or is there a physical reason why this difference is naturally of that order?

In the next section, we will see that questions like these also plague the (normal) Standard Model. We will see that these *theoretical* reasons to extend the Standard Model generally call for more symmetry.

1.3 Theoretical reasons to extend the Standard Model

In this section we study a number of phenomena that can in principle be explained by the Standard Model, but only if some of its parameters are very large, very small or finetuned to very specific values. These are not *hard* problems of the Standard Model; in principle the parameters can be 'just like this'. But it is also possible – and from a theoretical perspective this is preferable – that there is an underlying theory that can explain these particular values.

We can compare this to a person playing poker and getting four-of-a-kind aces many times in a row. In principle, there is a finite probability of a long list of hands with four aces, but any casino or opponent would investigate this player with great scrutiny. Cards in his sleeve are a much more probable explanation than great luck.

In this section, we discuss the strong CP problem, the Higgs hierarchy problem and the gauge unification possibility. Candidate solutions for these problems are respectively the Peccei-Quinn symmetry; an extended space-time symmetry, called supersymmetry and an extended and unified gauge symmetry. The last two symmetries in this list are important ingredients of chapter 4 of this thesis. In the next section, we discuss the so-called flavour problem. This problem, and its candidate solution, flavour symmetries are the main topic of this thesis.

1.3.1 The strong CP problem

In section 1.2.3, we discussed the fact that matter and antimatter behave differently under the laws of particle physics, as the Standard Model violates CP. In principle, CP violation can be related to two of the three forces of section 1.1, both the weak and the strong nuclear force. However, all CP violation observed so far comes from the weak sector. The CP violation in the strong interactions is thus either very small or vanishing.

In the Standard Model, CP violation in the strong sector is parameterized by a parameter called the theta angle. In principle, θ can take any value between 0 and 2π, which is the natural range for an angle. Measurements so far have not observed any non-zero value of the angle, but have restricted it to be very small: $\theta < 10^{-10}$. Now it might well be that θ 'just happens' to have a small value of, for instance, 5×10^{-11}. However, one is tempted to believe that θ might be *exactly* zero. In 1977, Roberto Peccei and Helen Quinn postulated a theory that predicts the theta-angle to be zero in a natural way. In this theory, θ is no longer a constant value (i.e. a parameter), but actually a dynamical field that is charged under a new symmetry, the Peccei-Quinn symmetry. An extra advantage is the presence of a dark matter candidate, called the axion.

In this thesis we do not discuss the Peccei-Quinn mechanism in more detail, but the framework it uses is very typical. Firstly, we noticed that there is an element of the Standard Model that cannot be explained in a natural way. Secondly, we gave an explanation using new fields and new symmetries. Lastly, we found that this solution also helps to solve other problems of the Standard Model, in this case the dark matter problem.

1.3.2 The hierarchy problem

The next theoretical challenge to the Standard Model is related to the mass of the Higgs boson. Unfortunately, the Higgs mass is the last great unknown of the Standard Model. Indirect measurements constrain the Higgs, if it exists, to be lighter than approximately 200 GeV [3][2]. A theoretical argument, the perturbativity bound, gives the same value.

Naively, this value of the Higgs mass – or in fact any other value – would not pose a problem. We would just need to assume a parameter of the right size. The problem is, that masses in particle physics are not just given by parameters. The masses given by the *bare parameters* can be significantly changed by the effects of virtual particles. These can be thought of as being created from the vacuum for a very short while before disappearing again in this vacuum in a process that is in line with the uncertainty principle between energy and time.

To see the effect of virtual particles on the Higgs mass, we study a Higgs boson propagating through the empty vacuum. This can be graphically represented by a line running from left to right as in figure 1.6. The line is dashed to indicate that the particle propagating is a so-called boson, a particle for which the spin quantum number is an integer, zero in this case.

Instead of 'just' propagating, the Higgs boson can do more interesting things, like budding of a second (virtual) Higgs particle and then immediately reabsorbing it (figure 1.7) or temporarily splitting in a fermion-antifermion pair. Fermions are particles whose spin quantum number is a half-integer and they are represented by continuous lines. The top quark couples most strongly to the Higgs (and is thus the heaviest) of all known fermions, so a top-antitop loop is most probable and this is shown in figure 1.8.

Figure 1.6:
The Higgs propagator.

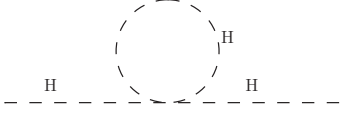

Figure 1.7:
The Higgs propagator with a Higgs loop.

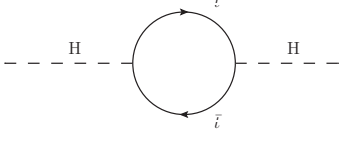

Figure 1.8:
The Higgs propagator with a top loop.

The diagrams 1.7 and 1.8 effect the Higgs mass squared: the Higgs loop in a positive way and the top-antitop loop in a negative way. The question is how large these corrections are. This is related to how much energy the particles in the loop can have. Even if the energy of the Higgs boson that is propagating is fixed, the energy of the short-lived particles in the loop can be much larger. Naively, the energy of the particles in the loop can go up to infinity.

Allowing virtual particles with infinite energies gives unsolvable problems for the theory. This can be circumvented by declaring that the virtual particles should be allowed to have energies at least as high as the next scale of new physics. Until this scale, the Standard Model is a good description of nature and we know what should be the physics of particles (including virtual particles) with these

[2]The gigaelectronvolt or GeV is a unit for energy or mass; according to Einstein's $E = mc^2$ these are equivalent. The mass of a proton is approximately 1 GeV and most processes in particle physics find place at an energy scale up to a few hundred GeV.

energies. Above this scale, we do not know what the physics is and we also do not know what is the effect of virtual particles of these energies.

The fundamental scale of the physics of the Standard Model is the scale where electroweak symmetry breaking takes place as alluded to in section 1.1. The other fundamental scale of particle physics is the scale of quantum gravity, the Planck scale introduced at the end of section 1.1. We do not know the details of the new theory that emerges at the Planck scale, but we can estimate the scale itself by an analysis of the fundamental constants of gravitation (Newton's constant G), relativity (the speed of light c) and quantum physics (the Planck constant h). Max Planck did this calculation immediately after the postulation of his constant and the scale he found turned out to be much larger than the (later discovered) electroweak scale. The Planck scale is 1.2×10^{19} GeV, while the electroweak scale is a mere 246 GeV.

Unless there is another scale of new physics between the electroweak scale and the Planck scale, we conclude that the virtual particles in the loops of figures 1.7 and 1.8 can have energies up to the Planck scale. Even if this energy is not infinite, it is very large and it leads to enormous corrections to the Higgs mass. To find a Higgs in the range where it should be, the bare parameter should not be around the Higgs mass squared, but around the Planck mass squared and it should be almost perfectly equal to the corrections. The difference between the original parameter and the corrections should be 10^{-34} times smaller than either of these. This is a strong finetuning and the chance that it happens 'naturally' is as small as a poker playing showing four aces nine times in a row.

There are two loopholes in the argument above and they serve as candidate solutions to the hierarchy (or finetuning) problem. The first focusses on the claim that the scale of quantum gravity is as large as 10^{19} GeV. A crucial assumption made here is that the known laws of gravity are valid at all intermediate scales. More specifically, the assumption is that gravity always spreads out over only three space dimensions. If there are extra dimensions, the scale of quantum gravity can be lower and the finetuning is less severe.

A second solution is related to the fact that there are both a positive and a negative correction to the Higgs mass squared. If these corrections cancel each other in a natural way, the finetuning problem is also evaded. This is the case if there is both a loop with a boson and one with a fermion that have related couplings to the Higgs field. This is not the case for the Higgs and the top of figures 1.7 and 1.8, but we can introduce a Higgs-like fermion ('Higgsino') and a top-like boson ('stop'). These give rise to diagrams 1.9 and 1.10, that cancel exactly to respectively 1.7 and 1.8.

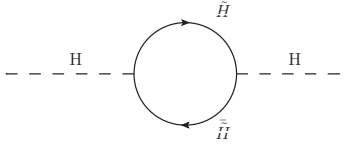

Figure 1.9:
The Higgs propagator with a Higgsino loop.

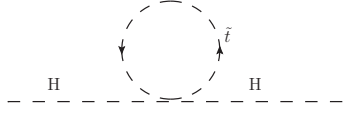

Figure 1.10:
The Higgs propagator with a stop loop.

The symmetry that gives a boson for every fermion in the theory and vice versa, is called supersymmetry. The superpartner of a Standard Model fermion is called a sfermion and its name is given by putting an s (of 'supersymmetric') in front of the name of the particle, for instance a stop as a partner to the top quark. The names of the supersymmetric partners of the Standard Model bosons are formed by adding '-ino' to the original names, giving photinos, Winos, Zinos, gluinos and Higgsinos.

If supersymmetry were exact, fermions and sfermions would have identical masses. This is not what we observe: for none of the Standard Model fermions, there is a boson with the same mass. The same holds for the known bosons. Obviously, supersymmetry cannot be an exact symmetry of nature, but it should be broken. The superpartners of the known particles are much heavier than their Standard Model counterparts. Still, if supersymmetry is to solve the finetuning problem, the gap may not be too large. The prediction is that if superpartners exist, their masses should be in the range of the LHC

and they should be discovered there. As of fall 2011 no signs of supersymmetry have been found (see e.g. [4] and [5]). This significantly constrains the parameter space for certain supersymmetric implementations, but by no means rules out supersymmetry at the LHC scale.

We conclude that supersymmetry can solve the finetuning problem related to the Higgs mass, but this comes with a price. We need to add quite a large new (broken) symmetry to the theory and the existence of many new particles is needed. The good news is that one of these particles typically can serve as the dark matter candidate and that supersymmetry enables the possibility of gauge unification, as described in the next section. Supersymmetry is an important ingredient of the models in chapters 2 and 4. The models described in chapter 5 are non-supersymmetric.

1.3.3 Gauge unification

The Standard Model is a consistent theory of three of the four forces of nature, as described in section 1.1. All of these forces couple to some of the matter particles as shown in figure 1.3 and they do so with their own strength. At small distances, the hierarchy of the forces is such that the strong nuclear force is the strongest, followed by the weak nuclear force. The electromagnetic force is relatively feeble.

Much like the Higgs mass discussed in the previous section, the coupling constant of a force is not just a parameter, but there are strong effects from virtual particles. To study these, we consider an electron somewhere in the vacuum.

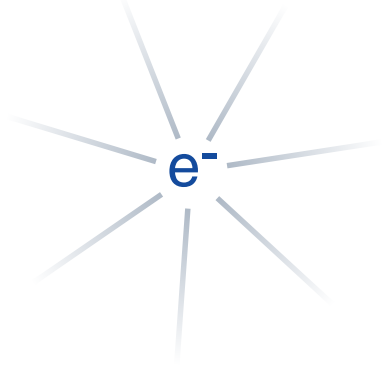

Figure 1.11: *An electron and the field created around it.*

The electron is an (electromagnetically) charged particle and it thus creates a strong field around it, represented by the grey lines in figure 1.11. Now if a virtual electron-positron pair is created in the vacuum, this pair will tend to align along the field lines, with the positron pointing towards the electron to partially shield it. The resulting situation is depicted in figure 1.12.

Due to the screening of the positrons, the strength of the field that we observe is less than the strength of the original field. How much less this is, depends on how far we have zoomed in. If we use very energetic photons to probe the electron, we can look deeper into the cloud of electron-positron pairs than when we use less energetic photons. We conclude that to energetic photons, the strength of the field of the electron is greater than it is to less energetic photons. This translates to the electromagnetic coupling constant growing with the energy scale we study it at.

If we study the strong nuclear force in detail, we see that not a screening effect, but an anti-screening effect dominates. The strong force is very strong at low energies, but it becomes less strong when the energy grows. The weak nuclear force starts in between the electromagnetic and the strong force. It becomes weaker as energy grows, but at a smaller pace than the strong nuclear force.

This allows us to pose an interesting question. If we look at higher and higher energy scales, the

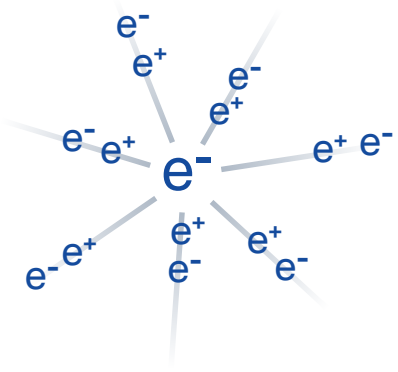

Figure 1.12: *An electron and the cloud of aligned positron-electron pairs around it.*

coupling constants of the three forces of the Standard Model grow towards each other. Is there an energy scale where all three of them become of comparable strength? In the Standard Model, the answer is 'no', as can be seen from figure 1.13. Plotted here is $1/\alpha$ for the three forces, where α is a dimensionless number that is proportional to the coupling constants squared.

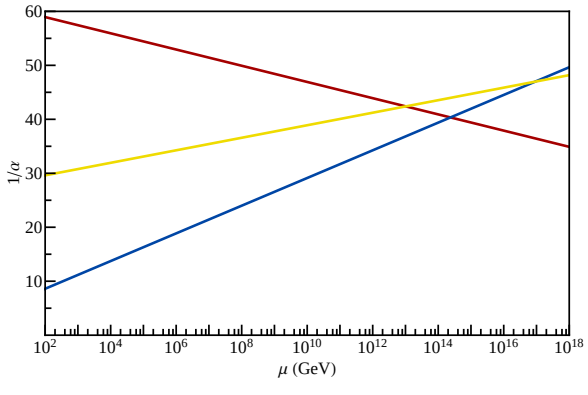

Figure 1.13: *The 'running' of the coupling constants of the Standard Model as a function of the scale μ they are observed at. Red: hypercharge, that is directly related to electromagnetism; yellow: the weak nuclear force and blue: the strong nuclear force. We observe that the three forces do not meet in one point.*

In a supersymmetric extension of the Standard Model, the superpartners of the known bosons and fermions can also contribute to the screening or anti-screening effects. They do so only if we probe the coupling constants at energies larger than their masses. In a theory with superpartners, the lines of the running coupling constants therefore have a kink at the energy scale that corresponds to the masses of the superpartners. This kink bends the running coupling constants in the right direction. In a theory with supersymmetry, it is possible that the three coupling constants of the Standard Model meet in one point. This is shown in figure 1.14. Note that this unification scale is higher than the candidate unification scale in the non-supersymmetric theory. This has to do with the fact that supersymmetric particles partly cancel the effect of their partners. In supersymmetry, the running of the coupling constants is slower, so they meet at a higher energy.

In figure 1.14 the three coupling constants go through one point, but after that they just continue to run and diverge again. If this is the case, there is probably no great importance of the three constants going through one point. There is a second possibility however. After the unification scale, the three forces may actually unite and form one superforce. Theories with this superforce are called Grand Unified Theories (GUTs). In a sense, these theories are much simpler than the Standard Model. The SM really needs three forces; in GUTs there is only one fundamental force, that has three manifestations after it gets broken. Also fermions can often be described more economically in

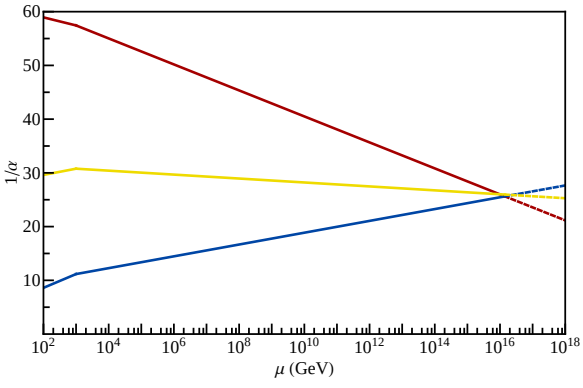

Figure 1.14: *The running of the coupling constants in a supersymmetric extension of the Standard Model. The three coupling constants seem to meet in one point.*

GUTs, as several particles that are unrelated in the SM, may have a common origin in Grand Unified Theories. In chapter 4 we study a particular GUT, the Pati–Salam theory, in more detail.

1.4 Flavour symmetries

There are many free parameters in the Standard Model. We already discussed some of them. The theta parameter of QCD in section 1.3.1; the Higgs mass (that eventually relates to two parameters λ and μ) in section 1.3.2 and the three gauge coupling constants in section 1.3.3. Together this gives six parameters.

By far the most parameters however, are related to the masses of the elementary fermions, that originate from the Yukawa couplings of the quarks and leptons to the Higgs field. In the original Standard Model, where neutrinos are massless, this amounts to 13 parameters. In a theory that includes neutrino masses, this number grows to 20 if neutrinos are particles of the Dirac type (not their own antiparticle) and to 22 if neutrinos are of the Majorana type (their own antiparticle).

When we look at the fermion masses and the way the mass eigenstates combine to form interaction eigenstates, there seems to be some structure. In principle, this apparent structure can just be the result of particular values of the 20 or 22 available free parameters. Some parameters then need to be tuned to 'special' values like 1, 1/2 or 1/3 to at least a few percent accuracy. Other parameters need to be quite large, with for instance the top quark to electron mass ratio being of the order of 340 000. This is all quite unnatural and unsatisfying from a theoretical physicist's point of view. We prefer to explain observed structures with physical arguments instead of with resort to coincidence.

The central claim of this thesis is that there may be new physics in the fermion mass sector that helps explaining the observed structures in the data. In this section, we first discuss some of the structures in the fermion sector. Then we sketch how family symmetries can explain these structures. The working of family symmetries is explained in more (mathematical) detail in chapter 2.

1.4.1 Structures in the fermion masses

In section 1.1 we introduced the three families of quarks and leptons of the Standard Model. We plot the measured masses of the fermions in figures 1.15 and 1.16 on respectively a linear and a logarithmic scale. In the top figure, we see that the top quark is much heavier than all the other particles, effectively dwarfing their masses.

The logarithmic plot holds more information. Firstly, we notice that the neutrinos are *much* lighter

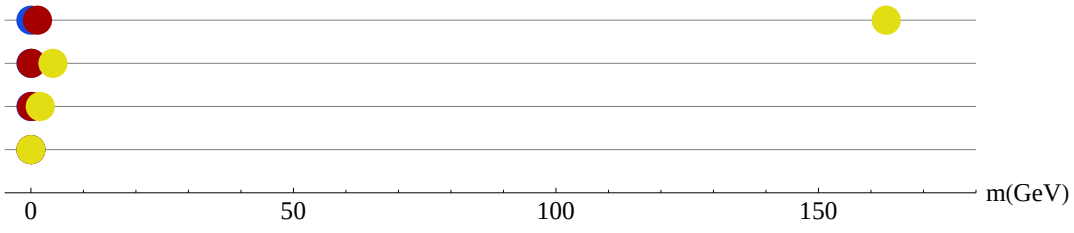

Figure 1.15: *The masses of the Standard Model fermions on a linear scale. The top quark appears right on the top line. All other quarks and all leptons appear on top of each other on the left side of the diagram.*

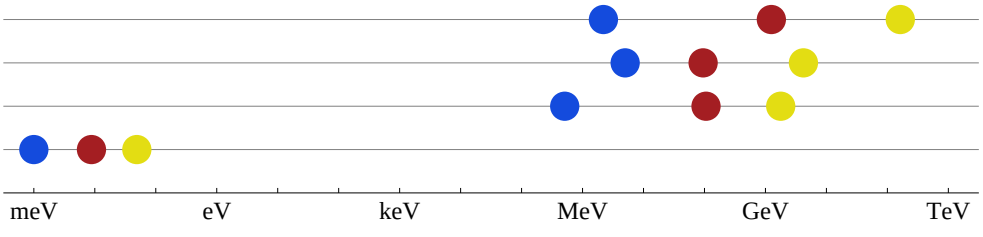

Figure 1.16: *The masses of the Standard Model fermions on a logarithmic scale. Top line from right to left: top quark, charm quark and up quark. Second line: bottom quark, strange quark and down quark. Third line: tau lepton, muon and electron. Bottom line: the three neutrinos. Their exact masses are not know at the moment, but from indirect measures, we conclude that their masses are in the milli electronvolt to electronvolt region.*

than all the other particles around. It is no wonder that up to 13 years ago, they were thought to be massless. This, combined with the observation that neutrinos are the only electrically neutral particles in the Standard Model, gives rise to the assumption that neutrino mass might come from an entirely other mechanism than quark and charged lepton masses. This mechanism is called the see-saw mechanism and is called such because it works in the same way as the seesaw in a children's playground. The neutrinos are on the seat that goes up and end up with a very small mass. The theory predicts the existence of other particles that sit on the seat that goes down. These particles are identified as new heavy ('righthanded') neutrinos or bosonic or fermion triplets. As much as the neutrinos are extremely light, these particles are very heavy and this might be the reason they are not observed so far, although there is some hope at the Large Hadron Collider. The seesaw and its consequences are discussed in more detail in section 2.1.4.

If we ignore the neutrinos, we can do a second interesting observation. All particles of the second generation are much heavier than all particles of the first generation, while all particles of the third generation are much heavier than all particles of the second generation. There seems to be quite a strict hierarchy between the generations. Actually, when we look at the gaps between the first and second and second and third generation, these are for each type of particle more or less of the same order. This relation is not exactly true; for instance, we see that the electron is slightly too light, while the down quark is a bit too heavy for the relation to hold. The masses of the Standard Model particles vary slightly with the energy scale we observe them at, due to a mechanism with virtual particles, much like what we described for the Higgs boson in section 1.3.2. At the scale of gauge unification, the relation described above holds much better.

Let's zoom in to the up-type quark sector. The mass of the top quark is given by a 'normal' parameter, that is approximately 1, while the charm quark is given by a small parameter and the up quark by a parameter that is small-squared (i.e. $m_c/m_t \approx m_u/m_c \ll 1$). Alternatively, we can describe the charm mass by a parameter that *is* normal, but now multiplied by a attenuating factor that is approximately the ratio of the top to the charm mass. The up-quark mass is now described by a third normal parameter, and the square of the attenuation factor. Froggatt and Nielsen gave a mechanism that describes the attenuation factors for the charm and up quarks, assuming they are charged under a type of charge that differs per generation. The Froggatt–Nielsen symmetry is thus the first family

symmetry we encounter in this thesis; we study the principles of the mechanism in more detail in section 2.3.1 and the Froggatt–Nielsen symmetry is also an important element of the model of chapter 4.

Evaluating the quark and charged lepton masses at the unification scale, yields two more interesting observations. The first is that at this scale the bottom quark and the tau lepton have the same mass to good accuracy. The second is that the strange quark is quite precisely three times lighter than the muon, known as the Georgi–Jarlskog relation. This might suggest that these masses are not given by unrelated parameters, but (in both cases) by one parameter that effects both masses. In the Pati–Salam GUT, Bottom-tau unification and the Georgi–Jarlskog relation can easily follow from symmetry principles and we use this in the construction of the model of section 4.

1.4.2 Structures in the fermion mixings

In figures 1.15 and 1.16 we plotted the masses of the quarks and leptons. In the weak interactions, not exactly these mass eigenstates react, but rather a very specific combination of them. There is a coupling between the top-quark, a W boson and a quark of the down type. We can define this quark as the interaction eigenstate b'. The b' quark does not have a uniquely defined mass. It is a mixture of the lightest, middle and heaviest eigenstate.

In figure 1.17 we show the mass eigenstates d, s and b that are linear combinations of the down-type quarks that couple to respectively the up, charm and top quark (the interaction eigenstates d', s' and b').

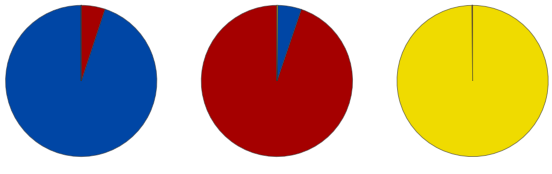

Figure 1.17: *Pie charts showing the flavour content of the three quark mass eigenstates. . Data taken from [6]*

The pie-charts of figure 1.17 are almost 'diagonal', meaning that the lightest mass eigenstate d is almost entirely the interaction eigenstate d' that couples to the up quark; in the second generation, we have $s \approx s'$ and in the third $b \approx b'$.

A priori, we would expect a mixing where each of the mass eigenstates is a mixture of significant portions of each of the interaction eigenstates. The data on the other hand seem to signal that coupling to the 'own' generation is preferred. Indeed in both chapter 4 and section 5.10.4 we describe mechanisms where at the leading order quarks couple diagonally and where the small slivers of red and blue (and the almost invisibly small piece of yellow) in figure 1.17 are given by correcting effects.

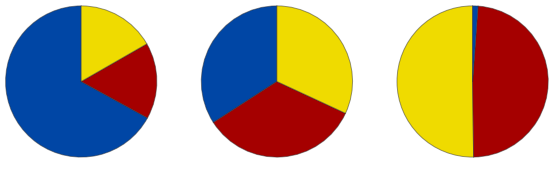

Figure 1.18: *Pie charts showing the flavour content of the three neutrino mass eigenstates. Data are average values from [7]*

The situation in the lepton sector is different. The mass eigenstates are mixtures of significant

portions of all three interaction eigenstates as shown in figure 1.18. In the last paragraph we mentioned that this is exactly what could be a priori be expected. However, there is more to it here. A closer look at the diagrams of figure 1.18 shows that the combinations seem to be special. The second mass eigenstate is an almost perfect equal combination of all three interaction eigenstates, while the third mass eigenstate is so for two of the three interaction eigenstates. This mixing pattern is called tribimaximal mixing [8]. It is interesting to note that it can be reproduced by a quite limited amount of new physics as shown in section 2.4. The words 'almost perfect' are important here. Recent measurements of the so-called reactor neutrino angle have shown that the thin sliver of blue in the rightmost diagram of 1.18 is unmistakeably there, ruling out the possibility of exact tribimaximal mixing as was in line with the data until very recently.

1.4.3 Models with family symmetries

To solve the numerical coincidence with the θ parameter (the strong CP problem), the Peccei-Quinn symmetry was introduced; supersymmetry can account for the numerical coincidence of the finetuning of the Higgs mass. In the same spirit, there is a symmetry related to the observations of the previous subsections.

The patterns we observed account to striking similarities and striking differences between the three generations. The new symmetry will therefore have to connect these generations. The words family symmetry and flavour symmetry are used interchangeably for this symmetry.

It is interesting to note that flavour symmetries work in a certain way perpendicular to the known gauge symmetries of the Standard Model. The electromagnetic force couples for instance one electron to a photon; the weak nuclear force can couple an electron neutrino to an electron and a W boson and the strong force couples for instance a blue up quark to a red one. Obviously, these three forces treat the particles within a generation very differently, according to their charges under the related symmetry. All this concerns couplings within a generation. The idea of family symmetries is to have very specific couplings between particles of different families and treat the three families different by charging them differently under the new symmetry. This is graphically represented in figure 1.19. The figure also explains why family symmetries are sometimes called horizontal symmetries.

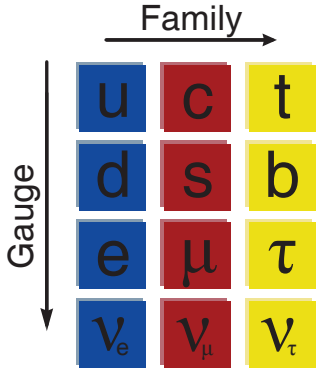

Figure 1.19: *A graphical representation of family and gauge symmetries*

The introduction of family symmetries concludes the content-part of this chapter. We conclude that the Standard Model provides an excellent description of the physics of elementary particles, but that there are reasons to extend it. One of these extensions is the introduction of flavour symmetries that form the heart of this thesis.

1.5 Outlook of this thesis

In this thesis we study different manifestations of flavour symmetries and their consequences. To be well-prepared for these models and their technical details, chapter 2 is a second introductory chapter. It is more technical than this chapter and contains not only an introduction to relevant concepts, but also to the mathematical formulation. The number of equations grows to 90 compared to zero in this chapter.

After a discussion of fermion masses in one and three families, chapter 2 discusses two well-known family-symmetric models. The model of Froggatt and Nielsen [9] mainly gives an explanation for the patterns found in the fermion masses as discussed in section 1.4.1. The model of Altarelli and Feruglio [10, 11] reproduces the tribimaximal mixing alluded to in section 1.4.2. In both cases the key element of the model is the assumption of an extra symmetry. We end the model sections with a balance: how much information is gained by assuming an extra symmetry and how much extra complications are the price that is paid for it.

The discussion of the Altarelli–Feruglio model contains a lot of information. This is true at a technical level – an example is the method of using driving superfields – but it also shows directions to proceed in. One of the conclusions is that the tribimaximal mixing pattern and in particular the limited possibility to have so-called next-to-leading order corrections to this mixing scheme points to the investigation of different mixing schemes.

Chapter 3 starts with a discussion about where to go now the measurement of non-zero reactor neutrino mixing angle has excluded exact tribimaximal mixing. After that, we consider a large class of candidate flavour symmetries and investigate to which mixing patterns they can give rise to. Tribimaximal mixing is one of them, but it is accompanied by a large family of other mixing patterns. Of particular interest are two mixing patterns that follow from relatively large groups ($\Delta(96)$ and $\Delta(384)$ respectively) that naturally predict the third neutrino mixing angle to be non-zero. This feature is not shared by other familiar groups and exactly what the most recent data point at.

Chapter 4 interprets the hint from the Altarelli–Feruglio model in a different way. This chapter describes a model in detail, in which the tribimaximal mixing pattern is replaced by the so-called bimaximal one. In first approximation this describes the data far worse than the tribimaximal case. The advantage lies in the fact that in the bimaximal case, corrections are possible and indeed needed.

The model of chapter 4 is thus a model of bimaximal mixing. The other important characteristic of the model is that it combines a flavour symmetry with a grand unified symmetry, the Pati–Salam GUT to be precise. We discuss the consequences of the combination of the two types of symmetries and show that in the interplay between the symmetries significant interference appears. The model can explain a wealth of data, but it becomes quite baroque. The Higgs sector is strongly extended and effects from renormalization group flow exclude much of the initially preferred parameter space.

Chapter 5 is inspired by another lesson learned from the Altarelli–Feruglio model. Supersymmetry and extra dimensions are no essential elements of family symmetric models, but at least one of them is needed for so-called flavon alignment in a model with two or more directions in flavour space. Both supersymmetry and extra dimensions are very interesting and well-motivated types of new physics, but it is important to see if flavour symmetry models can be constructed independent of them. The obvious way out, is to consider cases where just one direction in flavour space appears. Chapter 5 discusses a particular realization in which a multitude of Higgs fields transforms under a family symmetry. We give the scalar potential if there are three Higgs fields that transform as a triplet under A_4, the most popular family symmetry and continue to find all its minima. The scale of new physics in this set up is the electroweak breaking scale. The model thus provides predictions testable at the LHC and precision measurements can already constrain it. We finish the chapter by an elaborate discussion of these tests and applications to various implementations.

Chapter 6 does what a last chapter usually does. It summarizes and concludes the thesis. In this chapter we make a large balance of the positive and negative things about flavour symmetries and flavour symmetric model building seen in this thesis.

Chapter 2

Fermion masses in the Standard Model and beyond

> False facts are highly injurious to the progress of science, for they often endure long; but false views, if supported by some evidence, do little harm, for every one takes a salutary pleasure in proving their falseness.
>
> *Charles Darwin [12], The descent of man*

Flavour symmetries provide new ways to describe the apparent structure in the quark and lepton masses. To be able to appreciate this, we first study the way elementary-fermion masses are generated in the original Standard Model. In the first section of this chapter, we discuss fermion masses in the Standard Model with only one generation. We will see that the quark and charged lepton masses are generated straightforwardly, but that neutrino masses are quite challenging to the theorist already. In the next section, we extend the analysis to the familiar three generation Standard Model, counting how many new degrees of freedom are hidden in the fermion masses and mixing. In the two sections that follow, we describe the working of family symmetries. We include two relatively simple models: the Froggatt–Nielsen model, that explains the hierarchy among the generations in section 2.3 and the model of Altarelli and Feruglio, that reproduces the tribimaximal mixing pattern in section 2.4. Lastly, section 2.5 presents the conclusions of the chapter.

2.1 The one family Standard Model

In this section, we describe how the Standard Model can accommodate masses for the quarks and leptons in case there is a rather minimal number of them. We discuss a situation where there are only two quarks, one of the up-type and one of the down-type, that we simply call up and down. We also assume the existence of only one charged lepton, dubbed the electron and one neutrino, that we refer to as such.

As always, all information is contained in the Lagrangian. The most general $SU(3)_C \times SU(2)_L \times U(1)_Y$ gauge invariant Lagrangian with only renormalisable operators reads

$$\mathcal{L}_{\text{SM}} = \mathcal{L}_K + \mathcal{L}_{\text{gauge}} + \mathcal{L}_Y + V_{\text{Higgs}}. \tag{2.1}$$

Here, $\mathcal{L}_K$ are the kinetic terms for the quarks, the leptons and the Higgs field. The demand of invariance under *local* symmetry transformations, requires the appearance of gauge bosons in covariant derivatives. Their own kinetic terms and self-interactions are given in the second part of the Lagrangian $\mathcal{L}_{\text{gauge}}$. Kinetic and gauge terms are very well known since the original formulation of the Standard Model and we do not modify them in this thesis, except for the fact that we discuss a gauge group different from the Standard Model's in chapter 4. Even there, the extension is straightforward.

The last term in 2.1 is the potential for the Higgs field. If there is only one Higgs field, this is also very well-known. It is the famous Mexican hat potential, where the Higgs field drifts away to its minimum that is not at the origin, thereby breaking the electroweak symmetry. The value of the Higgs field at the minimum is called the vacuum expectation value or vev. This is schematically represented in figure 2.1. In case of more than one Higgs field, the potential might become more involved. In chapter 5 we study the most general potential for a three Higgs fields that transform together as a triplet of the flavour symmetry A_4 and the different vacuum expectation values these fields can be in. In the remainder of this chapter, we simply assume the existence of some Higgs potential that gives non-zero vevs for one or more Higgses and focus on the last term we did not discuss yet, the Yukawa interactions $\mathcal{L}_Y$.

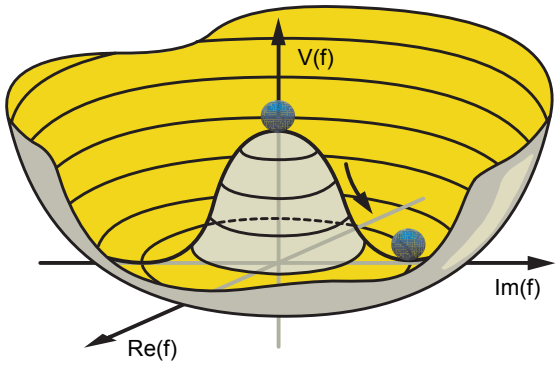

Figure 2.1: *A cartoon of the Higgs potential and its non-zero vacuum expectation value.*

2.1.1 Yukawa couplings

The terms in 2.1 that are of most importance for this chapter, are the terms in $\mathcal{L}_Y$, the Yukawa interactions between the Higgs fields and the quarks or leptons that eventually give rise to mass terms for the latter. To appreciate these, we first turn to elementary particles *below* the electroweak symmetry breaking (EWSB) scale. These particles and their relevant quantum numbers - the electromagnetic charge and the representation of the colour gauge group - are given in table 2.1

Field	symbol	$(SU(3)_C, U(1)_{\text{em}})$
up quark	u	(3, $\frac{2}{3}$)
down quark	d	(3, -$\frac{1}{3}$)
neutrino	ν	(1, 0)
electron	e	(1,-1)

Table 2.1: The quarks and leptons below the EWSB scale and their representations under the relevant gauge group.

Mass terms are constructed as quadratic terms in the fermion fields. They contain a spinor ψ that represents an incoming fermion as well as a barred spinor $\bar{\psi}$ that represents an outgoing fermion as shown in figure 2.2. Below the electroweak scale, fermion masses read

$$\begin{aligned}\mathcal{L}_{\text{mass}} &= m_u \bar{u}_L u_R + m_d \bar{d}_L d_R + m_e \bar{e}_L e_R + \text{h.c.} \\ &= m_u \bar{u} u + m_d \bar{d} d + m_e \bar{e} e \ .\end{aligned} \tag{2.2}$$

Note that in the definition of $\bar{\psi} = \psi^\dagger \gamma_0$, there is a complex conjugate. Therefore, a spinor $\bar{\psi}$ has the opposite quantum numbers as ψ. Thus, for instance, $\bar{u}$ is in the representation $(\bar{3}, -2/3)$ of

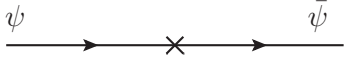

Figure 2.2: *A propagating fermion with a mass insertion according to equation (2.2)*

$SU(3) \times U(1)_{\text{em}}$. This ensures that all terms in the Lagrangian (2.2) are singlets of the colour times electromagnetic gauge group. In the term $m_u \bar{u} u$, we have $\bar{3} \times 3 \ni 1$ for colour and $-2/3 + 2/3 = 0$ for electric charge, etc. We did not include neutrino masses for reasons that are explained shortly.

Now we move to the Standard Model above the EWSB scale. This is a chiral theory, meaning that left-handed and righthanded fields are no longer treated on equal footing. In the left hand side of table 2.2, we repeat the content of table 2.1, this time taking the left- or righthandedness of the fields into account. On the right hand side, we add the Standard Model fields that correspond to the fields on the left. Standard Model fields have quantum numbers of $SU(3)_C$, $SU(2)_L$ and $U(1)_Y$. The colour group is the same as below the electroweak scale. The representations under $SU(2)_L$ are such that lefthanded fields are in the doublet representation, while righthanded fields are in the singlet representation. We normalize hypercharge such that the electric charge is given by $Q = I_3 + Y$, where I_3 is +(-)$\frac{1}{2}$ for the upper (lower) component of an $SU(2)_L$-doublet and zero for righthanded fields.

Field		$(SU(3)_C, U(1)_{\text{em}})$	Field		$(SU(3)_C, SU(2)_L, U(1)_Y)$
RH up quark	u_R	(3, $\frac{2}{3}$)	RH up quark	u_R	(3,1,$\frac{2}{3}$)
LH up quark	u_L	(3, $\frac{2}{3}$)	LH quark doublet	Q_L	(3,2,$\frac{1}{6}$)
LH down quark	d_L	(3, -$\frac{1}{3}$)			
RH down quark	d_R	(3, -$\frac{1}{3}$)	RH down quark	d_R	(3,1, -$\frac{1}{3}$)
(RH neutrino)	(ν_R)	(1,0)	(RH neutrino)	(ν_R)	(1,1,0)
LH neutrino	ν_L	(1,0)	LH Lepton doublet	L_L	(1,2,$-\frac{1}{2}$)
LH electron	e_L	(1,-1)			
RH electron	e_R	(1,-1)	RH electron	e_R	(1,1,-1)

Table 2.2: Elementary fermions below (left) and above (right) the scale of electroweak symmetry breaking. The righthanded neutrino is printed in grey to stress that its existence is uncertain as explained in the text.

Table 2.2 mentions a righthanded neutrino in grey. Indeed a non-particle physicist that would see a version of table 2.2 without it, would probably immediately add it to 'complete the symmetry' of the table, where for every lefthanded field in the left half of the table, there is also a righthanded field and for every doublet on the right, there are two singlets. In the original Standard Model, however, the righthanded neutrino is absent. The reason is simple: it has never been observed. This is a consequence of the fact that it is a singlet under the complete Standard Model gauge group. This means that, barring gravity, it cannot interact with any of the other particles, perfectly hiding its possible existence. For now we assume that there are no righthanded neutrinos and discuss the masses of the other particles of table 2.2. Later in this section, we explore the new physics possibilities that the inclusion of a righthanded neutrino offers.

In passing, we note that after electroweak symmetry breaking, neutrinos of any handedness are

singlets under the residual $SU(3)_C \times U(1)_{\text{em}}$ gauge group. This means that the only way in which neutrinos can interact is by the fact that they are part of a doublet *above* the electroweak scale. There is thus a huge gap between the energy that neutrinos normally have and the energy scale above which they can interact. This explains the claim made in section 1.2.1 that neutrinos can traverse lightmonths of lead without ever interacting.

The analogue of equation (2.2) above the electroweak scale reads[1]

$$\mathcal{L}_{\text{mass}} = y_u \begin{pmatrix} \bar{Q}^u_L & \bar{Q}^d_L \end{pmatrix} \begin{pmatrix} H^0_u \\ H^-_u \end{pmatrix} u_R + y_d \begin{pmatrix} \bar{Q}^u_L & \bar{Q}^d_L \end{pmatrix} \begin{pmatrix} H^+_d \\ H^0_d \end{pmatrix} d_R + y_e \begin{pmatrix} \bar{L}^\nu_L & \bar{L}^e_L \end{pmatrix} \begin{pmatrix} H^+_d \\ H^0_d \end{pmatrix} e_R + \text{h.c.} \quad (2.3)$$

Here H_d and H_u are Higgs fields with quantum numbers $(1, 2, +1/2)$ and $(1, 2, -1/2)$ respectively. Note that the Higgs fields are required by gauge invariance, as no terms with only left- and righthanded quarks or leptons can give an SM singlet. This is why direct mass terms (with a dimensionful coupling constant m_x) are forbidden and we have only indirect mass terms from interactions with the Higgs field. The coupling constants, the Yukawa couplings y_x are dimensionless. In the minimal Standard Model, only one independent Higgs field can be used as H_d and H_u can be related via $H_u = i\sigma_2 H_d^*$. In many extensions of the Standard Model, including the minimal supersymmetric Standard Model, this identification is not allowed and two separate Higgs fields are required. In this chapter, we use both H_d and H_u, keeping in mind that the two fields might be related .

After the neutral components of the Higgs fields develop vacuum expectation values of respectively v_{H_d} and v_{H_u}, the Higgs fields can be expanded around these minima

$$H_d = \frac{1}{\sqrt{2}} \begin{pmatrix} h^+_d \\ v_{H_d} + h^0_d \end{pmatrix}, \quad H_u = \frac{1}{\sqrt{2}} \begin{pmatrix} v_{H_u} + h^0_u \\ h^-_u \end{pmatrix} . \quad (2.4)$$

The factor $\sqrt{2}$ in (2.4) is just a convention to have both components conveniently normalized. In the minimal Standard Model, obviously, $v_{H_d} = v_{H_u}$ as the vev can be chosen real. In a two Higgs doublet model, the quadratic sum of the two vevs equals 'the' electroweak vacuum expectation value v_{ew}. The ratio of the two vacuum expectation values is an important parameter called $\tan\beta$.

$$v^2_{H_u} + v^2_{H_d} = v_{\text{ew}} = 246 \text{ GeV}^2 , \qquad \tan\beta = \frac{v_{H_u}}{v_{H_d}} . \quad (2.5)$$

The Higgs fields are complex $SU(2)$-doublets, so they have four real components each. If H_d and H_u are unrelated, this gives in total eight real components; if they are related as in the Standard Model, the number is only four. Three components correspond to Goldstone bosons that give mass to the W^+, W^- and Z bosons. In the Standard Model, these are the two charged components for the Ws and the imaginary part A of the expansion around the vev for the neutral Z. This leaves only one Higgs boson h.

In a two Higgs doublet model, the Goldstone boson for the W^+ is formed from a certain linear combination of the charged components h^+_d and h^-_u (or rather its conjugate), while the orthogonal combination becomes the physical charged Higgs. Typically, both vevs v_{H_d} and v_{H_u} are real. In that case, the Goldstone boson of the Z particle comes from a linear combination of the imaginary parts of h^0_d and h^0_u, but not of the real parts. The other linear combination of the imaginary parts becomes a pseudoscalar Higgs, while the real parts of h^0_d and h^0_u mix to two scalar Higgs bosons.

Inserting the Higgs vevs of (2.4) into equation (2.3) reproduces equation (2.2) with $m_u = y_u v_{H_u}/\sqrt{2}$, $m_d = y_d v_{H_d}/\sqrt{2}$ and $m_e = y_e v_{H_d}/\sqrt{2}$. This vev insertion is shown with a cross in figure 2.3. Inserting the terms with the active Higgs bosons gives fermion-Higgs vertices.

$$\begin{aligned} \mathcal{L}_{\bar{f}fH} = &\frac{y_u}{\sqrt{2}} \left(\bar{u}_L h^0_u u_R + \bar{d}_L h^-_u u_R \right) + \frac{y_d}{\sqrt{2}} \left(\bar{u}_L h^+_d d_R + \bar{d}_L h^0_d d_R \right) + \\ &\frac{y_e}{\sqrt{2}} \left(\bar{\nu}_L h^+_d e_R + \bar{e}_L h^0_d e_R \right) + \text{h.c.} \end{aligned} \quad (2.6)$$

[1] Alternative conventions can be found in the literature, where $y_{u,d,e}$ are given by the coefficients of the Hermitian conjugate of the main terms given in equation (2.3)

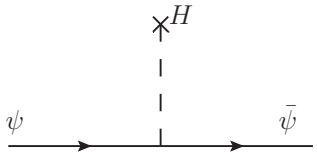

Figure 2.3: *A propagating fermion that gets a mass insertion by interacting with the Higgs field*

The absence of righthanded neutrinos in the spectrum of the Standard Model explains why there is no neutrino mass term in equations (2.2) and (2.3). Even if the righthanded neutrino has only trivial quantum numbers under the Standard Model gauge group, it would be needed to complete the fermion flow. In its absence, no coupling between the lefthanded neutrino in the lepton doublet and the (up-type) Higgs field can be constructed. At the time when the Standard Model was constructed, the neutrino was indeed thought to be massless. Its mass was only inferred much later by the observation of neutrino oscillations. Now we know that neutrinos have mass, we know that the content of this section cannot be the whole story.

In the next subsection we describe the way to extend the Standard Model with supersymmetry. In the six subsections that follow, we study the different possibilities to include neutrino masses in the Standard Model.

2.1.2 Fermion masses in supersymmetry

The Lagrangian that gives rise to fermion masses (2.3) contains elementary fermions and scalars (the Higgs fields). As mentioned in section 1.3.2, supersymmetry gives a boson for every fermion in the theory and vice versa. Those two states together (as well as one extra auxiliary field) form a supermultiplet or superfield. These are the building blocks of supersymmetric Lagrangians. In particular the superpotential $\mathcal{W}$ is relevant here. The superpotential is a holomorphic function of the superfields of the theory, meaning that it can contain the superfields, up to three of them, but not their Hermitian conjugates.

In the standard supersymmetry literature, it is customary not to reproduce the exact terms in (2.3), but terms that are basically its Hermitian conjugate, but then with $H^\dagger$ redefined to H, such that the Standard Model Higgs has negative hypercharge. In this case, the mass term for the up quark reads $y_u \bar{u}_R H_u \cdot Q_L$ and we need three superfields. Going from right to left, the first is a superfield that contains the quark doublet as fermionic component. Secondly there is a superfield with a Higgs doublet with hypercharge $+1/2$ as scalar component. The holomorphicity of the superpotential now explains the remark below equation (2.3). In the Standard Model, this Higgs field might be related to the Higgs field of the second term H_d via $H_u = i\sigma_2 H_d^*$, but in supersymmetry this is forbidden as it would render the superpotential non-holomorphic.

The third superfield is more problematic. It is the superfield that should give rise to $\bar{u}_R$. The bar implies complex conjugation, so having u_R as a fermionic component is not allowed. If instead we take its charge conjugate $(u_R)^c$ as an element, the corresponding supermultiplet does not need to be conjugated and is allowed in the superpotential. Due to the nature of charge conjugation, $(u_R)^c$ is itself a lefthanded field and can as such be written as $(u^c)_L$ – see for instance [13]. This has the extra advantage that all fermionic fields in the theory are now lefthanded, which allows them to be grouped together in grand unified multiplets. The best example is $SO(10)$ grand unification, where *all* Standard Model fermions are collected in a single 16-plet.

The generation of the superpotential terms for down quarks and electrons is similar to those for up quarks. In the minimal supersymmetric standard model (MSSM) the superpotential reads

$$\mathcal{W} = \mu \Phi_{H_u} \Phi_{H_d} - y_u \Phi_Q \Phi_{H_u} \Phi_{u^c} - y_d \Phi_Q \Phi_{H_d} \Phi_{d^c} - y_u \Phi_L \Phi_{H_d} \Phi_{e^c} \ . \tag{2.7}$$

We indicate supermultiplets with a capital Φ and a subscript that indicates the Standard Model component[2]. The first term in (2.7) gives rise to part of the Higgs potential. The other three terms reproduce the known fermion mass terms. Soft supersymmetry breaking terms are supposed to give additional contributions to the sfermion mass terms. These are terms that do not respect supersymmetry, but are added to the theory by hand to explain non-observation of sparticles so far. Note furthermore that in principle additional terms are possible in the superpotential (2.7). These are terms such as $\Phi_{u^c}\Phi_{d^c}\Phi_{d^c}$ or $\Phi_Q\Phi_{d^c}\Phi_L$ that violate respectively baryon number and lepton number and together can give rise to proton decay. They are absent however, if R-parity is imposed as an exact multiplicative symmetry.

Standard Model particles can be assigned R-parity $+1$, while sparticles (squarks, sleptons and Higgsinos) have -1. R-parity can be expressed in the spin, baryon and lepton quantum numbers. The lepton doublet has lepton number $+1$, while the anti-electron has -1; baryons, being made up of three quarks have baryon number $+1$, giving the individual quarks $+1/3$, while anti quarks have $-1/3$. R-parity is then defined as

$$R_p = (-1)^{3(B-L)+2s} \,. \tag{2.8}$$

A single subsection can never do justice to the rich phenomenology of supersymmetry and the MSSM. See for instance [14] for a more complete picture.

2.1.3 Dirac neutrinos

The most straightforward way to include neutrino masses is to allow the existence of righthanded neutrinos. Even if they are not observed themselves, their existence is motivated by the fact that they now allow the neutrinos that we do know to get a mass. This mass is of the same type as for the quarks and charged leptons and arises from the Yukawa interactions

$$\mathcal{L}_{\nu_D\text{-mass}} = y_\nu \begin{pmatrix} \bar{L}^\nu_L & \bar{L}^e_L \end{pmatrix} \begin{pmatrix} H^0_u \\ H^-_u \end{pmatrix} \nu_R + \text{h.c.} \tag{2.9}$$

If neutrinos get a mass term according to this mechanism, they are called Dirac neutrinos. Dirac particles are not identical to their antiparticles, for which all charges are reversed. We see that the righthanded neutrino can *a priori* be a non-Dirac (or Majorana) particle as it does not seem to have any charges.

The righthanded neutrino might have a different type of charge than the ones mentioned in table 2.2 though. A candidate charge is lepton number that was introduced above. The Standard Model seems to respect lepton number (and baryon number as well) as accidental symmetries, but we might promote it to a symmetry that we demand to be explicitly conserved. Indeed equation (2.9) respects lepton number as well, as opposed to the alternatives we will see in the next sections[3].

Just like the other fermions, below the EWSB scale, neutrinos get an effective mass as in equation 2.2 and righthanded and lefthanded components have the same mass, given by $y_\nu v_{H_u}/\sqrt{2}$. The dimensionless parameters y_ν have very small values: 10^{-12} to 10^{-15} depending on the exact neutrino masses. According to the logic of section 1.3, one might wonder whether there is a reason for this 'unnaturally small' value.

In this scenario, the universe is filled with extra light degrees of freedom from the otherwise unobservable righthanded neutrinos. If precision cosmological observations might measure these, this will credit the scenario. If there are experiments that observe lepton number violation, for instance in neutrinoless double beta decay, the scenario is discredited.

[2] As all multiplets contain lefthanded fermions, the subscript L can be dropped to prevent cluttered notation.

[3] Actually, there is a rare, non-perturbative process in the Standard Model, called sphaleron interactions [15, 16]. In these interactions nine quarks can be converted to three antileptons and both baryon number and lepton number are violated. The difference $B - L$ is still conserved and this is thus a better candidate for an exact symmetry than L itself. Assigning a lepton number to the righthanded neutrino automatically also gives it a $B - L$ charge.

2.1.4 Majorana neutrinos

Fermions that are their own anti particles are called Majorana fermions. The quarks and charged leptons of the Standard Model clearly are not Majorana particles, as they have a charge that is the opposite for the anti particles. Below the electroweak scale, (lefthanded) neutrinos are singlets under the residual Standard Model group, so they are indeed a candidate to be Majorana particles. For Majorana fermions, a second type of mass term is allowed[4].

$$\mathcal{L}_{\nu_M\text{-mass}} = \frac{1}{2} m_\nu \bar{\nu}_L (\nu_L)^c + \text{h.c.} \tag{2.10}$$

Because the charge conjugate of the lefthanded neutrino is itself righthanded, the explicit addition of a righthanded neutrino is not needed. Above the EWSB scale, lefthanded neutrinos are part of the lepton doublet, that is in a non-trivial representation of the electroweak group and can therefore not be a Majorana spinor. In the remainder of this section, we give four mechanisms that reproduce equation (2.10) below the electroweak scale. One of these uses an effective dimension-5 operator; the other three are versions of the so-called seesaw mechanism.

2.1.5 The Weinberg operator

The fields $\bar{\nu}_L$ and $(\nu_L)^c$ that appear in equation (2.10) are singlets of the residual gauge group after electroweak symmetry breaking. Above this scale, we can form Standard Model singlets from their counterparts $\bar{L}_L$ and $(L_L)^c$ by multiplying these by H_u. The so-called Weinberg operator can now provide an effective Majorana mass for neutrinos.

$$\mathcal{L}_{\nu_M\text{-eff}} = \frac{f_\nu}{M_X} \left[\begin{pmatrix} \bar{L}_L^\nu & \bar{L}_L^e \end{pmatrix} \begin{pmatrix} H_u^0 \\ H_u^- \end{pmatrix} \right] \left[\begin{pmatrix} H_u^0 & H_u^- \end{pmatrix} \begin{pmatrix} (L_L^\nu)^c \\ (L_L^e)^c \end{pmatrix} \right] . \tag{2.11}$$

Here, M_X is a – presumably large – mass scale that appears because of the fact that this operator is non-renormalizable. After the Higgs field gets its vev, a neutrino mass is generated.

$$m_\nu = \frac{f_\nu}{2} \frac{(v_{H_u})^2}{M_X} . \tag{2.12}$$

Typically, M_X is much larger than the Higgs vev. In many models it is as high as the Grand Unified scale of section 1.3.3. This implies that neutrino masses are much below the electroweak scale for 'natural' values of the dimensionless parameter f_ν. This might explain why the neutrinos are much lighter than the quarks and charged leptons as shown in figure 1.16.

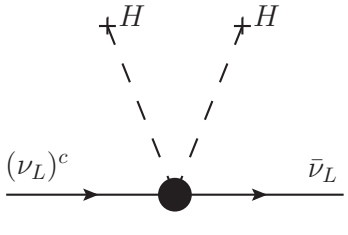

Figure 2.4: *The effective dimension 5 operator to generate a Majorana neutrino mass.*

The Weinberg operator is schematically given in figure 2.4. The 'blob' symbolizes the unknown physics behind the dimension-5 coupling. There are two ways to dissolve the blob using only 'normal' dimension-3 and -4 operators. These are given in figure 2.5.

[4]Some authors choose to define m_ν via the Hermitian conjugate of the main term in (2.10), i.e. $m_\nu \leftrightarrow {m_\nu}^*$. As the phase of m_ν is not observable, this is not a problem; all observables are the same in both conventions.

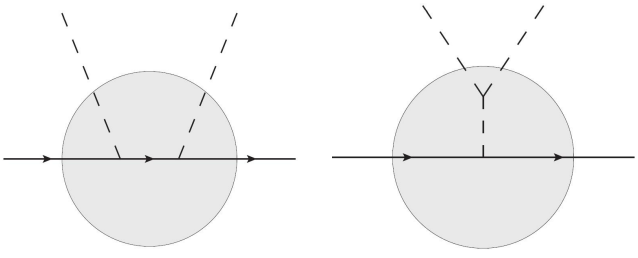

Figure 2.5: *The two ways to dissolve the effective Weinberg operator of figure 2.4*

Figure 2.5 contains intermediate particles: a fermion in the figure on the left and a boson in the figure on the right. These particles are assumed to be very heavy. In fact, the heavier the new particle is, the lighter is the lefthanded neutrino, just as on a seesaw in a children's playground: the higher one kid, the lower the other.

In all of the vertices of figure 2.5 two $SU(2)$ doublets meet. According to the group theory rule $2 \times 2 = 1 + 3$, the intermediate fermion or boson should thus be a singlet or a triplet. This can be used to classify the different seesaw mechanisms. An $SU(2)$-singlet fermion gives rise to the so-called type-I seesaw; an $SU(2)$-triplet boson to the seesaw of type-II and an $SU(2)$-triplet fermion to the type-III seesaw. Having an intermediate $SU(2)$-singlet boson is no option as can be seen from the right figure in 2.5. This would basically 'add nothing' to the fermion flow.

2.1.6 Type-I Seesaw

We first study the type-I seesaw, in which an intermediate $SU(2)$-singlet fermion appears in the diagram on the left of figure 2.5. The hypercharge of the field is calculated to be 0, giving it exactly the quantum numbers of the righthanded neutrino. The couplings between the lefthanded neutrino, the Higgs field and the righthanded neutrino are thus simply the Yukawa couplings of equation (2.9).

In section 2.1.3 we noticed that the righthanded neutrino might well be a Majorana particle, unless new exactly conserved charges like lepton number forbid this. If the righthanded neutrino is indeed a Majorana particle, a Majorana mass term analogous to equation (2.10) is also allowed. The mass might be very large as it does not have to be generated at the electroweak scale.

The (lefthanded) neutrino mass can be estimated from the diagram in figure 2.6. The two Yukawa interactions give a factor $\frac{1}{2}(y_\nu v_{H_2})^2$, while the propagator gives a factor $i/(\not{p} - M_M)$, that for low momenta can be approximated by $(-i)/M_M$, with M_M the righthanded neutrino Majorana mass.

$$m_\nu = \frac{{y_\nu}^2}{2} \frac{(v_{H_u})^2}{M_M} \,. \tag{2.13}$$

This is exactly of the form (2.12) if the high energy scale M_X and the Majorana mass scale M_M are related according to $M_X/f_\nu = M_M/y_\nu^2$.

The light neutrino mass of equation (2.13) can also be obtained from a more formal analysis. The total neutrino mass Lagrangian reads

$$\mathcal{L}_{\text{type}-\text{I}} = y_\nu \begin{pmatrix} \bar{L}_L^\nu \\ \bar{L}_L^e \end{pmatrix} \cdot \begin{pmatrix} H_u^0 \\ H_u^- \end{pmatrix} \nu_R + \frac{1}{2} M_M \overline{\nu_R} (\nu_R)^c + \text{h.c.} \tag{2.14}$$

After the Higgs fields obtain their vevs, this becomes

$$\begin{aligned} \mathcal{L}_{\mathcal{D}+\mathcal{M}} =& \frac{1}{2} m_D \overline{\nu_L} \nu_R + \frac{1}{2} m_D \overline{(\nu_R)^c} (\nu_L)^c + \frac{1}{2} M_M \overline{(\nu_R)^c} \nu_R + \text{h.c.} \\ =& \frac{1}{2} \begin{pmatrix} \overline{\nu_L} & \overline{(\nu_R)^c} \end{pmatrix} \begin{pmatrix} 0 & m_D \\ m_D & M_M \end{pmatrix} \begin{pmatrix} (\nu_L)^c \\ \nu_R \end{pmatrix} + \text{h.c.} \end{aligned} \tag{2.15}$$

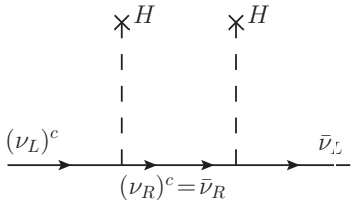

Figure 2.6: *The type-I seesaw.*

Here we used the spinor identity $\overline{\nu_L}\nu_R = \overline{(\nu_R)^c}(\nu_L)^c$. In the second line, we switched to a matrix notation. Finding the masses of the light and heavy neutrinos corresponds to finding the eigenvalues of this matrix.

$$m_{N,\,\nu} = \frac{M_M \pm \sqrt{1 + 4\frac{(m_D)^2}{M_M}}}{2} \simeq \begin{cases} M_M, & \text{For the heavy state } N. \\ -\frac{(m_D)^2}{M_M}, & \text{For the light state } \nu. \end{cases} \tag{2.16}$$

The last approximation is valid under the assumption that $M_M \gg m_D$ for reasons that are given above. The eigenstates ν and N of the mass matrix in (2.15) can be given in terms of the original states $(\nu_L)^c$ and ν_R

$$\begin{array}{lllll} \nu & \propto & (\nu_L)^c & + \frac{m_D}{M_M} & \nu_R\,, \\ N & \propto \frac{m_D}{M_M} & (\nu_L)^c & + & \nu_R\,. \end{array} \tag{2.17}$$

We see that the light neutrino is almost entirely the (conjugate of) the old lefthanded neutrino, i.e. the neutrino that was part of the lepton doublet.

2.1.7 Type-II Seesaw

Instead of fermionic, the messenger can also be bosonic. In that case, the two Higgses first 'fuse' to the new boson; this boson then couples to the fermion flow. The two Higgses are doublets of $SU(2)_L$, so the new boson can a priori be a singlet or a triplet and the hypercharge should be +1. Only a triplet can generate a neutrino-neutrino coupling. This mechanism is known as the type-II seesaw and depicted in figure 2.7.

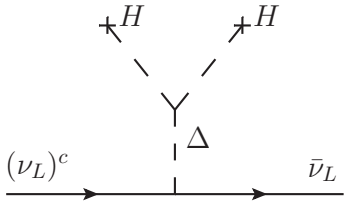

Figure 2.7: *The type-II seesaw.*

The bosonic triplet can be written as $\Delta = \begin{pmatrix} \Delta^{++}, & \Delta^{+}, & \Delta^{0} \end{pmatrix}^T$. It gives rise to a mass term when the third (electrically neutral) component gets a vacuum expectation value v_Δ

$$\mathcal{L}_{II} = g_\nu\, \bar{\nu}_L\, (\nu_L)^c\, v_\Delta\,. \tag{2.18}$$

Neutrino masses are very small if the vev of Δ is very small. This is indeed plausible as can be seen from the combined potential of the doublet and triplet Higgs fields. We show the analysis for the

case of the Standard Model with one doublet Higgs (so $H_u = i\sigma_2 H_d^*$ in equation (2.3)); the extension to multiple Higgs doublet models is straightforward.

$$V = V(H) + {M_T}^2 \Delta^\dagger \Delta + (\alpha H H \Delta + \alpha^* H^\dagger H^\dagger \Delta^\dagger) + ... \tag{2.19}$$

The first term is the normal Higgs potential $V(H) = \mu^2 H^\dagger H + \lambda (H^\dagger H)^2$; the next term is a mass term for the triplet Higgs and the last term is a cubic interaction between the doublet and triplet Higgses. Note that α is here a dimensionful parameter. The ellipsis contains quartic interaction terms with the triplet Higgs, like $H^\dagger H \Delta^\dagger \Delta$ or $(\Delta^\dagger \Delta)^2$, that are not relevant here, as their contribution is strongly suppressed with respect to those given in (2.19). If the doublet Higgs is sufficiently lighter than the triplet Higgs, the doublet obtains its vev $v_H = -\mu^2/2\lambda$ in the ordinary way. In terms of this vev and the one of the triplet, the potential now reads

$$V = V_0 + {M_T}^2 v_\Delta v_\Delta^* + \alpha \, {v_H}^2 v_\Delta + \alpha^* (v_H^*)^2 {v_\Delta}^* \, . \tag{2.20}$$

Demanding the first derivative with respect to v_Δ to be zero gives

$$\frac{\partial V}{\partial v_\Delta} = 0 \Rightarrow v_\Delta^* = (-)\alpha \frac{{v_H}^2}{{M_T}^2} \, . \tag{2.21}$$

This equation justifies the use of the word seesaw. The higher the scale of the triplet Higgs (or rather the presumably comparable scale of α and M_T), the lower the scale of v_Δ and hence the lighter the neutrinos. Indeed in many Grand Unified Theories, there is the relation

$$\alpha \simeq M_T \simeq M_R \, . \tag{2.22}$$

In that case, both the type-I and II seesaw predict neutrino masses of order ${v_H}^2/M_R$ and an analysis of neutrino masses should take into account both types of seesaw. We will see an example in the model of chapter 4.

2.1.8 Type-III Seesaw

Lastly, the intermediate particle can be a fermionic triplet that flows in the same channel as the fermionic singlet of the type-I seesaw. This type-III seesaw is sketched in figure 2.8.

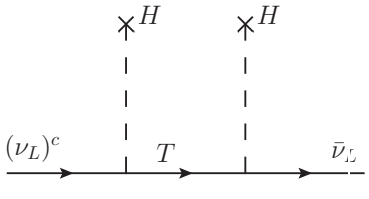

Figure 2.8: *The type-III seesaw. T denotes the fermionic triplet messenger.*

The seesaws of type-I, II and III are the only possibilities to generate neutrino masses with only renormalisable operators and only one intermediate messenger. Many suggestions exist in the literature of mechanisms that need more than one intermediate particle. They are known as the double seesaw, inverse seesaw, etc. See for instance [17] for a detailed discussion.

2.2 The three family Standard Model

In the previous section, we ignored the fact that there are three generations of quarks and leptons. In this section, we correct for this. We discuss the quarks sector first, then the lepton sector. The

inclusion of three families basically amounts to adding generation labels to the fields in the mass Lagrangian (2.3): $Q_L \to Q_{Li}$; $u_R \to u_{Rj}$ and $d_R \to d_{Rj}$. Obviously, $i, j = 1, 2, 3$. To prepare the supersymmetric model of chapter 4 (where H_u and H_d are unrelated) and the models of chapters 5 (where there are three copies of H_d in the triplet representation of a family symmetry group), we also allow the Higgs fields to come in several copies: $H_d \to H_a^d$ and $H_u \to H_b^u$, where a and b run from 1 to respectively n_d and n_u. We denote their vevs as $v_a^d e^{i\omega_a}$ and $v_b^u e^{i\omega_b}$, where the phases indicate that the vevs can be complex. With three families, the old coupling constants y_u and y_d now become matrices in generation space and in case of multiple Higgs fields even a vector of matrices.

2.2.1 Quark masses

The quark part of equation (2.3) becomes[5]

$$\mathcal{L}_{\text{Q mass}} = Y^u_{ijb} \bar{Q}_{Li} H^u_b u_{Rj} + Y^d_{ija} \bar{Q}_{Li} H^d_a d_{Rj} + \text{h.c.} \tag{2.23}$$

The crucial observation is that the fields here are given in the interaction basis and they do not correspond to mass eigenstates. If all Higgs fields obtain their vacuum expectation values, the Lagrangian contains mass terms and fermion-Higgs interactions.

$$\mathcal{L}_{\text{Q mass}} = (M^u)_{ij} \bar{u}_{Li} u_{Rj} + (M^d)_{ij} \bar{d}_{Li} d_{Rj} + \text{h.c.} \tag{2.24}$$

$$\begin{aligned} \mathcal{L}_{\bar{f}fH} =& \frac{Y^u_{ijb}}{\sqrt{2}} \left(\bar{u}_{Li}\, h_b^{u0}\, u_{Rj} + \bar{d}_{Li}\, h_b^{u-}\, u_{Rj} \right) + \\ & \frac{Y^d_{ija}}{\sqrt{2}} \left(\bar{u}_{Li}\, h_a^{d+}\, d_{Rj} + \bar{d}_{Li}\, h_a^{d0}\, d_{Rj} \right) + \text{h.c.} \end{aligned} \tag{2.25}$$

The mass matrices in the first Lagrangian are given by the expressions below. It is important that these are not diagonal in flavour space.

$$(M^u)_{ij} = \sum_b Y^u_{ijb} \frac{v_b^u e^{i\omega_b}}{\sqrt{2}} \,, \qquad (M^d)_{ij} = \sum_a Y^d_{ija} \frac{v_a^d e^{i\omega_a}}{\sqrt{2}} \,. \tag{2.26}$$

The same holds for the mass matrices of the Higgses. We have already seen this in the section about the one-family Standard Model, where for instance the neutral Goldstone boson can be a mixture of A_u and A_d.

A basis transformation related the weak interaction basis to a basis where the mass matrices are diagonal. To distinguish the mass basis, we put a hat on relevant fields and operators and use the letters $r, s, \ldots$ for the fermion family indices and $\alpha, \beta, \ldots$ for the Higgs copy indices. We focus on the mass terms first, leaving the diagonalization of the Higgs mass matrices to section 2.2.5.

The fermion fields in the mass basis are defined as

$$\begin{aligned} u_{Ri} &= V^u_{Rir} \hat{u}_{Rr}, \quad u_{Li} = V^u_{Lir} \hat{u}_{Lr} \,, \\ d_{Ri} &= V^d_{Rir} \hat{d}_{Rr}, \quad d_{Li} = V^d_{Lir} \hat{d}_{Lr} \,. \end{aligned} \tag{2.27}$$

Here $V^{u,d}_{L,R}$ are unitary matrices such that the mass matrices in the mass basis are diagonal

$$\begin{aligned} \hat{M}^u_{rs} &= (V^u_L)^\dagger{}_{ri}\, M^u_{ij}\, V^u_{RLjs} = \text{diag}(m_u, m_c, m_t) \,. \\ \hat{M}^d_{rs} &= (V^d_L)^\dagger{}_{ri}\, M^d_{ij}\, V^d_{Rjs} = \text{diag}(m_d, m_s, m_b) \,. \end{aligned} \tag{2.28}$$

For practical purposes, V^u_L (V^u_R) can be calculated as the matrix that has the normalized eigenvectors of $M^u M^{u\dagger}$ ($M^{u\dagger} M^u$) in its columns and idem in the down sector.

[5] Again, some authors choose to define the Yukawa couplings by the Hermitian conjugates of the terms in (2.23). Some formulas, such as those directly below equation (2.28) change, but all observables are the same.

The values on the diagonal of $\hat{M}^u$ and $\hat{M}^d$ are the quark masses. Experimentally, these are given by [6]

$$\begin{aligned} m_u &= 1.7 - 3.3\text{MeV}, & m_c &= 1.27^{+0.07}_{-0.09}\text{GeV}, & m_t &= 172.0 \pm 0.9 \pm 0.3\text{GeV}, \\ m_d &= 4.1 - 5.8\text{MeV}, & m_s &= 101^{+29}_{-21}\text{MeV}, & m_b &= 4.19^{+0.18}_{-0.06}\text{GeV}. \end{aligned} \tag{2.29}$$

The large uncertainties in the light (u, d, s) quarks is due to the fact that quarks only exist in hadrons and that most of the mass of a hadron is not in the constituent quarks, but due to QCD effects. It was mentioned in section 1.4.1 that quark masses vary with the energy they are observed at. The masses in (2.29) are evaluated at 2 GeV using the $\overline{\text{MS}}$ scheme for the u, d and s quark; the c and b mass are the running masses at the mass scale itself, again using the $\overline{\text{MS}}$ scheme and the top mass is from direct observations of top events.

2.2.2 The CKM matrix

The transformation to the mass basis implies that the weak interaction with the W boson is no longer diagonal. The coupling of the quarks in their mass basis to the W boson is governed by the famous Cabibbo-Kobayashi-Maskawa (CKM) matrix.

$$\begin{aligned} \mathcal{L}_{CC} =& \bar{u}_{Li}\gamma^\mu d_{Li} W^+_\mu + \text{h.c.} \\ =& \bar{\hat{u}}_{Lr}\gamma^\mu (V_{\text{CKM}})_{rs} \hat{d}_{Ls} W^+_\mu + \text{h.c.} \qquad V_{\text{CKM}} = (V^u_L)^\dagger V^d_L. \end{aligned} \tag{2.30}$$

The CKM matrix is the product of two unitary matrices, $(V^u_L)^\dagger$ and V^d_L and is as such unitary itself. A general 3×3 unitary matrix has nine real parameters. However, not all of these are observable, as some phases can be absorbed in the quark fields. All quarks can absorb a phase, except for one global phase. This removes five phases, leaving the CKM matrix with four real parameters. Three of these, θ^q_{12}, θ^q_{13} and θ^q_{23}, are mixing angles that control the mixing between the particles of two of the three generations and one, δ^q_{CP}, is a complex phase that gives rise to CP violation. It was this counting and the realization that CP violation in the quark sector can only occur in case of at least three generations that earned Makoto Kobayashi and Toshihide Maskawa [18] the Nobel Prize of 2008.

In this section, we discuss two parametrizations of the CKM matrix. The first one is in terms of the aforementioned three angles and one phase, the second in terms of the so-called Wolfenstein parameters. The Wolfenstein parametrization takes into account that the CKM matrix elements respect a hierarchy in which some of the terms are much larger than others.

In the standard parametrization [19], the CKM matrix is expressed as

$$\begin{aligned} V_{\text{CKM}} &= \begin{pmatrix} V_{ud} & V_{us} & V_{ub} \\ V_{cd} & V_{cs} & V_{cb} \\ V_{td} & V_{ts} & V_{tb} \end{pmatrix} = \begin{pmatrix} 1 & 0 & 0 \\ 0 & c_{23} & s_{23} \\ 0 & -s_{23} & c_{23} \end{pmatrix} \cdot \begin{pmatrix} c_{13} & 0 & s_{13}e^{-i\delta^q_{\text{CP}}} \\ 0 & 1 & 0 \\ -s_{13}e^{i\delta^q_{\text{CP}}} & 0 & c_{13} \end{pmatrix} \cdot \begin{pmatrix} c_{12} & s_{12} & 0 \\ -s_{12} & c_{12} & 0 \\ 0 & 0 & 1 \end{pmatrix} \\ &= \begin{pmatrix} c_{12}c_{13} & s_{12}c_{13} & s_{13}e^{-i\delta^q_{\text{CP}}} \\ -s_{12}c_{23} - c_{12}s_{13}s_{23}e^{i\delta^q_{\text{CP}}} & c_{12}c_{23} - s_{12}s_{13}s_{23}e^{i\delta^q_{\text{CP}}} & c_{13}s_{23} \\ s_{12}s_{23} - c_{12}s_{13}c_{23}e^{i\delta^q_{\text{CP}}} & -c_{12}s_{23} - s_{12}s_{13}c_{23}e^{i\delta^q_{\text{CP}}} & c_{13}c_{23} \end{pmatrix}. \end{aligned} \tag{2.31}$$

Here s_{ij} and c_{ij} are respectively the sine and the cosine of the mixing angles θ^q_{ij}. These three angles can be recovered from (2.31) by the following expressions

$$\sin\theta^q_{13} = |(V_{\text{CKM}})_{13}|\,, \quad \tan\theta^q_{12} = \frac{|(V_{\text{CKM}})_{12}|}{|(V_{\text{CKM}})_{11}|}\,, \quad \tan\theta^q_{23} = \frac{|(V_{\text{CKM}})_{23}|}{|(V_{\text{CKM}})_{33}|}\,. \tag{2.32}$$

The CP violating phase δ^q_{CP} can be recovered from the argument of the (1 3)-element of the CKM matrix. In practical calculations however, it is not always directly possible to eliminate the phases as

described above and arrive at the parametrization (2.31). In that case, $\delta^q_{\rm CP}$ can be calculated via

$$\delta^q_{\rm CP} = -\arg\left(\frac{\frac{(V_{\rm CKM})^*_{11}(V_{\rm CKM})_{13}(V_{\rm CKM})_{31}(V_{\rm CKM})^*_{33}}{c_{12}c^2_{13}s_{13}c_{23}} + c_{12}s_{13}c_{23}}{s_{12}s_{23}} \right) . \tag{2.33}$$

The mixing angles and the CP-violating phase are input to calculate the Jarlskog invariant of CP-violation [20]

$$J_{\rm CP} = {\rm Im}\Big[V_{ij}V_{ji}V^*_{ii}V^*_{jj}\Big] = c_{12}\ c^2_{13}\ c_{23}\ s_{12}\ s_{13}\ s_{23}\ \sin\delta^q_{\rm CP}\ . \tag{2.34}$$

In the second term ij = 12, 13 or 23 and no summation is assumed.

The experimental determinations of the values of the absolute values of the elements of the CKM matrix are [6]

$$|V_{\rm CKM}| = \begin{pmatrix} 0.9742 \pm 0.00015 & 0.2253 \pm 0.0007 & 0.00347^{+0.00016}_{-0.00012} \\ 0.2252 \pm 0.0007 & 0.97345^{+0.00015}_{-0.00016} & 0.0410^{+0.0011}_{-0.0007} \\ 0.00862^{+0.00026}_{-0.00020} & 0.0403^{+0.0011}_{-0.0007} & 0.999152^{+0.000030}_{-0.000045} \end{pmatrix} . \tag{2.35}$$

This is calculated under the assumption that the CKM matrix is unitary (this is theoretically well motivated as described above) and that there are no more than three generations. The direct constraint on for instance the (3 3)-element is much weaker: $|V_{tb}| = 0.88 \pm 0.07$.

The angles that correspond to the data in (2.35) and the CP phase that can be calculated separately are

$$\theta^q_{12} = 13.0^\circ, \quad \theta^q_{13} = 0.199^\circ, \quad \theta^q_{23} = 2.35^\circ, \quad \delta^q_{\rm CP} = 68.9^\circ. \tag{2.36}$$

These data support the claim made in section 1.4.2: the CKM matrix is almost diagonal. Although the first mass eigenstate is not exactly the first interaction eigenstate, the difference is not large, etc. Only the mixing between the first and the second mass eigenstates is of medium order, with the mixing parameter θ^q_{12} equal to 13.0°, while the other two mixing angles are tiny. This explains that there is only a small sliver of red respectively blue in the first two circles of figure 1.17 and almost no yellow.

The standard parametrization uses θ^q_{12}, θ^q_{13}, θ^q_{23} and $\delta^q_{\rm CP}$ to parameterize the CKM-matrix. Some of these parameters are very small. The Wolfenstein parametrization [21] is an alternative parametrization, in which all parameters are between 0.1 and 1. The first parameter λ is $\sin\theta^q_{12} \approx 0.23$. This is slightly smaller than 1 and allows a power expansion of the CKM matrix in powers of λ. To good accuracy the (1 2)-element of the CKM matrix is equal to λ, since $\cos\theta^q_{13} \approx 1$. The (2 3)-element is more or less equal to λ^2; we define the deviation A via $\sin\theta^q_{23} = A\lambda^2$. The (1 3)-element of the CKM matrix is of order λ^3. The real and imaginary part ρ and η of the coefficient are defined as $\sin\theta^q_{13}\ e^{i\delta^q_{\rm CP}} = A\lambda^3(\rho + i\eta)$. This gives the CKM matrix to third order in λ

$$V_{\rm CKM} = \begin{pmatrix} 1-\lambda^2/2 & \lambda & A\lambda^3(\bar\rho - i\bar\eta) \\ -\lambda & 1-\lambda^2/2 & A\lambda^2 \\ A\lambda^3(1-\rho-i\eta) & -A\lambda^2 & 1 \end{pmatrix} + \mathcal{O}(\lambda^4). \tag{2.37}$$

The Wolfenstein parameters are given by[6]

$$\lambda = 0.2246 \pm 0.0011, \quad A = 0.832 \pm 0.017, \quad \bar\rho = 0.130 \pm 0.018, \quad \bar\eta = 0.341 \pm 0.013. \tag{2.38}$$

2.2.3 Lepton masses

In sections 2.1.3 and 2.1.4 the Dirac or Majorana nature of neutrinos was discussed. If neutrinos are Dirac particles, the theory of lepton masses in three generations is an exact copy of the theory

[6]For calculations to higher order in λ two parameters $\bar\rho$ and $\bar\eta$ are preferred over ρ and η; these are defined as

$$\sin\theta^q_{13}\ e^{i\delta^q_{\rm CP}} = A\lambda^3(\rho + i\eta) = \frac{A\lambda^3(\bar\rho + i\bar\eta)\sqrt{1 - A^2\lambda^4}}{\sqrt{1-\lambda^2}[1 - A^2\lambda^4(\bar\rho + i\bar\eta)]} .$$

of quarks. The lepton analogue to the CKM matrix, often called the Pontecorvo-Maki-Nakagawa-Sakata (PMNS) matrix, can be parameterized in the same way as the CKM matrix in (2.31). There are small, but important differences if neutrinos are Majorana particles as we assume in the remainder of this section and in fact in most of this thesis.

The lepton masses below the electroweak scale are given by

$$\mathcal{L}_{\text{Lmass}} = (M^e)_{ij}\bar{e}_{Ri}e_{Lj} + (M^\nu)_{ij}\bar{\nu}_{Li}(\nu_L)^c_j + \text{h.c.} \tag{2.39}$$

The symmetric neutrino mass matrix $(M^\nu)_{ij}$ might originate from one or more of the seesaw mechanisms. In model building, the seesaws of type I and II or a combination of these are very popular. Indeed, in chapter 4 we show that in many grand unified models, both seesaws are automatically present and their contributions to the neutrino masses are comparable. In case of interplay of type I and II seesaw, the neutrino mass matrix reads

$$(M^\nu)_{ij} = -M^D_{iI}(M^R)^{-1}_{IJ}(M^D)^T_{Jj} + M^L_{ij}. \tag{2.40}$$

Here M^D is the Dirac mass matrix, given by $M^D_{iI} = \sum_a Y^\nu_{iIa}v^u_a/\sqrt{2}$; $i = 1,2,3$ is the index that counts the number of normal lefthanded neutrinos. I counts the number of right handed neutrino species. It need not run from 1 to 3, as there may be fewer or more righthanded neutrinos. M^L is the contribution of the type-II seesaw equal to $g^\nu_{ij}v_\Delta$.

The charged lepton masses are diagonalized as in equations (2.27) and (2.28)

$$e_{Ri} = V^e_{Rir}\hat{e}_{Rr}\ , \quad e_{Li} = V^e_{Lir}\hat{e}_{Lr}\ , \tag{2.41}$$

$$\hat{M}^e_{rs} = (V^e_L)^\dagger{}_{ri}M^e_{ij}V^e_{Rjs} = \text{diag}(m_e, m_\mu, m_\tau)\ . \tag{2.42}$$

The masses of the the electron, the muon and tau lepton can be measured much better than the quark masses, as they can be measured directly in detectors instead of only in hadrons. They are given by

$$\begin{aligned} m_e &= 0.510998910 \pm 0.000000013\text{MeV}\ , \\ m_\mu &= 105.658367 \pm 0.000004\text{MeV}\ , \\ m_\tau &= 1776.82 \pm 0.16\text{MeV}\ . \end{aligned} \tag{2.43}$$

The neutrinos are diagonalized via a single unitary matrix U^ν instead of two (left and right) as in the case for all Dirac particles.

$$\hat{M}^\nu_{rs} = (U^\nu)^\dagger_{ri}(M^\nu)_{ij}(U^\nu)^*_{js}\ , \tag{2.44}$$

$$\nu_L = (U_\nu)^*\hat{\nu}_L\ . \tag{2.45}$$

Neutrino masses are very hard to measure. Neutrinos rarely interact and they are almost always highly relativistic, meaning that only a tiny fraction of their energy is in the rest mass. The only direct signs for neutrino masses are from neutrino oscillations. These are not sensitive to the neutrino masses themselves, but to the differences between the squares of two of them. The results of solar neutrino oscillations (neutrinos from nuclear fusion in the center of the sun) and atmospheric neutrino oscillations (neutrinos formed when cosmic rays collide with air particles in the outer atmosphere) are given in table 2.3.

The three neutrino mass eigenstates are generically denoted as ν_1, ν_2 and ν_3. This ordering does *not* always correspond to the ordering from lightest to heaviest. The solar and atmospheric mass differences imply two gaps between the mass states, one much larger than the other. The states ν_1 and ν_2 are defined as the states separated by the solar mass gap, with ν_1 the lightest of the pair.

$$\Delta m^2_{\text{sol}} \equiv \Delta m^2_{12} \equiv m^2_2 - m^2_1\ . \tag{2.46}$$

The third neutrino ν_3 can be heavier or lighter than the solar pair; it is separated from them by the larger atmospheric gap. In the former case, the neutrino ordering is called normal, because just like with charged leptons and quarks, the gap between the third and second family is larger than the one between the first and the second one. If ν_3 is the lightest neutrino, the ordering is called inverted.

parameter	Ref. [22–24] best fit (1σ)	3σ-interval	Ref. [25–28] best fit (1σ)	3σ-interval	
$\Delta m^2_{\rm sol}\ [\times 10^{-5}{\rm eV}^2]$	$7.58^{+0.22}_{-0.26}$	$6.99 - 8.18$	$7.59^{+0.20}_{-0.18}$	$7.09 - 8.19$	
$\Delta m^2_{\rm atm}\ [\times 10^{-3}{\rm eV}^2]$	$2.35^{+0.12}_{-0.09}$	$2.06 - 2.81$	$2.50^{+0.09}_{-0.16}$	$2.14 - 2.76$	Normal hierarchy
			$2.40^{+0.08}_{-0.09}$	$2.13 - 2.67$	Inverted hierarchy

Table 2.3: *Neutrino oscillation parameters from two independent global fits [22–24] and [25–28].*

The definition of $\Delta m^2_{\rm atm}$ in terms of neutrino masses is different for the two orderings; it is a positive quantity given by the difference of the mass squared of ν_3 and of the solar doublet neutrino closest to it.

$$\Delta m^2_{\rm atm} = \begin{cases} m_3^2 - m_1^2, & \text{Normal ordering.} \\ m_2^2 - m_3^2, & \text{Inverted ordering.} \end{cases} \tag{2.47}$$

The neutrino oscillation parameters only contain information about the differences of (squares of) neutrino masses, not about the magnitude of the masses themselves. In one scenario, the lightest neutrino may be almost massless. The other masses are now given approximately by $\sqrt{\Delta m^2_{\rm sol}}$ and $\sqrt{\Delta m^2_{\rm atm}}$ (normal ordering) or both very close to $\sqrt{\Delta m^2_{\rm atm}}$ (inverted ordering). In this case, the words normal ordering and inverted ordering are often replaced by normal hierarchy and inverted hierarchy. In an other scenario, the neutrinos are relatively heavy and the differences between the neutrino masses is small compared to the masses themselves. This is called a quasi degenerate spectrum. The sum of quasi degenerate neutrino masses is constrained by cosmological data. Although the different groups do not agree on the bound [6], most report a value near 1.0 eV, requiring that the individual neutrinos have masses smaller than approximately 0.3 eV. Information on the absolute mass scale of neutrinos may also be found in the endpoint of tritium beta decay by the Katrin collaboration [29] or by one of the groups looking for neutrinoless double beta decay [30–34]. A schematic representation of the four possibilities for the neutrino hierarchy and ordering is given in figure 2.9.

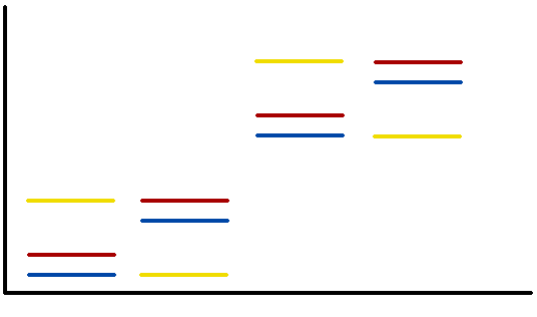

Figure 2.9: *Schematic representation of the normal hierarchy (NH), inverted hierarchy (IH) and quasi degenerate neutrinos with normal ordering (QD NO) and with inverted ordering (QD IO).*

2.2.4 The PMNS matrix

The Pontecorvo-Maki-Nakagawa-Sakata matrix parameterizes the flavour mixing in weak interactions of leptons. The PMNS matrix is defined as

$$V_{\rm PMNS} = (V_L^e)^\dagger V^\nu. \tag{2.48}$$

If neutrinos are Majorana particles, the PMNS matrix can be parameterized as

$$V_{\text{PMNS}} = \begin{pmatrix} V_{e1} & V_{e2} & V_{e3} \\ V_{\mu 1} & V_{\mu 2} & V_{\mu 3} \\ V_{\tau 1} & V_{\tau 2} & V_{\tau 3} \end{pmatrix} = R(\theta_{12}^l, \theta_{13}^l, \theta_{23}^l, \delta_{\text{CP}}^l) \times \begin{pmatrix} e^{i\varphi_1/2} & 0 & 0 \\ 0 & e^{i\varphi_2/2} & 0 \\ 0 & 0 & 1 \end{pmatrix} . \tag{2.49}$$

Here $R(\theta_{12}^l, \theta_{13}^l, \theta_{23}^l, \delta_{\text{CP}}^l)$ is the part of the mixing matrix that depends on the mixing angles and the Dirac CP-violating phase. This is identical to the parametrization of the CKM matrix in (2.31). The matrix on the right contains extra CP-violating phases, the so-called Majorana phases.

The mixing angles θ_{ij}^l and Dirac phase δ_{CP}^l can be inferred from the PMNS matrix via formulas analogous to (2.32) and (2.33). The Majorana phases can be written in terms of an auxiliary angle $\delta_e = \arg[e^{i\delta_{\text{CP}}^l}(V_{\text{PMNS}})_{13}]$ as

$$\varphi_1 = 2\,\arg[e^{i\delta_e}(V_{\text{PMNS}})_{11}^*] , \qquad \varphi_2 = 2\,\arg[e^{i\delta_e}(V_{\text{PMNS}})_{12}^*] . \tag{2.50}$$

The angles of the PMNS matrix are totally different to those of the CKM matrix. In the quark sector all angles are small to very small. In the lepton sector, the angle θ_{23}^l – the atmospheric angle – is very large. Possibly it has exactly the right value (45°) to produce maximal mixing in the (2 3) sector. The solar angle or θ_{12}^l is also very large, but significantly smaller than maximal ($45°$). The third mixing angle, θ_{13}^l is sometimes called the reactor angle. It is much smaller than the other two lepton mixing angles. Until recently, experimental data were compatible with a vanishing value of the angle [22, 23, 25, 26]. For the newest results, this is (just) below the 3σ range [24, 27, 28]. At the other end of the range, the angle can be almost as large as the Cabibbo angle, the largest angle in the CKM matrix.

In table 2.4 we give the mixing angles according to the two global fits also used in table 2.3. In the last column, we mention the values according to the tribimaximal mixing pattern, first introduced by Harrison, Perkins and Scott in 2002 and alluded to in section 1.4.2 [8]; see also [35–40]. We see that this pattern indeed fits the data rather well, although the agreement was a lot stronger with older datapoints. The fit significantly deteriorated when evidence for non-zero θ_{13} was found, first as a slight hint in global fits to accommodate slightly conflicting data, later from a dedicated search at the Tokai to Kamioka (T2K) experiment [41].

	Ref. [22–24]		Ref. [25–28]			
parameter	best fit (1σ)	3σ-interval	best fit (1σ)	3σ-interval		TBM values
$\sin^2\theta_{12}^l$	$0.312^{+0.017}_{-0.016}$	$0.265 - 0.364$	$0.312^{+0.017}_{-0.015}$	$0.27 - 0.36$		$1/3$
$\sin^2\theta_{23}^l$	$0.42^{+0.08}_{-0.03}$	$0.34 - 0.64$	$0.52^{+0.06}_{-0.07}$	$0.39 - 0.64$	NH	$1/2$
			0.52 ± 0.06	$0.39 - 0.64$	IH	
$\sin^2\theta_{13}^l$	0.025 ± 0.007	$0.005 - 0.050$	$0.013^{+0.007}_{-0.005}$	$0.001 - 0.035$	NH	0
			$0.016^{+0.008}_{-0.006}$	$0.001 - 0.039$	IH	

Table 2.4: *Neutrino oscillation parameters from two independent global fits [22–24] and [25–28] and the values of the tribimaximal mixing pattern. In the second fit, separate results for normal hierarchy (NH) and inverted hierarchy (IH) are given.*

If the neutrino mixing matrix is exactly equal to the tribimaximal Harrison-Perkins-Scott matrix, the absolute values of its elements are given by

$$|U_{\text{TBM}}| = \begin{pmatrix} \sqrt{2/3} & \sqrt{1/3} & 0 \\ \sqrt{1/6} & \sqrt{1/3} & \sqrt{1/2} \\ \sqrt{1/6} & \sqrt{1/3} & \sqrt{1/2} \end{pmatrix} . \tag{2.51}$$

All three phases of the PMNS matrix are unknown at the moment. The phase $\delta^l_{\rm CP}$ might be discovered together with the mixing angle θ_{13} in detectors near nuclear reactors [42–45]. The Majorana phases do not show up in oscillations, but might be inferred from nuclear decay processes. In particular, in neutrinoless double beta decay, a parameter $m_{\beta\beta}$ is probed that contains both phases.

$$\begin{aligned} m_{\beta\beta} &= \sum_{i=1-3} m_i (V_{\rm PMNS})^2_{ei} \\ &= m_1 \cos^2\theta^l_{12}\cos^2\theta^l_{13} e^{i\varphi_1} + m_2 \cos^2\theta^l_{13}\sin^2\theta^l_{12} e^{i\varphi_2} + m_3 \sin^2\theta^l_{13} e^{-2i\delta} \ . \end{aligned} \tag{2.52}$$

2.2.5 Diagonalizing the Higgs sector

This section discusses the diagonalization of the Higgs sector, necessary if there is more than one Higgs boson present. We will see that if more than one Higgs boson is present, generally this gives rise to flavour changing neutral currents (FCNCs) that are experimentally very tightly constrained. In chapter 5 we use these FCNCs to test certain multi-Higgs models.

We recall from equation (2.4) that the Higgs fields can be expanded around the vacuum expectation value according to

$$H^d_a = \frac{1}{\sqrt{2}} \begin{pmatrix} h^{d+}_a \\ v_a e^{i\omega_a} + \text{Re}\, h^{d0}_a + i\,\text{Im}\, h^{d0}_a \end{pmatrix} \ , \quad H^u_b = \frac{1}{\sqrt{2}} \begin{pmatrix} v_b e^{i\omega_b} + \text{Re}\, h^{u0}_b + i\,\text{Im}\, h^{u0}_b \\ h^{u-}_a \end{pmatrix} \ . \tag{2.53}$$

Now the interaction eigenstates $h_{u,d}$ mix to mass eigenstates of the Higgses ("physical Higgses") and a number of Goldstone bosons. As argued below equation (2.3), the states in H^d should thereby be compared with those in $-i\sigma_2 (H^u)^*$. Indeed in both cases, the charged states are positive.

In the neutral sector the mass eigenstates are formed according to

$$\hat{h}_\alpha = U_{\alpha a} h_a \ . \tag{2.54}$$

The vector h_a holds all neutral components of the original Higgs fields. Due to the complex conjugation alluded to above, Im h^{u0}_b carry minus signs

$$h_a = \left(\text{Re}\, h^{u0}_1 \ \cdots \ \text{Re}\, h^{u0}_{n_u},\ -\text{Im}\, h^{u0}_1 \ \cdots \ -\text{Im}\, h^{u0}_{n_u},\ \text{Re}\, h^{d0}_1 \ \cdots \ \text{Re}\, h^{d0}_{n_d},\ \text{Im}\, h^{d0}_1 \ \cdots \ \text{Im}\, h^{d0}_{n_d} \right) . \tag{2.55}$$

These $2(n_u+n_d)$ states give rise to the states in $\hat{h}_\alpha$: $2(n_u+n_d)-1$ physical Higgses and the Goldstone boson that gives a mass to the Z-boson.

$$\hat{h}_\alpha = \left(\hat{h}_1 \ \cdots \ \hat{h}_{2(n_u+n_d)-1},\ \pi^0 \right) . \tag{2.56}$$

In the charged sector we have likewise

$$\hat{h}^+_\alpha = S_{\alpha a} h^+_a \ . \tag{2.57}$$

The vector h^+_a holds the positive states from H^d and from $-i\sigma_2(H^u)^*$, while the vector $\hat{h}^+_\alpha$ contains the $n_u + n_d - 1$ positively charged scalars and the Goldstone boson that gives rise to the W^+ boson mass.

$$\begin{aligned} h^+_a &= \left((H^u)^+_1 \ \cdots h^{u+}_{n_u},\ h^{d+}_1 \ \cdots \ h^{d+}_{n_d} \right) , \\ \hat{h}^+_\alpha &= \left(\hat{h}^+_1 \ \cdots \ \hat{h}^+_{n_u+n_d-1},\ \pi^+ \right) . \end{aligned} \tag{2.58}$$

The expressions in (2.54) and (2.57) are needed to rewrite the fermion-Higgs interactions, equation (2.25) and its lepton analogue, in the mass basis. To keep the discussion clear and the formulas short, we only discuss the quark case in this section. The lepton case is completely analogous.

In the mass basis the part of the Lagrangian which includes interactions with the neutral Higgses – the first and fourth term of equation (2.25) – becomes

$$\mathcal{L}_{Y,n} = \overline{\hat{d}}_r (R^d)^\alpha_{rs} h_\alpha \frac{1+\gamma_5}{2} \hat{d}_s + \overline{\hat{u}}_r (R^u)^\alpha_{rs} h_\alpha \frac{1+\gamma_5}{2} \hat{u}_s + \text{h.c.} \tag{2.59}$$

Here we defined the coupling tensors R^d and R^u according to

$$\begin{aligned} (R^d)^\alpha_{rs} &= \left[V^{d\dagger}_{Lri} \frac{1}{\sqrt{2}} (U^{\dagger(2n_u+a)\alpha} + iU^{\dagger(2n_u+n_d+a)\alpha}) Y^d_{ija} V^d_{Rjs} \right], \\ (R^u)^\alpha_{rs} &= \left[V^{u\dagger}_{Lri} \frac{1}{\sqrt{2}} (U^{\dagger a\alpha} - iU^{\dagger(n_u+a)\alpha}) Y^u_{ija} V^u_{Rjs} \right]. \end{aligned} \tag{2.60}$$

In case the up-type and down-type Higgses are not separate, we can still use this formula with some small modifications. From the perspective of the down-type Higgs, there are no other Higgses, so $\text{Re}h^d_1$ is the first element of h_a in (2.55), so in R^d we should take $n_u = 0$. On the other hand, in R^u we should use $n_u = n_d$, because $-\text{Im}h^{u0}_1$ is the $(n_d+1)^{\text{th}}$ element of h_a.

The interactions with the charged Higgs in (2.25) become

$$\mathcal{L}_{Y,ch} = \overline{\hat{u}}_r (T^d)^\alpha_{rs} \hat{h}^+_\alpha \frac{1+\gamma_5}{2} \hat{d}_s + \overline{\hat{d}}_r (T^u)^\alpha_{rs} \hat{h}^-_\alpha \frac{1+\gamma_5}{2} \hat{u}_s + \text{h.c.} \tag{2.61}$$

The coupling tensors T are given by the following expressions that can also be used when there are no separate up-type Higgses ($n_u = 0$).

$$(T^d)^\alpha_{rs} = \left[V^{d\dagger}_{Lri} S^{\dagger(n_u+a)\alpha} Y^d_{ija} V^d_{Rjs} \right], \qquad (T^u)^\alpha_{rs} = \left[V^{u\dagger}_{Lri} S^{Ta\alpha} Y^u_{ija} V^u_{Rjs} \right]. \tag{2.62}$$

Expanding the Hermitian conjugate, the Lagrangian (2.59) can be written in terms of scalar and pseudoscalar couplings with non-chiral fermions.

$$\begin{aligned} \mathcal{L}_Y = \Big(& \overline{\hat{d}}_r \big((I^d)^\alpha_{r,s} + \gamma_5 (J^d)^\alpha_{r,s} \big) \hat{h}_\alpha \hat{d}_s + \overline{\hat{u}}_r \big((I^u)^\alpha_{r,s} + \gamma_5 (J^u)^\alpha_{r,s} \big) \hat{h}_\alpha \hat{u}_s \\ & + \overline{\hat{u}}_r \big(F^\beta_{r,s} + \gamma_5 G^\beta_{r,s} \big) \hat{h}^+_\beta \hat{d}_s + \overline{\hat{d}}_r \big(F^{\beta *}_{r,s} - \gamma_5 G^{\beta *}_{r,s} \big) \hat{h}^-_\beta \hat{u}_s \Big). \end{aligned} \tag{2.63}$$

The new coefficients are defined in the following way:

$$\begin{aligned} (I^{d,u})^\alpha_{r,s} &= \frac{1}{2} \Big((R^{d,u})^\alpha_{rs} + ((R^{d,u})^\alpha_{sr})^* \Big), \\ (J^{d,u})^\alpha_{r,s} &= \frac{1}{2} \Big((R^{d,u})^\alpha_{rs} - ((R^{d,u})^\alpha_{sr})^* \Big), \\ F^\beta_{r,s} &= \frac{1}{2} \Big((T^d)^\beta_{rs})^* - ((T^u)^\beta_{sr})^* \Big), \\ G^\beta_{r,s} &= \frac{1}{2} \Big((T^d)^\beta_{rs})^* + ((T^u)^\beta_{sr})^* \Big). \end{aligned} \tag{2.64}$$

The operators I, J, F and G determine whether flavour changing interactions are possible and what their strength is. Note that for particularly symmetric vevs of the Higgs fields, many of these operators are automatically zero, thus forbidding many flavour changing interactions or allowing them only if certain selection rules are met. We discuss some flavour changing interactions in chapter 5. The matrices I and J are important building blocks for the expressions there.

2.3 Fermion masses in family symmetric models

In section 1.4 family symmetries were introduced. We counted the number of free parameters and found that 20 or 22 of the parameters correspond to the fermion masses and mixings in respectively the neutrino-Dirac and neutrino-Majorana case. We also mentioned that some dimensionless

parameters are remarkably small. The Yukawa couplings of the first generation y_u, y_d and y_e are examples we have seen in this chapter. All of these are of the order 10^{-5}, with the electron Yukawa even smaller. If neutrinos are Dirac particles, their Yukawa couplings are even more tiny, being approximately 10^{-13}. We have seen that the type-I seesaw provided a 'solution' to this. New physics had to be introduced as the properties of the righthanded neutrino are now significantly different from those of the lefthanded one, but the parameters could all be of 'natural' magnitude. Even the new energy scale introduced was consistent with expectations.

The type-I seesaw provides a good example of some general philosophies that are also behind models with flavour symmetries. In section 1.4 we mentioned that there does not *need* to be something like flavour symmetries. In principle, the mass sector of the Standard Model can be the result of some God playing dice with 20 or 22 available parameters. From a theoretical point of view, however, alternative theories are preferable if they either manage to have much fewer parameters or if the parameters they have are less finetuned, meaning that the observed physics follows from a larger range of parameters. Ideally, a model does both.

The key ingredients of models with flavour symmetries are the matrices of Yukawa couplings Y^x_{ij}, $x \in \{u, d, e, \nu\}$ and comparable parameters in the seesaws. The models were already introduced in the text of section 1.4. In this section, we study in some more mathematical rigour how we can force the Yukawa and seesaw parameters to reproduce the physics we observe.

The best way to introduce family symmetries is probably by going through a remarkably simple, but efficient example, the Froggatt–Nielsen model [9], that we discuss in the next section. The Froggatt–Nielsen model uses an Abelian flavour symmetry. The models that the other chapters of this thesis are based on, use non-Abelian symmetries. Furthermore, these symmetries are often global and discrete. We discuss their properties at the end of this section and give an typical example, the model of Altarelli and Feruglio [10, 11], in the next section.

2.3.1 The Froggatt–Nielsen model

A first family symmetric model that we discuss is the Froggatt–Nielsen model, or rather a toy version of it. To focus only on the core issues we restrict the discussion to the charged lepton sector and ignore family mixing, i.e. we assume that only couplings diagonal in flavour space occur. Even in this simplified set up, there is a striking feature in the data, namely the huge hierarchy between the masses of the particles under consideration. The tau lepton is much heavier than the muon, which is itself again much heavier than the electron. The Froggatt–Nielsen mechanism provides an explanation to this by assigning different charges to the three fields.

The Yukawa Lagrangian for our simplified model reads

$$\mathcal{L} = y_e \begin{pmatrix} \nu_e \\ e \end{pmatrix} \cdot \begin{pmatrix} H_d^+ \\ H_d^0 \end{pmatrix} e^c + y_\mu \begin{pmatrix} \nu_\mu \\ \mu \end{pmatrix} \cdot \begin{pmatrix} H_d^+ \\ H_d^0 \end{pmatrix} \mu^c + y_\tau \begin{pmatrix} \nu_\tau \\ \tau \end{pmatrix} \cdot \begin{pmatrix} H_d^+ \\ H_d^0 \end{pmatrix} \tau^c. \tag{2.65}$$

After the Higgs fields obtains it vev, this gives a diagonal mass matrix for the three leptons.

$$\mathcal{L} = \frac{1}{\sqrt{2}} \begin{pmatrix} e & \mu & \tau \end{pmatrix} \begin{pmatrix} y_e v & & \\ & y_\mu v & \\ & & y_\tau v \end{pmatrix} \begin{pmatrix} e^c \\ \mu^c \\ \tau^c \end{pmatrix}. \tag{2.66}$$

The observation that the tau lepton, muon and electron have a huge hierarchy, now translates to $y_e \ll y_\mu \ll y_\tau$. Actual, a study of the data suggests

$$y_e : y_\mu : y_\tau \approx \lambda^5 : \lambda^2 : 1, \qquad \lambda = 0.2. \tag{2.67}$$

At this stage, λ is just a parameter with size 0.2. It appears because the data show that the logarithmic gaps between tau lepton and muon and between muon and electron are roughly 3:2 related. In chapter 4 the parameter λ is linked to the Cabibbo angle.

The central idea of Froggatt and Nielsen was that the huge mass gaps may be not a coincidence. They proposed a new $U(1)_{\rm FN}$ symmetry and to assign a new charge that differs over the three families as in table 2.5.

field	all doublets	e^c	μ^c	τ^c
FN-charge	0	5	2	0

Table 2.5: Frogatt and Nielsen's proposal for new charges for the charged leptons.

The Lagrangian (2.65) is now no longer a valid Lagrangian: no longer all terms are singlets of the full symmetry group. The first term for instance has $U(1)_{\rm FN}$-charge 0+0+5$\neq$ 0. This can be solved by introducing a new field, the so-called Froggatt–Nielsen messenger θ that has negative FN-charge as shown in table 2.6.

field	all doublets	e^c	μ^c	τ^c	θ
FN-charge	0	5	2	0	-1

Table 2.6: An update of table 2.5 that also includes the bosonic Froggatt–Nielsen messenger.

With the Froggatt–Nielsen messenger, it is possible to 'fix' the Lagrangian (2.65) by inserting appropriate powers of the messenger. This makes the first two terms in the Lagrangian non-renormalisable. We correct for this by dividing by appropriate powers of an assumedly high cut-off scale $M_{\rm FN}$. Like the three versions of the seesaw mechanism can dissolve the Weinberg operator, it is in principle possible to express the terms below in a combination of renormalisable operators, but here we stick to the effective operator approach.

$$\mathcal{L} = \frac{1}{M_{\rm FN}^5} y'_e \begin{pmatrix}\nu_e\\ e\end{pmatrix} \cdot \begin{pmatrix}H_d^+\\ H_d^0\end{pmatrix} \theta^5 e^c + \frac{1}{M_{\rm FN}^2} y'_\mu \begin{pmatrix}\nu_\mu\\ \mu\end{pmatrix} \cdot \begin{pmatrix}H_d^+\\ H_d^0\end{pmatrix} \theta^2 \mu^c + y'_\tau \begin{pmatrix}\nu_\tau\\ \tau\end{pmatrix} \cdot \begin{pmatrix}H_d^+\\ H_d^0\end{pmatrix} \tau^c \tag{2.68}$$

In the next step, the Froggatt–Nielsen-messenger θ acquires a vev just slightly below the cut-off scale $\langle\theta\rangle = \lambda\ M_{\rm FN}$, with $\lambda \approx 0.2$. For the exact mechanism of this symmetry breaking, there are several candidates. We present a supersymmetric case in which the $U(1)_{FN}$ is gauged such that θ gets its vev through a D-term. The corresponding potential is of the form

$$V_{D,\rm FN} = \frac{1}{2}(M_{\rm FI}^2 - g_{\rm FN}|\theta|^2 + ...)^2\ . \tag{2.69}$$

The gauge coupling constant of $U(1)_{\rm FN}$ is $g_{\rm FN}$ and $M_{\rm FI}^2$ denotes the contribution of the Fayet-Iliopoulos (FI) term. Dots in equation (2.69) represent e.g. terms involving the fields e^c and μ^c which are charged under $U(1)_{FN}$. These terms are however not relevant to calculate the VEV of the FN field and we omit them in the present discussion. $V_{D,FN}$ leads in the supersymmetric limit to

$$|\langle\theta\rangle|^2 = \frac{M_{\rm FI}^2}{g_{\rm FN}}\ . \tag{2.70}$$

This is identified as $\lambda^2 M_{\rm FN}^2$.

When both the Higgs and the FN-messenger have vacuum expectation values, the mass matrix is diagonal again.

$$\mathcal{L} = \frac{1}{\sqrt{2}} \begin{pmatrix}e & \mu & \tau\end{pmatrix} \begin{pmatrix} y'_e\lambda^5 v & & \\ & y'_\mu\lambda^2 v & \\ & & y'_\tau v \end{pmatrix} \begin{pmatrix}e^c\\ \mu^c\\ \tau^c.\end{pmatrix}\ . \tag{2.71}$$

The mass matrix looks a lot like the one in (2.66), but with the exception that the hierarchy is 'factored out' in the factors λ^2 and λ^5. The three remaining dimensionless couplings y'_e, y'_μ and y'_τ can all be of the same order and more or less of order 1.

Concluding, we see that the Froggatt–Nielsen mechanism can give a natural explanation for the charged lepton hierarchy and that it allows all dimensionless parameters to be of the same order. The price to be paid is the introduction of a new symmetry $U_{\rm FN}$ and of a new field θ as well as allowing non-renormalisable operators in the mass Lagrangian.

In terms of cold parameter-counting, the Froggatt–Nielsen symmetry is certainly not a progress. The addition of the symmetry did not reduce the number of free parameters of the model. We started with three parameters y_e, y_μ and y_τ and we ended with more parameters. Not only the analogous y'_e, y'_μ and y'_τ, but also the parameter λ that sets the scale of the messenger vev and some discrete parameters that give the FN-charges as shown in table 2.6. The gain that we have is not in having fewer parameters, but in 'more natural' parameters. Whether the gain in naturalness is worth the excess complexity should probably be seen as a matter of personal taste.

Ultimately, it is up to experiments to confirm or falsify the model. For confirmation, detection of the Froggatt–Nielsen messenger is necessary as well as showing that it has the correct couplings to the other particles. The theory is falsified if θ is not observed in experiments that would have the ability to detect it if it were to exist. However, close inspection of the formulas in this section show that the exact scale at which the messenger should exist, is unknown. The mass or the vev of θ does not appear in any formula, only the ratio $\langle\theta\rangle/M_{\rm FN}$. This lack of exact predictivity makes falsification of the theory very hard.

2.3.2 Global, non-Abelian, discrete symmetries

The Froggatt–Nielsen mechanism proved very apt in explaining the hierarchy between the three copies of a certain particle type, for instance the charged leptons of the previous section. In chapter 1 we discussed a second striking feature of the mass sector, the mixing patterns. Two of the three angles of the CKM matrix are very close to vanishing, with θ^l_{13} as small as 0.2°. In the PMNS matrix, at least two of the three angles are large and it is remarkable that the mixing pattern can be well described by the simple fractions $1/3$ and $1/2$ in table 2.4. Such mixing patterns cannot be reproduced with (an adaptation of) the Froggatt–Nielsen mechanism. To describe those, we need a different type of symmetries.

When selecting symmetries, one has to make three choices: local or global; Abelian or non-Abelian and continuous or discrete. It turns out that global, non-Abelian, discrete symmetries make good candidates for flavour symmetries.

To start with the first choice: local or global. When a symmetry is made local or gauged, this introduces many new degrees of freedom, e.g. in new gauge bosons. These complicate the theory and often lead to new sources of flavour changing neutral currents, which have not been observed. A global symmetry is enough for the aim we have set, constraining the Yukawa couplings.

The second choice is if the symmetry has to be Abelian or non-Abelian. Schur's lemma dictates that every complex irreducible representation of an Abelian symmetry group is one-dimensional. To be able to describe mixing patterns like the tribimaximal one, it is highly preferred to have three-dimensional representations. We conclude that candidate family symmetries should be non-Abelian. Having said that, many models have a non-Abelian symmetry as the main symmetry, but need additional Abelian symmetries as secondary or auxiliary symmetry groups. For instance, the full symmetry group of the model of chapter 4 is

$$G_f = S_4 \times Z_4 \times U(1)_{FN} \times U(1)_R \,. \tag{2.72}$$

The group S_4 is indeed non-Abelian. It ensures bimaximal mixing, a mixing pattern that is comparable to tribimaximal. The additional Z_4 is further needed to prevent some unwanted couplings and

separates the quark and the lepton sector as well as neutrinos and charged leptons within the latter. The Froggatt–Nielsen symmetry gives the quark and lepton mass hierarchies and the R-symmetry is a generalization of the better-known R-parity of supersymmetry. It separates supermultiplets with different functions (see for more details the next section).

Lastly, there is a choice between continuous and discrete symmetry groups. Although there exist many excellent models that use continuous groups, for obvious reasons mostly $SU(3)$ and $SO(3)$ (see for instance [46]), discrete groups are more popular. These have a richer choice in lower dimensional representations and the groups can be relatively small and simple (in the non-mathematical use of the word). Popular choices are the 12-element group A_4 and the 24-element S_4. For a review, see e.g. [47], that also contains a long list of references to the various models.

The prototype model of how a non-Abelian discrete symmetry can reproduce a given mixing pattern is the model of Altarelli and Feruglio [11]. We discuss this model in the next section, thereby also providing the general strategies of flavour symmetric model building.

2.4 The Altarelli–Feruglio model

2.4.1 Description of the model

The model of Altarelli and Feruglio [11] applies to the lepton sector of the Standard Model. The aim of the model is to produce a PMNS matrix that is exactly of the tribimaximal (TBM) form (2.51); until recently, this was in perfect accordance with all data and at the moment, it is still a very good approximation. To achieve TBM mixing, the lepton sector is required to be invariant not only under the symmetries of the Standard Model, but also under an additional horizontal symmetry. For this horizontal symmetry, the group A_4 is chosen. A_4 is a small discrete non-Abelian group, that is described in more detail below and in appendix 3.A. The important point here is that it has a three-dimensional representation. Actually, it is the smallest group with this property.

Much like in the Froggatt–Nielsen model, the Standard Model terms in themselves are not invariant under A_4 and the introduction of a new scalar field is required to save the symmetry. In the Froggatt–Nielsen model, this was the messenger θ; here three so-called flavons are used. Two of these flavons, φ_T and φ_S are triplets of A_4; a third ξ is a singlet.

In the next step, the flavons get a vacuum expectation value according to a specific pattern, thereby breaking the flavour symmetry. We show that the required patterns naturally appears from the minimization of a superpotential. In an earlier model [10], Altarelli and Feruglio showed that alternatively, this can be achieved in a set up with one extra dimension, where the fields are located at different branes.

The symmetry breaking by the vevs of the flavons is not complete. There are residual symmetries: Z_3 in the neutrino sector and Z_2 in the charged lepton sector. Naively, these are already the *tri* and *bi* of tribimaximal mixing. This breaking of the flavour symmetry into two different subgroups in the two lepton subsectors is the central point of flavour symmetric model building. It is now possible to write down the mass matrices of charged leptons and neutrinos. In the basis chosen by Altarelli and Feruglio, the charged lepton mass matrix is exactly diagonal. This implies $V_L^e = \mathbb{1}$, so the requirement that the PMNS matrix is equal to the tribimaximal one reduces to $V^\nu = V_{\mathrm{TBM}}$. The neutrino mass matrix is indeed of the form that generates this.

In the following, we first give some properties of the group A_4 needed to understand the Altarelli–Feruglio model. Then we give the derivation of the tribimaximal mixing as described in words above. In this part, the required form of the flavon vevs is simply assumed; it is subsequently derived. We continue with a brief discussion on higher-order corrections to the model and quark masses. We finish with a conclusion in the form of a balance.

2.4.2 Group theory of A_4

The group A_4 is a discrete group with 12 elements. Details of its group theory are given in appendix 3.A. Here we just present the information needed to understand the Altarelli–Feruglio model. A_4 has three irreducible representations, a trivial singlet 1 and two non-trivial one-dimensional representations $1'$ and $1''$ as well as a triplet representation 3. All 12 elements can be represented as products of two generating elements S and T that satisfy the following relations, thereby defining the 'presentation' of the group

$$S^2 = (ST)^3 = T^3 = 1\,. \tag{2.73}$$

The elements S and T can be represented as $(1,1)$, $(1,\omega)$, $(1,\omega^2)$ for the three one-dimensional representations. Here $\omega = e^{2\pi i/3}$ is a cube root of unity. In the three dimensional representation, we have

$$S = \frac{1}{3}\begin{pmatrix} -1 & 2 & 2 \\ 2 & -1 & 2 \\ 2 & 2 & -1 \end{pmatrix}\,; \quad T = \begin{pmatrix} 1 & 0 & 0 \\ 0 & \omega & 0 \\ 0 & 0 & \omega^2 \end{pmatrix}\,. \tag{2.74}$$

It can easily be checked that for all representations, the requirements (2.73) are met. However, only in the three-dimensional case, this happens in a non-trivial way for the generator S. Generating all 12 elements of A_4 is only possible with the three dimensional representations, that are therefore called faithful. Different bases than (2.74) are possible. In particular, a basis of A_4 in which the generator S is diagonal is often used. This basis and its relations to the Altarelli–Feruglio basis (2.74) are given in appendix 3.A.

The elements S and T in themselves generate the two maximal subgroups of A_4, the Abelian Z_2 and Z_3 as is clear from equation (2.73). Like in all groups, multiplication of two representations of A_4 gives again a sum of A_4 representations. The multiplication rules are given by

$$\begin{aligned} &1\times 1 = 1, \quad 1\times 1' = 1', \quad 1\times 1'' = 1'', \\ &1'\times 1' = 1'', \quad 1'\times 1'' = 1, \quad 1''\times 1'' = 1', \\ &1\times 3 = 3, \quad 1'\times 3 = 3, \quad 1''\times 3 = 3, \\ &3\times 3 = 1 + 1' + 1'' + 3 + 3. \end{aligned} \tag{2.75}$$

If α is a singlet of one of the types 1, 1′ and 1″ and $(\beta_1,\beta_2,\beta_3)$ is a triplet, the explicit form of the products on the third line is given by $(\alpha\,\beta_1,\ \alpha\,\beta_2,\ \alpha\,\beta_3)$; $(\alpha\,\beta_3,\ \alpha\,\beta_1,\ \alpha\,\beta_2)$ and $(\alpha\,\beta_2,\ \alpha\,\beta_3,\ \alpha\,\beta_1)$ respectively. The elements of the last product can be given as a function of the elements of two triplets $\alpha = (\alpha_1,\ \alpha_2,\ \alpha_3)$ and $\beta = (\beta_1,\ \beta_2,\ \beta_3)$

$$\begin{aligned} (\alpha\,\beta)_1 &= \alpha_1\beta_1 + \alpha_2\beta_3 + \alpha_3\beta_2\,; \\ (\alpha\,\beta)_{1'} &= \alpha_1\beta_2 + \alpha_2\beta_1 + \alpha_3\beta_3\,; \\ (\alpha\,\beta)_{1''} &= \alpha_1\beta_3 + \alpha_2\beta_2 + \alpha_3\beta_1\,; \\ (\alpha\,\beta)_{3;\mathrm{sym}} &= \tfrac{1}{3}(2\alpha_1\beta_1 - \alpha_2\beta_3 - \alpha_3\beta_2,\ -\alpha_1\beta_2 - \alpha_2\beta_1 + 2\alpha_3\beta_3,\ -\alpha_1\beta_3 + 2\alpha_2\beta_2 - \alpha_3\beta_1)\,; \\ (\alpha\,\beta)_{3;\mathrm{asym}} &= \tfrac{1}{2}(\alpha_2\beta_3 - \alpha_3\beta_2,\ \alpha_1\beta_2 - \alpha_2\beta_1,\ \alpha_3\beta_1 - \alpha_1\beta_3)\,. \end{aligned} \tag{2.76}$$

From the third line in (2.75), we see that the product of three triplets $(3\times 3)_3\ \times 3$ can also give a singlet. This is possible with the first product of two triplets in the symmetric or antisymmetric combination. In the next subsection, we need the singlet of the combination $(\alpha\ \alpha\ \beta)$. This selects the symmetric combination for the first product.

$$(\alpha\ \alpha\ \beta)_1 = \big((\alpha\ \alpha)_{3;\mathrm{sym}} \times \beta\big)_1 = \frac{2}{3}(\alpha_1^2\beta_1 - \alpha_2\alpha_3\beta_1,\ \alpha_3^2\beta_2 - \alpha_1\alpha_2\beta_2,\ \alpha_2^2\beta_3 - \alpha_1\alpha_3\beta_3)\,. \tag{2.77}$$

2.4.3 The model

In the AF model, the symmetry group A_4 works in the family direction. We choose to put the three copies of the lepton doublet (holding the lefthanded electron + electron neutrino; muon + muon neutrino and tau + tau neutrino) together in a triplet L of A_4. The righthanded charged leptons

(or rather their lefthanded antiparticles as explained in section 2.1.2) are not combined in a triplet; instead, they are assumed to be in the three different one dimensional representations: e^c in 1; μ^c in $1'$ and τ^c in $1''$. The Higgs fields (separate H^u and H^d because of the supersymmetric context) are family blind and thus in the trivial singlet representation.

There are three flavons: we want the triplet φ_T to couple only to the charged leptons and the triplet φ_S as well as the (trivial) singlet ξ to couple only to the neutrinos. The two triplets are indistinguishable at this moment: both are singlets of all Standard Model gauge groups and triplets of A_4, so we cannot use one of the already used symmetries to ensure this separation. Instead, a second, auxiliary, symmetry is invoked – the Abelian Z_3 in this case. The charges of all fields, as shown in table 2.7 are exactly such that all wanted couplings are guaranteed, while the unwanted couplings are forbidden.

Field	L	e^c	μ^c	τ^c	$H_{u,d}$	φ_T	φ_S	ξ
A_4	3	1	$1'$	$1''$	1	3	3	1
Z_3	ω	ω^2	ω^2	ω^2	1	1	ω	ω

Table 2.7: The A_4 and Z_3 representations of the fields in the Altarelli–Feruglio model.

The superpotential for the mass terms becomes

$$\begin{aligned}\mathcal{W} =& \frac{y_e}{\Lambda} e^c H_d(\varphi_T L)_1 + \frac{y_\mu}{\Lambda}\mu^c H_d(\varphi_T L)_{1''} + \frac{y_\tau}{\Lambda}\tau^c H_d(\varphi_T L)_{1'} + \\ & \frac{x_a}{\Lambda^2}\xi H_u H_u (LL)_1 + \frac{x_b}{\Lambda^2} H_u H_u (LL\varphi_S)_1 + ...\end{aligned} \tag{2.78}$$

Terms such as $y'_e/\Lambda\ e^c H_d(\varphi_S L)_1$ or $x'_b/\Lambda\ (LL\varphi_T)_1$ that would couple flavons to the 'wrong' sectors are indeed absent due to the extra Z_3 symmetry. We recall from equation (2.11) that the terms with two Ls give rise to a neutrino mass term, while the first three terms obviously lead to charged lepton masses. The dots at the end of equation (2.78) refer to terms suppressed by higher powers of Λ.

In [48] and [49] it was shown that models cannot reproduce maximal atmospheric mixing ($\theta^l_{23} = 45°$) if the flavour symmetry is exact. The flavour symmetry thus needs to be broken. This occurs when the flavons φ_T, φ_S and ξ develop vacuum expectation values in very specific directions in the A_4 space; the next subsection show how this follows from an analysis of their superpotential. The vev of φ_T is such that it is invariant under the T-generator of A_4 (equation 2.73). This means that terms in the Lagrangian that are dependent on φ_T (and φ_T only) will have a residual symmetry after A_4 is broken by φ_T taking its vacuum expectation value. This symmetry is the Abelian Z_3. As only the charged lepton mass terms depend on φ_T, we say that Z_3 is the residual symmetry in the charged lepton sector.

Similarly, φ_S gets a vacuum expectation value that is invariant under the S generator and the singlet ξ gets a constant vev, that does not break A_4. As a result, the neutrino sector has a residual Z_2 symmetry generated by S. Basically, the *tri* of the residual Z_3 in the charged lepton sector and the *bi* of the residual Z_2 for the neutrinos are the main ingredients of tribimaximal mixing. The explicit forms of the vacuum expectation values of the flavons are

$$\langle\varphi_T\rangle = v_T(1,\ 0,\ 0); \qquad \langle\varphi_S\rangle = v_S(1,\ 1,\ 1); \qquad \langle\xi\rangle = v_\xi. \tag{2.79}$$

The effective Lagrangian after the flavons and the Higgses obtain their vacuum expectation values is

$$\begin{aligned}\mathcal{L} =& \frac{v_d v_T}{\Lambda}(y_e e^c e + y_\mu \mu^c \mu + y_\tau \tau^c \tau) \\ & + \frac{x_a v_u^2 v_\xi}{\Lambda^2}(\nu_e\nu_e + 2\nu_\mu\nu_\tau) + \frac{x_b 2 v_u^2 v_S}{3\Lambda^2}(\nu_e\nu_e + \nu_\mu\nu_\mu + \nu_\tau\nu_\tau - \nu_e\nu_\mu - \nu_e\nu_\tau - \nu_\mu\nu_\tau) \\ & + \text{h.c.} + ...\end{aligned} \tag{2.80}$$

The charged lepton mass matrix is now diagonal, with the masses given by

$$m_e = y_e v_d \frac{v_T}{\sqrt{2}\Lambda}, \quad m_\mu = y_\mu v_d \frac{v_T}{\sqrt{2}\Lambda}, \quad m_\tau = y_\tau v_d \frac{v_T}{\sqrt{2}\Lambda}. \tag{2.81}$$

All masses are suppressed from the electroweak scale by a factor $\frac{v_T}{\Lambda}$ (and a factor $\cos\beta$ from v_d). The model so far does not explain the hierarchy in the masses, although it is possible to combine the model with the Froggatt–Nielsen model of section 2.3.1.

In the neutrino sector, the mass matrix reads

$$M_\nu = \frac{v_u^2}{\Lambda} \begin{pmatrix} a + 2b/3 & -b/3 & -b/3 \\ -b/3 & 2b/3 & a - b/3 \\ -b/3 & a - b/3 & 2b/3 \end{pmatrix}. \tag{2.82}$$

Here a and b are dimensionless parameters given by

$$a = \frac{2x_a v_\xi}{\Lambda}, \quad b = \frac{2x_b v_S}{\Lambda}. \tag{2.83}$$

The neutrino mass matrix (2.82) is diagonalized exactly by the tribimaximal mixing matrix (2.51)

$$\hat{M}_\nu = U^\dagger M_\nu U^* = \begin{pmatrix} a+b & 0 & 0 \\ 0 & a & 0 \\ 0 & 0 & -a+b \end{pmatrix}, \qquad U = \begin{pmatrix} \sqrt{2/3} & 1/\sqrt{3} & 0 \\ -1/\sqrt{6} & 1/\sqrt{3} & -1/\sqrt{2} \\ -1/\sqrt{6} & 1/\sqrt{3} & 1/\sqrt{2} \end{pmatrix}. \tag{2.84}$$

This is the main result of this section. Using a relatively limited amount of new ingredients, it is possible to exactly predict the neutrino mixing matrix.

A few comments are in order. Firstly on the ratio between the various flavon vevs and the cut-off scale. This ratio should be smaller than 1 in order to sensibly cut off the superpotential (2.78) after the given terms. A lower limit emerges from the mass of the tau lepton in equation (2.81), where the parameter y_τ should be smaller than 4π to be in the perturbative regime. If we assume that for all three flavons the vevs are of the same order of magnitude, we find

$$\frac{0.00080}{\cos\beta} \lesssim \frac{v_T}{\Lambda} \approx \frac{v_S}{\Lambda} \approx \frac{v_\xi}{\Lambda} \lesssim 1\,. \tag{2.85}$$

Secondly, not only a neutrino mixing matrix, but also a relation between the neutrino masses is found. In [10] it was shown that the atmospheric and solar mass differences can be accommodated in the normal hierarchy and that there is an extra relation between the parameter of neutrinoless double beta decay and the third neutrino mass. This makes the model testable in future neutrino experiments. Thirdly, using the atmospheric mass difference, the absolute scale of Λ itself can be limited to

$$\Lambda < 1.8 \times 10^{15}\ \text{GeV}. \tag{2.86}$$

The model described so far assumes that neutrinos are Majorana particles, but does not use one of the three seesaw mechanism to generate their masses. Instead, the effective Weinberg operator of section 2.1.5 is used. This seems reasonable, given that the couplings of fermions, Higgs fields and flavons are already effective operators due to the extra flavon insertions. Addition of a righthanded neutrino to the model is possible and a version of the model that uses the type-I seesaw can be written down, giving the same general conclusions, but differing in many details such as the relations between the neutrino masses.

2.4.4 Flavon vacuum alignment

In this subsection, we show how the flavons can obtain the vevs of equation (2.79). Note that the ordinary Higgs fields are singlets under the family symmetries and that the flavons are singlets under

the electroweak gauge group. The potentials of the Higgs fields and the flavons therefore decouple and should be studied separately. For the Higgses, this is just the superpotential of the MSSM.

In the flavon sector, we would like to build a potential for the fields φ_S, φ_T and ξ such that their minima are as in (2.79). This turns out to be possible only if new fields are introduced again, the so-called driving fields. They do not develop vevs themselves but merely help the 'normal' flavons to do so[7]. The driving fields, that we write as φ_0^S, φ_0^T and ξ_0 have the same A_4 and Z_3 charges as the fields they correspond to. To be able to have a non-trivial minimum, a second copy of the field ξ is needed as well; it is called $\tilde{\xi}$ and has exactly the same charges as ξ.

At this stage also a new symmetry is introduced. It is a continuous R-symmetry $U(1)_R$ that has the usual R-parity as a subgroup. The working of R-symmetry on superfields and supercoordinates is such that consistent terms in a superpotential should always have total R-charge 2, see e.g. [14] for more details. The R-charges in the model of Altarelli and Feruglio are given in table 2.8. It can be seen that all terms in the flavour symmetry breaking superpotential have to be linear in one of the driving fields. The Altarelli–Feruglio model does not discuss quarks, but extensions of it that do, will have the same R-charges for quarks as for leptons. In that way, baryon number violating operators that mediate proton decay are forbidden in the same way as in supersymmetric models with R-parity conservation.

Field	L	e^c	μ^c	τ^c	$H_{u,d}$	φ_T	φ_S	ξ	$\tilde{\xi}$	φ_0^T	φ_0^S	ξ_0
A_4	3	1	$1'$	$1''$	1	3	3	1	1	3	3	1
Z_3	ω	ω^2	ω^2	ω^2	1	1	ω	ω	ω	1	ω	ω
$U(1)_R$	1	1	1	1	0	0	0	0	0	2	2	2

Table 2.8: The representations of the fields in the Altarelli–Feruglio model after inclusion of the driving fields.

The requirement of invariance under A_4, Z_3 and $U(1)_R$ allows us to write down the so-called driving superpotential.

$$\begin{aligned}\mathcal{W}_d =& M(\varphi_0^T\varphi_T)_1 + g_0(\varphi_0^T\varphi_T\varphi_T)_1 + \\ & g_1(\varphi_0^S\varphi_S\varphi_S)_1 + g_2\tilde{\xi}(\varphi_0^S\varphi_S)_1 + g_3\xi_0(\varphi_S\varphi_S)_1 + g_4\xi_0\xi^2 + g_5\xi_0\xi\tilde{\xi} + g_6\xi_0\tilde{\xi}^2 + \mathcal{O}(1/\Lambda)\,.\end{aligned} \tag{2.87}$$

Note that the field that appears in the term with g_2 is $\tilde{\xi}$ and not ξ. So far, there was no difference between these two fields and we are free to define $\tilde{\xi}$ as the combination that couples to $(\varphi_0^S\varphi_S)_1$ in the superpotential.

The scalar potential follows from the superpotential, soft supersymmetry breaking terms and D-terms. Given the large scale of Λ found in equation (2.86), we assume that the masses of soft breaking are much smaller than the mass scales in w_d and we minimize the scalar potential in the supersymmetric limit, taking soft susy breaking terms into account later, for instance to select the minimum described below over the trivial minimum. In the supersymmetric limit the scalar potential reads

$$V = \sum_i \left|\frac{\partial \mathcal{W}}{\partial \phi_i}\right|^2 + \cdots \tag{2.88}$$

Requiring supersymmetry to be conserved and thus $V = 0$ requires the derivatives of the superpo-

[7]The fact that the driving superfields do not develop vevs strictly holds only in the exact supersymmetric phase, while in the broken phase they develop a vev proportional to the common soft breaking scale [50–52], usually denoted as $m_{\rm SUSY}$. This could have a relevant impact on flavour violating processes, as studied in a series of papers [53–57]

tential to all components of the driving fields to be zero. This leads to a set of seven equations.

$$\begin{aligned}
\frac{\partial \mathcal{W}_d}{\partial \varphi_{01}^T} &= M\varphi_{T1} + \frac{2g_0}{3}\Big(\varphi_{T1}^2 - \varphi_{T2}\varphi_{T3}\Big),\\
\frac{\partial \mathcal{W}_d}{\partial \varphi_{02}^T} &= M\varphi_{T3} + \frac{2g_0}{3}\Big(\varphi_{T2}^2 - \varphi_{T1}\varphi_{T3}\Big),\\
\frac{\partial \mathcal{W}_d}{\partial \varphi_{03}^T} &= M\varphi_{T2} + \frac{2g_0}{3}\Big(\varphi_{T3}^2 - \varphi_{T1}\varphi_{T2}\Big),\\
\frac{\partial \mathcal{W}_d}{\partial \varphi_{01}^S} &= g_2\tilde{\xi}\varphi_{S1} + \frac{2g_1}{3}\Big(\varphi_{S1}^2 - \varphi_{S2}\varphi_{S3}\Big),\\
\frac{\partial \mathcal{W}_d}{\partial \varphi_{02}^S} &= g_2\tilde{\xi}\varphi_{S3} + \frac{2g_1}{3}\Big(\varphi_{S2}^2 - \varphi_{S1}\varphi_{S3}\Big),\\
\frac{\partial \mathcal{W}_d}{\partial \varphi_{03}^S} &= g_2\tilde{\xi}\varphi_{S2} + \frac{2g_1}{3}\Big(\varphi_{S3}^2 - \varphi_{S1}\varphi_{S2}\Big),\\
\frac{\partial \mathcal{W}_d}{\partial \xi_0} &= g_4\xi^2 + g_5\xi\tilde{\xi} + g_6\tilde{\xi}^2 + g_3\Big(\varphi_{S1}^2 + 2\varphi_{S2}\varphi_{S3}\Big).
\end{aligned} \tag{2.89}$$

The first three and the last four equations of (2.89) can be separately solved and a non-trivial solution is given by

$$\begin{aligned}
&\varphi_T = (v_T, 0, 0), \qquad v_T = -\frac{3M}{2g},\\
&\xi = v_\xi,\\
&\tilde{\xi} = 0,\\
&\varphi_S = (v_S, v_S, v_S), \qquad v_S^2 = -\frac{g_4}{3g_3}v_\xi^2.
\end{aligned} \tag{2.90}$$

This is indeed of the form (2.79) and breaks the A_4 flavour symmetry to Z_3 and Z_2 respectively in the charged lepton and neutrino sectors.

2.4.5 Higher order corrections and quark masses

So far we have proven that it is possible to obtain the tribimaximal lepton mixing in leading order (LO) in a $1/\Lambda$ expansion. The lepton superpotential also contains next-to-leading order (NLO) terms, that is terms with one additional flavon. These slightly break the TBM prediction. The same holds for NLO terms in the driving superpotential, as these drive the vacuum expectation values of the flavons away from the values in (2.90). A third source of deviations from the predicted limit comes from the fact that the mass matrices (and thus the mixing matrices) are calculated at a very high scale, up to 1.8×10^{15} GeV according to equation (2.86). Renormalization effects between this scale and the scale where they are observed should be taken into account, although they are generally relatively small; see chapter 4 for a discussion of Yukawa coupling renormalization in a similar model.

These corrections are very welcome, as the observed neutrino mass mixing matrix is exactly of the tribimaximal type. However, as the tribimaximal pattern already fits the data rather well (certainly before the recent signal of non-zero θ_{13}^l), the deviations should be small – in particular the correction to θ_{12}^l should be tiny. We do not discuss the full NLO computation of masses and mixings in the Altarelli–Feruglio model here, but instead present the main conclusion. In order for the NLO corrections not to spoil the LO conclusions, the ratio between the vev of any of the flavons to the cut-off scale Λ should be smaller than a few percent. The upper limit of v_X/Λ in equation (2.85) becomes 0.05 instead of 1.

The aim of the Altarelli–Feruglio model is the reproduction of the lepton mixing matrix. Quarks are thus not considered in the most basic version of the model. Addition of quarks to the model is of course possible and it can be done in several ways. In the most simple extension, the quark doublet

transforms in the same way as the lepton doublet, while the anti-quarks of both types transform in the same way as the charged anti-leptons. In this case, at the leading order, the quark mixing matrix is the unit matrix. This is a reasonable approximation, given that the quark mixing angles are fairly small, but the required NLO corrections seem to be larger than those allowed in the lepton sector, which is not entirely satisfactory. We find that while the (extended) model fits the data quite well at leading order, it is hard to improve this at higher orders.

2.4.6 A balance

The original model of Altarelli and Feruglio was published in 2005. At that time, the tribimaximal mixing pattern was well-known in the literature (it was published in 2002 by Harrison, Perkins and Scott). The TBM mixing pattern was in accordance with the experimental data, although the experimental errors were still large. Neutrino oscillations have given new results in the last years. In particular, there now seems to be a signal for a θ_{13}^l angle that is relatively large. This would require a rather large correction to this angle, while such corrections are not allowed for the other two angles. Interestingly enough, a comparably large correction is needed to introduce the Cabibbo angle in the CKM matrix that is the unity at leading order. Alternative models that require the same (larger) corrections in both sectors may address this point; in chapter 4 we provide a model with this mechanism. In chapter 3, we investigate mixing patterns that give non-zero mixing patterns at the leading order.

Even if the question of NLO corrections is not answered completely satisfactory, the tribimaximal pattern is still an interesting start for modelbuilding. The Altarelli–Feruglio model can provide this mixing, but, as in the case of the Froggatt–Nielsen mechanism, it requires the introduction of a rather large number of extra fields and symmetries.

The main ingredient of the model is the horizontal symmetry A_4. It has subgroups Z_2 and Z_3 that are at the basis of the tribimaximal mixing. The introduction of the fields φ_S and φ_T seems therefore very reasonable. It is those fields that break in exactly the right directions for the TBM mixing pattern to arrive.

Tribimaximal mixing requires that the Z_2 and Z_3 residual symmetries are not only created by the flavons, but also transmitted in the right way to respectively the neutrinos and the charged leptons. Unfortunately, both φ_S and φ_T are triplets of A_4 (and singlets of the Standard Model gauge group), so a priori both of them would couple to both sectors. To prevent this, a rather *ad hoc* Z_3 symmetry is introduced. This symmetry also requires a new particle: the fourth term in equation (2.78) with two Higgs fields and two lepton doublets is invariant under the Standard Model gauge group and under A_4 with or without ξ and it needs this field only to be safe under Z_3. This chain of action-and-reaction of addition of new fields and symmetries makes the model slightly baroque and unfortunately, this will not be much better (actually quite a bit worse) in more ambitious ones, such as the model of chapter 4 that also aims at reproducing the CKM matrix and some relations between particles of different type.

The version of the Altarelli–Feruglio model described here is supersymmetric. An earlier version of the model [10] has a setting with extra dimensions. We stress that neither are fundamental elements of the model or of non-Abelian flavour models in general. In principle the questions whether flavour symmetries exist in nature and whether supersymmetry or extra dimensions are introduced – for instance to solve the hierarchy problem – should be answered separately, both from a theoretical and from an experimental point of view. The problem is that the theoretical methods developed so far only succeed in giving the right vacuum alignment for two or more flavons in settings with supersymmetry or extra dimensions. We have shown that with supersymmetry the right flavon alignment is possible, but that this is non-trivial. New driving fields had to be introduced as well as a second copy of ξ. We note that it is possible in some other models to find a supersymmetric vacuum without driving fields. The A_5 model of Feruglio and Paris [58] is an elegant example. Alternatively, one can consider models that are non-supersymmetric and do not have extra dimensions. This is discussed in chapter 5 where the role of the flavons is basically given to a multiplet of Higgs bosons.

Concluding we state that the model of Altarelli and Feruglio succeeds in reproducing the tribimaximal mixing pattern in an impressive way. The 'cost' of this is the introduction of quite a number of new symmetries and fields and from an theoretical-economical perspective, one may question whether the gained predictively is worth the price. The last words of this section have the same message as those in section 2.3.1 on the Froggatt–Nielsen mechanism. Ultimately it is up to experiments to confirm or disprove the sometimes very specific predictions of the model.

2.5 Conclusions of the chapter

In this chapter we discussed how fermion masses appear in the Standard Model (extended to include neutrino masses) and in supersymmetric variations. To focus on the different operators that appear, we first studied the case where the Standard Model has only one family. Next we allowed for three family copies of the fermionic content in accordance with observations. We found that with more than one generation, mass eigenstates and flavour eigenstates do not coincide. This gives rise to the CKM and PMNS mixing matrices.

We studied the experimentally found masses and mixing angles of the elementary fermions. The trained eye of the theoretical physicist immediately sees patterns here. We stressed that these patterns do not need to imply new physics. Even if some of the 20 or 22 free parameters of the Standard Model plus neutrinos have some unnatural values, it is perfectly consistent and describes everything that is measured. On the other hand, these patterns are compelling enough to at least justify a thorough study of different possibilities to explain them using symmetry principles.

We studied two simplified models: the Froggatt–Nielsen model, that gives an explanation for the hierarchies of the charged fermion masses and the Altarelli–Feruglio model that explains the emergence of a neutrino mixing close to the tribimaximal mixing pattern. These models are very interesting, but they leave some questions unanswered. For instance, we found no clear way to include quarks and quark mixing in the Altarelli–Feruglio model. Furthermore, we mentioned that the tribimaximal mixing pattern is not be the only phenomenologically interesting mixing pattern. In particular models that accommodate non-zero θ_{13}^l either at first order or naturally via corrections are appealing. In the following chapters we will see examples of both these approaches.

Chapter 3

Mixing patterns of finite modular groups

> The most amazing thing happened to me to me tonight. I was coming here, on the way to the lecture, and I came in through the parking lot. And you won't believe what happened. I saw a car with the licence plate ARW 357. Can you imagine? Of all the millions of licence plates in the state, what was the chance that I would see that particular one tonight? Amazing!
>
> *(attributed to) Richard Feynman*

3.1 Introduction
From bimaximal to tribimaximal to which neutrino mixing?

Slightly over a decade ago neutrino oscillations were discovered. Shortly after this observation, it was found that the PMNS neutrino mixing matrix can be characterized by two large mixing angles and one significantly smaller, possibly vanishing one. It was soon speculated that the neutrino mixing might correspond to a special pattern. Early data were in accordance with so-called bimaximal (BM) mixing [59–61] that is characterized by $\sin^2\theta^l_{23} = \sin^2\theta^l_{12} = 1/2$ and $\sin^2\theta^l_{13} = 0$.

More precise measurements of the solar angle θ^l_{12} showed that the corresponding mixing is in fact not maximal; it is currently off by approximately 6 σ. Instead, for a long time, the data were compatible with the tribimaximal (TBM) mixing pattern [8] of figure 1.18 and table 2.4. TBM mixing has $\sin^2\theta^l_{12} = 1/3$ and the other two angles identical to the bimaximal values: the mixing corresponding to the atmospheric angle θ^l_{23} is still maximal and the reactor angle θ^l_{13} is still vanishing. Both the bimaximal mixing and the tribimaximal mixing can emerge when horizontal symmetry groups are assumed along the lines of section 2.4. In particular the small discrete groups A_4 and S_4 are often used. See e.g. [47, 62] for reviews.

As mentioned in the previous chapter, recent data by the T2K collaboration gives evidence for non-zero reactor mixing angle. This signal is in accordance with earlier hints that a small but non-zero reactor angle can alleviate tensions between oscillation data extracted from KamLAND and from solar neutrinos and also in accordance with the first data of Double Chooz [63]. In table 2.4 we presented two recent independent fits of the neutrino oscillation data. In both fits, the hypothesis of zero θ_{13} is excluded by more than 3σ. The new neutrino oscillation data do not match the tribimaximal pattern anymore, at least not at the three sigma level. The detection of non-zero θ_{13} can lead to four directions in flavour-symmetry model-building space.

A first conclusion can be that the most important prediction of tribimaximal mixing, a vanishing reactor mixing angle, is not observed. The falsification of this most popular implementation of

flavour symmetries can be seen as a general argument against the use of flavour symmetries in general and a sign that one should give up on the approach. Secondly – and less negatively – one can keep the idea of flavour symmetries, but use them to build models that are less constraining in their predictions. An example is a model that provides tribimaximal mixing with a single finetuning instead of three as in the Standard Model. If this parameter is not exactly tuned this way, near-tribimaximal mixing results. The models of chapter 5 – motivated in a different way – are examples of such models.

Thirdly, one can try to reconcile the predictions with the data by allowing next-to-leading order (NLO) effects to alter the precise prediction. These corrections then modify the prediction of zero $\sin^2\theta_{13}$ and, most likely, also modify the two other mixing angles. In models where quark and neutrino mixing have a common origin, NLO corrections in the quark sector also follow. At the end of section 2.4 we found that the requirement that the solar mixing angle should have only minor corrections in order to keep fitting the data, is quite restricting. Possibly, the old bimaximal mixing pattern is a better starting point: both the solar and the reactor angle are far away from the data at first order and they require comparable corrections in order to fit the data. This was done in [64] and is further explored in chapter 4.

A fourth possibility is to assume a different mixing pattern at leading order, preferably one that has a non-zero prediction for θ_{13} already at the lowest level. In this chapter we pursue this last option. We systematically consider all mixing patterns that are generated by a class of discrete groups of which A_4 and S_4 are the first members. See e.g. for [65, 66] for other scans of candidate groups and [67] for an analysis of how groups like these can naturally occur when an $SU(3)_F$ symmetry gets broken.

The key to generate this class of groups is in (2.73) and its analogue for S_4. Both A_4 and S_4 are generated by two elements, generally called S and T that satisfy two relations that make them subgroups of the modular group Γ

$$S^2 = (ST)^3 = 1 \ . \tag{3.1}$$

The groups A_4 and S_4 are selected by additionally requiring a third relation between the generators. Both are of the form

$$T^N = 1 \ . \tag{3.2}$$

$N = 3$ corresponds to A_4 and $N = 4$ to S_4. In section 3.2 we show that the list of groups generated by generalizing this relation is infinite, but that only a finite number of these contains three dimensional irreducible representations. For all these groups G_f we investigate in section 3.3 to which lepton mixing patterns it can naturally give rise when we assume that the flavour dynamics breaks the group, but ensures residual symmetries G_e and G_ν in respectively the charged lepton and the neutrino sectors.

As expected, tribimaximal mixing and bimaximal mixing occur in this list as well as several other candidate mixing-patterns. Some of these are closer to the data than others. Four mixing patterns are particularly interesting. These are related to two groups of the type $\Delta(6n^2)$ with respectively $n = 4$ and $n = 8$ (where $n = 2$ corresponds to S_4) that give rise to four mixing patterns that are quite close to the data as shown in table 3.1. In particular the patterns `M3` and `M4` are compatible with the present data at the 2σ level. Note that this is possible only because of the prediction of non-zero θ_{13}^l. We discuss the patterns `M1` to `M4` in more detail in section 3.4. In section 3.5 we present the conclusions of the chapter.

3.2 Finite modular groups and their representations

As mentioned in the introduction, the groups A_4 and S_4 have a common presentation in terms of two generators S and T satisfying for $N = 3$ or 4

$$S^2 = (ST)^3 = 1 \quad , \qquad T^N = 1 \quad . \tag{3.3}$$

For $N = 5$ the group A_5 follows. With this group added, the list contains the proper symmetry groups of the five platonic solids, that can be grouped into three dual pairs: cube/octahedron,

group	pattern	$\sin^2\theta_{12}$	$\sin^2\theta_{23}$	$\sin^2\theta_{13}$
$\Delta(96)$	M1	$\frac{8-2\sqrt{3}}{13}$ ≈ 0.349	$\frac{5+2\sqrt{3}}{13}$ ≈ 0.651	$\frac{2-\sqrt{3}}{6}$ ≈ 0.045
	M2	$\frac{8-2\sqrt{3}}{13}$ ≈ 0.349	$\frac{8-2\sqrt{3}}{13}$ ≈ 0.349	$\frac{2-\sqrt{3}}{6}$ ≈ 0.045
$\Delta(384)$	M3	$\frac{4}{8+\sqrt{2}+\sqrt{6}}$ ≈ 0.337	$\frac{4-\sqrt{2}+\sqrt{6}}{8+\sqrt{2}+\sqrt{6}}$ ≈ 0.424	$\frac{4-\sqrt{2}-\sqrt{6}}{12}$ ≈ 0.011
	M4	$\frac{4}{8+\sqrt{2}+\sqrt{6}}$ ≈ 0.337	$\frac{4+2\sqrt{2}}{8+\sqrt{2}+\sqrt{6}}$ ≈ 0.576	$\frac{4-\sqrt{2}-\sqrt{6}}{12}$ ≈ 0.011
Central value [24]		0.312	0.420	0.025
Central value [27,28]		0.312	0.520	0.014

Table 3.1: *Four of the mixing patterns produced by the groups we consider. In particular patterns* M3 *and* M4 *can be very close to the experimental data.*

dodecahedron/icosahedron and the self-dual tetrahedron. Also the group A_5 has been used in flavour symmetric model building, see for instance [58], where the Golden Ratio mixing pattern is derived. It fits the data with a precision comparable to the tribimaximal pattern and has the same $\theta_{13} = 0$ prediction.

A natural question is whether these presentations extend to other finite groups for $N > 5$. It turns out that this is possible, although for $N \geq 7$ a fourth relation will be required next to the three already given to ensure that the groups considered are finite [68]. Though not excluded as candidates for a flavour symmetry, infinite discrete groups have the disadvantage that they can possess infinitely many irreducible representations of a given dimensionality, which makes them less appealing for model building as they eventually allows to reproduce any mixing pattern. In particular, we will be interested in the groups in this series that have three dimensional representations [69], as these can then be used to build models of lepton mixing.

We will embed the previous groups into an infinite set of finite groups, related to the modular group. To be able to study this set, we first study the modular group (over **Z**) itself, which is an discrete *infinite* group.

The (inhomogeneous) modular group Γ is the group of linear fractional transformations acting on a variable z:

$$z \to \frac{az+b}{cz+d}\,. \tag{3.4}$$

The parameters a, b, c and d are integers and $ad - bc = 1$. Obviously, a transformation described by parameters $\{a, b, c, d\}$ is identical to a transformation defined by $\{$-a, -b, -c, -$d\}$.

As is clear from the definition, Γ is isomorphic to the group $PSL(2,Z) = SL(2,Z)/\{\pm I\}$. Here $SL(2,Z)$ (the *homogeneous* modular group) is the group of 2×2 matrices with integer entries and determinant equal to one and to get $PSL(2,Z)$ (the *inhomogeneous* modular group), two matrices that only differ by an overall sign are identified as M and $-M$ determine the same transformation.

The modular group Γ is generated by two elements S and T satisfying [70]:

$$S^2 = (ST)^3 = 1 \quad . \tag{3.5}$$

Note again that these relations are also satisfied by the generators of A_4, S_4 and A_5, although they are not sufficient to define these groups uniquely. With respect to the behaviour of the parameter z, S and T can be represented by the transformations

$$S : z \to \frac{-1}{z} \quad . \qquad T : z \to z + 1. \tag{3.6}$$

This corresponds to the two following matrices of $SL(2,Z)$:

$$S = \begin{pmatrix} 0 & 1 \\ -1 & 0 \end{pmatrix} \quad , \qquad T = \begin{pmatrix} 1 & 1 \\ 0 & 1 \end{pmatrix} \quad . \tag{3.7}$$

We now generalize this construction by replacing integers by integers modulo N. Given a natural number $N > 1$, the homogeneous finite modular group $SL(2,Z_N)$ is defined as the group of 2×2 matrices with entries that are integers modulo N and determinant equal to one modulo N. Again, the inhomogeneous groups are defined by identifying in $SL(2,Z_N)$ two opposite matrices

$$\Gamma_N \sim PSL(2,Z_N) \equiv SL(2,Z_N)/\{\pm I\} \; .$$

For each N these groups are finite.

The order of the homogeneous finite modular groups $SL(2,Z_N)$ is [70,71]

$$\Big|SL(2,Z_N)\Big| = N^3 \prod_{p|N} \left(1 - \frac{1}{p^2}\right) \tag{3.8}$$

The product extends to the prime p divisors of N. For $N = 2$, the identity I and its opposite $-I$ are indistinguishable and therefore $\Gamma_2 \equiv SL(2,Z_2)$. For $N > 2$ they are distinguishable and the order of the inhomogeneous groups is half of that of the homogeneous ones

$$\Big|\Gamma_N\Big| = \frac{1}{2}\Big|SL(2,Z_N)\Big| \quad . \tag{3.9}$$

In table 3.2 we list the order of $SL(2,Z_N)$ and Γ_N, as well as the groups Γ_N is isomorhic to, for $2 \leq N \leq 11$

N	2	3	4	5	6	7	8	9	10	11
$\lvert SL(2,Z_N)\rvert$	6	24	48	120	144	336	384	648	720	1320
$\lvert\Gamma_N\rvert$	6	12	24	60	72	168	192	324	360	660
$\Gamma_N \sim$	S_3	A_4	S_4	A_5	$(S_3 \times A_4)$	$PSL(2,7)$			$(S_3 \times A_5)$	$PSL(2,11)$

Table 3.2: *Properties of* $SL(2,Z_N)$ *and* Γ_N *for* $2 \leq N \leq 11$.

The group Γ_2 has six elements and coincide with the permutation group S_3. For $N = 3,4,5$, the groups Γ_N coincide with the proper symmetry groups of the Platonic solids and we have [71]: $\Gamma_3 \sim A_4$, $\Gamma_4 \sim S_4$ and $\Gamma_5 \sim A_5$. Our proposal is to investigate the whole series Γ_N. Notice that, if we regard the matrices S and T of equation (3.7) as representative of elements of Γ_N, we find that, besides the relations in equation (3.5), they also satisfy $T^N = 1$. However, in general, further relations are required to define the complete presentation of the corresponding group. For instance, Γ_7 is characterized by

$$S^2 = (ST)^3 = 1 \quad , \qquad T^7 = 1 \quad , \qquad (ST^{-1}ST)^4 = 1 \quad . \tag{3.10}$$

The group Γ_7 is isomorphic to the group[1] $PSL(2,7)$. Note that without including the last relation in (3.10), the matrices S and T can generate a group of infinite order.

The group $SL(2,Z_N)$ is a double covering of the group Γ_N, for $N > 2$. There is a homomorphism between these two groups and the inhomogeneous group, Γ_N, can be regarded as an unfaithful copy of its homogeneous counterpart $SL(2,Z_N)$ (except for $N = 2$ where the relation is an isomorphism). As a consequence, all irreducible representations of Γ_N are also irreps of $SL(2,Z_N)$.

[1]The 7 in $PSL(2,7)$ stands for the Galois field of order 7, so a better notation would be $PSL(2,GF_7)$. It is non-trivial that $PSL(2,Z_7)$ is isomorphic to $PSL(2,GF_7)$. Actually, only for prime N the numbers 0 to $(N-1)$ with addition and multiplication modulo N form a finite field.

In the following we will recall the complete classification of the irreducible representations of $SL(2, Z_N)$. In this way we will obtain all the representations of the group we are interested in, Γ_N, plus additional representations that we will discard.

We now like to find all three-dimensional representations of $SL(2, Z_N)$ (and thus of Γ_N). To study the irreps of $SL(2, Z_N)$, we consider the three possible situations for N

1) N is prime.

2) N is a power of a prime.

3) N is the product $\prod_p p^{\lambda_p}$ of primes and powers of primes.

We start with the case where N is a prime p. As remarked before, if $p = 2$, we have $\Gamma_2 = S_3$, which has two one-dimensional and one two-dimensional representations, but no three-dimensional ones. The dimensions d and multiplicities μ of the irreducible representations of $SL(2, Z_p)$ (p an *odd* prime) as a function of p are given in table 3.3.

We find that $SL(2, Z_N)$ has three dimensional irreps only for the primes 3, 5 and 7. The only related Γ_N groups that can have three dimensional irreps are thus A_4, A_5 and $PSL(2, 7)$. We indeed find that A_4 has a three dimensional irrep, while A_5 and $PSL(2, 7)$ have two, in the latter case, a complex-conjugate pair. These representations are explicitly given in table 3.4 in a basis where T is diagonal.

d	μ	$d = 3$ if	μ if $d = 3$	related Γ_n.
1	1^*	-	-	-
$p+1$	$\frac{1}{2}(p-3)$	~~$p=2$~~	-	-
p	1	$p = 3$	1	A_4
$p-1$	$\frac{1}{2}(p-1)$	~~$p=4$~~	-	-
$\frac{1}{2}(p+1)$	2	$p = 5$	2	A_5
$\frac{1}{2}(p-1)$	2	$p = 7$	2	$PSL(2, 7)$

Table 3.3: *Dimensions d and multiplicities μ of the irreducible representations of $SL(2, Z_p)$, p being an odd prime and the possibility to have three dimensional representations. If the candidate three-dimensional representation is related to even p in the third column, it is crossed. *In the case $p = 3$, there are two extra 1d representations from the last row.*

Next, we consider the case where N is a power p^λ of a prime. We separately discuss the cases where p is an odd prime and where $p = 2$. In table 3.5 we list the irreducible representations d of $SL(2, Z_{p^\lambda})$ with $p > 2$ and $\lambda > 1$, and the multiplicities μ of these representations. This table should be understood as follows. Given an integer $\bar{\lambda} > 1$, all groups $SL(2, Z_{p^\lambda})$ with $\lambda < \bar{\lambda}$ are unfaithful copies of the group $SL(2, Z_{p^{\bar{\lambda}}})$. It follows that the representations of $SL(2, Z_{p^\lambda})$ with $1 \leq \lambda < \bar{\lambda}$ are also representations of the group $SL(2, Z_{p^{\bar{\lambda}}})$. The irreducible representations of $SL(2, Z_{p^{\bar{\lambda}}})$ are given by those of table 3.3 ($\lambda = 1$) and by those listed in table 3.5, with $\lambda = 2, ..., \bar{\lambda}$. For instance, if $\bar{\lambda} = 3$ we should include both $\lambda = 2$ and $\lambda = 3$ from table 3.5. As a check we can compute the order of $SL(2, Z_{p^{\bar{\lambda}}})$ from tables 3.3 and 3.5 and we find $p^{3\bar{\lambda}}(1 - 1/p^2)$ in agreement with eq. (3.8). From table 3.5 it is easy to prove that for $p > 2$ and $\lambda > 1$ there are no other irreducible three-dimensional representations, apart from those already given in table 3.3. This concludes the discussion for $p > 2$.

The case $p = 2^\lambda$ is more complicated and a separate discussion for each λ is needed. Again the representations of $SL(2, Z_{2^\lambda})$ are also representations of the group $SL(2, Z_{2^{\bar{\lambda}}})$ for $1 \leq \lambda < \bar{\lambda}$. For $\lambda > 4$ there are no three-dimensional irreducible representations, different from those already induced by $\lambda = 2, 3, 4$ [72–74]. In table 3.6 we summarize the irreducible representations of $SL(2, Z_{2^\lambda})$ ($\lambda = 1, 2, 3, 4$). We conclude that Γ_4, Γ_8 and Γ_{16} can give "new" three dimensional irriducible representations and are interesting from a model building point of view.

N	S	$\frac{1}{2\pi i}\log(T)$
3	$\frac{1}{3}\begin{pmatrix} -1 & 2 & 2 \\ 2 & -1 & 2 \\ 2 & 2 & -1 \end{pmatrix}$	$\mathtt{diag}\left(0, \frac{1}{3}, \frac{2}{3}\right)$
5	$\frac{1}{\sqrt{5}}\begin{pmatrix} 1 & \sqrt{2} & \sqrt{2} \\ \sqrt{2} & -\phi & \frac{1}{\phi} \\ \sqrt{2} & \frac{1}{\phi} & -\phi \end{pmatrix}$	$\mathtt{diag}\left(0, \frac{1}{5}, \frac{4}{5}\right)$
	$-\frac{1}{\sqrt{5}}\begin{pmatrix} 1 & \sqrt{2} & \sqrt{2} \\ \sqrt{2} & \frac{1}{\phi} & -\phi \\ \sqrt{2} & -\phi & \frac{1}{\phi} \end{pmatrix}$	$\mathtt{diag}\left(0, \frac{2}{5}, \frac{3}{5}\right)$
7	$\frac{2}{\sqrt{7}}\begin{pmatrix} s_1 & s_2 & s_3 \\ s_2 & -s_3 & s_1 \\ s_3 & s_1 & -s_2 \end{pmatrix}$	$\mathtt{diag}\left(\frac{2}{7}, \frac{1}{7}, \frac{4}{7}\right)$
	$\frac{2}{\sqrt{7}}\begin{pmatrix} s_1 & s_2 & s_3 \\ s_2 & -s_3 & s_1 \\ s_3 & s_1 & -s_2 \end{pmatrix}$	$\mathtt{diag}\left(\frac{5}{7}, \frac{6}{7}, \frac{3}{7}\right)$

Table 3.4: *Three dimensional irreducible representations of* Γ_N, $N = 3, 5, 7$.*We have defined* $\phi \equiv \frac{1+\sqrt{5}}{2}$ *and* $s_j \equiv \sin(\frac{j\pi}{7})$.

d	$p^{\lambda-1}(p+1)$	$p^{\lambda-1}(p+1)$	$\frac{1}{2}p^{\lambda-2}(p^2-1)$
μ	$\frac{1}{2}p^{\lambda-2}(p-1)^2$	$\frac{1}{2}p^{\lambda-2}(p^2-1)$	$4p^{\lambda-1}$

Table 3.5: *Dimensions* d *and multiplicities* μ *of the "new" irreducible representations of* $SL(2, Z_{p^\lambda})$, p *being an odd prime and* $\lambda > 1$. *See the text for explanations.*

Lastly, we consider the case where N is a product of primes and powers of primes

$$N = \prod_p p^{\lambda_p}. \tag{3.11}$$

Now the group $SL(2, Z_N)$ factorizes as

$$SL(2, Z_N) = \prod_p SL(2, Z_{p^{\lambda_p}}) \tag{3.12}$$

Two examples can be checked on the second line of table 3.2: $SL(2, Z_6) = SL(2, Z_2) \times SL(2, Z_3)$ (the number of elements satisfies $144 = 6 \times 24$) and $SL(2, Z_{10}) = SL(2, Z_2) \times SL(2, Z_5)$ (where the number of elements satisfies $720 = 6 \times 120$). Due to the special position of Γ_2, in these two cases, also the relations $\Gamma_6 = \Gamma_2 \times \Gamma_3 = S_3 \times A_4$ and $\Gamma_{10} = \Gamma_2 \times \Gamma_5 = S_3 \times A_5$ hold, as given on the lowest line.

Clearly, three dimensional representations of these product groups can be constructed using the three-dimensional representation of one of the groups and one-dimensional representations of all the others. Therefore, the cases where N is a product do not give new patterns.

In conclusion all independent three-dimensional representations of the finite modular groups can be studied by considering the six groups $SL(2, Z_N)$ ($N = 3, 4, 5, 7, 8, 16$). We have 33 distinct irreducible triplets. From table 3.3 we see that one is associated to $N = 3$, two are related to $N = 5$ and two to $N = 7$. Moreover, from table 3.6, we see that 4 irreducible triplets corresponds to $N = 4$, while $N = 8$ introduces 8 new irreducible triplets and finally 16 other independent irreducible triplets are associated to $N = 16$.

The full list of these 33 triplets is explicitly given in Appendix A of ref. [74], in terms of the S and T elements, in the basis where the T generator is diagonal. Of these 33 $SL(2, Z_N)$ representations

d	1	2	3	4	6	8	12	24	Order	Note
$SL(2,Z_2)$	2	1							6	Isomorphic to S_3
$SL(2,Z_4)$	4	2	4						48	Double cover of S_4
$SL(2,Z_8)$	4	6	12	2	6				384	
$SL(2,Z_{16})$	4	6	28	2	26	6	2	2	3072	

Table 3.6: *Dimensions d and multiplicities of the irreducible representations of $SL(2,Z_{2^\lambda})$, for $\lambda < 5$. For each group all the irreducible representations are listed [72–74].*

only a smaller subset are also representations of the corresponding inhomogeneous group Γ_N: those satisfying the relations in eq. (3.5). They are 19 and we collect them in table 3.4 and 3.7. In the latter table, the elements S are given in terms of a matrix

$$\mathcal{S} \equiv \frac{1}{2}\begin{pmatrix} 0 & \sqrt{2} & \sqrt{2} \\ \sqrt{2} & -1 & 1 \\ \sqrt{2} & 1 & -1 \end{pmatrix} \tag{3.13}$$

N	S	$\frac{1}{2\pi i}\log(T)$
4	$\mathcal{S}$	$\mathtt{diag}\left(0, \frac{1}{4}, \frac{3}{4}\right)$
	$-\mathcal{S}$	$\mathtt{diag}\left(\frac{2}{4}, \frac{3}{4}, \frac{1}{4}\right)$
8	$\mathcal{S}$	$\mathtt{diag}\left(\frac{6}{8}, \frac{7}{8}, \frac{3}{8}\right)$
	$\mathcal{S}$	$\mathtt{diag}\left(\frac{2}{8}, \frac{5}{8}, \frac{1}{8}\right)$
	$-\mathcal{S}$	$\mathtt{diag}\left(\frac{6}{8}, \frac{1}{8}, \frac{5}{8}\right)$
	$-\mathcal{S}$	$\mathtt{diag}\left(\frac{2}{8}, \frac{3}{8}, \frac{7}{8}\right)$
16	$\mathcal{S}$	$\mathtt{diag}\left(\frac{14}{16}, \frac{5}{16}, \frac{13}{16}\right)$
	$\mathcal{S}$	$\mathtt{diag}\left(\frac{2}{16}, \frac{11}{16}, \frac{3}{16}\right)$
	$-\mathcal{S}$	$\mathtt{diag}\left(\frac{6}{16}, \frac{13}{16}, \frac{5}{16}\right)$
	$-\mathcal{S}$	$\mathtt{diag}\left(\frac{10}{16}, \frac{3}{16}, \frac{11}{16}\right)$
	$\mathcal{S}$	$\mathtt{diag}\left(\frac{10}{16}, \frac{15}{16}, \frac{7}{16}\right)$
	$\mathcal{S}$	$\mathtt{diag}\left(\frac{6}{16}, \frac{1}{16}, \frac{9}{16}\right)$
	$-\mathcal{S}$	$\mathtt{diag}\left(\frac{2}{16}, \frac{7}{16}, \frac{15}{16}\right)$
	$-\mathcal{S}$	$\mathtt{diag}\left(\frac{14}{16}, \frac{9}{16}, \frac{1}{16}\right)$

Table 3.7: Three dimensional irreducible representations of Γ_N, $N = 4, 8, 16$. The matrix $\mathcal{S}$ is defined in the text.

In the next section we will study the application of Γ_N with $N = 3$, 4, 5, 7, 8 or 16 to the lepton sector. We suppose that the group functions as a horizontal symmetry group, that after it gets broken leaves a residual G_e symmetry in the charged lepton sector and a residual G_ν in the neutrino sector. Both G_e and G_ν are expressed in the generators S and T.

In the cases $N = 3$, 4, 5 and 7, this is straightforward, but in the cases $N = 8$ and 16 an extra complication occurs. In these cases, the representations given by S and T are not faithful and generate subgroups of Γ_8 and Γ_{16} of order 96 and 384 respectively. These are the groups $\Delta(96)$ and $\Delta(384)$ that we study in sections 3.3.5 and 3.3.6. They belong to the series $\Delta(n^2)$ [75–77] that also $\Delta(24) \sim S_4$ is part of and are isomorphic to the semi-direct products of $Z_2 \times Z_2$ and S_3.

3.3 Lepton mixing patterns from Γ_N

In this section we classify the lepton mixing patterns arising from the candidate flavour symmetry groups mentioned in the previous section. We have $G_f = \Gamma_N$ for $N = 3$, 4, 5 and 7, while for $N = 8$ and 16 G_f is the subgroup of Γ_N that can be constructed from the S and T generators mentioned in table 3.7.

We aim at a complete classification under the following rules. We work in a certain leading order approximation, where the neutrino mass matrix and the charged lepton mass matrix are separately invariant under the subgroups G_ν and G_e of G_f, respectively. As has been discussed in detail in the literature [78, 79], this framework in which the misalignment between neutrino and charged lepton mass matrices is associated with the non-trivial breaking of a flavour symmetry is particularly interesting and predictive. Given G_f, we will scan all possible subgroups G_ν and G_e with the following restrictions.

Firstly we assume that neutrinos are Majorana particles as strongly hinted to by their light masses. The Majorana character of neutrinos shows up in the choice of G_ν. With a single generation, the only transformation of a Majorana neutrino leaving invariant its mass term is a change of sign. If there are three generations, it can be shown [78, 80] that the appropriate invariance group of the neutrino sector generalizes to the product of two commuting parities, the Klein group $Z_2 \times Z_2$, allowing for an independent relative change of sign of any neutrino.

Secondly, we discard non-Abelian residual symmetries for the charged leptons since the non-Abelian character of the subgroup would result in a complete or partial degeneracy of the mass spectrum, which is not in accordance with the hierarchy among the charged lepton masses. Hence, we choose G_e to be a cyclic group Z_n or a subgroup of these groups, such as $Z_2 \times Z_2$.

Thirdly, to minimize double counting and to select only those mixing patterns that reflect the properties of the full group G_f, we will ask that the subgroups $G_\nu = Z_2 \times Z_2$ and G_e generate the full group G_f.

Once we specify a three-dimensional representation ρ of G_f for the lepton doublets, the elements $g_{\nu i}$ of the subgroup G_ν and g_{ei} of the subgroup G_e are given by matrices $\rho(g_{\nu i})$ and $\rho(g_{ei})$. These matrices leave the neutrino mass matrix m_ν and the combination $(m_e^\dagger m_e)$ invariant[2].

$$\rho(g_{\nu i})^T m_\nu\, \rho(g_{\nu i}) = m_\nu\ , \qquad \rho(g_{ei})^\dagger (m_e^\dagger m_e) \rho(g_{ei}) = (m_e^\dagger m_e) \quad . \tag{3.14}$$

The matrices $\rho(g_{\nu i})$ and $\rho(g_{ei})$ can be diagonalized by two unitary transformations Ω_ν and Ω_e. This follows from the facts that ρ is a unitary representation and that G_ν and G_e are Abelian

$$\rho(g_{\nu i})_{\rm diag} = \Omega_\nu^\dagger\, \rho(g_{\nu i})\, \Omega_\nu \quad , \qquad \rho(g_{ei})_{\rm diag} = \Omega_e^\dagger\, \rho(g_{ei})\, \Omega_e \quad . \tag{3.15}$$

By the above invariance requirements Ω_ν and Ω_e are also the transformations that diagonalize m_ν and $(m_e^\dagger m_e)$, respectively.

$$(m_\nu)_{\rm diag} = \Omega_\nu^T m_\nu \Omega_\nu, \qquad (m_e^\dagger m_e)_{\rm diag} = \Omega_e^\dagger (m_e^\dagger m_e) \Omega_e\ . \tag{3.16}$$

The lepton mixing matrix is, up to phase redefinitions, given by

$$U_{\rm PMNS} = \Omega_e^\dagger \Omega_\nu\ . \tag{3.17}$$

Phase redefinitions $\Omega_e \to \Omega_e K_e$ and $\Omega_\nu \to \Omega_\nu K_\nu$, with K_e and K_ν diagonal matrices of phases, can be used to make the eigenvalues of m_ν real and positive and to eliminate all but three phases in $U_{\rm PMNS}$. One of these is the Dirac CP phase $\delta^l_{\rm CP}$ that can be measured in neutrino oscillations (at least if $\theta^l_{13} \neq 0$); two others are Majorana phases. These cannot be predicted in our approach as

[2] In our convention, $SU(2)_L$ doublets are on the right of m_e

the neutrino masses remain unconstrained by the above requirements. When relevant, we report $|\sin\delta^l_{\rm CP}|$ and the Jarlskog CP-invariant of equation (2.34).

The fact that the actual neutrino and charged lepton masses are not fixed by the requirements (3.14) and (3.15), means that these relations only fix the lepton mixing matrix up to interchange of rows and columns. We can use this to our advantage to obtain a $U_{\rm PMNS}$ that is in closest agreement with the data. Even if there is evidence of non-zero θ^l_{13} now, this angle is very small. We recall from (the lepton analogue of) equation (2.32) that the sine of this angle is given by the absolute value of the $(1\ 3)$ element of the mixing matrix and therefore, we choose to represent the smallest element of the mixing matrices at the $(1\ 3)$ position. Now we are just allowed an extra interchange of the first and second column and of the second and third row.

We choose to order the first and second columns such that the $(1\ 1)$ element is larger in absolute value than the $(1\ 2)$ element. Equation (2.32) tells us that $\tan\theta^l_{12}$ is then smaller than 1 and this implies $\sin^2\theta^l_{12} < 1/2$ in accordance with the data in table 2.4. Next, we mention a slight tension between the two global neutrino oscillation fits reported in table 2.4. The fit [24] seems to point at a value of $\sin^2\theta_{23}$ smaller than $1/2$, implying that the $(2\ 3)$ element of the PMNS matrix is larger than the $(3\ 3)$ element. On the other hand the fit [27,28] very slightly favours $\sin^2\theta_{23} > 1/2$, which can be reproduced if the two above mentioned elements are ordered the other way around.

Equations (3.14) and (3.15) also show that the PMNS mixing matrix is invariant, when the matrices representing the elements of G_ν and/or G_e change overall sign. Furthermore, when these matrices are complex conjugated, the lepton mixing matrix becomes conjugated as well. We do not discuss these cases separately.

In the next six subsections, we systematically consider the cases $N = 3$, 4, 5, 7, 8 and 16. In each of the cases we present the conjugacy classes of the group with their order and a list of the Abelian subgroups that the group possesses. We consider all possible Abelian subgroups G_e that the charged lepton sector can be invariant under (as explained above, G_ν of the neutrino sector is fixed to be one of the Klein groups). For all these cases, we find the corresponding lepton mixing matrix and we comment on the compatibility with the data of these patterns.

3.3.1 The group $\Gamma_3 \sim A_4$

The group A_4 is the group of even permutations of four elements. Directly related, A_4 is also the symmetry group of the regular tetrahedron, the simplest of the Platonic solids. The group has three inequivalent one-dimensional irreducible representations 1, $1'$ and $1''$ and one three dimensional irrep. As explained in section 3.2, it can be generated by elements S and T that satisfy

$$S^2 = (ST)^3 = T^3 = 1\ . \tag{3.18}$$

In the T-diagonal (Altarelli–Feruglio) basis of the three dimensional representation, S and T are given in table 3.4. The twelve elements of the group A_4 are members of four classes, with order 1, 2, 3 and 3 respectively as shown in table 3.8. We name these classes $a\mathcal{C}_b$, where a refers to the number of elements and b the order.

Class	Order	# Elements	Elements
$1\mathcal{C}_1$	1	1	E
$3\mathcal{C}_2$	2	3	S, T^2ST, ST^2ST
$4\mathcal{C}_3^{(1)}$	3	4	T, ST, TS, STS
$4\mathcal{C}_3^{(2)}$	3	4	T^2,$(ST)^2$, $(TS)^2$, $(STS)^2$

Table 3.8: *Conjugacy classes of* A_4

There is a unique $Z_2 \times Z_2$ Klein group, that is equal to the class of order 2 and there are four Z_3s. We

can assume that each of these is generated by an element of the first class of order 3 as shown in table 3.9.

Subgroup		Generators
$Z_2 \times Z_2$	K	S, T^2ST
Z_3	C_1	T
	C_2	ST
	C_3	TS
	C_4	STS

Table 3.9: *Abelian subgroups of A_4 and their generators.*

The fact that there is only a single Klein group, automatically fixes G_ν. It also forces G_e to be one of the Z_3 groups, as it cannot also be the Klein group. The choices of G_e are all equivalent. In all cases the Klein group and the Z_3-group together generate the full group A_4 and we obtain the so-called magic mixing matrix as the lepton mixing matrix [81,82].

$$U_{\rm PMNS} = \frac{1}{\sqrt{3}} \begin{pmatrix} 1 & 1 & 1 \\ 1 & \omega & \omega^2 \\ 1 & \omega^2 & \omega \end{pmatrix} . \tag{3.19}$$

In this mixing pattern, both the solar and atmospheric mixing are maximal and θ_{13} fulfills $\sin^2\theta_{13} = 1/3$. This pattern also leads to a Dirac CP phase $|\delta_{CP}| = \pi/2$ and $|J_{CP}| = 1/(6\sqrt{3}) \approx 0.096$.

We comment about the fact that in this scheme A_4 cannot reproduce the tribimaximal mixing. However there are many models in the literature that obtain TBM mixing from A_4, including the model of section 2.4. The key is that in these models, the neutrinos are invariant under a Klein group generated not only by S, but also by the so-called $(\mu\,\tau)$-invariant matrix U

$$U = \begin{pmatrix} 1 & 0 & 0 \\ 0 & 0 & 1 \\ 0 & 1 & 0 \end{pmatrix} . \tag{3.20}$$

This matrix is not an element of A_4. Invariance under U can therefore not be forced by A_4. It can however appear as an accidental symmetry because of the matter content of a specific model and/or auxiliary symmetries that are present next to A_4. The matrix U is actually an element of S_4 and since this group also has a Z_3 subgroup, we will find tribimaximal mixing in the next section. The combination of S_4 and tribimaximal mixing is indeed also often seen in the literature.

The group A_4 appears in many places in this thesis and details of its group theory, such as Clebsch Gordan rules are thus often needed. We derive those properties in appendix 3.A that follows this chapter.

3.3.2 The group $\Gamma_4 \sim S_4$

The next group we consider is S_4. It is the symmetric group of (even and odd) permutations of four elements. As such, it is twice as large as A_4, having twenty-four elements. S_4 is also the symmetry group of two of the Platonic solids, the cube and the octahedron. It has five irreps: two one-dimensional, one two-dimensional and two inequivalent three-dimensional. The group can be generated by two elements S and T that satisfy

$$S^2 = (ST)^3 = T^4 = 1 . \tag{3.21}$$

Specific realizations of S and T in the three-dimensional representation are given in table 3.7. We see that the two triplets are related by an overall change of sign of both $\rho(S)$ and $\rho(T)$. As explained in the introduction of this section these two cases lead to equivalent lepton mixing matrices and do not need to be discussed separately.

The group S_4 has five conjugacy classes, whose elements are listed in table 3.10. The Abelian subgroups are Klein groups as well as groups of order 3 and 4, as given in table 3.11. One of the Klein groups K is a conjugacy class on itself, making it a normal subgroup.

Class	Elements
$1\mathcal{C}_1$	E
$6\mathcal{C}_2$	$S, ST^2ST, T^3ST, T^2ST^2, ST^3ST^2, ST^2ST^3$
$3\mathcal{C}_2$	T^2, ST^2ST^2, ST^2S
$8\mathcal{C}_3$	$ST, ST^3, TS, T^3S, T^2ST, ST^3ST, T^3ST^2, T^2ST^3$
$6\mathcal{C}_4$	$T, ST^2, T^3, STS, T^2S, ST^3S$

Table 3.10: *Conjugacy classes of S_4*

Subgroup		Generators
$Z_2 \times Z_2$	K	T^2, ST^2S
	K_1	S, ST^2ST^2
	K_2	T^2, ST^2ST^3
	K_3	ST^2S, ST^3ST^2
Z_3	C_1	ST
	C_2	TS
	C_3	T^3ST^2
	C_4	T^2ST^3
Z_4	Q_1	T
	Q_2	ST^2
	Q_3	STS

Table 3.11: *Abelian subgroups $Z_2 \times Z_2$, Z_3 and Z_4 of S_4 and their generators. K is a normal subgroup.*

The possible mixing patterns are listed below. From table 3.11 we se that we have several different possible choices for G_ν and G_e. Some of them do not generate the entire group S_4 and can be disregarded. For instance K together with any other subgroup in table 3.11 always generate a group smaller than S_4.

In the next three paragraphs, we consider the three choices of G_e: it can be a Z_3 , Z_4 or Klein subgroup. We focus on choices of the G_e and G_ν where it is possible to generate the full group S_4. Because of the potential presence of many phases in the lepton mixing matrix, we report the absolute values of its elements. This is enough to calculate all three mixing angles.

Mixing patterns with $G_\nu = Z_2 \times Z_2$ and $G_e = Z_3$

When the lepton sector is invariant under an element of order 3, the full group S_4 can be generated if neutrino sector is invariant under a klein group K_i, but not K. We then obtain the tribimaximal mixing pattern, as anticipated upon in the discussion of A_4.

$$||U_{\rm PMNS}|| = \begin{pmatrix} \frac{2}{\sqrt{6}} & \frac{1}{\sqrt{3}} & 0 \\ \frac{1}{\sqrt{6}} & \frac{1}{\sqrt{3}} & \frac{1}{\sqrt{2}} \\ \frac{1}{\sqrt{6}} & \frac{1}{\sqrt{3}} & \frac{1}{\sqrt{2}} \end{pmatrix} \quad . \tag{3.22}$$

When we pick the invariant Klein group K for the neutrino sector, it is not possible to generate the full group S_4, but a subgroup is generated instead. In this case, the subgroup is A_4 and the corresponding mixing pattern is the magic matrix of (3.19).

Mixing patterns with $G_\nu = Z_2 \times Z_2$ and $G_e = Z_4$

If we assume the lepton sector to be invariant under an element of order 4, the mixing pattern obtained can be

$$||U_{\rm PMNS}|| = \begin{pmatrix} \frac{1}{\sqrt{2}} & \frac{1}{\sqrt{2}} & 0 \\ \frac{1}{2} & \frac{1}{2} & \frac{1}{\sqrt{2}} \\ \frac{1}{2} & \frac{1}{2} & \frac{1}{\sqrt{2}} \end{pmatrix} \quad . \tag{3.23}$$

An example is when $G_\nu = K_1$ and $G_e = Q_1$. This mixing pattern is bimaximal. As mentioned in the introduction, the mixing pattern itself does not describe the data well, as the solar angle is maximal and thus too large. However, with next-to-leading order corrections included, it may be very relevant, in particular since the order of magnitude of the correction to the solar and reactor angle are similar. Furthermore, the corrections in the lepton sector might be related to the generation of the Cabibbo angle, which is also approximately of the same size via quark-lepton complementarity; see e.g. [83–87] and the discussion in chapter 4.

Mixing patterns with $G_\nu = Z_2 \times Z_2$ and $G_e = Z_2 \times Z_2$

When both the neutrino sector and the charged lepton sector are assumed to be invariant under (different) Klein groups, the lepton mixing matrix can be the same as in the previous case. When the full group S_4 is generated, for instance by K_1 and K_2, the mixing pattern is the bimaximal mixing of equation (3.23).

This concludes the discussion for S_4. The group can be used to reproduce two of the most popular mixing patterns in the literature, tribimaximal and bimaximal mixing. In the case of bimaximal mixing, this is possible in two ways, with very different residual symmetries in the charged lepton sector. As for A_4, the group theory of S_4 will be important in many places of this thesis, in particular in chapter 4. We derive the Clebsch-Gordan rules and transformation rules of different bases into each other in appendix 3.B.

3.3.3 The group $\Gamma_5 \sim A_5$

The third subgroup of the modular group is A_5. It can be defined as the group of even permutations of 5 elements and has 60 elements and five conjugacy classes. Relevant Abelian subgroups are $Z_2 \times Z_2$, Z_3 and Z_5. In total, there are 21 of them. Due to the growing number of elements, we no longer list all classes and generators of Abelian subgroups. Instead, these are collected in appendix 3.C at the end of this chapter.

The group has two inequivalent irreducible triplets. Two candidates for $\rho(S)$ and $\rho(T)$ are mentioned in table 3.4. We checked that if the set $\{S,\ T\}$ is given by one pair of matrices given in the table, that then the others can be written as $\{S' = T^2ST^3ST^2,\ T' = T^2\}$ and that this is a second independent representation that satisfies the algebra

$$S^2 = (ST)^3 = T^5 = 1 \ . \tag{3.24}$$

In the following three subsections, we describe the lepton mixing when the neutrino residual symmetry is a Klein groups and the one of the charged leptons is either Z_3, Z_5 or $Z_2 \times Z_2$.

Mixing patterns with $G_\nu = Z_2 \times Z_2$ and $G_e = Z_3$

When we take G_ν a Klein group and we take G_e generated by an element of order 3, we get the mixing pattern

$$||U_{\rm PMNS}|| = \frac{1}{\sqrt{6}} \begin{pmatrix} \sqrt{2}\phi & \frac{\sqrt{2}}{\phi} & 0 \\ \frac{1}{\phi} & \phi & \sqrt{3} \\ \frac{1}{\phi} & \phi & \sqrt{3} \end{pmatrix} \approx \begin{pmatrix} 0.934 & 0.357 & 0 \\ 0.252 & 0.661 & 0.707 \\ 0.252 & 0.661 & 0.707 \end{pmatrix} \quad . \tag{3.25}$$

This mixing pattern is for instance generated by $G_\nu = K_1$ and $G_e = C_1$. The mixing angles are vanishing θ_{13} and maximal θ_{23} together with $\sin^2\theta_{12} = \frac{1}{3}(2-\phi) = \frac{1}{6}(3-\sqrt{5}) \approx 0.127$. Obviously, $J_{CP} = 0$. This is the pattern mentioned by Lam [80]. It would need large corrections to the solar mixing angle in order to match the current data.

Mixing patterns with $G_\nu = Z_2 \times Z_2$ and $G_e = Z_5$

When the lepton sector is invariant under an element of order 5, the mixing pattern becomes

$$||U_{\rm PMNS}|| = \begin{pmatrix} \cos\theta_{12} & \sin\theta_{12} & 0 \\ \sin\theta_{12}/\sqrt{2} & \cos\theta_{12}/\sqrt{2} & 1/\sqrt{2} \\ \sin\theta_{12}/\sqrt{2} & \cos\theta_{12}/\sqrt{2} & 1/\sqrt{2} \end{pmatrix} \approx \begin{pmatrix} 0.851 & 0.526 & 0 \\ 0.372 & 0.602 & 0.707 \\ 0.372 & 0.602 & 0.707 \end{pmatrix} \quad . \tag{3.26}$$

with $\tan\theta_{12} = 1/\phi$. This pattern is generated for any choice of G_ν and G_e. Again, we find vanishing θ_{13} and maximal atmospheric mixing θ_{23}, this time together with $\sin^2\theta_{12} \approx 0.276$. Obviously $J_{CP} = 0$. This mixing pattern was discussed before e.g. in [58,88]. As mentioned at the beginning of section 3.2, its agreement with the data is of the same order as the tribimaximal mixing pattern.

Mixing patterns with $G_\nu = Z_2 \times Z_2$ and $G_e = Z_2 \times Z_2$

In case both the neutrino sector and the charged lepton sector are invariant under a Klein group, the mixing reads

$$||U_{\rm PMNS}|| = \frac{1}{2} \begin{pmatrix} \phi & 1 & \phi^{-1} \\ \phi^{-1} & \phi & 1 \\ 1 & \phi^{-1} & \phi \end{pmatrix} \approx \begin{pmatrix} 0.809 & 0.5 & 0.309 \\ 0.309 & 0.809 & 0.5 \\ 0.5 & 0.309 & 0.809 \end{pmatrix} \quad . \tag{3.27}$$

Excluding the case in which G_ν and G_e are the same group, we always find the pattern in equation(3.27) to be generated. The mixing angles which can be extracted from equation(3.27) are: $\sin^2\theta_{13} \approx 0.095$ and $\sin^2\theta_{12} = \sin^2\theta_{23} \approx 0.276$. Interchange of the second and third row gives $\sin^2\theta_{23} \approx 0.724$. Also in this case there is no non-trivial Dirac CP phase, i.e. $J_{CP} = 0$. We mention that although the $(1\ 2)$-angle is in good agreement with the data, $\sin^2\theta_{13}$ is too large even now it is clearly established to be non-zero and also the atmospheric mixing angle is too far away from maximum in order to fit the data.

3.3.4 The group $\Gamma_7 \sim PSL(2,7)$

For N equal to 7, the modular subgroup Γ_N is isomorphic to $PSL(2,7)$ [89, 90]. We recall from the previous section that the group can be generated from two generators S and T only if a fourth non-trivial relation is satisfied. A presentation of the group is then

$$S^2 = (ST)^3 = T^7 = (ST^{-1}ST)^4 = 1 \ . \tag{3.28}$$

Possible matrix representations for S and T are given in table 3.4. The two representations there are each others complex conjugates and thus trivially give rise to the same mixing patterns. The group

$PSL(2,7)$ has six conjugacy classes mentioned in table 3.C.3 in the appendix after this chapter and a total of 71 relevant Abelian subgroups of the type Z_3, Z_4, Z_7 and $Z_2 \times Z_2$. These are collected in table 3.C.4. In the following four paragraphs, we discuss the lepton mixing when the charged leptons are invariant under each of these groups, while the neutrinos are fixed to be invariant under the Klein group. None of these mixing patterns are very close to the neutrino data.

Mixing patterns with $G_\nu = Z_2 \times Z_2$ and $G_e = Z_3$

When the neutrino sector is invariant under a Klein group and the charged lepton sector under an element of order 3, it is possible to generate the whole group $PSL(2,7)$ with the elements of G_e and G_ν and we find the following mixing pattern

$$\begin{aligned} ||U_{\rm PMNS}|| &= \frac{1}{\sqrt{6}} \begin{pmatrix} \sqrt{\frac{1}{2}\left(5+\sqrt{21}\right)} & 1 & \frac{1}{2}(5-\sqrt{21})\sqrt{\frac{1}{2}(5+\sqrt{21})} \\ 1 & 2 & 1 \\ \frac{1}{2}(5-\sqrt{21})\sqrt{\frac{1}{2}(5+\sqrt{21})} & 1 & \sqrt{\frac{1}{2}\left(5+\sqrt{21}\right)} \end{pmatrix} \\ &\approx \begin{pmatrix} 0.894 & 0.408 & 0.187 \\ 0.408 & 0.816 & 0.408 \\ 0.187 & 0.408 & 0.894 \end{pmatrix} \quad . \end{aligned}$$

The mixing angles are $\sin^2\theta_{13} = \frac{1}{12}\left(5-\sqrt{21}\right) \approx 0.035$ and $\sin^2\theta_{12} = \sin^2\theta_{23} = \frac{1}{14}\left(7-\sqrt{21}\right) \approx 0.173$. If the second and third row are interchanged, the atmospheric mixing is given by $\sin^2\theta_{23} = \frac{1}{14}\left(7+\sqrt{21}\right) \approx 0.827$. The CP violating phase fulfills $|\sin\delta_{CP}| = \sqrt{7/8} \approx 0.935$ and thus $|J_{CP}| = 1/(24\sqrt{3}) \approx 0.024$. One possible choice of G_ν and G_e is: $G_\nu = K_1$ and $G_e = C_1$.

Mixing patterns with $G_\nu = Z_2 \times Z_2$ and $G_e = Z_4$

If we take the lepton sector invariant under an element of order 4, we can generate the following mixing pattern

$$\begin{aligned} ||U_{\rm PMNS}|| &= \frac{1}{2} \begin{pmatrix} \sqrt{\frac{1}{2}\left(3+\sqrt{7}\right)} & 1 & \frac{1}{2}\left(3-\sqrt{7}\right)\sqrt{3+\sqrt{7}} \\ 1 & \sqrt{2} & 1 \\ \frac{1}{2}\left(3-\sqrt{7}\right)\sqrt{3+\sqrt{7}} & 1 & \sqrt{\frac{1}{2}\left(3+\sqrt{7}\right)} \end{pmatrix} \\ &\approx \begin{pmatrix} 0.840 & 0.5 & 0.210 \\ 0.5 & 0.707 & 0.5 \\ 0.210 & 0.5 & 0.840 \end{pmatrix} \quad . \end{aligned} \tag{3.29}$$

The mixing angles are given by $\sin^2\theta_{13} = \frac{1}{8}\left(3-\sqrt{7}\right) \approx 0.044$, $\sin^2\theta_{12} = \sin^2\theta_{23} = \frac{1}{9}\left(5-\sqrt{7}\right) \approx 0.262$. After interchange of the second and third rows, $\sin^2\theta_{23}$ is equal to $\frac{1}{9}\left(4+\sqrt{7}\right) \approx 0.738$. The Jarlskog invariant fulfills $|J_{CP}| = 1/32 \approx 0.031$ and $|\sin\delta_{CP}| = \frac{1}{4}\sqrt{13-\sqrt{7}} \approx 0.804$. This pattern is produced for example for $G_\nu = K_1$ and $G_e = Q_1$.

Mixing patterns with $G_\nu = Z_2 \times Z_2$ and $G_e = Z_7$

If the charged lepton sector is invariant under an element of order 7, the mixing takes the form

$$||U_{\rm PMNS}|| = 2\sqrt{\frac{2}{7}} \begin{pmatrix} s_2 s_3 & s_1 s_3 & s_1 s_2 \\ s_1 s_2 & s_2 s_3 & s_1 s_3 \\ s_1 s_3 & s_1 s_2 & s_2 s_3 \end{pmatrix} \approx \begin{pmatrix} 0.815 & 0.452 & 0.363 \\ 0.363 & 0.815 & 0.452 \\ 0.452 & 0.363 & 0.815 \end{pmatrix} \quad . \tag{3.30}$$

For the mixing angles we find $\sin^2\theta_{13} \approx 0.132$ and $\sin^2\theta_{12} \approx 0.235$; $\sin^2\theta_{23}$ is approximately equal to 0.235 or, after interchange of rows, to 0.765. CP violation is characterized by $|J_{CP}| = 1/(8\sqrt{7}) \approx$

0.047.This pattern arises from any possible combination of a Klein group and an element of order seven.

Mixing patterns with $G_\nu = Z_2 \times Z_2$ and $G_e = Z_2 \times Z_2$

If both the neutrino sector and the charged lepton sector are invariant under a Klein group, the unique mixing pattern, compatible with our requirements, is

$$||U_{\rm PMNS}|| = \frac{1}{2}\begin{pmatrix} \sqrt{2} & 1 & 1 \\ 1 & \sqrt{2} & 1 \\ 1 & 1 & \sqrt{2} \end{pmatrix} \quad . \tag{3.31}$$

We find for the mixing angles $\sin^2\theta_{13} = 1/4$, $\sin^2\theta_{12} = 1/3$ and $\sin^2\theta_{23} = 1/3$ or $2/3$. The quantity $|\sin\delta_{CP}|$ is $3\sqrt{7}/8 \approx 0.992$ and $|J_{CP}| = \sqrt{7}/32 \approx 0.083$. One choice of G_ν and G_e leading to this particular pattern is $G_\nu = K_1$ and $G_e = K_3$.

3.3.5 The subgroup $\Delta(96)$ of Γ_8

The next group to consider is Γ_8. As explained at the end of section 3.2, it does not have three-dimensional faithful representations. Instead the three-dimensional representations given in table 3.7 can generate at most a subgroup of order 96. This group $\Delta(96)$ is also known as the tetrakisoctahedral group ${}^4O$.

The group $\Delta(96)$ has ten conjugacy classes as given in table 3.C.5; a list of generating elements for the Abelian subgroups $Z_2 \times Z_2$, Z_3, Z_4 and Z_8 can be found in table 3.C.6 and that of the Z_2 symmetries in table 3.C.7. The reason for mentioning the latter is explained shortly. There are ten irreducible representations: two singlets, one doublet, six triplets (two of which unfaithful) and one sextet. The character table of $\Delta(96)$ can be found in [75, 76]. The elements S and T of the four faithful three-dimensional representations are given in table 3.7. They are related to each other by an overall change of sign and/or complex conjugation and thus give rise to the same mixing patterns. S and T fulfill the relations

$$S^2 = (ST)^3 = T^8 = (ST^{-1}ST)^3 = 1 \, . \tag{3.32}$$

In the following we discuss all possible combinations of G_e and $G_\nu = Z_2 \times Z_2$ case by case. We encounter two new instances: firstly, we come across situations in which a certain combination of types of subgroups employed for G_e and $G_\nu = Z_2 \times Z_2$ does not allow to generate the original group $\Delta(96)$.

Secondly, it can be checked that the generating elements of the groups Q_1, Q_2 and Q_3 for the faithful irreducible triplets (to which we assign the left-handed lepton generations) are represented by matrices which have two degenerate eigenvalues. As a consequence, it is not possible to distinguish among the three generations of leptons with these groups. On themselves they cannot be used to generate G_e. However, a combination of two of them or a combination with an additional Z_2-generating element, resolves the degeneracy. For this reason we also include the cases $G_e = Z_2 \times Z_4$ and $G_e = Z_4 \times Z_4$ in our discussion.[3]

[3]We do not discuss all possible types of $Z_2 \times Z_4$ and $Z_4 \times Z_4$ subgroups, but only those in which the Z_4 group alone is not sufficient to distinguish the three generations of leptons.

Mixing patterns with $G_\nu = Z_2 \times Z_2$ and $G_e = Z_3$

We first discus the case where the neutrino sector is invariant under a Klein group and the charged lepton sector under an element of order 3. The generated mixing pattern reads

$$||U_{\rm PMNS}|| = \frac{1}{\sqrt{3}} \begin{pmatrix} \frac{1}{2}(\sqrt{3}+1) & 1 & \frac{1}{2}(\sqrt{3}-1) \\ 1 & 1 & 1 \\ \frac{1}{2}(\sqrt{3}-1) & 1 & \frac{1}{2}(\sqrt{3}+1) \end{pmatrix} \approx \begin{pmatrix} 0.789 & 0.577 & 0.211 \\ 0.577 & 0.577 & 0.577 \\ 0.211 & 0.577 & 0.789 \end{pmatrix}. \tag{3.33}$$

This leads to the following mixing angles: $\sin^2\theta_{13} = \frac{2-\sqrt{3}}{6} \approx 0.045$ and $\sin^2\theta_{12} = \sin^2\theta_{23} = \frac{8-2\sqrt{3}}{13} \approx 0.349$. Alternatively, the second and third row can be exchanged, giving $\sin^2\theta_{23} = \frac{5+2\sqrt{3}}{13} \approx 0.651$ instead. The fact that this pattern is close to the data, including a prediction for non-zero reactor mixing angle, makes the pattern very interesting. It is discussed in more detail in section 3.4. We refer to the two sets of mixing angles here as `M2` and `M1` respectively. A viable choice of G_e and G_ν leading to this pattern is $G_e = C_1$ and $G_\nu = K_1$.

It is interesting to note that this mixing pattern can also be realized when the flavour group is S_4, although this does not happen when neutrinos are Majorana particles and thus required to satisfy $G_\nu = Z_2 \times Z_2$. If neutrinos are instead Dirac particles, $G_\nu = Z_4$ may be chosen. Together with any choice for a Z_3 subgroup as residual symmetry in the lepton sector, the pattern `M1` or `M2` follows.

Mixing patterns with $G_\nu = Z_2 \times Z_2$ and $G_e = Z_8$

If the original group $\Delta(96)$ is generated through the elements of G_e and G_ν, the resulting mixing pattern is bimaximal, see equation (3.23). One possible choice of G_e and G_ν is $G_e = O_1$ and $G_\nu = K_1$.

Mixing patterns with $G_\nu = Z_2 \times Z_2$ and $G_e = Z_2 \times Z_4$

As discussed above, we also consider the Z_4 subgroup contained in G_e to be one of the subgroups which are represented by matrices with degenerate eigenvalues (Q_1, Q_2 or Q_3) for the irreducible faithful triplet. These are only sufficient to describe the charged leptons when combined with an additional Z_2-group. The mixing pattern that arises if all our requirements are passed, is again the bi-maximal one of equation (3.23). An example of G_e and G_ν is $G_e = V_1 \times Q_1$ and $G_\nu = K_1$.

Three cases that do not generate the full group $\Delta(96)$

Lastly, we study the cases where G_ν is given by a Klein group and G_e is given by either

- a Z_4 group, but not Q_1, Q_2 or Q_3 (that have degenerate eigenvalues),
- a Klein group $Z_2 \times Z_2$ or
- a product $Z_4 \times Z_4$, where the each of the Z_4 groups is given by one of Q_1, Q_2 or Q_3 .

None of the possible choices allows us to generate the original group $\Delta(96)$ using the elements of the subgroups G_e and G_ν.

3.3.6 The subgroup $\Delta(384)$ of Γ_{16}

The last group we consider in this chapter is Γ_{16}. Just like Γ_8, none of the three-dimensional representations is faithful. The eight triplets in table 3.7 instead generate a subgroup of order 384. Like the group of the previous section, it is part of the series $\Delta(6n^2)$, this time with $n = 8$.

The group $\Delta(384)$ has 24 conjugacy classes and a total of 145 Z_n subgroups as given in the appendix. As not only the Z_2 elements, but also some of the Z_4 and Z_8 elements have degenerate eigenvalues, candidates for G_e also include $Z_4 \times Z_2$, $Z_4 \times Z_4$, $Z_4 \times Z_8$, $Z_8 \times Z_2$ and $Z_8 \times Z_8$. In these cases, the order 4 and 8 elements should come from Q_{1-3} and O_{1-3}.

The matrix representations for the elements S and T that can generate the group $\Delta(384)$ are given in table 3.7. The elements S and T satisfy four non-trivial relations

$$S^2 = (ST)^3 = T^{16} = (ST^{-1}ST)^3 = 1 \; . \tag{3.34}$$

We observe that the eight faithful triplets of table 3.7 come in two groups of four, where the matrices in each group are related by an overall sign change and/or complex conjugation. The two groups are related by observing that if one set of S and T matrices satisfies the presentation (3.34), then so does any odd power of it, smaller than 16.

In the following, we calculate the mixing patterns that follow when G_ν is taken to be a Klein group and G_e is a Z_n-group, a Klein group or any of the product groups mentioned above.

Mixing patterns with $G_\nu = Z_2 \times Z_2$ and $G_e = Z_3$

The case we discuss is the one where the neutrino sector is invariant under a Klein group and the charged lepton sector under an element of order 3. The generated mixing pattern reads

$$\begin{aligned} ||U_{\rm PMNS}|| &= \frac{1}{\sqrt{3}} \begin{pmatrix} \frac{1}{2}\sqrt{4+\sqrt{2}+\sqrt{6}} & 1 & \frac{1}{2}\sqrt{4-\sqrt{2}-\sqrt{6}} \\ \frac{1}{2}\sqrt{4+\sqrt{2}-\sqrt{6}} & 1 & \frac{1}{2}\sqrt{4-\sqrt{2}+\sqrt{6}} \\ \sqrt{1-\frac{1}{\sqrt{2}}} & 1 & \sqrt{1+\frac{1}{\sqrt{2}}} \end{pmatrix} \\ &\approx \begin{pmatrix} 0.810 & 0.577 & 0.107 \\ 0.497 & 0.577 & 0.648 \\ 0.312 & 0.577 & 0.754 \end{pmatrix} \; . \end{aligned} \tag{3.35}$$

With the ordering chosen in eq. (3.35), the mixing angles are

$$\begin{aligned} \sin^2\theta_{13} &= \frac{4-\sqrt{2}-\sqrt{6}}{12} \approx 0.011 \; , \\ \sin^2\theta_{12} &= \frac{4}{8+\sqrt{2}+\sqrt{6}} \approx 0.337 \; , \\ \sin^2\theta_{23} &= \frac{4-\sqrt{2}+\sqrt{6}}{8+\sqrt{2}+\sqrt{6}} \approx 0.424 \; . \end{aligned} \tag{3.36}$$

If we exchange the second and third rows in $U_{\rm PMNS}$, the atmospheric mixing changes to

$$\sin^2\theta_{23} = \frac{4+2\sqrt{2}}{8+\sqrt{2}+\sqrt{6}} \approx 0.576 \; . \tag{3.37}$$

We observe that CP is conserved in both cases. We refer to these two patterns as `M3` and `M4`. Both patterns are very close to the data, with interestingly, `M3` favoured by the global neutrino fit [24] and `M4` by the fit [27,28]. Similar to the case where the mixing patterns `M1` and `M2` could be generated by S_4 instead of $\Delta(96)$ if neutrinos are Dirac particles, we find that these patterns can also be generated by the 'simpler' group $\Delta(96)$ if the neutrino are allowed to be Dirac particles invariant under a Z_3 symmetry and charged leptons under a Z_8 symmetry.

Mixing patterns with $G_\nu = Z_2 \times Z_2$ and $G_e = Z_{16}$

We now study mixing patterns where the neutrinos are invariant under a Klein group and the charged leptons under one of the Z_{16} groups. It is possible to generate the full group $\Delta(384)$ for instance with K_2 and Y_1. The mixing pattern that follows is the bimaximal mixing pattern (3.23)

Mixing patterns with $G_\nu = Z_2 \times Z_2$ and $G_e = Z_8 \times Z_2$

When the charged lepton sector is invariant under a $Z_8 \times Z_2$ group, with the Z_8 either O_1, O_2 or O_3, the full group $\Delta(384)$ is generated for instance if $G_e = O_1 \times V_2$ and $G_\nu = K_1$. The resulting mixing pattern is the familiar bimaximal one of equation (3.23).

Cases that do not generate the full group $\Delta(384)$

There are seven additional cases where G_e is in accordance with the requirements set in this section. When combined with any G_ν that is a Klein group, it is not possible to recover the complete group $\Delta(384)$. These cases are

- G_e is a Z_4 subgroup, unequal to Q_1, Q_2 or Q_3,
- G_e is a Z_8 subgroup, unequal to O_1, O_2 or O_3,
- G_e is a Klein group,
- G_e is a product group $Z_4 \times Z_2$, with the Z_4 factor given by either Q_1, Q_2 or Q_3,
- G_e is a product group $Z_4 \times Z_4$, with both Z_4 factors from Q_{1-3},
- G_e is a product group $Z_4 \times Z_8$, with the Z_4 factor from Q_{1-3} and the Z_8 factor from O_{1-3} or
- G_e is a product group $Z_8 \times Z_8$ with both Z_8 factors from O_{1-3}.

This concludes all cases where the residual symmetry in the neutrino sector is a Klein group. There is one pattern that does not respect this rule, but that might be worth mentioning.

$$V = \begin{pmatrix} \cos\pi/16 & \sin\pi/16 & 0 \\ -\sin\pi/16 & \cos\pi/16 & 0 \\ 0 & 0 & 1 \end{pmatrix} \approx \begin{pmatrix} 0.981 & 0.195 & 0 \\ -0.195 & 0.981 & 0 \\ 0 & 0 & 1 \end{pmatrix} . \tag{3.38}$$

This can be produced by a number of residual subgroups, including Z_4 and Z_4 (e.g. Q_1 and Q_{18}); Z_4 and Z_8 (e.g. Q_1 and O_{24}); Z_4 and Z_16 (e.g. Q_4 and Y_{12}); Z_8 and Z_8 (e.g. O_1 and O_{24}) and, lastly, Z_8 and Z_{16} (e.g. O_{24} and Y_{12}). Obviously, this is not a valuable pattern for neutrinos, but it might be relevant for quarks. If the two residual subgroups are those of the up- and down-quark sectors, the result is quite close to the CKM matrix. In a first approximation, one angle slightly smaller than the Cabibbo angle is generated. Subleading corrections may lead to the two other angles and possibly to very small effects on the neutrino mixing matrix. In the spirit of this chapter, we refrain from giving a more concrete model building realization. This is likely to be quite complicated, as now there are different residual symmetries in all four sectors (charged leptons, neutrinos, up and down quarks). In a realization with flavons, preventing them to couple to the wrong sectors is likely to be non-trivial.

3.4 Four interesting mixing patterns

In this section we comment on the four mixing patterns `M1` to `M4`. All of these points are close to the current data on the neutrino mixing angles as shown already in table 3.1 at the beginning of this chapter and as graphically illustrated in figure 3.1.

Both (pairs of) mixing patterns appeared when $G_\nu = Z_2 \times Z_2$ and $G_e = Z_3$ was chosen for a group of the type $\Delta(6n^2)$. When these two subgroups are chosen in $\Delta(24) \sim S_4$ one gets the tribimaximal

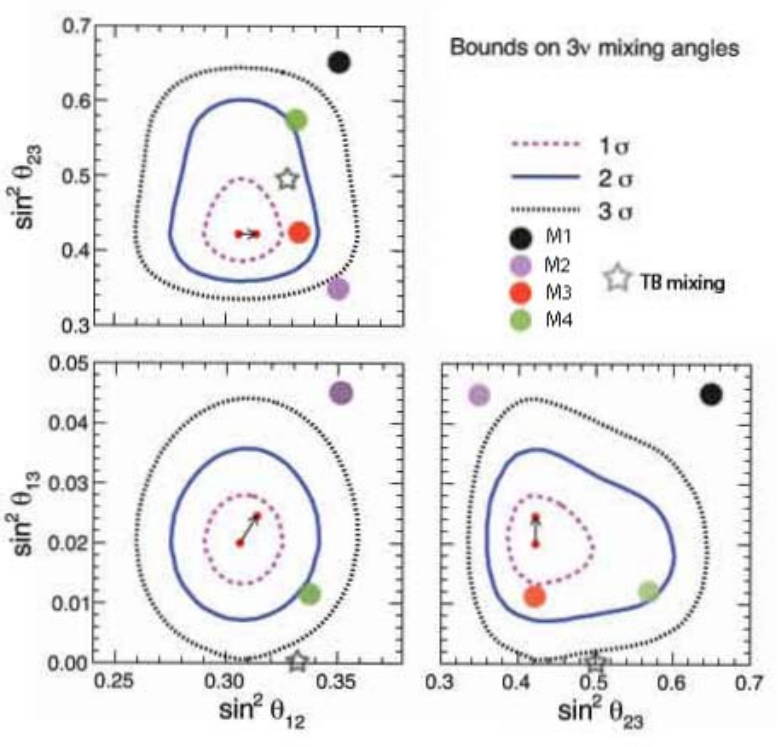

Figure 3.1: *Values of* $\sin^2\theta_{ij}$ *for the four different mixing patterns* `M1` *(black),* `M2` *(violet),* `M3` *(red) and* `M4` *(green) as well as the tribimaximal mixing pattern (star). The contours show the* 1σ *(pink dashed line),* 2σ *(blue solid line) and* 3σ *(black dotted line) levels and are taken from [24]. The small dots indicate the best fit values of the mixing angles and the arrows the effect of the new estimates of the reactor antineutrino flux. Note that in the* $\sin^2\theta_{12}$-$\sin^2\theta_{13}$ *plane the points of* `M1` *and* `M2` *as well as of* `M3` *and* `M4` *lie on top of each other, since they only differ in the value of* $\sin^2\theta_{23}$.

mixing pattern given by equation (3.22), or, with the phases reintroduced in the standard way by

$$U_{\rm TBM} = \begin{pmatrix} \sqrt{\frac{2}{3}} & \frac{1}{\sqrt{3}} & 0 \\ -\frac{1}{\sqrt{6}} & \frac{1}{\sqrt{3}} & \frac{1}{\sqrt{2}} \\ -\frac{1}{\sqrt{6}} & \frac{1}{\sqrt{3}} & -\frac{1}{\sqrt{2}} \end{pmatrix} \tag{3.39}$$

The two new patterns are quite similar to tribimaximal mixing. This can be seen from the fact that also these patterns can be brought into a form in which the second column has three entries equal to $1/\sqrt{3}$. Indeed, the TBM mixing matrix can be modified by a rotation in the $(1\ 3)$ plane acting from the right

$$U_{\rm PMNS} = U_{\rm TBM} U_{13}(\alpha) \qquad \text{with} \qquad U_{13}(\alpha) = \begin{pmatrix} \cos\alpha & 0 & \sin\alpha \\ 0 & 1 & 0 \\ -\sin\alpha & 0 & \cos\alpha \end{pmatrix} \quad . \tag{3.40}$$

It is immediate to show that, by taking $\alpha = -\pi/12$ and $\alpha = \pi/24$, the resulting mixing matrices are identical, in absolute value, to the matrices in equations (refeq:mixD96) and (3.35), respectively. Such perturbations from TB mixing with α arbitrary have been already discussed in the literature [91–96]. For generic α, the mixing angles read

$$\sin^2\theta_{12} = \frac{1}{2+\cos 2\alpha}\ , \quad \sin^2\theta_{23} = \frac{1}{2} - \frac{\sqrt{3}\sin 2\alpha}{4+2\cos 2\alpha}\ , \quad \sin^2\theta_{13} = \frac{2}{3}\sin^2\alpha\ . \tag{3.41}$$

For small α, we can expand the results

$$\sin^2\theta_{12} \approx \frac{1}{3} + \frac{2\alpha^2}{9}\,, \quad \sin^2\theta_{23} \approx \frac{1}{2} - \frac{\alpha}{\sqrt{3}}\,, \quad \sin^2\theta_{13} \approx \frac{2\alpha^2}{3} \tag{3.42}$$

showing that the deviation from the value of TB mixing of $\sin^2\theta_{12}$, the best measured quantity among the three mixing angles, is quadratic in α, whereas the leading correction to $\sin^2\theta_{23} = 1/2$ is linear in α, allowing reasonably large deviations from its maximal value as indeed still allowed by the data.

3.5 Conclusions of the chapter

Recent results of the T2K experiment and of a global fit of the neutrino oscillation data point to non-vanishing θ_{13} at the 3σ level. The best fit value of θ_{13} is around $0.15 \div 0.16$, smaller than the ones of the other angles, but much larger than 0.02, the 1σ experimental error on the solar angle θ_{12}. If future data confirm this result, many models giving rise at LO to mixing patterns with vanishing θ_{13}, such as TB mixing, become disfavoured, because corrections, expected in these models, generically lead to too small θ_{13}.

A particular elegant mechanism to produce simple mixing patterns is based on discrete flavour symmetries. The latter are broken in a non-trivial way and as a consequence give rise to mixing angles whose values only depend on the properties of the flavour symmetry, but not on lepton masses. After the T2K data the natural question is whether such symmetries still remain a valuable tool to describe flavour mixing. In the beginning of the chapter we have given four possible answers to this question, ranging from 'probably not' to 'possible with the right types of flavour symmetries'.

In this chapter we have scanned a large category of candidate flavour-symmetries. The discrete flavour group G_f is chosen to be a modular subgroup Γ_N or, in specific cases a subgroup hereof. G_f is supposed to be broken in such a way that the relevant mass matrices m_ν and $m_e^\dagger m_e$ have a residual invariance under the subgroups G_ν and G_e, respectively. The lepton mixing matrix originates from the mismatch of these two subgroups and from their specific embedding into G_f. We rediscovered the lepton mixing matrices that correspond to tribimaximal mixing, bimaximal mixing and the golden ratio mixing from the 'smaller' groups A_4, S_4 and A_5 in the list of G_f. The group $PSL(2,7)$ generates several mixing patterns, but none of them is particularly close to the data given by neutrino oscillations. The groups $\Delta(96)$ and $\Delta(384)$ provide us with two (or four if a degeneracy is taken into account) very interesting mixing patterns. In particular the pattern reproduced by $\Delta(384)$ is remarkably close to their experimental best fit values. More precise measurements are expected to show if the agreement between the patterns and the data are just coincidental or if they might be related by a deeper mechanism. If the latter is the case, the first thing on a theorist's to-do list should obviously be a concrete model that derives these mixing angles and generates some additional predictions.

Appendices to chapter 3

In the previous chapter, we studied six groups of the type Γ_N. The groups A_4 and S_4, corresponding respectively to $N = 4$ and $N = 5$, occur at many other places in this thesis. In the first two appendices here, we carefully derive their group theoretical properties. In the third appendix, we list some properties of the other finite modular groups under discussion, A_5, $PSL(2,7)$, $\Delta(96)$ and $\Delta(384)$.

3.A The alternating group A_4

The group A_4 is the group of even permutations of four elements. It thus has $4!/2 = 12$ elements. A general permutation of them can be seen as a mapping $p : i \mapsto p(i)$, with $i = 1 \cdots 4$. The mappings can be represented as

$$p = \begin{pmatrix} 1 & 2 & 3 & 4 \\ p(1) & p(2) & p(3) & p(4) \end{pmatrix} . \tag{3.A.1}$$

This is often simply represented as $p = \big(p(1),\ p(2),\ p(3),\ p(4)\big)$. With only four elements, only a limited number of structures is available for permutations. Apart from the identity, these are transpositions, double transpositions, three-cycles and four-cycles.

A transposition is the interchange of two elements, while leaving the other two elements inert. The interchange of i_1 and i_2 is represented as $i_1 \mapsto i_2 \mapsto i_1$ or as $(i_1,\ i_2)$ in the so-called cycle notation. A single transposition is obviously an odd permutation, so it is not an element of A_4, but it is an important building block for permutations that are in A_4.

A double transpositions, the combined and unrelated interchange of two pairs of elements is an even permutation and thus an element of A_4. They can be represented as $i_1 \mapsto i_2 \mapsto i_1$ and $i_3 \mapsto i_4 \mapsto i_3$ or simply as $(i_1,\ i_2)\ (i_3,\ i_4)$. With four elements present, there are three double transpositions, one for each of the three ways to pair the numbers 1 to 4. Obviously (double) transpositions square to the identity, giving an important property of these transformations.

The third type are three-cycles $i_1 \mapsto i_2 \mapsto i_3 \mapsto i_1$, while the fourth element i_4 is inert. This is also written as $(i_1,\ i_2,\ i_3)$. A three-cycle can be seen as a combination of two transpositions, for instance as $(i_1,\ i_3) \circ (i_1,\ i_2)$. There are eight three-cycles in A_4: there are four ways to pick the three elements (there are four choices for the single element that has to be left out) and each of these gives rise to two three-cycles, one being the square of the other. The third power of any element gives the identity. Four-cycles lastly, can be written as the product of three transpositions and as such are no elements of A_4.

We can call one of the double transpositions S and one of the three-cycles T. It follows that all elements of A_4 can be written as simple combinations of S and T. It is in particular relevant to mention that the element ST is a three-cycle and as such satisfies $(ST)^3 = 1$. In table 3.A.1 we mention the 12 elements of A_4 in permutation notation, in cycle notation and as a product of S and T.

Permutation	Cycle	$f[S,\ T]$	Order	Class
(1, 2, 3, 4)	-	$\mathbb{1}$	1	E
(1, 3, 4, 2)	(2, 3, 4)	$(ST)^2$	3	$4C_3^{(2)}$
(1, 4, 2, 3)	(2, 4, 3)	ST	3	$4C_3^{(1)}$
(2, 1, 4, 3)	(1, 2) (3, 4)	S	2	$3C_2$
(2, 3, 1, 4)	(1, 2, 3)	T	3	$4C_3^{(1)}$
(2, 4, 3, 1)	(1, 2, 4)	$(STS)^2$	3	$4C_3^{(2)}$
(3, 1, 2, 4)	(1, 3, 2)	T^2	3	$4C_3^{(2)}$
(3, 2, 4, 1)	(1, 3, 4)	TS	3	$4C_3^{(1)}$
(3, 4, 1, 2)	(1, 3) (2, 4)	T^2ST	2	$3C_2$
(4, 1, 3, 2)	(1, 4, 2)	STS	3	$4C_3^{(1)}$
(4, 2, 1, 3)	(1, 4, 3)	$(TS)^2$	3	$4C_3^{(2)}$
(4, 3, 1, 2)	(1, 4) (2, 3)	ST^2ST	2	$3C_2$

Table 3.A.1: *The 12 elements of A_4 with their permutation and cycle notation; the way to write them in S and T; the order and the class they belong to.*

In the discussion above, the group A_4 works on four abstract points. A very natural interpretation is possible, where the four points $(1,\ 2,\ 3,\ 4)$ are the four vertices of a tetrahedron. An operation $i_1 \mapsto i_2 \cdots$ represents the corresponding interchange of the vertices. Even permutations of the four vertices are exactly the rotations that leave the tetrahedron invariant, while odd permutations represent reflections.

We define S as the double transposition (1, 2) (3, 4) that interchanges vertices 1 and 2 as well as 3 and 4. It can be represented by a rotation over $180°$ over the axis connecting the middles of the edges 1-2 and 3-4. The three-cycle T is defined as the anti-clockwise rotation over $120°$ in the 1-2-3 plane, leaving vertex 4 invariant. This is shown in figure 3.A.1

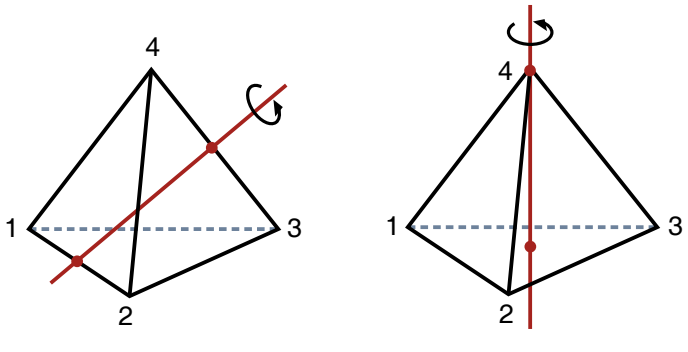

Figure 3.A.1: *The generating elements S and T of A_4.*

In section 3.3.1 we calculated the conjugacy classes of A_4. The group has four classes: E containing the identity, $3C_2$ containing the three elements of order 2 (including S) and two classes $4C_3$ and $4C_3'$ with order 3 elements (one containing T and the other T^2). The order and the conjugacy class any element belongs to are also given in table 3.A.1. For finite groups, the number of irreducible representations (irreps) up to equivalence is equal to the number of classes. Their dimensions are

related to the order of the group according to

$$\sum_{a\in I} d_a^2 = \text{order(G)} \tag{3.A.2}$$

Because A_4 has four classes, it should also have four irreps. The only way to satisfy equation (3.A.2) is if three of them have dimension 1 and one has dimension 3. The irreps of A_4 can thus be characterized as $\mathbf{1}$, $\mathbf{1}'$, $\mathbf{1}''$ and $\mathbf{3}$.

Next we construct the character table. We use the following requirements

- In the trivial representation, all elements are represented as 1.
- The identity operation, contained in the class E is represented by the number 1 for all three one-dimensional representations and by the (3×3) identity matrix (with trace 3) for the three-dimensional representation
- The elements of $3C_2$ should be represented by $+1$ or -1 in the irreps $\mathbf{1}'$ and $\mathbf{1}''$ since they square to the identity.
- The elements of $4C_3$ and $4C_3'$ should be represented by 1, $\omega \equiv e^{2\pi i/3}$ or ω^2 in the irreps $\mathbf{1}'$ and $\mathbf{1}''$ as the identity is their third power.
- The irreps satisfy an orthonormality relation:

$$\frac{1}{\text{order(G)}}\sum_{i\in G}\chi^I(i)\big(\chi^J(i)\big)^* = \delta^{IJ}\ .$$

  Here $\chi^I(i)$ stands for the character of the element i in the irreducible representation I.

When we apply these conditions, there are just two character tables possible. One of them is given in table 3.A.2; the other simply has the irreps $1'$ and $1''$ interchanged[4].

	E	$3C_2$ (containing S)	$4C_3$ (containing T)	$4C_3'$ (containing T^2)
$\mathbf{1}$	1	1	1	1
$\mathbf{1}'$	1	1	ω	ω^2
$\mathbf{1}''$	1	1	ω^2	ω
$\mathbf{3}$	3	-1	0	0

Table 3.A.2: *The character table of A_4.*

Two explicit representations are popular in the literature. In the representation of Ma and Rajasekaran (MR) [97], the element S is diagonal in the three-dimensional representation. It has the further advantage that all elements are represented by real matrices in the triplet representation. In the basis of Altarelli and Feruglio (AF) [10,11] the element T is chosen diagonal (and complex). The representations of S and T in the various irreducible representations and in the bases of MR and AF are given in table 3.A.3. Both representations are used in this thesis: the AF representation in chapters 2 and 3 and the MR representation in chapter 5.

The bases of Ma and Rajasekaran and of Altarelli and Feruglio are related by a basis transformation

$$M_{\text{MR}} = \Omega^\dagger M_{\text{AF}}\Omega\,, \qquad \Omega = \frac{1}{\sqrt{3}}\begin{pmatrix}1 & 1 & 1\\ 1 & \omega & \omega^2\\ 1 & \omega^2 & \omega\end{pmatrix}\ . \tag{3.A.3}$$

[4] In the original definition of Altarelli and Feruglio [11] the opposite definition for $1'$ and $1''$ is chosen. The 'Altarelli-Feruglio basis' given below is therefore not the original one, but it shares the most important property, namely that the T matrix is diagonal in the triplet representation.

Irrep	Ma and Rajasekaran		Altarelli and Feruglio	
$\mathbf{1}$	$S=1$	$T=1$	$S=1$	$T=1$
$\mathbf{1'}$	$S=1$	$T=\omega$	$S=1$	$T=\omega$
$\mathbf{1''}$	$S=1$	$T=\omega^2$	$S=1$	$T=\omega^2$
$\mathbf{3}$	$S=\begin{pmatrix}1&0&0\\0&-1&0\\0&0&-1\end{pmatrix}$	$T=\begin{pmatrix}0&1&0\\0&0&1\\1&0&0\end{pmatrix}$	$S=\begin{pmatrix}-1&2&2\\2&-1&2\\2&2&-1\end{pmatrix}$	$T=\begin{pmatrix}1&0&0\\0&\omega^2&0\\0&0&\omega\end{pmatrix}$

Table 3.A.3: *The generating elements S and T of A_4 in the bases of Ma and Rajasekaran and of Altarelli and Feruglio.*

The multiplication rules for A_4 can be constructed from the character table by demanding that the characters satisfy the multiplication rules. We find

$$\begin{aligned}
&1 \times r = r \text{ for all representations } r,\\
&1' \times 1' = 1'', \quad 1'' \times 1'' = 1, \quad 1' \times 1'' = 1,\\
&1' \times 3 = 3, \quad 1'' \times 3 = 3,\\
&3 \times 3 = 1 + 1' + 1'' + 3 + 3.
\end{aligned} \tag{3.A.4}$$

In the last product, one of the resulting triplets can be chosen to be symmetric and the other to be antisymmetric in the elements of the original triplets.

Lastly, we construct the Clebsch-Gordan (CG) coefficients of the products above. We use α_i to indicate the elements of the first representation of the product and β_j to indicate those of the second representation. The products are then linear in α_i and β_j. The coefficients follow from the requirement that the products (3.A.4) 'commute' with S and T transformations. For instance if $(\alpha \times \beta)_{1'}$ indicates the $1'$ in the product 3×3, we should have $\big((T_3\alpha) \times (T_3\beta)\big)_{1'} = T_{1'}(\alpha \times \beta)_{1'}$. All results are given in table 3.A.4.

The calculation of the Clebsch-Gordan coefficients concludes this appendix. The multiplication rules and the CG coefficients of A_4 are the starting point for the analyses in the main chapters of this thesis.

	Ma-Rajasekaran	Altarelli-Feruglio
$1 \times r = r$	r	r
$1' \times 1' = 1''$	$\alpha\beta$	$\alpha\beta$
$1' \times 1'' = 1$	$\alpha\beta$	$\alpha\beta$
$1'' \times 1'' = 1'$	$\alpha\beta$	$\alpha\beta$
$1' \times 3 = 3$	$\alpha(\beta_1,\ \omega\beta_2,\ \omega^2\beta_3)$	$\alpha(\beta_3,\ \beta_1,\ \beta_2)$
$1'' \times 3 = 3$	$\alpha(\beta_1,\ \omega^2\beta_2,\ \omega\beta_3)$	$\alpha(\beta_2,\ \beta_3,\ \beta_1)$
$3 \times 3 \ni 1$	$\alpha_1\beta_1 + \alpha_2\beta_2 + \alpha_3\beta_3$	$\alpha_1\beta_1 + \alpha_2\beta_3 + \alpha_3\beta_2$
$3 \times 3 \ni 1'$	$\alpha_1\beta_1 + \omega^2\alpha_2\beta_2 + \omega\alpha_3\beta_3$	$\alpha_1\beta_2 + \alpha_2\beta_1 + \alpha_3\beta_3$
$3 \times 3 \ni 1''$	$\alpha_1\beta_1 + \omega\alpha_2\beta_2 + \omega^2\alpha_3\beta_3$	$\alpha_1\beta_3 + \alpha_2\beta_2 + \alpha_3\beta_1$
$3 \times 3 \ni 3_S$	$\frac{1}{2}\begin{pmatrix}\alpha_2\beta_3 + \alpha_3\beta_2\\ \alpha_1\beta_3 + \alpha_3\beta_1\\ \alpha_1\beta_2 + \alpha_2\beta_1\end{pmatrix}$	$\frac{1}{3}\begin{pmatrix}2\alpha_1\beta_1 - \alpha_2\beta_3 - \alpha_3\beta_2\\ -\alpha_1\beta_2 - \alpha_2\beta_1 + 2\alpha_3\beta_3\\ -\alpha_1\beta_3 + 2\alpha_2\beta_2 - \alpha_3\beta_1\end{pmatrix}$
$3 \times 3 \ni 3_{AS}$	$\frac{1}{2}\begin{pmatrix}\alpha_2\beta_3 - \alpha_3\beta_2\\ -\alpha_1\beta_3 + \alpha_3\beta_1\\ \alpha_1\beta_2 - \alpha_2\beta_1\end{pmatrix}$	$\frac{1}{2}\begin{pmatrix}\alpha_2\beta_3 - \alpha_3\beta_2\\ \alpha_1\beta_2 - \alpha_2\beta_1\\ -\alpha_1\beta_3 + \alpha_3\beta_1\end{pmatrix}$

Table 3.A.4: *The Clebsch-Gordan coefficients for A_4 in the two bases used in this thesis, when α_i and β_j represent the elements of the terms of the product.*

3.B The symmetric group S_4

The group S_4 is the group of all permutations of 4 elements. It has 24 elements that are of order 1, 2, 3 and 4. The irreps are of one-dimensional (twice), two-dimensional (once) and three-dimensional (twice). We denote the two one-dimensional irreps as $\mathbf{1_1}$ and $\mathbf{1_2}$ instead as $\mathbf{1}$ and $\mathbf{1'}$ to use the common notation in S_4 models. The details of the classes and irreps can be calculated in the same way as in the previous section. This is summarized in the extended character table 3.B.1.

Class	χ_{1_1}	χ_{1_2}	χ_2	χ_{3_1}	χ_{3_2}	Elements
E	1	1	2	3	3	$\mathbb{1}$
$3C_2$	1	1	2	-1	-1	T^2, ST^2S, ST^2ST^2
$6C_2$	1	-1	0	1	-1	$S, T^3ST, TST^3, T^2ST^2, ST^2ST, TST^2S$
$8C_3$	1	1	-1	0	0	$TS, ST, (TS)^2, (ST)^2, T^2ST, TST^2, T^3ST^2, T^2ST^3$
$6C_4$	1	-1	0	-1	1	$T, T^3, ST^2, T^2S, STS, TST$

Table 3.B.1: *Character table of the S_4 discrete group. In the last column we have reported the elements for each class in terms of the generators S and T of the group.*

As for A_4, all elements can be generated as by two elements, S of order 2 and T of order 4 that satisfy $(ST)^3 = \mathbb{1}$. S_4 is also the symmetry group of the octahedron. S, T and ST can the be represented respectively by a rotation over $180°$ on an axis through two opposing edges; a rotation of 90 degrees on an axis through the centres of two opposing faces and a rotation over $180°$ on an axis through two opposite vertices as given in figure 3.B.1

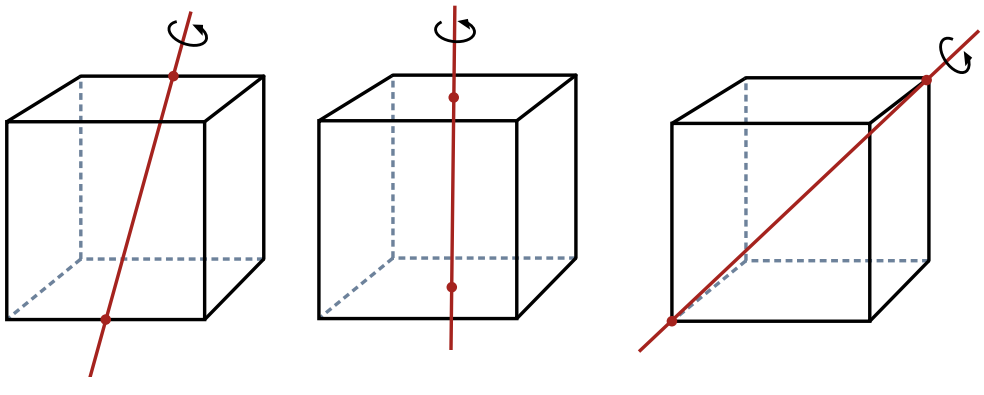

Figure 3.B.1: *Graphical representation of the elements S, T and ST of S_4.*

Many matrix representations can be used for S_4. In chapter 4 we choose a representation in which neither S nor T is diagonal in the three dimensional representations. We present this basis as well as S and T diagonal bases in table 3.B.2. There we also report the matrices that diagonalize our S and T elements according to $M_{\text{chap4}} = \Omega^\dagger_{2,S,T} M_{2;S,T-\text{diag}} \Omega_{2,S,T}$.

The product rules can be constructed from the character table. They read

$$\begin{aligned}
&1 \times r = r \text{ for all representations } r, \\
&1_2 \times 1_2 = 1_1\,, \quad 1_2 \times 2 = 2\,, \quad 1_2 \times 3_1 = 3_2\,, \quad 1_2 \times 3_2 = 3_1\,, \\
&2 \times 2 = 1_1 + 1_2 + 2\,, \quad 2 \times 3_1 = 3_1 + 3_2\,, \quad 2 \times 3_2 = 3_1 + 3_2\,, \\
&3_1 \times 3_1 = 3_2 \times 3_2 = 1_1 + 2 + 3_1 + 3_2\,, \quad 3_1 \times 3_2 = 1_2 + 2 + 3_1 + 3_2\,.
\end{aligned} \tag{3.B.1}$$

For each of the bases the Clebsch-Gordan rules can be calculated. We report those for the basis used in chapter 4 in table 3.B.3.

Irrep	Basis of chapter 4		
$\mathbf{1_1}$	$S=1$	$T=1$	
$\mathbf{1_2}$	$S=-1$	$T=-1$	
$\mathbf{2}$	$S=\frac{1}{2}\begin{pmatrix}1&\sqrt{3}\\ \sqrt{3}&-1\end{pmatrix}$	$T=\begin{pmatrix}-1&0\\ 0&1\end{pmatrix}$	
$\mathbf{3_1}$	$S=\begin{pmatrix}0&0&-1\\ 0&1&0\\ -1&0&0\end{pmatrix}$	$T=\begin{pmatrix}-1&0&0\\ 0&0&-1\\ 0&1&0\end{pmatrix}$	
$\mathbf{3_2}$	$S=\begin{pmatrix}0&0&1\\ 0&-1&0\\ 1&0&0\end{pmatrix}$	$T=\begin{pmatrix}1&0&0\\ 0&0&1\\ 0&-1&0\end{pmatrix}$	

Irrep	S-diagonal basis		Diagonalizing matrix
$\mathbf{1_1}$	$S=1$	$T=1$	
$\mathbf{1_2}$	$S=-1$	$T=-1$	
$\mathbf{2}$	$S=\begin{pmatrix}-1&0\\ 0&1\end{pmatrix}$	$T=\frac{1}{2}\begin{pmatrix}1&\sqrt{3}\\ \sqrt{3}&-1\end{pmatrix}$	$\Omega_2=\frac{1}{2}\begin{pmatrix}-1&\sqrt{3}\\ \sqrt{3}&1\end{pmatrix}$
$\mathbf{3_1}$	$S=\begin{pmatrix}1&0&0\\ 0&1&0\\ 0&0&-1\end{pmatrix}$	$T=\frac{1}{2}\begin{pmatrix}0&-\sqrt{2}&-\sqrt{2}\\ \sqrt{2}&-1&1\\ \sqrt{2}&1&-1\end{pmatrix}$	$\Omega_S=\frac{1}{\sqrt{2}}\begin{pmatrix}0&-1&1\\ \sqrt{2}&0&0\\ 0&1&1\end{pmatrix}$
$\mathbf{3_2}$	$S=\begin{pmatrix}-1&0&0\\ 0&-1&0\\ 0&0&1\end{pmatrix}$	$T=\frac{1}{2}\begin{pmatrix}0&\sqrt{2}&\sqrt{2}\\ -\sqrt{2}&1&-1\\ -\sqrt{2}&-1&1\end{pmatrix}$	$''$

Irrep	T-diagonal basis		Diagonalizing matrix
$\mathbf{1_1}$	$S=1$	$T=1$	
$\mathbf{1_2}$	$S=-1$	$T=-1$	
$\mathbf{2}$	$S=\frac{1}{2}\begin{pmatrix}1&\sqrt{3}\\ \sqrt{3}&-1\end{pmatrix}$	$T=\begin{pmatrix}-1&0\\ 0&1\end{pmatrix}$	
$\mathbf{3_1}$	$S=\frac{1}{2}\begin{pmatrix}0&-\sqrt{2}&-\sqrt{2}\\ -\sqrt{2}&1&-1\\ -\sqrt{2}&-1&1\end{pmatrix}$	$T=\begin{pmatrix}-1&0&0\\ 0&-i&0\\ 0&0&i\end{pmatrix}$	$\Omega_T=\frac{1}{\sqrt{2}}\begin{pmatrix}\sqrt{2}&0&0\\ 0&-i&i\\ 0&1&1\end{pmatrix}$
$\mathbf{3_2}$	$S=\frac{1}{2}\begin{pmatrix}0&\sqrt{2}&\sqrt{2}\\ \sqrt{2}&-1&1\\ \sqrt{2}&1&-1\end{pmatrix}$	$T=\begin{pmatrix}1&0&0\\ 0&i&0\\ 0&0&-i\end{pmatrix}$	$''$

Table 3.B.2: *The generating elements S and T of S_4 in the basis of chapter 4, and in S- and T-diagonal ones.*

Product rule	Clebsch-Gordan coefficients
$\mathbf{1_1} \times \mathbf{r} = \mathbf{r}$	r
$\mathbf{1_2} \times \mathbf{1_2} = \mathbf{1_1}$	$\alpha\beta$
$\mathbf{1_2} \times \mathbf{2} = \mathbf{2}$	$\begin{pmatrix} -\alpha\beta_2 \\ \alpha\beta_1 \end{pmatrix}$
$\mathbf{1_2} \times \mathbf{3_2} = \mathbf{3_1}$ and $\mathbf{1_2} \times \mathbf{3_1} = \mathbf{3_2}$	$\begin{pmatrix} \alpha\beta_1 \\ \alpha\beta_2 \\ \alpha\beta_3 \end{pmatrix}$
$\mathbf{2} \times \mathbf{2} = \mathbf{1_1}$	$\alpha_1\beta_1 + \alpha_2\beta_2$
$\mathbf{2} \times \mathbf{2} = \mathbf{1_2}$	$\alpha_1\beta_2 - \alpha_2\beta_1$
$\mathbf{2} \times \mathbf{2} = \mathbf{2}$	$\begin{pmatrix} \alpha_1\beta_2 + \beta_1\alpha_2 \\ \alpha_1\beta_1 - \alpha_2\beta_2 \end{pmatrix}$
$\mathbf{2} \times \mathbf{3_1} = \mathbf{3_1}$ and $\mathbf{2} \times \mathbf{3_3} = \mathbf{3_2}$	$\begin{pmatrix} \alpha_1\beta_1 \\ -\frac{1}{2}(\sqrt{3}\alpha_1 + \alpha_2)\beta_2 \\ \frac{1}{2}(\sqrt{3}\alpha_1 - \alpha_2)\beta_3 \end{pmatrix}$
$\mathbf{2} \times \mathbf{3_1} = \mathbf{3_2}$ and $\mathbf{2} \times \mathbf{3_2} = \mathbf{3_1}$	$\begin{pmatrix} \alpha_1\beta_1 \\ -\frac{1}{2}(\alpha_1\sqrt{3}\alpha_2)\beta_2 \\ -\frac{1}{2}(\alpha_1 + \sqrt{3}\alpha_2)\beta_3 \end{pmatrix}$
$\mathbf{3_1} \times \mathbf{3_1} = \mathbf{1_1}$, $\mathbf{3_1} \times \mathbf{3_1} = \mathbf{1_1}$ and $\mathbf{3_1} \times \mathbf{3_2} = \mathbf{1_2}$	$\alpha_1\beta_1 + \alpha_2\beta_2 + \alpha_3\beta_3$
$\mathbf{3_1} \times \mathbf{3_1} = \mathbf{2}$ and $\mathbf{3_2} \times \mathbf{3_2} = \mathbf{2}$	$\begin{pmatrix} \sqrt{3}(-\alpha_2\beta_2 + \alpha_3\beta_3) \\ 2\alpha_1\beta_1 - \alpha_2\beta_2 - \alpha_3\beta_3 \end{pmatrix}$
$\mathbf{3_1} \times \mathbf{3_2} = \mathbf{2}$	$\begin{pmatrix} 2\alpha_1\beta_1 - \alpha_2\beta_2 - \alpha_3\beta_3 \\ \sqrt{3}(\alpha_2\beta_2 - \alpha_3\beta_3) \end{pmatrix}$
$\mathbf{3_1} \times \mathbf{3_1} = \mathbf{3_1}$, $\mathbf{3_1} \times \mathbf{3_2} = \mathbf{3_1}$ and $\mathbf{3_2} \times \mathbf{3_2} = \mathbf{3_2}$	$\begin{pmatrix} \alpha_2\beta_3 + \alpha_3\beta_2 \\ \alpha_1\beta_3 + \beta_3\alpha_1 \\ \alpha_1\beta_2 + \alpha_2\beta_1 \end{pmatrix}$
$\mathbf{3_1} \times \mathbf{3_1} = \mathbf{3_2}$, $\mathbf{3_1} \times \mathbf{3_2} = \mathbf{3_2}$ and $\mathbf{3_2} \times \mathbf{3_2} = \mathbf{3_1}$	$\begin{pmatrix} -\alpha_2\beta_3 + \alpha_3\beta_2 \\ \alpha_1\beta_3 - \beta_3\alpha_1 \\ -\alpha_1\beta_2 + \alpha_2\beta_1 \end{pmatrix}$

Table 3.B.3: *The Clebsch-Gordan coefficients for S_4 in the bases used in chapter 4. Again α_i and β_j represent the elements of the terms of the product.*

3.C Tables of Abelian subgroups for A_5, $PSL(2,7)$, $\Delta(96)$ and $\Delta(384)$

The groups A_5, $PSL(2,7)$, $\Delta(96)$ and $\Delta(384)$ were very important in chapter 3, but they do not reappear in this thesis. Hence we refrain from giving their full group theoretical properties, such as character tables. These can be found in the mathematical and/or physical literature, e.g. [58,75,76,89]. In this appendix we just report the relevant Abelian subgroups of the groups, as these can be used as candidates for G_e and G_ν as described in the chapter.

3.C.1 Abelian subgroups of A_5

The group A_5 has five irreducible representations, namely the trivial singlet, two triplets and one four- and one five-dimensional representation. In the tables below the five conjugacy classes and all relevant subgroups of A_5 are given, together with a typical element or generator of them expressed in the elements S and T. We mention that all subgroups of a certain type are similar to each other.

Class	Typical element
$1\mathcal{C}_1$	E
$15\mathcal{C}_2$	S
$20\mathcal{C}_3$	ST
$12\mathcal{C}_5^{(1)}$	T, T^4
$12\mathcal{C}_5^{(2)}$	T^2, T^3

Table 3.C.1: *Conjugacy classes in* A_5

Subgroup		Generators	Subgroup		Generators
$Z_2 \times Z_2$	K_1	$S, T^2ST^3ST^2$	Z_3	C_1	ST
	K_2	T^4ST, ST^3ST^2S		C_2	TS
	K_3	TST^4, ST^2ST^3S		C_3	TST^3
	K_4	T^2ST^3, ST^2ST		C_4	T^2ST^2
	K_5	T^3ST^2, TST^2S		C_5	T^3ST
Z_5	R_1	T		C_6	ST^3ST
	R_2	ST^2		C_7	ST^2ST^3
	R_3	T^2S		C_8	ST^3ST^2
	R_4	TST		C_9	ST^2ST^4
	R_5	TST^2		C_{10}	ST^2ST^2S
	R_6	T^2ST			

Table 3.C.2: *Generators of Abelian subgroups of* A_5.

3.C.2 Abelian subgroups of $PSL(2,7)$

Apart from the two complex conjugated three-dimensional representations $PSL(2,7)$ has one singlet, one six-, one seven- and one eight-dimensional representation. All classes and relevant subgroups of $PSL(2,7)$ are collected in the tables below. The cyclic subgroups are similar to each other, while the Klein groups can be divided into two categories, where each order-two element is part of both.

Class	Typical element	Class	Typical element
$1\mathcal{C}_1$	E	$21\mathcal{C}_2$	S
$56\mathcal{C}_3$	ST	$42\mathcal{C}_4$	ST^3
$24\mathcal{C}_7^{(1)}$	T, T^2, T^4	$24\mathcal{C}_7^{(1)}$	T^3, T^5, T^6

Table 3.C.3: *Conjugacy classes in* $PSL(2,7)$

Subgroup		Generators	Subgroup		Generators
$Z_2 \times Z_2$	K_1	S, T^2ST^3ST	Z_3	C_1	ST
	K_2	S, TST^3ST^2		C_2	TS
	K_3	$T^4ST^3, T^2ST^4ST^2$		C_3	TST^5
	K_4	T^4ST^3, ST^4ST^3S		C_4	T^2ST^4
	K_5	T^5ST^2, ST^4ST^3S		C_5	T^3ST^3
	K_6	T^2ST^5, ST^3ST^4S		C_6	T^4ST^2
	K_7	T^3ST^4, ST^3ST^4S		C_7	T^5ST
	K_8	$T^3ST^4, T^2ST^4ST^2$		C_8	TST^3S
	K_9	T^6ST, ST^5ST^6		C_9	T^2ST^4S
	K_{10}	TST^6, ST^4ST^4		C_{10}	ST^2ST^5
	K_{11}	T^2ST^5, ST^4ST^4		C_{11}	ST^2ST^4
	K_{12}	T^6ST, ST^3ST^3		C_{12}	T^4ST^2S
	K_{13}	TST^6, ST^2ST		C_{13}	ST^5ST^2
	K_{14}	T^5ST^2, ST^2ST		C_{14}	ST^4ST^2
				C_{15}	ST^3ST
Z_4	Q_1	T^3S		C_{16}	ST^2ST^4S
	Q_2	ST^3		C_{17}	ST^4ST^2S
	Q_3	TST^3		C_{18}	TST^4ST^5
	Q_4	T^2ST^2		C_{19}	TST^4ST
	Q_5	TST^2		C_{20}	TST^3ST^4
	Q_6	T^3ST		C_{21}	TST^5ST^2
	Q_7	T^2ST		C_{22}	T^2ST^5ST
	Q_8	TST^5S		C_{23}	TST^5ST
	Q_9	T^2ST^3S		C_{24}	ST^3ST^5ST
	Q_{10}	T^3ST^2S		C_{25}	$ST^2ST^4ST^6$
	Q_{11}	ST^3ST^4		C_{26}	$ST^2ST^4ST^2$
	Q_{12}	ST^4ST^3		C_{27}	$ST^2ST^4ST^5$
	Q_{13}	ST^2ST^3		C_{28}	ST^2ST^4ST
	Q_{14}	ST^3ST^2	Z_7	P_1	T
	Q_{15}	ST^5ST		P_2	STS
	Q_{16}	ST^2ST^2S		P_3	T^2S
	Q_{17}	TST^4ST^2		P_4	TST^4
	Q_{18}	T^2ST^4ST		P_5	T^4ST
	Q_{19}	TST^5ST^3		P_6	ST^2
	Q_{20}	$T^2ST^5ST^2$		P_7	T^2ST^3

Table 3.C.4: *Generators of Abelian subgroups of* $PSL(2,7)$*.*

3.C.3 Abelian subgroups of $\Delta(96)$

The group $\Delta(96)$ has ten irreducible representations: two singlets, one doublet, six triplets and one sextet. In this appendix we list the conjugacy classes and the generators for the relevant Abelian subgroups of $\Delta(96)$. As explained in the text of section 3.3.5, these are of the type $Z_2 \times Z_2$, Z_3, Z_4 and Z_8. Also $Z_4 \times Z_2$ and $Z_4 \times Z_4$ can be used for specific choices of the Z_4 generator, namely Q_1, Q_2 or Q_3.
All Klein groups except K are similar to each other and so are the sixteen Z_3 subgroups C_i and all six Z_8 subgroups O_i. The twelve Z_4 subgroups Q_i fall into three categories applying similarity transformations belonging to $\Delta(96)$: the first contains Q_1, Q_2 and Q_3, the second one Q_4, Q_5 and Q_6 and the third the others Q_7, ..., Q_{12}. The generators of Q_{1-6} all commute. The product group $Q_4 \times Q_5 \times Q_6$ is a normal subgroup of ${}^4O$, since the elements of order two fill the class $3C_2$ and those of order 4 fill the class $6C_4$.

Class	Typical element	Class	Typical element
$1\mathcal{C}_1$	E	$3\mathcal{C}_2$	T^4
$12\mathcal{C}_2$	S	$32\mathcal{C}_3$	ST
$3\mathcal{C}_4^{(1)}$	T^2	$3\mathcal{C}_4^{(2)}$	T^6
$6\mathcal{C}_4$	ST^2ST^4	$12\mathcal{C}_4$	ST^4
$12\mathcal{C}_8^{(1)}$	T, T^5	$12\mathcal{C}_8^{(2)}$	T^3, T^7

Table 3.C.5: *Conjugacy classes in* $\Delta(96)$

Subgroup		Generators	Subgroup		Generators
$Z_2 \times Z_2$	K	T^4, ST^4S, ST^4ST^4	Z_8		
	K_1	ST^4ST^4, S		O_1	T
	K_2	T^4, ST^2ST		O_2	ST^2
	K_3	ST^4S, T^7ST		O_3	T^2S
	K_4	ST^4ST^4, T^6ST^2		O_4	STS
	K_5	ST^4S, TST^7		O_5	ST^4ST
	K_6	T^4, ST^6ST^3		O_6	T^5ST
Z_3	C_1	ST	Z_4		
	C_2	ST^3			
	C_3	ST^5		Q_1	T^2
	C_4	ST^7		Q_2	ST^2S
	C_5	T^2ST		Q_3	ST^2ST^2
	C_6	T^2ST^3		Q_4	ST^4ST^2
	C_7	T^4ST		Q_5	ST^6ST^2
	C_8	T^3ST^4		Q_6	ST^2ST^4
	C_9	T^6ST		Q_7	ST^4
	C_{10}	TST^2		Q_8	T^3ST
	C_{11}	T^3ST^2		Q_9	ST^6ST
	C_{12}	T^5ST^2		Q_{10}	T^2ST^2
	C_{13}	T^4ST^3		Q_{11}	TST^3
	C_{14}	T^2ST^5		Q_{12}	ST^2ST^3
	C_{15}	TST^4			
	C_{16}	TST^6			

Table 3.C.6: *List of elements generating the subgroups* $Z_2 \times Z_2$, Z_3, Z_4 *and* Z_8 *of* $\Delta(96)$.

Z_2 groups									
V_1	ST^6ST^3	V_2	ST^2ST	V_3	TST^2S	V_4	T^4ST^2ST	V_5	TST^7
V_6	S	V_7	T^2ST^6	V_8	T^5ST^3	V_9	T^4ST^4	V_{10}	T^7ST
V_{11}	T^3ST^5	V_{12}	T^6ST^2	V_{13}	ST^4S	V_{14}	ST^4ST^4	V_{15}	T^4

Table 3.C.7: *List of generating elements of the Z_2 subgroups of $\Delta(96)$.*

3.C.4 Abelian subgroups of $\Delta(384)$

The group $\Delta(384)$ has 24 irreducible representations: two singlets, one doublet, 14 triplets (six of which unfaithful) and seven sextets. In this appendix, we list its relevant Abelian subgroups. There are 27 Z_2 subgroups, from which 13 Klein groups can be constructed. Furthermore, there are 64 Z_3 subgroups, 18 Z_4 subgroups, 24 Z_8 subgroups and 12 Z_{16} subgroups. As mentioned in the text about mixing patterns from $\Delta(384)$, apart from G_e being a Klein group or a Z_n group, also $Z_4 \times Z_2$, $Z_4 \times Z_4$, $Z_4 \times Z_8$, $Z_8 \times Z_2$ and $Z_8 \times Z_8$ can be considered.

All Klein groups, except K are similar to each other. The same holds for all Z_3 and Z_{16} subgroups.The Z_4 and Z_8 subgroups fall into three and five categories respectively. Of the Z_4 elements, all of Q_{1-6} commute. The first category contains the elements of Q_1, Q_2 and Q_3 with only two unique eigenvalues; the second category contains the elements of Q_4, Q_5 and Q_6 and the third one contains all other elements. A similar structure can be found in the Z_8 subgroups, where all of O_{1-12} commute and five categories are formed by respectively O_{1-3}; O_{4-6}; O_{7-9}; O_{10-12} and all others.

Class	Typical element	Class	Typical element
$1\mathcal{C}_1$	E	$3\mathcal{C}_2$	T^8
$24\mathcal{C}_2$	S	$128\mathcal{C}_3$	ST
$3\mathcal{C}_4^{(1,2)}$	T^4 / T^{12}	$6\mathcal{C}_4$	ST^4ST^8
$24\mathcal{C}_4$	ST^8	$3\mathcal{C}_8^{(1-4)}$	T^2 / T^6 / T^{10} / T^{14}
$6\mathcal{C}_8^{(1-6)}$	ST^2ST^4 / ST^2ST^6 / ST^2ST^8	$24\mathcal{C}_8^{(1,2)}$	ST^4 / ST^{12}
	ST^2ST^{10} / ST^2ST^{12} / ST^4ST^{10}	$24\mathcal{C}_{16}^{(1-4)}$	T / T^3 / T^5 / T^7

Table 3.C.8: *Conjugacy classes in* $\Delta(384)$

Z_2 groups							
V_1	TST^2S	V_2	$ST^{14}ST^7$	V_3	T^3ST^6S	V_4	$T^5ST^{10}S$
V_5	ST^2ST^9	V_6	ST^6ST^3	V_7	$ST^{10}ST^5$	V_8	ST^2ST
V_9	TST^{15}	V_{10}	$ST^{13}ST^{10}$	V_{11}	T^5ST^{11}	V_{12}	TST^3ST^5
V_{13}	$T^{15}ST$	V_{14}	T^4ST^{12}	V_{15}	T^6ST^{10}	V_{16}	T^8ST^8
V_{17}	$ST^6ST^{10}S$	V_{18}	ST^3ST^6	V_{19}	$ST^8ST^{12}ST^{12}$	V_{20}	T^2ST^{14}
V_{21}	$T^{11}ST^5$	V_{22}	S	V_{23}	ST^9ST^2	V_{24}	T^9ST^7
V_{25}	ST^8S	V_{26}	ST^8ST^8	V_{27}	T^8		

Table 3.C.9: *List of generating elements of the* Z_2 *subgroups of* $\Delta(384)$.

Klein groups			
K	T^8, ST^8S, ST^8ST^8	K_1	ST^8S, $T^{11}ST^5$
K_2	ST^8S, TST^{15}	K_3	ST^8S, $T^{15}ST$
K_4	ST^8S, T^5ST^{11}	K_5	ST^8ST^8, T^6ST^{10}
K_6	ST^8ST^8, T^4ST^{12}	K_7	ST^8ST^8, T^2ST^{14}
K_8	ST^8ST^8, S	K_9	T^8, $ST^{14}ST^7$
K_{10}	T^8, $ST^{10}ST^5$	K_{11}	T^8, ST^6ST^3
K_{12}	T^8, ST^2ST		

Table 3.C.10: *List of generating elements of the Klein groups contained in* $\Delta(384)$.

Z_3 groups							
C_1	ST	C_2	TS	C_3	ST^3	C_4	T^3S
C_5	T^5S	C_6	T^7S	C_7	T^9S	C_8	$T^{11}S$
C_9	TST^{14}	C_{10}	T^2ST^{13}	C_{11}	T^3ST^{12}	C_{12}	T^4ST^{11}
C_{13}	T^5ST^{10}	C_{14}	T^6ST^9	C_{15}	T^7ST^8	C_{16}	T^8ST^7
C_{17}	T^9ST^6	C_{18}	$T^{10}ST^5$	C_{19}	$T^{11}ST^4$	C_{20}	$T^{12}ST^3$
C_{21}	$T^{13}ST^2$	C_{22}	$T^{14}ST$	C_{23}	TST^{12}	C_{24}	T^2ST^{11}
C_{25}	T^3ST^{10}	C_{26}	T^4ST^9	C_{27}	T^5ST^8	C_{28}	T^6ST^7
C_{29}	T^7ST^6	C_{30}	T^8ST^5	C_{31}	T^9ST^4	C_{32}	$T^{10}ST^3$
C_{33}	$T^{11}ST^2$	C_{34}	$T^{12}ST$	C_{35}	TST^{10}	C_{36}	T^2ST^9
C_{37}	T^3ST^8	C_{38}	T^4ST^7	C_{39}	T^5ST^6	C_{40}	T^6ST^5
C_{41}	T^7ST^4	C_{42}	T^8ST^3	C_{43}	T^9ST^2	C_{44}	$T^{10}ST$
C_{45}	TST^8	C_{46}	T^2ST^7	C_{47}	T^3ST^6	C_{48}	T^4ST^5
C_{49}	T^5ST^4	C_{50}	T^6ST^3	C_{51}	T^7ST^2	C_{52}	T^8ST
C_{53}	TST^6	C_{54}	T^2ST^5	C_{55}	T^3ST^4	C_{56}	T^4ST^3
C_{57}	T^5ST^2	C_{58}	T^6ST	C_{59}	TST^4	C_{60}	T^2ST^3
C_{61}	T^3ST^2	C_{62}	T^4ST	C_{63}	TST^2	C_{64}	T^2ST

Table 3.C.11: *List of generating elements of the Z_3 subgroups of $\Delta(384)$.*

Z_4 groups							
Q_1	T^4	Q_2	ST^4S	Q_3	ST^4ST^4		
Q_4	ST^4ST^8	Q_5	ST^8ST^4	Q_6	ST^4ST^{12}		
Q_7	ST^8	Q_8	TST^7	Q_9	T^2ST^6	Q_{10}	T^3ST^5
Q_{11}	T^4ST^4	Q_{12}	T^5ST^3	Q_{13}	T^6ST^2	Q_{14}	T^7ST
Q_{15}	ST^2ST^5	Q_{16}	ST^6ST^7	Q_{17}	$ST^{10}ST^9$	Q_{18}	$ST^{14}ST^{11}$

Table 3.C.12: *List of generating elements of the Z_4 subgroups of $\Delta(384)$.*

Z_8 groups					
O_1	T^2	O_2	ST^2S	O_3	$ST^{14}ST^{14}$
O_4	ST^6ST^4	O_5	ST^4ST^6	O_6	$ST^{10}ST^{14}$
O_7	ST^2ST^4	O_8	ST^2ST^{14}	O_9	ST^4ST^2
O_{10}	ST^2ST^8	O_{11}	ST^6ST^{14}	O_{12}	ST^8ST^2
O_{13}	ST^4	O_{14}	T^4S	O_{15}	TST^{11}
O_{16}	TST^3	O_{17}	T^2ST^{10}	O_{18}	T^2ST^2
O_{19}	T^3ST^9	O_{20}	T^3ST	O_{21}	ST^2ST^3
O_{22}	ST^6ST	O_{23}	$ST^{10}ST^3$	O_{24}	$ST^{14}ST$

Table 3.C.13: *List of generating elements of the Z_8 subgroups of $\Delta(384)$.*

Z_{16} groups							
Y_1	T	Y_2	ST^2	Y_3	STS	Y_4	ST^6
Y_5	ST^{10}	Y_6	ST^{14}	Y_7	TST^5	Y_8	TST^9
Y_9	TST^{13}	Y_{10}	ST^4ST	Y_{11}	ST^8ST	Y_{12}	$ST^{12}ST$

Table 3.C.14: *List of generating elements of the Z_{16} subgroups of $\Delta(384)$.*

Chapter 4

The interplay between GUT and flavour symmetries in a Pati–Salam $\times$ S_4 model

> Il semble que la perfection soit atteinte non quand il n'y a plus rein à ajouter, mais quand il n'y a plus rein à retrancher.
>
> It seems that perfection is reached not when there is nothing more to add, but when there is nothing more to remove.
>
> *Antoine de Saint-Exupéry [98], Terre des Homes*

4.1 Introduction

In this chapter we investigate the possibility to combine flavour symmetries with Grand Unified Theory (GUT) symmetries. The desire to combine these two symmetries has three roots. Firstly, it is partly data-driven. There are structures that can be explained well by grand unified explanations and others that are well explained using flavour symmetries. As far as these concern the elementary masses, as a rule of thumb relations between the different family copies of a certain type of particle (e.g. charged leptons) can have explanations in family symmetries, while relations between different types of particles in one generation (e.g. the muon and the strange quark) might be explained by grand unified symmetries.

Secondly, there are aesthetic reasons to combine the two symmetries. Family symmetries reduce the number of fermionic representations by grouping particles of different families in single irreducible representations; grand unified symmetries do exactly the same with different particle types within a generation. Thirdly, there is the coincidence that in many models scale of family physics is close to the assumed GUT scale - see e.g. equation (2.86) and figure 1.14.

Flavour-GUT models have been constructed before, for references see e.g. [47]. In our opinion, these analyses emphasize the difficulty in the construction of a flavour GUT model which naturally lead to realistic fermion phenomenology and to a fair explanation of the gauge symmetry breaking chain to get $SU(3)_C \times U(1)_{em}$. In particular, the combinations of the constraints arising by the flavour symmetry and by the GUT group may lead to wrong predictions for the fermion masses and mixings. For instance if the lepton mixing is tribimaximal at the GUT scale and at leading order, it is not necessarily so at a low energy scale and to all orders in different perturbing parameters. The problem is usually avoided by recurring to non-minimal Higgs or flavon field content and by assuming peculiar symmetry breaking patterns of the GUT gauge symmetry and ascribing quite often at type-II seesaw as the origin of the neutrino masses. Moreover these patterns are often not supported by the study of the scalar Higgs potential, leaving open the question if such peculiar

patterns may be actually realized or not.

In this chapter we perform as complete an analysis as possible. The chapter is divided into three parts. The first part is introductory. In section 4.2, we list several patterns that can be seen in the mass sector and that may be explained by family symmetry pattern or GUT patterns. The section ends with a 'wishlist' of relations that the model we construct in the rest of the chapter should be able to reproduce. In section 4.3 we introduce the flavour part of the model and add some additional wishes to the list. Section 4.4 introduces the Pati–Salam GUT that the model in the next sections is based on.

In the second part, we construct the described model. Section 4.5 gives the contents of the model and in sections 4.6 and 4.7 we give the results respectively at leading order and next-to-leading order in the number of flavons inserted. Subleading effects are very important to obtain agreement with the data in models based on the bimaximal mixing pattern and we find that after section 4.7 all points of the wishlist are satisfied.

Section 4.8 is a bridge between the second and the third part of the chapter. In this section we show that the flavons used in sections 4.6 and 4.7 can indeed have the vacuum expectation values they are assumed to. This introduces extra complications as driving fields are needed, but this is not more than in the non-GUT model of Altarelli and Feruglio discussed in chapter 2.

In sections 4.9 and 4.10 we study respectively the Higgs alignment and the effects of renormalization group running. Here is becomes clear that the combination of flavour and GUT symmetries leads to unexpected interference effects. In fact some of the positive conclusions of the second part of the chapter have to be withdrawn.

Lastly, in section 4.11, we perform an analysis of the phenomenological consequences of our model on near-future neutrino experiments and in section 4.12 we present our conclusions.

4.2 A detailed look on patterns in the elementary fermion masses

In chapters 1 and 2 some patterns in the mass sector of the Standard Model were introduced. In section 1.4.1 we found that the masses in both quark sectors as well as in the charged lepton sector are highly hierarchical with comparable gaps between the third and second generation and the second and first generation on a logarithmic scale. In section 2.3.1 we discussed the Froggatt–Nielsen mechanism that can explain these structures in a natural way.

The model described in section 2.3.1 discusses only the charged lepton sector. Extension to the quark sector is obviously possible. From figure 1.16 we see that the gaps between the charged lepton and down quark states are comparable, while the gaps between the up quark states are clearly larger. The ratios between the muon and the tau mass and between the electron mass and the muon mass used in section 2.3.1 were λ^2 and λ^3 respectively, with $\lambda = 0.2$. This does also reasonably well describe the mass gaps in the down-type quark sector, although the strange quark is slightly too light. In the up-type quark sector, the gaps are larger and can be parameterized by ratios of λ^4 and λ^3 between the charm and the top and between the up and the charm respectively.

The other simplifying assumption in section 2.3.1 is the absence of off-diagonal terms. This is clearly not realistic. The presence of off-diagonal terms is necessary for the generation of mixing matrices. In the quark sector, where the mixing is relatively weak, the off-diagonal terms should be small. It is exactly the key point of the Froggatt–Nielsen mechanism to generate terms that are naturally small and in the model we study in this chapter, we show how we can use this at our convenience. To explain the larger mixing angles of the lepton sector, that might furthermore be close to special mixing patterns such as the tribimaximal or bimaximal one, the use of discrete non-Abelian flavour symmetries might be more appropriate.

While the Froggatt–Nielsen mechanism can provide relations between the ratios of masses of par-

ticles of the same type – charged leptons in the example of section 2.3.1 – it does not help much to explain patterns between particles of different type. Still, these relations might be present. A first hint might be given by the fact that the second (down-type quarks) and third line (charged leptons) in figure 1.16 are quite close together, allowing for the possibility of relations between charged lepton and down-type quark masses.

At low energy scales, such relations do not quite exist. For none of the three generations the charged lepton has the same mass as a quark or a simple multiple of it. When we discussed the Altarelli–Feruglio model in section 2.4, we found that flavour symmetries are often implemented at a high scale and that there are renormalization effects. If we run the renormalization group backwards we can evaluate the quark and lepton Yukawa couplings at a high scale and the corresponding masses are graphically depicted in figure 4.1. We find evidence for two relations. The first is bottom-tau unification

$$m_b = m_\tau. \tag{4.1}$$

The second relation goes by the name of the Georgi–Jarlskog relation [99] and it connects the muon mass with the mass of the strange quark

$$m_\mu = 3m_s \tag{4.2}$$

Both relations are supposed to hold at the scale of Grand Unification or slightly below. Given that this is far above the electroweak scale, the Higgs field does not have a vacuum expectation value here. The word 'mass', equal to the product of the relevant Yukawa coupling with the Higgs vev should thus be taken with a grain of salt. Technically, all particles are massless at this scale. What is meant is that the Yukawa couplings, evaluated at this scale, satisfy the given relations.

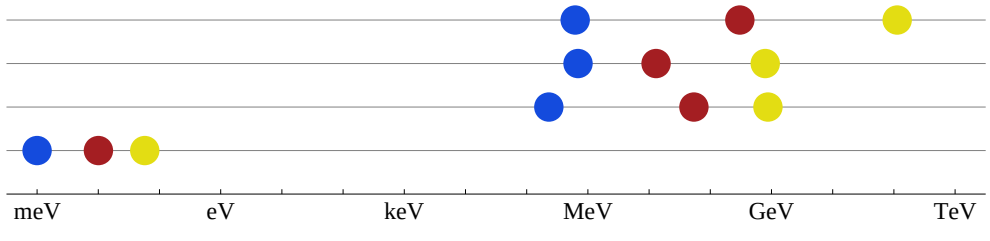

Figure 4.1: *The masses of the Standard Model fermions when evolved to a scale of* 10^{12} *GeV in the MSSM with tan* β *= 50 as discussed below.*

Lastly, we would like to explain the fact that the top quark is much heavier than the bottom quark and the tau lepton. In theories with more than one Higgs boson (for instance any supersymmetric theory), this may be explained by $\tan\beta$ or comparable quantities that give information about the relative vev of the Higgs that couples to the up- and down-sector. This large $\tan\beta$ itself should then follow from Higgs physics.

In table 4.1 we summarize the results mentioned in this section: the table contains the masses of the quarks and charged leptons at the scale of their own mass (or, if this is unavailable, at 2 GeV). The table also gives the masses at a high energy scale calculated in [100] using the renormalization group running of the MSSM with large $\tan\beta = 50$. We choose a value of 10^{12} GeV for the high energy scale. In section 4.9 we find that this is indeed close to the relevant scale for the generation of fermion masses.

The errors for the quarks are rather large, but the bottom-tau unification and the Georgi–Jarlskog relation are realized well within the margins of error. We also show ratios of the small Yukawa couplings with certain powers of $\lambda = 0.2$ such that the resulting couplings are of order 1. As a note of caution, we mention that the specific value of the high scale and of $\tan\beta$ are both slightly arbitrary and that the model inspired by the relations in the table does not have the MSSM as low energy limit. Therefore we perform a simple one-loop renormalization analysis in section 4.10.

As mentioned in chapter 2, not many parameters of the neutrino masses are known. It will be the aim of a family symmetric model to reproduce the solar and atmospheric mass differences of table 2.3.

	Generation 1	Generation 2	Generation 3
Charged Leptons	$m_e(m_e) = 0.51\,\text{MeV}$ $m_e(10^{12}\text{GeV}) = 0.23\,\text{MeV}$ $y_e(10^{12}\text{GeV}) = 6.6 \times 10^{-5}$ $y_e(10^{12}\text{GeV})/\lambda^6 = 1.0$	$m_\mu(m_\mu) = 106\,\text{MeV}$ $m_\mu(10^{12}\text{GeV}) = 54\,\text{MeV}$ $y_\mu(10^{12}\text{GeV}) = 0.016$ $y_\mu(10^{12}\text{GeV})/\lambda^3 = 1.9$	$m_\tau(m_\tau) = 1.78\,\text{GeV}$ $m_\tau(10^{12}\text{GeV}) = 875\,\text{MeV}$ $y_\tau(10^{12}\text{GeV}) = 0.25$ $y_\tau(10^{12}\text{GeV})/\lambda = 1.25$
Down-type Quarks	$m_d(2\text{GeV}) = 5.0 \pm 2.0\,\text{MeV}$ $m_d(10^{12}\text{GeV}) = 0.69^{+0.31}_{-0.29}\,\text{MeV}$ $y_d(10^{12}\text{GeV}) = \left(2.0^{+0.9}_{-0.8}\right) \times 10^{-4}$ $y_d(10^{12}\text{GeV})/\lambda^6 = 3.1^{+1.4}_{-1.3}$	$m_s(2\text{GeV}) = 95 \pm 25\,\text{MeV}$ $m_s(10^{12}\text{GeV}) = 13 \pm 4\,\text{MeV}$ $y_s(10^{12}\text{GeV}) = \left(3.7 \pm 1.2\right) \times 10^{-3}$ $y_s(10^{12}\text{GeV})/\lambda^3 = 0.46 \pm 0.14$	$m_b(m_b) = 4.20 \pm 0.07\,\text{GeV}$ $m_b(10^{12}\text{GeV}) = 0.79^{+0.05}_{-0.04}\,\text{GeV}$ $y_b(10^{12}\text{GeV}) = 0.22^{+0.01}_{-0.01}$ $y_b(10^{12}\text{GeV})/\lambda = 1.14^{+0.07}_{-0.05}$
Up-type Quarks	$m_u(2\text{GeV}) = 2.2^{+0.8}_{-0.7}\,\text{MeV}$ $m_u(10^{12}\text{GeV}) = 0.62^{+0.26}_{-0.22}\,\text{MeV}$ $y_u(10^{12}\text{GeV}) = \left(3.6^{+1.5}_{-1.3}\right) \times 10^{-6}$ $y_u(10^{12}\text{GeV})/\lambda^8 = 1.4^{+0.6}_{-0.5}$	$m_c(m_c) = 1.25 \pm 0.09\,\text{GeV}$ $m_c(10^{12}\text{GeV}) = 0.304^{+0.046}_{-0.045}\,\text{GeV}$ $y_c(10^{12}\text{GeV}) = \left(1.7 \pm 0.3\right) \times 10^{-3}$ $y_c(10^{12}\text{GeV})/\lambda^5 = 5.5 \pm 0.8$	$m_t(m_t) = 162.9 \pm 2.8\,\text{GeV}$ $m_t(10^{12}\text{GeV}) = 113.2^{+8.9}_{-7.7}\,\text{GeV}$ $y_t(10^{12}\text{GeV}) = 0.65^{+0.05}_{-0.04}$ $y_t(10^{12}\text{GeV})/\lambda = 3.2^{+0.3}_{-0.2}$

Table 4.1: *Parameters of quark and charged lepton masses evaluated at low scales and at a scale of* 10^{12} *GeV, calculated in [100] in the MSSM with* $\tan\beta = 50$*. For the charged leptons no error bars are given. In principle, their values are known to much higher precision. This extra information is not useful, as model dependent choices (e.g. the exact value of* $\tan\beta$*) bring in much more uncertainty.*

The actual neutrino masses themselves and in particular their ordering should then be a prediction of the specific model.

We conclude this section with a 'wishlist' of properties of the masses of quarks and leptons that a complete model should be able to reproduce:

- Find the right masses for the third family, in particular the large top mass.
- Suppress the second family masses: $m_\mu/m_\tau = m_s/m_b = \lambda^2$ and $m_c/m_t = \lambda^4$.
- Suppress the first family masses even stronger: $m_e/m_\tau = m_d/m_b = \lambda^5$ and $m_u/m_t = \lambda^7$.
- Reproduce the bottom-tau and strange-muon relations.
- Reproduce the atmospheric and solar mass differences
- Predict the absolute neutrino mass scale and the neutrino hierarchy.

Next to properties of the masses, we would also like to reproduce or predict properties of the mixings of the elementary fermions. The choices of our model regarding mixing are discussed in the next section.

4.3 Bimaximal versus tribimaximal mixing

At the end of section 2.4 we discussed the next-to-leading order (NLO) corrections to the Altarelli–Feruglio model, or rather to a simple extension of it that contains quarks. The leading order (LO) results of this model were exact tribimaximal mixing in the lepton sector and no mixing at all in the quark sector. We mentioned that these leading order mixing patterns were very accurate in the neutrino sector, perhaps even too accurate. The measured value of the solar mixing angle is very close to the tribimaximal value. The deviations can be at most of order λ^2, where λ is still defined as a parameter with value 0.2. The measurement error for the atmospheric mixing angle is rather large, but also here the central value agrees very well with the tribimaximal prediction and corrections no larger than of order λ^2 are favoured. The size of corrections in the (1 2) and (2 3) sector naturally imply very small corrections to the reactor mixing angle. This angle was zero at leading order and thus θ_{13}^l very close to zero is a prediction of the model – one that is in contradiction with the latest data. In the Wolfenstein picture, the parameter λ is defined as the size of the Cabibbo angle. If the LO result has no quark mixing, this should all be generated at NLO, thus requiring much larger corrections in the quark than in the lepton sector.

As described in section 2.4 NLO terms contain an extra flavon with respect to the leading order. We recall that the suppression of NLO terms is v_X/Λ with v_X the vev of any flavon and Λ the cut-off scale of the model. In models that have zero quark mixing at leading order and that reproduce the Cabibbo angle at the NLO, we thus need

$$\frac{v_X}{\Lambda} \approx \lambda = 0.2. \tag{4.3}$$

Good care must be taken to ensure that the two other mixing angles of the CKM matrix do not obtain values as large as the Cabibbo angle, but in general it is possible to have these vanishing also at NLO and to produce them only at the next-to-next-to-leading order. See also figure 4.2.

It is clear that the size of NLO corrections $v_X/\Lambda \approx 0.2$ is incompatible with the $v_X/\Lambda \lesssim 0.05$ found at the end of section 2.4 from lepton considerations. Now there are three possibilities. The first option entails a complete separation of the flavon-induced physics of the quark and lepton sectors. Instead of one value of v_X/Λ, there are separate values for v_{X_q}/Λ (large) and v_{X_l}/Λ (small). These two values of the flavon vevs might come from flavons that barely talk to each other or even from different symmetry groups in the two sectors. Obviously, the idea of separating the flavour aspects

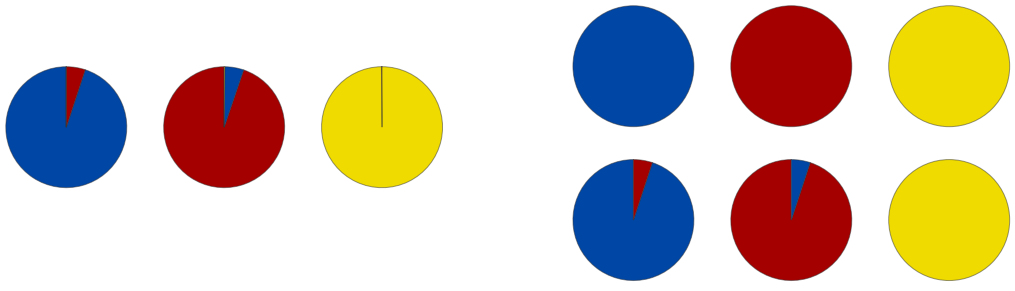

Figure 4.2: *Left: pie charts showing the flavour content of the three quark eigenstates. Right: the no-mixing predictions of a typical flavour model at LO (upper line) and a NLO result, where θ_{12} is corrected to the size of the observed Cabibbo angle. The other two mixing angles follow at higher orders, hence the absence of the red sliver in the third mass eigenstate (lower line).*

of quark and lepton physics is badly compatible with the concept of a unified description of the two sectors as discussed in the next section.

In both other options a single value of $v_X/\Lambda \approx 0.2$ is assumed. In a second scenario, the couplings of flavons to the Yukawa terms are tailored such that only in the quark sector there is a correcting term with just one extra flavon (thus giving a large correction), while in the lepton sector, the first correcting term has two extra flavons, leading to a much smaller correction of order $(v_X/\Lambda)^2$. This tailoring is highly non-trivial and might require the addition of more than one additional Z_n symmetry.

Thirdly, one can accept large corrections in both the quark and the lepton sector. In that case, however, the tribimaximal mixing pattern is not a good leading order result, as the near-perfect agreement with the data gets completely destroyed at the NLO. This is graphically shown in figure 4.3.

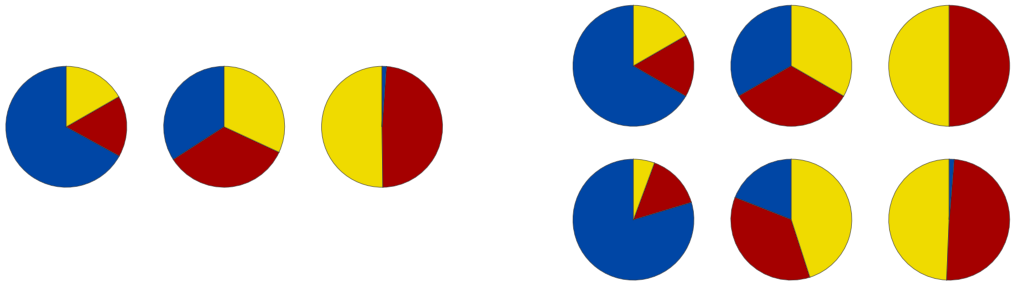

Figure 4.3: *Left: pie charts showing the flavour content of the three neutrino eigenstates. Right: The tribimaximal mixing pattern (upper line) and a possible NLO result if corrections of the size λ are allowed. We have used $\delta\theta^l_{12} = -0.7\theta_C$, $\delta\theta^l_{13} = 0.5\theta_C$. The (2 3) angle is not corrected. This is indeed the case in some models and allows for a more fair comparison with figure 4.4*

The fact that the quark sector requires a relatively large NLO correction, seems to suggest a lepton mixing pattern that also requires large corrections, i.e. one that at leading order described the data less perfect than the tribimaximal pattern. An interesting new piece of evidence are the so-called quark-lepton complementarity relations.

$$\theta^l_{12} + \theta^q_{12} \simeq \pi/4 + \mathcal{O}(\lambda^2)\,, \qquad \theta^l_{23} + \theta^q_{23} \simeq -\pi/4 + \mathcal{O}(\lambda^2)\,. \tag{4.4}$$

We note that there does not seem to be such a relation between the (1 3)-angles. In the quark sector, this angle is tiny (of the order of λ^3); in the lepton sector, the T2K result points to a value slightly

smaller than λ. There is certainly no angle close to $\pi/4$ involved. The complementarity relations point at a description in which the quark and lepton mixing angles are not only related by being part of a powerseries with a comparable expansion parameter (v_X/Λ), but may even be connected even stronger. In the next section we discuss the grand unified model of Pati and Salam, in which there is indeed a strong relationship between quark and lepton mass matrices as leptons may be seen as the fourth colour. In minimal Pati–Salam models one finds equal mass matrices for charged leptons and down-type quarks

$$M_e = M_d \ . \tag{4.5}$$

This obviously implies a common source for the mixing angles. The model described in this chapter is not a minimal Pati–Salam model and there are significant corrections to equation (4.5), but the idea of a common source for quark and lepton mixing angles remains.

The bimaximal pattern of section 3.3.2 is a candidate mixing pattern that matches the criteria above[1]. At leading order, both the (1 2) and (2 3) mixing angles in the lepton sector are maximal (45°), while the third lepton mixing angle as well as all quark mixing angles are zero. An elaborate model [64] exists in the literature where bimaximal mixing in the lepton sector is derived from a S_4 discrete symmetry. Our model can be seen as an revision of [64] in order to include a realistic description of the quark sector.

One way to realize bimaximal mixing at leading order is now if the neutrino mass matrix is diagonalized by a maximal angle in the (1 2) sector[2], while for all charged particles (that is, charged leptons and both types of quarks), the mixing is maximal in the (2 3) sector. Writing a rotation in the (i j) plane of a mass matrix over an angle α as $R_{ij}(\alpha)$, we get

$$\begin{aligned} V_{\text{CKM}} &= (V_L^u)^\dagger V_L^d = R_{23}(-\frac{\pi}{4}) \times R_{23}(\frac{\pi}{4}) = \mathbb{1} \\ V_{\text{PMNS}} &= (V_L^e)^\dagger V^\nu = R_{23}(-\frac{\pi}{4}) \times R_{12}(\frac{\pi}{4}) \ . \end{aligned} \tag{4.6}$$

These maximal mixing angles can originate from mass matrices that are relatively simple; they have many zeroes in the elements we do not want to get mixed. In this chapter, we choose the following realization for the neutrino mass matrix at leading order[3]

$$M^\nu \propto \begin{pmatrix} k_0 & k_1\lambda & 0 \\ k_1\lambda & k_0 & 0 \\ 0 & 0 & k_0 \end{pmatrix} \ . \tag{4.7}$$

The charged particle mass matrices (generically denoted as M^x) are given at leading order by

$$M^x \propto \begin{pmatrix} 0 & 0 & 0 \\ 0 & y_b & y_a \\ 0 & -y_b & y_a \end{pmatrix} \quad \rightarrow \quad M^x (M^x)^\dagger \propto \begin{pmatrix} 0 & 0 & 0 \\ 0 & y_a^2 + y_b^2 & y_a^2 - y_b^2 \\ 0 & y_a^2 - y_b^2 & y_a^2 + y_b^2 \end{pmatrix} \ . \tag{4.8}$$

Here, y_a will eventually be leading in the generation of the third generation masses and y_b in those of the second generation. The relative smallness of the second generation masses is explained by a positive Froggatt–Nielsen charge; y_b should therefore not be read as a true parameter of the model, but rather as an effective parameter after 'dilution' by the Froggatt–Nielsen mechanism[4]. At this

[1] It is amusing to see that the first references to the bimaximal mixing pattern are some four years older than those to the tribimaximal mixing pattern. From a modern point of view, the tribimaximal pattern is more natural since already at first order it reproduces decent agreement with the data. Obviously, this was not known in the first years of neutrino oscillations. As long as the solar mixing angle were in agreement with an maximal angle, the bimaximal pattern was considered a good leading order fit; when it was found that θ_{12}^l is significantly smaller than 45°, it was dismissed for a while. Approximately ten years after its first postulation, the pattern re-emerged as a pattern feasible with large next-to-leading order effects

[2] We recall that the CKM and PMNS matrix are respectively defined as $V_{\text{CKM}} = (V_L^u)^\dagger V_L^d$ and $V_{\text{PMNS}} = (V_L^e)^\dagger V^\nu$, where V^ν is the matrix that appears in the diagonalization of the neutrinos (2.44) and V_L^x, $x \in \{u, d, e\}$ are the matrices that diagonalize $M^x M^{x\,\dagger}$.

[3] The appearance of λs in this formula makes it look like a NLO expression instead of a LO result. However, the matrix with just the k_0 elements is proportional to the identity and does not allow the determination of V^ν as it is invariant under the action of any unitary matrix.

[4] This implies again that some terms in the mass matrix are larger than others; this choice follows from consistent qualification of LO and NLO effects.

level of approximation, the first generation particles are still massless; their masses are generated by higher order effects.

At next-to-leading-order, the Cabibbo angle should be reproduced in the quark sector, while keeping the two other mixing angles small. In the lepton sector, there should be a large correction to the (1 2) mixing angle. The (2 3) angle should not be corrected at this order, as the data suggest at most a λ^2 deviation from the maximal value. From the input-side, there is no preference for a specific behaviour of the (1 3) mixing angle. In our model, the correction is large, of order λ. This is good news in view of the latest data.

This pattern of NLO corrections can be generated as follows. In the neutrino mass matrix (4.7), the only correction is in the (3 3) element

$$(M^\nu) \propto \begin{pmatrix} k_0 & k_1\lambda & 0 \\ k_1\lambda & k_0 & 0 \\ 0 & 0 & k_0 + k_2\lambda^2 \end{pmatrix} . \tag{4.9}$$

This is still diagonalized by $R_{12}(\frac{\pi}{4})$. In the charged sector, NLO terms should give non-zero elements in the (1 2) and (1 3) elements, but not in the first column.

$$M^x \propto \begin{pmatrix} 0 & y_d\lambda & y_c\lambda \\ 0 & y_b & y_a \\ 0 & -y_b & y_a \end{pmatrix} \quad \rightarrow \quad M^x(M^x)^\dagger \propto \begin{pmatrix} 0 & (y_a y_c - y_b y_d)\lambda & (y_a y_c + y_b y_d)\lambda \\ (y_a y_c - y_b y_d)\lambda & y_a^2 + y_b^2 & y_a^2 - y_b^2 \\ (y_a y_c + y_b y_d)\lambda & y_a^2 - y_b^2 & y_a^2 + y_b^2 \end{pmatrix} . \tag{4.10}$$

This is diagonalized by a combination of rotations over all three mixing angles

$$V_L^x = R_{23}(\frac{\pi}{4}).R_{13}(f\lambda).R_{12}(g\lambda) . \tag{4.11}$$

Here, f and g are functions of the parameters of the mass matrix and we ignored complex phases. It is easy to see that in the diagonalization of the mass matrices in (4.10), the $(1\ 2)$ rotation originates dominantly from the second families, while the $(1\ 3)$ rotation comes from the third families. The parameters y_a, y_b, y_c, y_d in equation (4.10) generically stand for parameters in the mass matrices of all three types of charged particles.

In our model, the parameters y_a and y_c are universal for up quarks, down quarks and charged leptons, while y_b and y_d are the same for e and d, but different for u. This relates to the fact that the hierarchy is larger in the up sector than in the two other sectors. The Higgs content of our model is such that the coupling that gives mass to the second generation charged leptons and down-type quarks does not have an analogue for the up-type quarks. The mass of the charm quark eventually follows from a term whose d and e analogue is subleading. This has two positive consequences. Firstly that the mass gap between top and charm is indeed larger than between the bottom and the strange and between the tau lepton and the muon. Secondly that the parameter f of equation (4.11) is the same for all three types of particles, while g is the same for charged leptons and down quarks, but different for up quarks.

$$f = f_e = f_d = f_u$$

$$g_e = g_d \neq g_u$$

The mixing matrices at next-to-leading order read

$$\begin{aligned} V_{\text{PMNS}} = (V_L^e)^\dagger V^\nu =& \Big[R_{12}(-g_e\lambda)R_{13}(-f\lambda)R_{23}\big(-\frac{\pi}{4}\big)\Big]R_{12}\big(\frac{\pi}{4}\big) \\ =& R_{23}\big(-\frac{\pi}{4}\big)R_{13}(\tilde{f}\lambda)R_{12}\big(\frac{\pi}{4} - \tilde{g}_e\lambda\big) , \\ V_{\text{CKM}} = (V_L^u)^\dagger V_L^d =& \Big[R_{12}(-g_u\lambda)R_{13}(-f\lambda)R_{23}\big(-\frac{\pi}{4}\big)\Big]\Big[R_{23}\big(\frac{\pi}{4}\big)R_{13}(f\lambda)R_{12}(g_d\lambda)\Big] \\ =& R_{12}\big((g_d - g_u)\lambda\big) . \end{aligned} \tag{4.12}$$

Going from the first to the second line, we note that the rotation matrices in different sectors do not commute, hence the introduction of parameters $\tilde{f}$ and $\tilde{g_e}$. The lepton rotation in the (2 3) sector is still $-\pi/4$ up to corrections of order λ^2; the (1 2) mixing angle is corrected by an term of order λ from the maximal LO result and a large angle in the (1 3) sector is generated. For the quarks, only the Cabibbo angle is generated and it is of order λ as required; the other two angles are generated at even higher orders. The bimaximal leading order and next-to-leading order results for leptons are graphically summarized in figure 4.4; for quarks, it is the same as in figure 4.2.

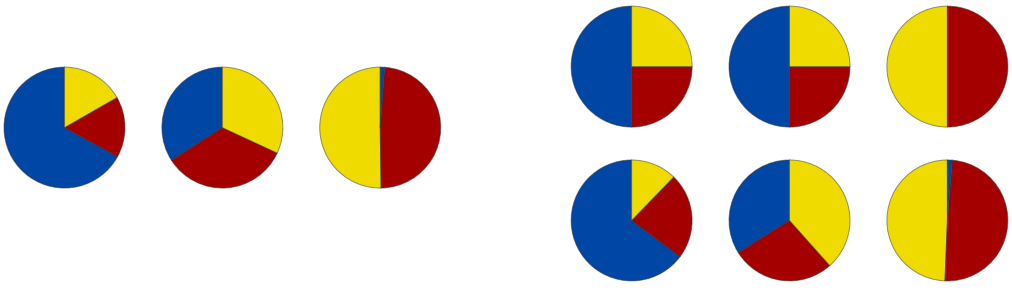

Figure 4.4: *Left: pie charts showing the flavour content of the three neutrino eigenstates. Right: The bimaximal mixing pattern (upper line) and a possible NLO result if corrections of the size λ are allowed in the (1 2) and (1 3) but not the (2 3) sector as in the model of this chapter. We have used $\delta\theta^l_{12} = -0.7\theta_C$ and $\delta\theta^l_{13} = 0.5.\theta_C$*

We end this section with a continuation of the wishlist we ended the previous section with. With respect to mixing angles in the lepton and quark sectors, the model should have the following properties.

- Show bimaximal lepton mixing and no quark mixing at leading order.
- At next-to-leading order, have a correction of order λ to the (1 2) mixing angles of both leptons and quarks.
- The two other angles in the CKM matrix should be generated by higher order effects, such that $\theta^q_{23} \sim \lambda^2$ and $\theta^q_{13} \sim \lambda^3$.
- The atmospheric mixing angle θ^l_{23} may not get a NLO correction; its deviation from maximal is at most λ^2.
- The model should give a value or range for the reactor mixing angle θ^l_{13}. When the model was first constructed, $\theta^l_{13} > 0$ was only hinted at and the result $\theta^l_{13} = \mathcal{O}(\lambda)$ was a prediction – one that is indeed supported by the current stream of data.

We have already seen that if the neutrino and charged fermion mass matrices at NLO are given by respectively (4.9) and (4.10) all wishes can be realized, so basically the wishlist collapses to the realization of these two matrices.

4.4 The Grand Unified Theory of Pati and Salam

In section 1.3.3 we introduced grand unified theories (GUTs). The main motivation was the observation that the three gauge couplings of an supersymmetric extension of the Standard Model go through one point when plotted against energy. From this scale on, there might not be three separate gauge forces, but one GUT-force instead. From a theoretical point of view, the main gain is that the description of the gauge sector is thus much simpler.

Also in the elementary fermion sector, grand unified theories offer a much simpler picture. We recall from table 2.2 on page 21 that five or six representations are needed to describe the fermions of one family of the Standard Model, depending on the question whether the righthanded neutrino is taken into account or not. In this chapter we assume it exists. Six representations is already a relatively low number. The lefthanded lepton doublet contains two states, one that below the electroweak phase transition becomes an electron and one that becomes a neutrino. The states of the righthanded up and down quarks (or, equivalently, anti-up or anti-down quarks) both describe three colour states. The lefthanded quark doublet even contains six states: three colours of up and three of down quarks. These states are depicted in figure 4.5.

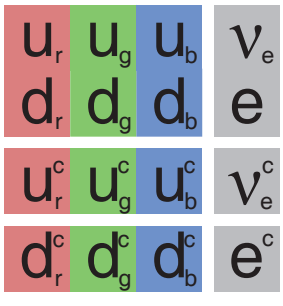

Figure 4.5: *The sixteen fermion states of the Standard Model grouped in six representations*

The way in which the fermions are grouped in figure 4.5 immediately suggests two possible unifications. Firstly, the difference between left- and righthanded fields are striking. While lefthanded fields are in a doublet, righthanded fields are in two separate singlets. The hypercharge is exactly such that these may be the two components of an $SU(2)_R$-doublet. This righthanded $SU(2)$ should then be present at high energies, but broken above the Standard Model scale. The assumption of this left-right symmetry closes the second horizontal gap in figure 4.5, thereby making it much more symmetric and compact.

Secondly, the position of the leptons right next to the quarks makes it tempting to see the leptons as a fourth colour. This is indeed possible if the $SU(3)$ gauge group of QCD is extended to $SU(4)$ at higher energies. As a result, the vertical gap in figure 4.5 is closed as well and all sixteen Standard Model states are described in just two representations, one lefthanded and one righthanded. We refer to these as F_L and F^c respectively. The fact that the theory is now completely left-right symmetric ensures anomaly cancellation.

The fact that quarks and leptons are treated on equal footing at high energies, with the symmetry broken in a very specific way, allows the bottom-tau unification and the mass relation (4.2) between muons and strange quarks. It is also essential in the generation of the mixing matrices from combined effects in both sectors.

The gauge group described above is known as the Pati–Salam grand unified theory [101]. Technically, it does not give a unified description. Even at high energies, the gauge group is the product of three groups and not a single group as is the case in the more conventional GUTs such as $SU(5)$ or $SO(10)$. Still, due to the unification of quarks and leptons and the fact that lefthanded and righthanded fields are treated on the same footing, we refer to it as a GUT.

The Pati–Salam Gauge group $SU(4)_{C'} \times SU(2)_L \times SU(2)_R$ is broken down to the Standard Model in two steps. At a very high scale M_C, the group $SU(4)_{C'}$ of extended colour breaks down to QCD $SU(3)_C$ times an additional $U(1)_{B-L}$. The charges of the known particles under this force are exactly the differences between their baryon and lepton number. At an intermediate scale M_R, $SU(2)_R \times U(1)_{B-L}$ is broken to $U(1)_Y$, the hypercharge of the Standard Model, according to $Y = T_{3R} + (B - L)/2$. The Standard Model gauge group now exists until the scale of electroweak symmetry breaking,

where the symmetry breaking ends at $SU(3)_C \times U(1)_{\rm em}$:

$$\begin{aligned} & SU(4)_{C'} \times SU(2)_L \times SU(2)_R \\ \xrightarrow{M_C} & SU(3)_C \times SU(2)_L \times SU(2)_R \times U(1)_{B-L} \\ \xrightarrow{M_R} & SU(3)_C \times SU(2)_L \times U(1)_Y \\ \xrightarrow{M_{\rm ew}} & SU(3)_C \times U(1)_{\rm em} \end{aligned} \tag{4.13}$$

We stress that the Pati–Salam GUT is not the only GUT that unifies many fermions in a single representation. In the $SU(5)$ GUT of Georgi and Glashow [102], the righthanded down quarks and the lepton doublet exactly have the right quantum numbers of the $\bar{5}$ of $SU(5)$, while the righthanded up quarks, the quark doublet and the righthanded electron together just fit in the anti-symmetric tensor representation 10. According to Georgi and Glashow, the arguments of unification are so strong that they are led "inescapably to the conclusion that $SU(5)$ is the gauge group of the world." In the $SO(10)$ GUT, the unification is even stronger as all 15 Standard Model particles plus the righthanded neutrino fit in the single 16 representation.

The choice for the Pati–Salam GUT over $SU(5)$ relates to the quark-lepton complementarity relations. In minimal $SU(5)$, one does not have equal charged lepton and down-type quark mass matrices as in equation (4.5). Instead the relation is $M_e \sim M_d^T$ and as result, a correction of order λ to the solar angle does not correspond to the Cabibbo angle of the CKM matrix.

On the other hand a reason to prefer Pati–Salam over $SO(10)$ is related to the type-I and type-II seesaw mechanisms. In these two GUT contexts, we expect both left-handed (LH) and right-handed (RH) neutrino Majorana mass matrices to be present. As a result, the effective LH neutrino mass matrix (4.7) gets contributions from both the type-I and II seesaw. In general, and this happens also in our proposal, this interplay introduces two mass scales and a highly non-trivial flavour structure for the effective neutrino mass matrix. It is difficult to find a realistic description of the PMNS matrix. For this reason, a hierarchy between the two contributions is usually assumed. We can reproduce quark-lepton complementarity in our model, if the type-II seesaw is dominant.

This possibility has already been investigated in several flavour GUT models, for example in [90,103–105] in the context of the $SO(10)$ GUT. However in [106] it was proven that the type-II dominance is not a viable solution in such GUTs. In the Pati–Salam context, there is more freedom and the eventual dominance of one of the two contributions could be realized. In this chapter we study the gauge Higgs potential and we verify that a type-II dominance can be justified, even if it puts strong constraints on the model building realization.

4.5 The flavour model building

In section 3.3.2 we found that the bimaximal mixing pattern can be reproduced by the 24-element discrete group S_4. For the group theory of S_4, we refer to appendix 3.B. In this section, we use a basis of S_4 different than the one in chapter 3. Obviously, the physical results are independent of the representation used. The representation chosen here makes the origin of the mixing effects from the charged lepton or neutrino sector more apparent. The transformations from this basis to bases with diagonal S or T is given in the appendix.

The spontaneous symmetry breaking of S_4 is responsible for the flavour structure of the matrices in equations (4.7) and (4.8): S_4 is broken down to two distinct subgroups and it is the presence of this mismatch at the LO which allows to construct M^ν and M^x. More in detail, the different subgroups to which S_4 is broken down are the subgroups that preserve the vevs of the flavons. In order to determine these structures, it is necessary to identify the elements of the group which leave the vevs of the flavons invariant under their action. Doing so, we find that S_4 is broken down to $Z_2 \times Z_2$ in the neutrino sector, originated by the elements ST^2S and T^3ST of the classes $3\mathcal{C}_2$ and $6\mathcal{C}_2$ respectively.

In the charged fermion sector, we find that S_4 is broken down to a $Z_2 \times Z_2$ group, distinct to the one in the neutrino sector, generated by the two elements T^2 and ST^2ST^3 of the classes $3\mathcal{C}_2$ and $6\mathcal{C}_2$ respectively.

It was already mentioned in section 2.3.2 that next to the non-Abelian S_4 auxiliary Abelian symmetries are required for a complete model. The complete flavour group is

$$G_f = S_4 \times Z_4 \times U(1)_{FN} \times U(1)_R \,. \tag{4.14}$$

The other terms in G_f carry out specific roles: the Abelian Z_4 symmetry is required to avoid dangerous terms in the superpotential, it helps to keep the different sectors of the model, quarks from leptons and neutrinos from charged leptons, separated; it is also useful in the generation of the flavon vacuum alignment. The continuous Frogatt-Nielsen (FN) Abelian symmetry, $U(1)_{FN}$, is introduced to justify charged fermion mass hierarchies. As in section 2.3.1, the (righthanded fields of the) first and second generation are assigned non-zero FN-charge, albeit a lower one than the one in section 2.3.1. This relates to the fact that mass terms for the first and second family often already require multiple (ordinary) flavons. The continuous R-symmetry $U(1)_R$, was introduced in section 2.4. It simplifies the constructions of the scalar potential. We stress again that the supersymmetric context is of great utility in the discussion of the scalar potential and helps in the gauge coupling running, but a similar non-supersymmetric model can in principle be constructed as well. In this chapter we only deal with SM particles and therefore we use the same symbols for a supermultiplet and its even R-parity components.

4.5.1 The matter, Higgs and flavon content of the model

As discussed in section 4.4, all fermionic matter of the SM plus a righthanded neutrino is contained in two Pati–Salam multiplets. The lefthanded multiplet F_L contains the quark and the lepton doublets, while the righthanded multiplet F^c contains the righthanded up quark, down quark, charged lepton and neutrino

$$\begin{aligned} \mathbf{SU(3)_C \times SU(2)_L \times U(1)_Y} &\quad\to\quad \mathbf{PS} \\ (3,\,2,\,1/6)_Q + (1,\,2,\,-1)_L &\quad\to\quad (4,\,2,\,1) \\ (\overline{3},\,1,\,-2/3)_{u^c} + (\overline{3},\,1,\,1/3)_{d^c} + (1,\,1,\,1)_{e^c} + (1,\,1,\,0)_{\nu^c} &\quad\to\quad (\overline{4},\,1,\,2)\,. \end{aligned} \tag{4.15}$$

The three copies of the LH supermultiplet are combined in the three-dimensional representation 3_1 of S_4, while the three families of the RH supermultiplet are in one of the 1-dimensional representations, 1_2, 1_2 and 1_1 respectively. The fact that we can put different representations within one family in different representations of the family symmetry group is essential here. Note that this would not be possible in (minimal) $SO(10)$, where all Standard Model particles are in one sixteen dimensional representation. The first two families are also charged under $U(1)_{FN}$ by two units. This suppresses their masses with respect to the third family ones. Further suppression of the first family with respect to the second is due to their different Z_4 charges that necessitate multiple flavon insertions already.

All the properties of the matter fields are summarized in table 4.2 and the unifying aspects are stressed in figure 4.6. Instead of 18 matter representations, as in the Standard Model, our model just needs four.

Our model contains five flavon fields that develop vacuum expectation values: two S_4 triplets (φ and φ') that, because of their Z_4 charge, deal at LO only with the Dirac Yukawa couplings of quarks and leptons, and two fields, one singlet (σ) and one triplet (χ), that, by Z_4, deal at LO only with the Majorana masses of neutrinos. The fifth flavon is the Froggatt–Nielsen messenger, which we indicate with θ. Their properties are shown in table 4.3. Under the continuous R-symmetry, the matter superfields transform as $U(1)_R = 1$, while all the flavons are neutral. Additional $U(1)_R = 2$ driving flavons are introduced in section 4.8. These help the original flavons obtaining their vevs.

Fermion masses and mixings arise from the spontaneous breaking of the flavour symmetry by means

Matter	F_L	F_1^c	F_2^c	F_3^c
PS	$(4,2,1)$	$(\overline{4},1,2)$	$(\overline{4},1,2)$	$(\overline{4},1,2)$
S_4	3_1	1_2	1_2	1_1
$U(1)_{FN}$	0	2	2	0
Z_4	1	1	i	$-i$

Table 4.2: *Transformation properties of the matter fields. Note that the PS assignments should be read in agreement with* $SU(4)_C \times SU(2)_L \times SU(2)_R$.

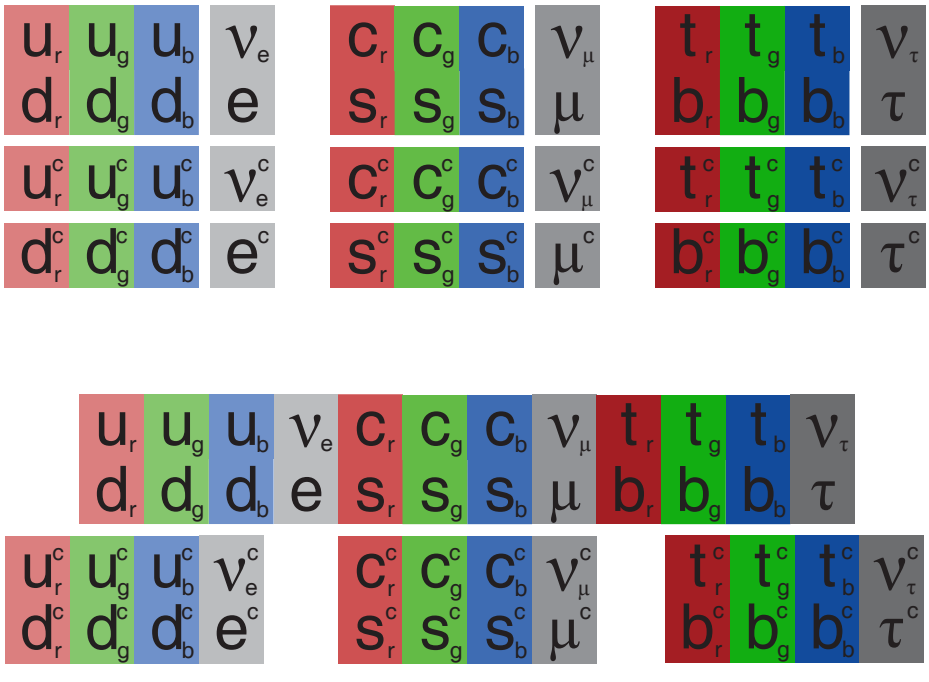

Figure 4.6: *The forty-eight fermion states of the Standard Model grouped in eighteen representations as in the SM (upper line) or in four representations as in our model (lower line)*

Flavons	θ	φ	φ'	χ	σ
S_4	1_1	3_1	3_2	3_1	1_1
$U(1)_{FN}$	-1	0	0	0	0
Z_4	1	i	i	1	1

Table 4.3: *The flavon field content and their transformation properties under the flavour symmetries. All flavon fields are singlet of the gauge group.*

of the flavons which develop vevs according to the following configuration: at LO we have

$$\langle\varphi\rangle = \begin{pmatrix} 0 \\ 1 \\ 1 \end{pmatrix} v_\varphi \ , \qquad \langle\varphi'\rangle = \begin{pmatrix} 0 \\ 1 \\ -1 \end{pmatrix} v_{\varphi'} \ , \tag{4.16}$$

$$\langle\chi\rangle = \begin{pmatrix} 0 \\ 0 \\ 1 \end{pmatrix} v_\chi \ , \qquad \langle\sigma\rangle = v_\sigma \ , \tag{4.17}$$

$$\langle\theta\rangle = v_\theta \ . \tag{4.18}$$

In this section we simply assume this vev alignment and we prove it to be a natural solution of the minimization of the scalar potential in section 4.8. Furthermore we assume that the FN messenger and the other flavons have vevs of the same order of magnitude: it results partly from the minimization procedure and partly from the constraints coming form the comparison with the measured mass hierarchies, as it will be clearer in the following.

The Higgs fields of our model relevant to build the fermion mass matrices transform under the gauge group and under the Z_4 factor of the flavour symmetry: in table 4.4 we summarize their transformation rules. The first three fields, ϕ, ϕ' and ρ, deal at LO only with the Dirac Yukawa couplings. Due to the Z_4 charges, ϕ and ϕ' are responsible for the third family and the charm quark masses, while ρ is responsible for the strange and μ masses. The field $\rho \sim (15, 2, 2)$ being in the adjoint of $SU(4)_C$ may develop vev along the $SU(4)_C$ direction diag$(-3, 1, 1, 1)$. This implies that the leptons which get mass via this field are a factor 3 heavier than the corresponding quarks and therefore this field is very useful to describe the second family, at least in the down sector, reproducing the well known Georgi–Jarlskog relation [99], $m_\mu \approx 3m_s$, at the high energy scale. As we show in the next sections, in order to recover the up-quark mass hierarchies the ρ projection along the light doublet Higgses, v^u_ρ and v^d_ρ, has to point only in the down direction: the requirement $v^u_\rho = 0$ can be realized only if the Higgs field content contains two identical copies of the Higgs field $(1, 2, 2)$ and this justifies the presence of both ϕ and ϕ'.

Finally, as we show in detail in the following sections, the field Δ_R is necessary to conclude the PS symmetry breaking pattern and to recover the SM gauge group through its spontaneous symmetry breaking vev. At the same time, when Δ_R develops a vev, it gives a Majorana mass to the right-handed neutrinos thus contributing to the effective neutrino mass matrix through the usual type-I seesaw mechanism. A second source for the neutrino mass matrix comes from Δ_L, in terms of the type-II seesaw mechanism.

Higgses	ϕ, ϕ'	ρ	Δ_L	Δ_R
PS	$(1, 2, 2)$	$(15, 2, 2)$	$(\overline{10}, 3, 1)$	$(10, 1, 3)$
Z_4	1	-1	1	-1

Table 4.4: *The Higgs fields responsible of generating fermion mass matrices and their transformation under the gauge and the Abelian flavour symmetries. All Higgs fields are singlets under $S_4 \times U(1)_{FN} \times U(1)_R$, while they can transform non-trivially under the Z_4 factor.*

In our scheme the neutrino mass matrix is dominated by type-II seesaw. As already stated in the two previous sections, the flavour structure of the effective neutrino mass matrix in equation (4.7) arises from an interplay between the two seesaw sources. In the PS context $m_D \sim M_u$ and this suggests a hierarchical structure for the type-I contribution, which does not agree with the flavour structure in (4.7). We show that, given $m_D \sim M_u$, the required flavour structure for the Majorana RH neutrino mass necessary to recover equation (4.7) is not allowed in our model. This suggests to find a construction in which the type-II contributions are dominating over the type-I and we show that such a feature puts strong constraints on the model building.

4.6 Fermion mass matrices at leading order

In this and the next section, we present the most important results: the fermion mass matrices and the resulting masses and mixings of the fermions. We first discuss the results at leading order in the flavon insertions. As expected for a model of bimaximal mixing, the results do not match the data very closely and next-to-leading order effects are very important as well. These are the topic of the next section.

The central object in the study of the fermion mass matrices is the matter superpotential, $\mathcal{W}_Y$. This Yukawa superpotential can be written as a sum of two pieces,

$$\mathcal{W}_Y = \mathcal{W}_{Dir} + \mathcal{W}_{Maj}. \tag{4.19}$$

These contain respectively terms with Dirac and Majorana structures. We study the superpotential making a power expansion in terms of flavon/Λ, distinguishing between leading and subleading couplings.

4.6.1 Dirac mass terms

We first study the Dirac matter superpotential at LO

$$\begin{aligned}\mathcal{W}^{LO}_{Dir} \;=\;& y_1 \frac{1}{\Lambda} F_L F^c_3 (\phi + \phi')\varphi + \\ &+ y_2 \frac{1}{\Lambda^3} F_L F^c_2 \theta^2 \rho \varphi' + \sum_{i=1}^{4} y_{3,(i)} \frac{1}{\Lambda^5} F_L F^c_2 \theta^2 (\phi + \phi') X^{(1)}_i + \\ &+ \sum_{i=1}^{3} y_{4,(i)} \frac{1}{\Lambda^4} F_L F^c_1 \theta^2 \rho X^{(2)}_i + y_5 \frac{1}{\Lambda^5} F_L F^c_1 \theta^2 (\phi + \phi') \chi^3 \,.\end{aligned} \tag{4.20}$$

Here we use a compact notation to avoid the proliferation of coefficients: the term $X^{(1,2)}_i$ represents a list of products defined as

$$\begin{aligned} X^{(1)}_i &\equiv \{\varphi^3,\, \varphi^2\varphi',\, \varphi\varphi'^2,\, \varphi'^3\}\,, \\ X^{(2)}_i &\equiv \{\varphi^2,\, \varphi\varphi',\, \varphi'^2\}\,. \end{aligned} \tag{4.21}$$

Each term represents all the different S_4 contractions which can be constructed with those flavons; furthermore we indicate with $y_1(\phi+\phi')$ the combination $y^{(1)}_1\phi + y^{(2)}_1\phi'$ and similarly for $y_{3,\,(i)}$ and y_5.

When the flavour symmetry is broken, the model describes a non-minimal PS model in which the Yukawa couplings present a well defined structure. Then, when the PS gauge symmetry is broken to the SM gauge group ϕ, ϕ' and the colour singlet component of ρ mix in four light Higgses, two up-type and two down-type, $h_{u,d}$ and $h'_{u,d}$. Thus at the EW scale ϕ, ϕ' and ρ have non-vanishing projections to the light Higgs components that acquire a vev. We indicate these components as $v^{u,d}_{\phi}$, $v^{u,d}_{\phi'}$ and $v^{u,d}_{\rho}$. As already said, we need to impose that the ρ field has no projection along the up direction: $v^u_\rho = 0$. This can be realized because in terms of the light Higgs up-vevs, $v^u_1 = \langle h_u \rangle$ and $v^u_2 = \langle h'_u \rangle$, v^u_ρ is given by

$$v^u_\rho = U_{13} v^u_1 + U_{23} v^u_2\,. \tag{4.22}$$

The matrix U is introduced in appendix 4.A. The constraint $v^u_2 = -U_{13}/U_{23} v^u_1$ can be imposed thanks to the freedom we have in the superpotential and in the soft potential[5]. Note that we could relax the condition $v^u_\rho = 0$ allowing a mild hierarchy between v^u_ρ and v^d_ρ, for example of order λ^2, without affecting the final mass hierarchies, but in the following, for simplicity, we work under the assumption that $v^u_\rho = 0$.

[5]This requirement, imposed *by hand*, could be motivated by some symmetry argument, but to introduce a mechanism that could explain $v^u_\rho = 0$, it would be necessary deeply modifying the structure of our model. In the present chapter we just assume this fine-tuning and we refer to the Appendix 4.A.2 for further details. We note that the fine-tuning we introduce in the model is similar to the fine-tuning which is universally accepted whenever the MSSM has to be recovered.

The final Dirac fermion mass matrices we get are given by

$$M_e^{LO} = -3\begin{pmatrix} 0 & 0 & 0 \\ 0 & y_2 & 0 \\ 0 & -y_2 & 0 \end{pmatrix} v_\rho^d \lambda^3 + \begin{pmatrix} 0 & 0 & 0 \\ 0 & 0 & y_1 \\ 0 & 0 & y_1 \end{pmatrix} v_\phi^d \lambda \,, \tag{4.23}$$

$$M_d^{LO} = \begin{pmatrix} 0 & 0 & 0 \\ 0 & y_2 & 0 \\ 0 & -y_2 & 0 \end{pmatrix} v_\rho^d \lambda^3 + \begin{pmatrix} 0 & 0 & 0 \\ 0 & 0 & y_1 \\ 0 & 0 & y_1 \end{pmatrix} v_\phi^d \lambda \,, \tag{4.24}$$

$$M_u^{LO} = m_D^{LO} = \begin{pmatrix} 0 & 0 & 0 \\ 0 & y_3 & 0 \\ 0 & -y_3 & 0 \end{pmatrix} v_\phi^u \lambda^5 + \begin{pmatrix} 0 & 0 & 0 \\ 0 & 0 & y_1 \\ 0 & 0 & y_1 \end{pmatrix} v_\phi^u \lambda \,. \tag{4.25}$$

We used the compact notation $y_i v_\phi^{u/d}$ to indicate $y_i^{(1)} v_\phi^{u/d} + y_i^{(2)} v_{\phi'}^{u/d}$ and absorbed all non-relevant CG coefficients. Note that y_3 is the sum of the different $y_{3,\,(i)}$ and that, by construction, $y_{1,2,3}$ can be considered complex coefficients with modulus of order 1. Note also that the different numerical coefficients between charged leptons and down quarks originate from to the presence of ρ instead of ϕ (ϕ') in the superpotential. The operators which should give contributions to the first families (those proportional to y_4 and y_5) are vanishing, thanks to the special flavon vev alignment. As a final comment, we are neglecting at this level of approximation the contributions to $M_{e,d}^{LO}$ coming from the operators proportional to y_3: these terms, which preserve the anti-alignment of the second and third entries of the second columns, are λ^2 suppressed with respect to the LO ones proportional to y_2.

The quark and lepton masses of the second and the third generation follow from (4.23)–(4.25)

$$\begin{aligned} m_\mu &\equiv -3\sqrt{2} y_2 v_\rho^d \lambda^3 \,, & m_\tau &\equiv \sqrt{2} y_1 v_\phi^d \lambda \,, \\ m_s &\equiv \sqrt{2} y_2 v_\rho^d \lambda^3 \,, & m_b &\equiv \sqrt{2} y_1 v_\phi^d \lambda \,, \\ m_c &\equiv \sqrt{2} y_3 v_\phi^u \lambda^5 \,, & m_t &\equiv \sqrt{2} y_1 v_\phi^u \lambda \,. \end{aligned} \tag{4.26}$$

We note that the top-quark Yukawa does not come from a renormalizable coupling; it has the same suppression as the other third family fermion masses. Obviously, the dominance of the top-quark mass should be justified by the hierarchy between v_ϕ^u and v_ϕ^d. The mass matrices in (4.23)–(4.25) are diagonalized by a maximal rotation in the sector (23), i.e. $U_e = V_d = V_u = R_{23}(\pi/4)$, while the fermion mass hierarchies are given by

$$\left|\frac{m_\mu}{m_\tau}\right| \sim \left|\frac{m_s}{m_b}\right| \sim \mathcal{O}(\lambda^2) \,, \qquad \left|\frac{m_c}{m_t}\right| \sim \mathcal{O}(\lambda^4) \,. \tag{4.27}$$

Furthermore, at the cut off, we recover some relations among the masses of different fermions: the $b - \tau$ unification and the Georgi–Jarlskog relation [99]

$$|m_\tau| = |m_b| \,, \qquad |m_\mu| = 3|m_s| \,. \tag{4.28}$$

Finally we should comment of the relative value of the top and of the bottom masses:

$$\left|\frac{m_t}{m_b}\right| = \left|\frac{y_1^{(1)} v_\phi^u + y_1^{(2)} v_{\phi'}^u}{y_1^{(1)} v_\phi^d + y_1^{(2)} v_{\phi'}^d}\right| \,. \tag{4.29}$$

Note that usually this ratio is proportional to $\tan\beta$, the ratio between the up- and down-vevs of the light Higgses, but this is not the case: indeed the light Higgses are combinations of ϕ, ϕ' and ρ and therefore we can define $\tan\beta$ as

$$\tan\beta \equiv \frac{\sqrt{(v_\phi^u)^2 + (v_{\phi'}^u)^2}}{\sqrt{(v_\phi^d)^2 + (v_{\phi'}^d)^2 + (v_\rho^d)^2}} \neq \left|\frac{m_t}{m_b}\right| \,. \tag{4.30}$$

4.6.2 Majorana mass terms

We now discuss the part of the superpotential which contains the Majorana couplings. At LO it is given by[6]

$$\mathcal{W}_{Maj}^{LO} = \tilde{k}_0\, F_L F_L \Delta_L + \sum_{i=1}^{2} \frac{\tilde{k}_{1,(i)}}{\Lambda}\, F_L F_L \Delta_L X_i^{(3)} + \sum_{i=1}^{3} \frac{\tilde{k}_{2,(i)}}{\Lambda^2} F_L F_L \Delta_L X_i^{(4)} + z_1\, F_3^c F_3^c \Delta_R \,. \tag{4.31}$$

This uses the compact notation

$$\begin{aligned} X^{(3)} &\equiv \{\chi,\, \sigma\}\,, \\ X^{(4)} &\equiv \{\chi^2,\, \chi\sigma,\, \sigma^2\}\,. \end{aligned} \tag{4.32}$$

This superpotential is responsible for giving the following Majorana LH and RH neutrino mass matrices:

$$M_L = \begin{pmatrix} k_0 & k_1\lambda & 0 \\ k_1\lambda & k_0 & 0 \\ 0 & 0 & k_0 + k_2\lambda^2 \end{pmatrix} v_L\,, \qquad M_R = \begin{pmatrix} 0 & 0 & 0 \\ 0 & 0 & 0 \\ 0 & 0 & z_1 \end{pmatrix} v_R\,. \tag{4.33}$$

Here v_L, v_R are the vevs of $\Delta_{L,R}$ respectively. At every order in λ, there is a diagonal contribution, parameterized by one of the $\tilde{k}_i$. The collective effect is captured in the effective parameter k_0 of order 1.

$$k_0 \equiv \tilde{k}_0 + \tilde{k}_{1,(2)}\lambda + \tilde{k}_{2,(1)}\lambda^2 + \tilde{k}_{2,(3)}\lambda^2 \tag{4.34}$$

In the same spirit we define k_1 and k_2

$$\begin{aligned} k_1 &\equiv \tilde{k}_{1,(1)} + \tilde{k}_{2,(2)}\lambda\,, \\ k_2 &\equiv -\tilde{k}_{2,(1)}\,. \end{aligned} \tag{4.35}$$

While M_L corresponds to the type-II contribution to the effective neutrino mass matrix, M_R provides a type-I term. Even at this approximation level, we note the tension between the two seesaw contributions: $m_\nu^{\text{(type-II)}} \equiv M_L$ presents a maximal rotation in the (12) sector, while it is easy to verify that $m_\nu^{\text{(type-I)}} \equiv m_D M_R^{-1} m_D^T$ shows a democratic structure on the (23) sector which corresponds to a maximal rotation here. To recover the mass matrix in (4.7) it is necessary that the type-II contribution dominates over the type-I terms: in this case it is sufficient to identify a with k_0, b with $k_1\lambda$ and c with $k_0 + k_2\lambda^2$.

The neutrino masses can be written as

$$|m_{1,2}|^2 = \Big(|k_0|^2 \mp 2|k_0|\,|k_1|\,\cos(\theta_{k_0} - \theta_{k_1})\lambda + |k_1|^2\,\lambda^2\Big) v_L^2\,, \tag{4.36}$$

$$|m_3|^2 = \Big(|k_0|^2 + 2|k_0|\,|k_2|\,\cos(\theta_{k_0} - \theta_{k_2})\lambda^2\Big) v_L^2\,. \tag{4.37}$$

Here θ_{k_i} is the argument of the complex number k_i. The definition of the solar mass difference implies that $|m_1|$ is smaller than $|m_2|$. This requires $\cos(\theta_{k_0} - \theta_{k_1}) > 0$. We see that in most of parameter space the spectrum is quasi degenerate, as the unsuppressed term with $|k_0|^2$ that appears in all three masses dominates over the other terms that are λ or λ^2 suppressed.

We also see that in most of the parameter space $|m_3|$ is the central eigenvalue: indeed $|m_1|$ ($|m_2|$) is shifted down (up) from the central value $|k_0|^2 v_L^2$ by a term proportional to λ, while $|m_3|$ stays closer to this central value as it is only shifted by a term proportional to λ^2. Having $|m_3|$ as the central eigenvalue is obviously in contradiction with experimental data. We conclude that our model is only viable when the term $2|k_0|\,|k_1|\,\cos(\theta_{k_0} - \theta_{k_1})\lambda$ is suppressed. This is clearly possible if either $|k_0|$ or $|k_1|$ or $\cos(\theta_{k_0} - \theta_{k_1})$ (or a combination of them) is small. In particular, the latter condition means that

[6] Regarding the terms which contribute to M_R, we consider at LO only the first non vanishing term in the superpotential.

k_0 and k_1 are almost perpendicular in the complex plane. We now investigate on these different scenarios, calculating the solar and atmospheric mass squared differences. Taking as definition of Δm^2_{atm} the mass squared difference between the heaviest and the lightest neutrinos, we have different results for normal (NO) and inverse (IO) mass ordering as given by

$$\begin{aligned}
\Delta m^2_{sol} &\equiv m_2^2 - m_1^2 \\
&= 4|k_0||k_1|\cos(\theta_{k_0}-\theta_{k_1})\lambda\, v_L^2\,, \\
\Delta m^2_{atm} &\equiv \begin{cases} \Delta m^2_{atmNO} \equiv (m_3^2 - m_1^2) \\ \Delta m^2_{atmIO} \equiv (m_2^2 - m_3^2) \end{cases} \\
&= \underbrace{2|k_0||k_1|\cos\left(\theta_{k_0}-\theta_{k_1}\right)\lambda\, v_L^2}_{\Delta m^2_{sol}/2} \mp\big(|k_1|^2 - 2|k_0||k_2|\cos\left(\theta_{k_0}-\theta_{k_2}\right)\big)\lambda^2\, v_L^2\,.
\end{aligned} \tag{4.38}$$

On the right-hand side of the last equation, the first term is suppressed by λ; the second one only by λ^2. We would be tempted to conclude that the first term gives the dominant contribution: it is however exactly this term that must be suppressed in order to avoid $|m_3|$ as the central eigenvalue. Furthermore, this term is equal to half of the solar mass squared difference that is about 30 times as small as the atmospheric splitting (see table 2.3). As a result, to recover a value for Δm^2_{atm} close to the measured one, we need that the second term on the right-hand side of equation (4.38) is the dominant one. We can estimate the ratio between the two terms by calculating r, the ratio of the two mass squared differences:

$$\begin{aligned}
(r_{NO,IO})^{-1} &\equiv \frac{\Delta m^2_{atmNO,IO}}{\Delta m^2_{sol}} \\
&= \frac{2|k_0||k_1|\cos\left(\theta_{k_0}-\theta_{k_1}\right)\lambda \mp \big(|k_1|^2 - 2|k_0||k_2|\cos\left(\theta_{k_0}-\theta_{k_2}\right)\big)\lambda^2}{4|k_0||k_1|\cos\left(\theta_{k_0}-\theta_{k_1}\right)\lambda} \\
&= \frac{1}{2} \mp \frac{|k_1|^2 - 2|k_0||k_2|\cos\left(\theta_{k_0}-\theta_{k_2}\right)}{4|k_0||k_1|\cos\left(\theta_{k_0}-\theta_{k_1}\right)}\lambda\,.
\end{aligned} \tag{4.39}$$

The natural range of this quantity r^{-1} would be something like $[0.3-0.7]$ (central value 0.5 and corrections of order λ). However, measurements give $r = 0.032^{+0.006}_{-0.005} \approx \lambda^2$, or in other words $1/r \sim 30 \sim \lambda^{-2}$. We conclude that

$$\frac{4|k_0||k_1|\cos\left(\theta_{k_0}-\theta_{k_1}\right)}{\big||k_1|^2 - 2|k_0||k_2|\cos\left(\theta_{k_0}-\theta_{k_2}\right)\big|} \approx \lambda^3\,. \tag{4.40}$$

The most natural explanation may be assuming that $\cos\left(\theta_{k_0}-\theta_{k_1}\right)$ is very small. In that case the absolute values of all parameters can still be of order one, which was part of the naturalness requirement of the model. Neutrinos present a quasi degenerate (QD) spectrum and both normal and inverse ordering are possible. The typical scale of neutrino masses v_L is given in this case by

$$v_L^2 = \frac{\Delta m^2_{atm}}{\lambda^2\big||k_1|^2 - 2|k_0||k_2|\cos\left(\theta_{k_0}-\theta_{k_2}\right)\big|} \approx (0.1\text{eV})^2\,. \tag{4.41}$$

Possible alternative solutions of equation 4.40 that give a non-QD spectrum can be obtained only by admitting the parameters belong to a larger and less natural, range, $\lambda^2 - \lambda^{-2}$. In this case when k_0 is of order λ^{-2} and $\cos\left(\theta_{k_0}-\theta_{k_1}\right) \sim \lambda$ while $k_{1,2}$ still of order one a inverse hierarchical (IH) spectrum can be obtained. Another possibility to get an IH spectrum is having k_0 and $\cos\left(\theta_{k_0}-\theta_{k_1}\right)$ of order one, $k_1 \sim \lambda^{-1}$ and $k_2 \sim \lambda^2$. Finally a normal hierarchical (NH) spectrum can be obtained only in the case in which $k_2 \sim \lambda^{-2}$, $\cos\left(\theta_{k_0}-\theta_{k_1}\right)$ and k_1 of order 1 and $k_0 \sim \lambda^2$.

At this moment, we conclude that the quasi-degenerate hierarchy (with either ordering) is the most natural outcome of our model, while normal and inverse hierarchy solutions are also possible, albeit with slightly unnatural values of the parameters. In section 4.10 we find that the renormalization flow dramatically changes these predictions.

4.6.3 Mixing matrices at Leading Order

As anticipated, the mixing pattern at leading order is the bimaximal pattern that does not describe the data very well. Only considering the NLO contributions, which we study in the next section, the model agrees with the measurements.

$$V = \mathbb{1} \ , \qquad U = R_{23}\left(-\frac{\pi}{4}\right) R_{12}\left(\frac{\pi}{4}\right) = \begin{pmatrix} 1/\sqrt{2} & -1/\sqrt{2} & 0 \\ 1/2 & 1/2 & -1/\sqrt{2} \\ 1/2 & 1/2 & +1/\sqrt{2} \end{pmatrix} \ . \tag{4.42}$$

4.7 Fermion mass matrices at higher orders

The NLO contributions in the mass matrices originate from two sources: the first are the higher order terms in the superpotential, while the others come from the insertion of the NLO flavon vevs in the operators in equations (4.20, 4.31). In section 4.8 we show how the flavons develop vevs and how they are corrected. Here we anticipate the results, reporting the flavon vevs in a form which is useful for the discussion in this section:

$$\begin{aligned} \langle\varphi\rangle &= \begin{pmatrix} 0 \\ 1 \\ 1 \end{pmatrix} v_\varphi + \begin{pmatrix} 1 \\ 0 \\ 0 \end{pmatrix} \delta v_\varphi \ , & \langle\varphi'\rangle &= \begin{pmatrix} 0 \\ 1 \\ -1 \end{pmatrix} v_{\varphi'} + \begin{pmatrix} 1 \\ 0 \\ 0 \end{pmatrix} \delta v_{\varphi'} \ , \\ \langle\chi\rangle &= \begin{pmatrix} 0 \\ 0 \\ 1 \end{pmatrix} v_\chi + \begin{pmatrix} 0 \\ 1 \\ 0 \end{pmatrix} \delta^2 v_\chi \ , & \langle\sigma\rangle &= v_\sigma \ . \end{aligned} \tag{4.43}$$

Some comments are in place: the subleading corrections are suppressed with respect the LO terms as $\delta v/v \sim \lambda$ and $\delta^2 v/v \sim \lambda^2$ for each flavon; NLO corrections to the second and third entries of $\langle\varphi\rangle$ and $\langle\varphi'\rangle$ are present, but they present the same structure of the LO terms and can be re-absorbed; similarly, the NLO corrections to the third entry of $\langle\chi\rangle$ and to $\langle\sigma\rangle$ are present, but they can be re-absorbed into the LO terms; the other entries of $\langle\chi\rangle$ do not receive any corrections at NLO. If we consider the NNLO approximation level, i.e. corrections of relative order λ^2 with respect the LO terms, we see that the second and the third entries of $\langle\varphi\rangle$ ($\langle\varphi'\rangle$) are not (anti-)aligned anymore and that the second entry of $\langle\chi\rangle$ is filled in. It is interesting that the first entry of $\langle\chi\rangle$ is still vanishing at this level. We will see the relevance of this structure in a while.

4.7.1 Dirac mass terms

The Dirac matter superpotential at NLO is given by

$$\begin{aligned} \mathcal{W}_{Dir}^{NLO} = & \sum_{i=1}^{3} y_{6,(i)} \frac{1}{\Lambda^2} F_L F_3^c (\phi + \phi') X_i^{(5)} + \\ & + \sum_{i=1}^{3} y_{7,(i)} \frac{1}{\Lambda^4} F_L F_2^c \theta^2 \rho X_i^{(6)} + \sum_{i=1}^{8} y_{8,(i)} \frac{1}{\Lambda^6} F_L F_2^c \theta^2 (\phi + \phi') X_i^{(7)} + \\ & + \sum_{i=1}^{6} y_{9,(i)} \frac{1}{\Lambda^5} F_L F_1^c \theta^2 \rho X_i^{(8)} + \sum_{i=1}^{7} y_{10,(i)} \frac{1}{\Lambda^6} F_L F_1^c \theta^2 (\phi + \phi') X_i^{(9)} + \\ & + \sum_{i=1}^{13} y_{11,(i)} \frac{1}{\Lambda^7} F_L F_1^c \theta^2 (\phi + \phi') X_i^{(10)} \ . \end{aligned} \tag{4.44}$$

We adopt a compact notation similar to the one in equation (4.20):

$$\begin{aligned}
X_i^{(5)} &\equiv \{\varphi\sigma,\, \varphi\chi,\, \varphi'\chi\}\,, \\
X_i^{(6)} &\equiv \{\varphi'\sigma,\, \varphi\chi,\, \varphi'\chi\}\,, \\
X_i^{(7)} &\equiv \{\varphi^3\chi,\, \varphi^2\varphi'\chi,\, \varphi\varphi'^2\chi,\, \varphi'^3\chi,\, \varphi^3\sigma,\, \varphi^2\varphi'\sigma,\, \varphi\varphi'^2\sigma,\, \varphi'^3\sigma\}\,, \\
X_i^{(8)} &\equiv \{\varphi^2\chi,\, \varphi\varphi'\chi,\, \varphi'^2\chi,\, \varphi^2\sigma,\, \varphi\varphi'\sigma,\, \varphi'^2\sigma\}\,, \\
X_i^{(9)} &\equiv \{\varphi^4,\, \varphi^3\varphi',\, \varphi^2\varphi'^2,\, \varphi\varphi'^3,\, \varphi'^4,\, \chi^4,\, \chi^3\sigma\}\,, \\
X_i^{(10)} &\equiv \{\varphi^4\chi,\, \varphi^3\varphi'\chi,\, \varphi^2\varphi'^2\chi,\, \varphi\varphi'^3\chi,\, \varphi'^4\chi,\, \varphi^4\sigma,\, \varphi^3\varphi'\sigma,\, \varphi^2\varphi'^2\sigma,\, \varphi\varphi'^3\sigma, \\
&\qquad \varphi'^4\sigma,\, \chi^5,\, \chi^4\sigma,\, \chi^3\sigma^2\}\,.
\end{aligned} \tag{4.45}$$

Note that not all of these terms are non-vanishing when the flavons develop a vev: in particular $X_i^{(9)}$ for any i do not give a contribution when the LO vevs are considered: only when the corrections to the vevs are introduced, they contribute to the mass matrices. For this reason also the terms with $X_i^{(10)}$ are taken into account, even if they are suppressed by an additional Λ. The other terms which are vanishing at this order of approximation are $X_i^{(8)}$ for $i = 4, 5, 6$ and $X_i^{(10)}$ for $i = 6, \ldots, 13$. When flavons and Higgs fields develop vevs, we get the following Dirac mass matrices:

$$M_e^{NLO} = -3 \begin{pmatrix} 0 & 0 & 0 \\ \tilde{y}_4 & 0 & 0 \\ \tilde{y}_9 & 0 & 0 \end{pmatrix} v_\rho^d \lambda^5 - 3 \begin{pmatrix} 0 & \tilde{y}_7\lambda & 0 \\ 0 & \tilde{y}_2 & 0 \\ 0 & -\tilde{y}_2 & 0 \end{pmatrix} v_\rho^d \lambda^3 + \begin{pmatrix} 0 & 0 & \tilde{y}_6\lambda \\ 0 & 0 & \tilde{y}_1 \\ 0 & 0 & \tilde{y}_1 \end{pmatrix} v_\phi^d \lambda\,, \tag{4.46}$$

$$M_d^{NLO} = \begin{pmatrix} 0 & 0 & 0 \\ \tilde{y}_4 & 0 & 0 \\ \tilde{y}_9 & 0 & 0 \end{pmatrix} v_\rho^d \lambda^5 + \begin{pmatrix} 0 & \tilde{y}_7\lambda & 0 \\ 0 & \tilde{y}_2 & 0 \\ 0 & -\tilde{y}_2 & 0 \end{pmatrix} v_\rho^d \lambda^3 + \begin{pmatrix} 0 & 0 & \tilde{y}_6\lambda \\ 0 & 0 & \tilde{y}_1 \\ 0 & 0 & \tilde{y}_1 \end{pmatrix} v_\phi^d \lambda\,, \tag{4.47}$$

$$M_u^{NLO} = \begin{pmatrix} 0 & 0 & 0 \\ \tilde{y}_5 & 0 & 0 \\ \tilde{y}_{10} & 0 & 0 \end{pmatrix} v_\phi^u \lambda^7 + \begin{pmatrix} 0 & \tilde{y}_8\lambda & 0 \\ 0 & \tilde{y}_3 & 0 \\ 0 & -\tilde{y}_3 & 0 \end{pmatrix} v_\phi^u \lambda^5 + \begin{pmatrix} 0 & 0 & \tilde{y}_6\lambda \\ 0 & 0 & \tilde{y}_1 \\ 0 & 0 & \tilde{y}_1 \end{pmatrix} v_\phi^u \lambda\,. \tag{4.48}$$

At this order, the neutrino Dirac matrix still equals the up-type quark matrix $m_D^{NLO} = M_u^{NLO}$. In the above equations we used the definitions

$$\begin{aligned}
\tilde{y}_1 &\equiv y_1 + y_{6,(1)}\lambda\,, \\
\tilde{y}_2 &\equiv y_2 + y_{7,(1)}\lambda\,, \\
\tilde{y}_3 &\equiv y_3 + \textstyle\sum_{i=5}^{8} y_{6,(i)}\lambda\,, \\
\tilde{y}_4 &\equiv \mathcal{F}_1[y_{9,(i)}] + \frac{1}{\lambda} y_4 \left(\frac{\delta v_{\varphi'}}{v_{\varphi'}} - \frac{\delta v_\varphi}{v_\varphi} \right)\,, \\
\tilde{y}_5 &\equiv \mathcal{F}_2\left[y_{11,(i)}\right] + \frac{1}{\lambda}\mathcal{F}_3\left[y_{10,(i)};\, \frac{\delta v_\varphi}{v_\varphi},\, \frac{\delta v_{\varphi'}}{v_{\varphi'}}\right] + \frac{1}{\lambda^2}\mathcal{F}_4\left[y_5;\, \frac{\delta^2 v_\chi}{v_\chi}\right]\,, \\
\tilde{y}_6 &\equiv (y_{6,(2)} + y_{6,(3)}) + \frac{1}{\lambda} y_1 \frac{\delta v_\varphi}{v_\varphi}\,, \\
\tilde{y}_7 &\equiv (y_{7,(2)} + y_{7,(3)}) + \frac{1}{\lambda} y_2 \frac{\delta v_{\varphi'}}{v_{\varphi'}}\,, \\
\tilde{y}_8 &\equiv \textstyle\sum_{i=1}^{4} y_{8,(i)} + \frac{1}{\lambda} \sum_{i=2}^{4} y_{3,(i)} \frac{\delta v_{\varphi'}}{v_{\varphi'}}\,, \\
\tilde{y}_9 &\equiv \mathcal{F}_5[y_{9,(i)}] + \frac{1}{\lambda} y_4 \left(\frac{\delta v_{\varphi'}}{v_{\varphi'}} + \frac{\delta v_\varphi}{v_\varphi} \right)\,, \\
\tilde{y}_{10} &\equiv \mathcal{F}_6\left[y_{11,(i)}\right] + \frac{1}{\lambda}\mathcal{F}_7\left[y_{10,(i)};\, \frac{\delta v_\varphi}{v_\varphi},\, \frac{\delta v_{\varphi'}}{v_{\varphi'}}\right]\,.
\end{aligned} \tag{4.49}$$

In the previous definitions we can see that each $\tilde{y}$ is the sum of two pieces: the first refers to the terms in equation (4.44) when the LO flavon vevs are considered; the second comes from the terms in equation (4.20) where the NLO flavon vevs are introduced. The only exception is $\mathcal{F}_3$ which refers to the term proportional to $X_i^{(9)}$ in equation (4.44) and that give contribution only when the NLO flavon vevs are considered. These two parts are of the same order of magnitude, since $\delta v/v \sim \lambda$ and $\delta^2 v/v \sim \lambda^2$. Note that $\mathcal{F}_i$ are distinct linear combinations of the arguments in the square brackets. The expressions in equations (4.46, 4.47, 4.48) are valid at NLO level. Note that the (anti-)alignment between the second and third entries of the (second) third families are still preserved. When considering higher order terms, this feature is lost and the $(1,1)$ entry of each mass matrix is filled.

The values for the charged fermion masses given in equation (4.26) are modified only by substituting the coefficients y_i with their tilde-versions:

$$y_1 \to \tilde{y}_1 \ , \qquad y_2 \to \tilde{y}_2 \ , \qquad y_3 \to \tilde{y}_3 \ . \tag{4.50}$$

At this approximation level, the first family masses are not yet well-described, because they are too small. We come back to these light masses in section 4.7.4.

4.7.2 Majorana mass terms

Moving to the Majorana part of the matter superpotential at NLO, we get

$$\begin{aligned}
\mathcal{W}_{Maj}^{NLO} \ = & \sum_{i=1}^{3} \frac{k_{3,(i)}}{\Lambda^3} F_L F_L \Delta_L X_i^{(11)} + \frac{z_2}{\Lambda^4} F_2^c F_2^c \theta^4 \Delta_R + \\
& + \frac{z_{3,(1)}}{\Lambda^4} F_2^c F_3^c \theta^2 \Delta_R \varphi\varphi' + \sum_{i=2}^{3} \frac{z_{3,(i)}}{\Lambda^5} F_2^c F_3^c \theta^2 \Delta_R X_{i-1}^{(12)} + \sum_{i=4}^{6} \frac{z_{3,(i)}}{\Lambda^6} F_2^c F_3^c \theta^2 \Delta_R X_{i-3}^{(13)} + \\
& + \sum_{i=1}^{4} \frac{z_{4,(i)}}{\Lambda^5} F_1^c F_3^c \theta^2 \Delta_R X_i^{(1)} + \sum_{i=5}^{12} \frac{z_{4,(i)}}{\Lambda^6} F_1^c F_3^c \theta^2 \Delta_R X_{i-4}^{(14)} + \\
& + \frac{z_5}{\Lambda^6} F_1^c F_2^c \theta^4 \Delta_R \varphi\chi + \sum_{i=1}^{2} \frac{z_{6,(i)}}{\Lambda^6} F_1^c F_1^c \theta^4 X_i^{(15)} \ .
\end{aligned} \tag{4.51}$$

As usual we used compact notation with

$$\begin{aligned}
X_i^{(11)} &\equiv \{\chi^3,\, \chi^2\sigma,\, \sigma^3\} \ , \\
X_i^{(12)} &\equiv \{\varphi\varphi'\chi,\, \varphi\varphi'\sigma\} \ , \\
X_i^{(13)} &\equiv \{\varphi^2\chi^2,\, \varphi\varphi'\chi^2,\, \varphi'^2\chi^2\} \ , \\
X_i^{(14)} &\equiv \{\varphi^3\chi,\, \varphi^2\varphi'\chi,\, \varphi\varphi'^2\chi,\, \varphi'^3\chi,\, \varphi^3\sigma,\, \varphi^2\varphi'\sigma,\, \varphi\varphi'^2\sigma,\, \varphi'^3\sigma\} \ , \\
X_i^{(15)} &\equiv \{\varphi^2,\, \varphi'^2\} \ .
\end{aligned} \tag{4.52}$$

A few comments are in place. Note that all the terms proportional to k_3 can be reabsorbed by a redefinition of $\tilde{k}_{0,1,2}$ and that the only new structure which corrects $\mathcal{M}_L$ comes from the term $F_L F_L \Delta_L \chi$ when we consider the subleading corrections of $\langle\chi\rangle$: as a result the entries $(1,3)$ and $(3,1)$ of $\mathcal{M}_L$ are filled in by terms proportional to λ^3. Regarding the contributions to the Majorana mass matrix for the RH neutrinos, it is important to see that the terms proportional to $z_{3,(i)}$ with $i = 1, \ldots, 3$ and to $z_{4,(i)}$ with $i = 1, \ldots, 4$ are vanishing, due to the particular flavon vev alignment of the model. As a consequence all the NLO contributions to $\mathcal{M}_R$ are of the order of λ^6, apart that one to the entry $(2,2)$ which is of the order of λ^4. Finally, we note that each entry of $\mathcal{M}_R$ is independent from all the others, being F_i^c singlets of the flavour symmetry, and therefore all the z_i are free parameters with

modulus of order 1. We listed only the dominant contributions, but the higher order terms would correspond to subleading corrections, which we can safely neglect in the following.

As a result of this analysis the Majorana masses for LH and RH neutrinos are given by

$$M_L^{NLO} = \begin{pmatrix} k'_0 & k'_1\lambda & k'_3\lambda^3 \\ k'_1\lambda & k'_0 & 0 \\ k'_3\lambda^3 & 0 & k'_0 + k'_2\lambda^2 \end{pmatrix} v_L \ , \qquad M_R^{NLO} = \begin{pmatrix} z_6\lambda^6 & z_5\lambda^6 & z_4\lambda^6 \\ z_5\lambda^6 & z_2\lambda^4 & z_3\lambda^6 \\ z_4\lambda^6 & z_3\lambda^6 & z_1 \end{pmatrix} v_R \ . \tag{4.53}$$

With the notation k'_i we account for all the redefinitions done on the parameters. As already stated when discussing the LO mass matrices, the contributions to the effective light-neutrino mass matrix come from the type-I and type-II seesaw mechanisms. The resulting NLO $m_\nu^{\text{(type-I)}}$ is given by

$$\begin{aligned} m_\nu^{\text{(type-I)}} &= m_D^{NLO}(M_R^{NLO})^{-1}(m_D^{NLO})^T \\ &= \begin{pmatrix} \tilde{y}_6^2\lambda^2 & \tilde{y}_1\tilde{y}_6\lambda & \tilde{y}_1\tilde{y}_6\lambda \\ \tilde{y}_1\tilde{y}_6\lambda & \tilde{y}_1^2 & \tilde{y}_1^2 \\ \tilde{y}_1\tilde{y}_6\lambda & \tilde{y}_1^2 & \tilde{y}_1^2 \end{pmatrix} \frac{(v_\phi^u)^2\lambda^2}{z_1 v_R} \ , \end{aligned} \tag{4.54}$$

This is diagonalized by a maximal rotation in the $(2\ 3)$ sector and not in the $(1\ 2)$ sector as demanded by equation 4.6. As a result, we need that the type-I seesaw contribution suppressed with respect to type-II seesaw one by at least a factor of order λ^2. Using equation (4.50), this translates to

$$\frac{m_t^2}{z_1 v_R} \leq \lambda^2 k'_0 v_L \ . \tag{4.55}$$

We remind here that v_L, v_R are the vevs of Δ_L and Δ_R respectively. In particular v_L is the vev developed by the SM $(1,3,1)$ triplet component of Δ_L and it is induced once the EW symmetry is broken. As we show in detail in the next sections the physical SM triplet $T \sim (1,3,1)$ arises by the mixing between the SM $(1,3,1)$ components of Δ_L and of two additional fields, Σ and Σ' transforming under the PS gauge symmetry as (1,3,3). The vev $\langle T \rangle$ of the $SU(2)_L$ triplet T is related to its mass M_T through the following expression

$$\langle T \rangle \simeq \alpha_{ij} \frac{v_i^u v_j^u}{M_T} \ . \tag{4.56}$$

Here α_{ij} are numerical coefficients arising by the details of the scalar potential and $v_1^u = \langle h_u \rangle \, , v_2^u = \langle h'_u \rangle$ are the vevs of the two up-type light Higgs doublets needed for the realization of our model (see appendix 4.A for details). Since v_L is the projection of $\langle T \rangle$ along Δ_L, neglecting fine tuned cases it is expected that

$$v_L \sim \langle T \rangle \ . \tag{4.57}$$

From equation (4.55) we need therefore that M_T and v_R satisfy

$$M_T \leq \lambda^2 \left(\frac{k'_0 z_1 \alpha_{ij} v_i^u v_j^u}{m_t^2} \right) v_R \, . \tag{4.58}$$

At the same time neutrino mass data imply that

$$k'_0 \alpha_{ij} \frac{v_i^u v_j^u}{M_T} \leq \mathcal{O}(1) \text{ eV} \, . \tag{4.59}$$

Combining the constraints of (4.58)–(4.59) we see that in the most natural scenario, assuming $\alpha_{ij} = 1$, M_T and v_R satisfy

$$\begin{gathered} v_R \gtrsim 30 \, M_T \ , \\ 10^{12} \, \text{GeV} \lesssim M_T \lesssim 10^{13} \, \text{GeV} \ . \end{gathered} \tag{4.60}$$

Nevertheless if we allow the numerical factors α_{ij} laying in the range $0.1 - 10$, then M_T, and consequently v_R, can be reduced even of two and one orders of magnitude respectively

$$10^{10} \, \text{GeV} \lesssim M_T \lesssim 10^{12} \, \text{GeV} \ . \tag{4.61}$$

In the following discussion of lepton mixing and in the phenomenological analysis, we assume that indeed type-II seesaw is dominating and neglect the type-I contributions. In the section devoted to the study of the scalar potential we justify this assumption and find the region of the parameters space where the type-II seesaw indeed dominates over type-I.

4.7.3 Mixing angles at the Next-to-Leading Order

Looking at equations (4.46)–(4.48) and (4.53) we see that the fermion mass matrices are of the required form as in (4.9) and (4.10). The resulting mixing matrices are modified with respect to the LO approximation and interesting new features follow. In the quark sector, the CKM matrix receives deviations from unity and at NLO the angle θ_{12}^q is not vanishing anymore:

$$\theta_{12}^q = \frac{\lambda}{\sqrt{2}} \frac{|\tilde{y}_7\tilde{y}_3 - \tilde{y}_2\tilde{y}_8|}{|\tilde{y}_2|\,|\tilde{y}_3|} \,. \tag{4.62}$$

Looking at this result, the meaning of the parameter λ is clear: it is defined as the ratio of the flavon vevs over the cut-off of the theory, but it also determines the order of magnitude of the Cabibbo angle. This justifies our initial assumption that λ is equal to 0.2. If the second columns of the up- and down-quark matrices are not proportional to each other, we can generate a non-vanishing Cabibbo angle θ_{12}^q, while the two other angles in the CKM matrix are still vanishing.

In the lepton sector, the PMNS is of the bimaximal form with large corrections as discussed in section 4.3. The solar and reactor angles are given by

$$\theta_{13}^l = \frac{\lambda}{2}\left|\frac{\tilde{y}_6}{\tilde{y}_1} - \frac{\tilde{y}_7}{\tilde{y}_2}\right|, \tag{4.63}$$

$$\theta_{12}^l = \frac{\pi}{4} - \frac{\lambda}{2}\left|\frac{\tilde{y}_6}{\tilde{y}_1} + \frac{\tilde{y}_7}{\tilde{y}_2}\right|. \tag{4.64}$$

As it is easy to see, the reactor angle and the deviation from the maximal value of the solar angle are of order λ and therefore the model is now in agreement with the experimental data[7], fulfilling the weak, but not the strong complementarity relations (4.4). At this approximation level, the atmospheric angle remains maximal. The relatively large value of θ_{13}^l was a prediction when this model was first presented.

4.7.4 Higher order effects

At the next-to-next-to-leading order (NNLO) and even higher orders, many new terms appear in the superpotential. However, only a few of them lead to new terms in the mass matrices, while the rest can be absorbed in redefinitions of the parameters as in equation (4.49). For this reason we do not report the full list of NNLO contributions, but we just comment on the physical consequences. Three effects are worth mentioning.

- As expected, the masses of the first families are strongly suppressed. We find that the down quarks and the electron masses are suppressed by a factor of λ^6 and the up-quark mass by a factor of λ^8. This leads to the following mass hierarchies in accordance with the wishlist of section 4.2
$$\left|\frac{m_d}{m_b}\right| \sim \left|\frac{m_e}{m_\tau}\right| \sim \lambda^5 \,, \qquad\qquad \left|\frac{m_u}{m_t}\right| \sim \lambda^7 \,. \tag{4.65}$$
- The (anti-)alignment of the (23) and (33) elements of the Dirac mass matrices in (4.46–4.48) gets broken as the new terms appear. The new elements are λ^2 suppressed with respect to the older

[7]Deriving equation (4.64), we already neglect the corrections which increase the value of the solar angle, instead of decreasing it

terms. As a result, the matrix that diagonalizes $M_i\, M_i^\dagger$, with $i = e, u, d$, has no longer an exact maximal mixing in the (2 3) sector. In the lepton sector, this translates to a λ^2 deviation from maximality in the atmospheric angle of the PMNS matrix. In the quark sector, the angle θ_{23}^q becomes of order λ^2. It is interesting to note that θ_{13}^q remains vanishing at this order. It only appears when even stronger suppressed terms are taken into account and is of order λ^3, in accordance with the Wolfenstein parametrization [21].

- The third columns of the mass matrices in (4.46)–(4.47) are proportional to v_ϕ^d, while the second column of M_d^{NLO} is proportional to v_ρ^d and that one of M_e^{NLO} to $-3v_\rho^d$. Therefore, also at NLO, equations (4.28) are fulfilled. At the NNLO level, terms proportional to v_ρ^d appear in the third columns of charged lepton and down-type quark matrices and terms proportional to v_ϕ^d in the second columns. The new terms are $\lambda^2 \approx 5\%$ suppressed with respect to the old entries. We thus expect deviations from the relations $|m_\tau| = |m_b|$ and $|m_\mu| = 3|m_s|$ at the 5% level.

After giving the right masses to the first generation fermions and introducing the (2 3) and (1 3) mixing angles in the CKM matrix, all points at the wishlists at the end of sections 4.2 and 4.3 are satisfied. So far, the model is successful. However, its success is based on a number of assumptions: that the flavons can indeed have the vacuum expectation value structure mentioned; that the Higgs fields indeed break the symmetry in the way assumed and that the values of fermion parameters derived at the high energy scale are still useful to describe physics when they are measured at low energy scales. These assumptions are studied in more detail in the next few sections.

4.8 The flavon scalar potential

In this section we comment on the vacuum alignment mechanism which explains the flavon vevs as in equations (4.16)–(4.18). It turns out that our desired alignment is exactly the one presented in [64], once we transform all the fields in our basis. Note indeed that it is possible to identify each flavon of table 4.3 with the flavons in [64], by simply comparing the transformation properties under the full flavour group:

$$\varphi \longrightarrow \varphi_l\ , \qquad \varphi' \longrightarrow \chi_l\ , \qquad \chi \longrightarrow \varphi_\nu\ , \qquad \sigma \longrightarrow \xi_\nu\ . \tag{4.66}$$

We use the unitary matrix Ω_T of appendix 3.B to move from the basis in [64] to our basis,

$$\begin{pmatrix} 1 & 0 & 0 \\ 0 & -i/\sqrt{2} & i/\sqrt{2} \\ 0 & 1/\sqrt{2} & 1/\sqrt{2} \end{pmatrix}\ . \tag{4.67}$$

We find (up to irrelevant phases) the following flavon vev alignment[8]. We comment about the presence of equivalent solutions below.

$$\varphi \propto \begin{pmatrix} 0 \\ 1 \\ 1 \end{pmatrix}\ , \qquad \varphi' \propto \begin{pmatrix} 0 \\ 1 \\ -1 \end{pmatrix}\ , \qquad \chi \propto \begin{pmatrix} 0 \\ 0 \\ 1 \end{pmatrix}\ . \tag{4.68}$$

These vacuum alignments correspond to equations (4.16)–(4.17).

The correct flavon vacuum alignment is ensured by a set of driving superfields among the same lines as described in section 2.4 dealing with a context similar to our model. All the driving fields transform as $U(1)_R = 2$ under the continuous R-symmetry and they appear linearly in the superpotential. In table 4.8 we show the driving fields and their transformation properties under $S_4 \times Z_4$.

It is easy to determine the correspondence between our set of driving fields and those of [64]:

$$D_R \longrightarrow \varphi_l^0\ , \qquad \varphi_R \longrightarrow \chi_l^0\ , \qquad \chi_R \longrightarrow \varphi_\nu^0\ , \qquad \sigma_R \longrightarrow \xi_\nu^0\ . \tag{4.69}$$

[8] The vevs of the fields φ and φ' is recovered by applying the unitary matrix in equation (4.67) to an equivalent configuration of equation (51) in [64], resulting from the application of the element $(TS)^2$ to (51) and of the element T to (18) of [64]

Driving	D_R	φ_R	χ_R	σ_R
S_4	2	3_2	3_1	1_1
Z_4	-1	-1	1	1

Table 4.5: *The driving field content and their transformation properties under $S_4 \times Z_4$. They are all singlets under the gauge group and the FN symmetry, while they transform as $U(1)_R = 2$ under the continuous R-symmetry.*

We now construct the driving superpotential w_d, which contains only flavons and driving fields and in particular neither matter fields nor Higgses, and look for the conditions that minimize the scalar potential,

$$V = \sum_i \left| \frac{\partial w_d}{\partial \Phi_i} \right|^2 + m_i^2 |\Phi_i|^2 + \dots \tag{4.70}$$

We write Φ_i to collectively denote all the scalar fields of the theory; m_i^2 are soft masses and dots stand for D-terms for the fields charged under gauge group and possible additional soft breaking terms. Since m_i^2 are expected to be much smaller that the mass scales involved in w_d, it is reasonable to minimize V in the supersymmetric limit and to account for soft breaking effects subsequently.

Since our flavon and driving field content exactly corresponds to the one in [64], we already know that the vev alignment in (4.16)–(4.17) represents an isolated minimum of the scalar potential. We only need to identify the relations which link the vevs v_φ, $v_{\varphi'}$, v_χ and v_σ among each other in our model. We therefore study the potential that can be constructed from the flavon driving fields and the ordinary flavons

$$\begin{aligned} w_d \; &= f_1 D_R \varphi\varphi + f_2 D_R \varphi'\varphi' + f_3 D_R \varphi\varphi' + f_4 \varphi_R \varphi\varphi' + \\ &+ M_1 \Lambda \chi_R \chi + f_5 \chi_R \chi\sigma + f_6 \chi_R \chi\chi + \\ &+ M_2^2 \Lambda^2 \sigma_R + M_3 \Lambda \sigma_R \sigma + f_7 \sigma_R \sigma\sigma + f_8 \sigma_R \chi\chi \; , \end{aligned} \tag{4.71}$$

The first line deals with only the fields φ and φ' and the other two with χ and σ. As also explained in [64], this leads to the alignment in equations (4.16, 4.17) where the vevs satisfy

$$\begin{gathered} f_1 v_\varphi^2 + f_2 v_{\varphi'}^2 + \sqrt{3} f_3 v_\varphi v_{\varphi'} = 0 \; , \\ v_\sigma = -\frac{M_1}{f_5} \; , \qquad\qquad v_\chi^2 = \frac{f_5^2 M_2^2 - f_5 M_1 M_3 + f_7 M_1^2}{2 f_5^2 f_8} \; . \end{gathered} \tag{4.72}$$

The solution in equations (4.16, 4.17, 4.72) is not unique, but it is possible to introduce a set of soft supersymmetric breaking parameters, which selects this solution as the lowest minimum of the scalar potential.

It is interesting to note the presence of an other source of uncertainty in our solution, which minimizes V. Given the symmetry of w_d and the field configurations of (4.16, 4.17, 4.72), by acting on them with elements of the flavour symmetry group $S_4 \times Z_4$, we can generate other minima of the scalar potential. These alternative solutions however are physically equivalent to those of the original set and it is not restrictive to analyze the model by choosing as local minimum that one in equations (4.16, 4.17, 4.72).

The Froggatt–Nielsen field can acquire a vev through a D-term as given in equation (2.70)

$$|v_\theta|^2 = |\langle\theta\rangle|^2 = \frac{M_{FI}^2}{g_{FN}} \; . \tag{4.73}$$

It is relevant to underline that the vevs in (4.72, 4.73), depend on mass parameters: all these mass scales naturally have the same order of magnitude and as a result $v_X/\Lambda_f \sim \lambda$. The only exceptions are the vevs of φ and φ', which depend on a flat direction. In the model, we simply assume that their vevs have values of the same order as all the other flavon vevs.

4.8.1 Higher order contributions

In this section we briefly comment on the corrections which enter in the flavon vevs, once the higher order contributions are taken into account. We leave all details to appendix 4.B.

In the superpotential w_d, the flavons which contribute to the Dirac mass terms, φ and φ', and those which contribute to the Majorana mass terms, χ and σ, at LO belong to two separate sectors, indeed any mixing term is prevented due to the Z_4 symmetry. This situation is not preserved at NLO, since the fields χ and σ are neutral under the Z_4 symmetry and therefore we can add each of them to all the terms in w_d. This leads to modifications to the LO vev alignment of (4.16) and it turns out that the first entries of $\langle\varphi\rangle$ and $\langle\varphi'\rangle$ are filled in, while the second and third entries are corrected by terms which can be however absorbed into the LO ones, without spoiling the alignment. Also the vevs in equation (4.17) receive some corrections: the first and second entries of $\langle\chi\rangle$ still vanish and the NLO contributions to the third entry can again be absorbed into the LO term. This discussion justifies the results showed in equation (4.43).

Corrections from the NNLO contributions are without particular alignments: in particular, the second and third entries of $\langle\varphi\rangle$ and $\langle\varphi'\rangle$ are no longer related, and also the second entry of $\langle\chi\rangle$ gets a non-zero value. It is interesting to note that the first entry of $\langle\chi\rangle$ remains zero.

4.9 Higgs scalar potential

In this section we present the study of the Higgs potential in our model. It is an interesting example of how the introduction of flavour symmetries and the assumptions made to get the correct mass matrices have non-negligible consequences on the Higgs sector. As a result, the study of the Higgs scalar potential and of the gauge and the running Yukawa couplings in a general non-flavour PS context does not strictly hold. Note that even if the following analysis refers to our particular choice of fields and symmetries, our conclusions can be taken as a general hint for a very large class of models that combine a discrete flavour symmetry with a grand unified scenario: indeed our model building strategy shares common features with other constructions. In particular the Higgs fields usually transform under the flavour symmetry G_f – in our case under the Z_4 part of it. This has direct consequences on the implementation of the grand unified symmetry breaking. Moreover type-II seesaw dominance and particular patterns of vanishing projections of the heavy Higgs fields on the light Higgs doublets are frequently required to get the correct fermion mass matrices.

In table 4.6 we list all the Higgs fields which are necessary to reproduce the correct mass matrices and to implement the desired PS symmetry breaking pattern. This extends table 4.4 that only contains that appear in the Yukawa superpotentials. The fields in table 4.6 carry one of the labels 'min' (from 'minimal'), 'ext' (from 'extended') or 'new'. This refers to the question whether they occur already in minimal Pati–Salam scenarios, only in extended (non-minimal) realizations or are new to our construction that combines GUT with flavour.

Some of these Higgs fields are already present in the minimal version of PS models [107]: typically a (15,1,1) multiplet – as the fields A and B in table 4.6 – is used to break $SU(4)_C$ down to $SU(3)_C \times U(1)_{B-L}$ and to induce the vevs of the couple of $(10,1,3) \oplus (\overline{10},1,3)$ – corresponding to the fields $\Delta_R \oplus \overline{\Delta}_R$ in table 4.6. The latter vevs breaks $SU(2)_R \times U(1)_{B-L}$ into the SM hypercharge $U(1)_Y$ concluding the symmetry breaking chain from the PS gauge group to the SM $SU(3)_C \times SU(2)_L \times U(1)_Y$. The field that triggers the EW symmetry breaking is usually a bidoublet (1,2,2) – as ϕ or ϕ' in table 4.6. The fields $(\overline{10},3,1) \oplus (10,3,1)$ – the fields $\Delta_L \oplus \overline{\Delta}_L$ in table 4.6 – do not develop vevs at tree level in the usual minimal PS model, but only when next to leading order terms are taken into account; these are typically suppressed by the Planck scale, as already stated in [107]. For this reason in the minimal PS the type-II seesaw contributions to the effective neutrino masses are almost negligible.

We identify three main reasons for which the existent studies of the symmetry breaking patterns in

Higgses	ϕ	ϕ'	ρ	ξ	Δ_L	Δ_R
PS	$(1,2,2)$	$(1,2,2)$	$(15,2,2)$	$(1,1,1)$	$(\overline{10},3,1)$	$(10,1,3)$
Z_4	1	1	-1	-1	1	-1
	min	new	ext	new	ext	min
Higgses	$\overline{\Delta}_L$	$\overline{\Delta}_R$	A	B	Σ	Σ'
PS	$(10,3,1)$	$(\overline{10},1,3)$	$(15,1,1)$	$(15,1,1)$	$(1,3,3)$	$(1,3,3)$
Z_4	1	-1	1	-1	1	-1
	ext	min	min	new	ext	new

Table 4.6: *All the Higgs fields of the model and their transformation properties under the gauge group and under Z_4. All Higgs fields are invariant under the other factors of the flavour symmetry group G_f. The labels 'min', 'ext' and 'new' indicate whether the field is present in minimal PS models, in extended ones or only in our realization.*

the PS context have to be modified and this automatically justifies the presence of the new fields in table 4.6.

- The assumption $v_\rho^u = 0$ necessary to distinguish the up-quark sector from the others and to recover the up-quark mass hierarchies can be realized only if we include two identical copies of bidoublet (1,2,2), ϕ and ϕ' (see details in appendix 4.A), and we then impose that four $SU(2)_L$ doublets (2 up-type and 2 down-type) remain light;

- Since the fields ρ, Δ_R and $\overline{\Delta}_R$ transform non-trivially under the flavour symmetry Z_4, it is necessary to introduce two copies of (15,1,1) multiplets, A and B, with opposite Z_4 charges, 1 and -1 respectively: A is responsible of inducing the breaking of $SU(2)_R$ through its coupling with Δ_R and $\overline{\Delta}_R$; B allows the coupling of the bidoublets ϕ, ϕ' with the bidoublet ρ. In this way all of these three fields have a non-vanishing projection on the light Higgs $SU(2)_L$ doublets;

- The component of Δ_L which corresponds to the usual SM triplet (1,3,1) can develop a vev once the EW symmetry is broken only in the presence of a trilinear coupling with the $SU(2)_L$ Higgs doublets. This coupling cannot be constructed with only the Higgs fields $\Delta_L \oplus \overline{\Delta}_L$ and the field content given in table 4.6. For this reason we need an additional field that mediates this coupling and the simplest choice would be a bitriplet $\Sigma \sim (1,3,3)$ that can couple with the fields ϕ, ϕ' or ρ and at the same time can mix with Δ_L, when Δ_R develops vev at the $SU(2)_R$ breaking scale. However, once more, the presence of the Z_4 symmetry obliges the introduction of two distinct (1,3,3) Higgs fields, Σ and Σ', with opposite Z_4 charges, 1 and -1 respectively. In this way Σ can couple to the bidoublets ϕ, ϕ' or ρ, while Σ' can mix with Δ_L. Finally, we need a new ingredient that mixes Σ with Σ': a PS singlet ξ charged -1 under Z_4 can do the job.

The scalar part of the superpotential is then given by[9]

$$\begin{aligned}\mathcal{W} =& \frac{1}{2}M_\phi\,\phi\phi + \frac{1}{2}M_{\phi'}\,\phi'\phi' + M_{\phi\phi'}\,\phi\phi' + \frac{1}{2}M_\rho\,\rho\rho + M_{\Delta_L}\,\Delta_L\overline{\Delta}_L + \\ &+ M_{\Delta_R}\,\Delta_R\overline{\Delta}_R + \frac{1}{2}M_A\,AA + \frac{1}{2}M_B\,BB + \frac{1}{2}M_\Sigma\Sigma\Sigma + \frac{1}{2}M_{\Sigma'}\Sigma'\Sigma' + \frac{1}{2}M_\xi\xi\xi + \\ &+ \lambda_\xi\Sigma\Sigma'\xi + \lambda_{\xi AB}AB\xi + \lambda_{\phi\rho}\phi B\rho + \lambda_{\phi'\rho}\phi' B\rho + \frac{1}{3}\lambda_A AAA + \\ &+ \frac{1}{2}\lambda_B BBA + \lambda_L\Delta_L\overline{\Delta}_L A + \lambda_R\Delta_R\overline{\Delta}_R A + \\ &+ \frac{1}{2}\lambda_{\phi\Sigma}\phi\phi\Sigma + \frac{1}{2}\lambda_{\phi'\Sigma}\phi'\phi'\Sigma + \lambda_{\phi\phi\Sigma}\phi'\phi\Sigma + \frac{1}{2}\lambda_{\rho\Sigma}\rho\rho\Sigma + \\ &+ \lambda_{\Delta\Sigma'}\Delta_L\overline{\Delta}_R\Sigma' + \overline{\lambda}_{\Delta\Sigma'}\Delta_R\overline{\Delta}_L\Sigma' + \frac{1}{3}\lambda_\Sigma\Sigma\Sigma\Sigma + \frac{1}{2}\lambda_{\Sigma'}\Sigma'\Sigma'\Sigma\,.\end{aligned} \tag{4.74}$$

The vacuum configuration at the GUT breaking scale is given by[10]

$$\langle\Delta_R\rangle = \left\langle\overline{\Delta}_R\right\rangle = M_R\,, \qquad \langle A\rangle = M_{C_1}\,, \qquad \langle B\rangle = M_{C_2}\,, \qquad \langle\xi\rangle = V_\xi\,. \tag{4.75}$$

The vevs $\langle A\rangle$ and $\langle B\rangle$ break the $SU(4)_C$ to $SU(3)_C\times U(1)_{B-L}$, while $\langle\Delta_R\rangle$ and $\left\langle\overline{\Delta}_R\right\rangle$ break $SU(4)_C\times SU(2)_R$ into $SU(3)_C\times U(1)_Y$. Therefore, given our field content, the colour breaking scale, $M_C = \mathrm{Max}(M_{C_1}, M_{C_2})$, is never smaller than the $SU(2)_R$ breaking scale, M_R. We may expect that $(M_{C_1}\sim M_{C_2}) = M_C$ but in principle they could be different. Finally V_ξ is expected to be close to the flavour breaking scale, due to the ξ gauge singlet nature.

The F-derivative system obtained by the superpotential (4.74) reads

$$\begin{aligned}&M_{\Delta_R} + \frac{3}{\sqrt{2}}\lambda_R M_{C_1} = 0\,,\\ &M_B M_{C_2}\sqrt{2}\lambda_B M_{C_1}M_{C_2} + \lambda_{AB\xi}M_{C_1}V_\xi = 0\,,\\ &M_A M_{C_1} + \frac{1}{\sqrt{2}}\lambda_B M_{C_2}^2 - \frac{2}{\sqrt{3}}\lambda_R M_R^2 + \sqrt{2}\lambda_A M_{C_1}^2 + \lambda_{AB\xi}M_{C_2}V_\xi = 0\,,\\ &M_\xi V_\xi + \lambda_{AB\xi}M_{C_1}M_{C_2} = 0\,.\end{aligned} \tag{4.76}$$

By solving the previous equations, we can express the mass parameters that enter in the superpotential in term of the dimensionless parameters λ_i and the physical breaking scales. All details regarding the mass spectrum are reported in the appendix 4.A, but some comments are in place. As in the minimal supersymmetric PS [107] when the singlet component of A develops a vev, there is an accidental $SU(3)$ symmetry involving Δ_R and $\overline{\Delta}_R$. When the singlet components of these fields acquire a vev the accidental symmetry is broken to $SU(2)$ giving rise to 5 Goldstone Bosons (GBs). At the same time $SU(2)_R\times U(1)_{B-L}$ is broken down to $U(1)_Y$, eating 3 of the 5 GBs. Therefore 2 of them, namely δ^{++} and $\overline{\delta}^{++}$ are left massless, down to the SUSY soft breaking scale ~ 1 TeV. This is a well known prediction of SUSY PS theories, which can be tested at LHC [108–111]. On the other hand, contrary to the minimal case described in [107], due to the mixing between the Higgs fields A and B, no colour octet is lighter than M_R.

In order to assure type-II dominance and to get the correct PS symmetry breaking pattern, it is necessary that $M_T \le M_R \le M_C \le V_\xi$. In the next section we present the constraints on the parameters that can be derived from this special mass ordering. For the moment, we just assume this scheme. Below we give the spectrum of the states that become massive at scales between M_{susy} and V_ξ. We express the states with the quantum numbers they would have under the Standard Model gauge group.

[9] All the Higgs fields are neutral under the continuous $U(1)_R$. The scalar superpotential explicitly breaks it, while preserving the usual R-parity. The terms in equation (4.74) can be generated from a $U(1)_R$-conserving superpotential in which the breaking is mediated by additional fields, which are $U(1)_R = 2$ and develop non-vanishing vevs. For instance the mass term $M_\phi\,\phi\phi$ can originate from a trilinear term $X\,\phi\phi$, when $\langle X\rangle = M_\phi$. Similarly the trilinear coupling $\lambda_\xi\Sigma\Sigma'\xi$ could originate by the non-renormalizable term $X\,\Sigma\Sigma'\xi/\Lambda'$, when $\langle X\rangle/\Lambda' = \lambda_\xi$ and Λ' is the energy scale of the dynamics of the field X. In our model we simply assume the existence of the terms in equation (4.74) in the superpotential and allow for an explicit breaking of the $U(1)_R$ symmetry in this sector.

[10] We redefine $\langle\Delta_R\rangle = v_R$ as $\langle\Delta_R\rangle = M_R$ in order to adapt to the usual notation.

1. At V_ξ

   At this scale we have two heavy $SU(2)_L$ triplets given in section 4.A.3.

2. Between V_ξ and M_C In this range a number of fields become massive. These are

   - all the SM singlets given in section 4.A.1 except one, called ξ_0,
   - the colour triplets given in section 4.A.1,
   - the colour octets given in section 4.A.1,
   - the heavy doublets given in section 4.A.2,
   - the two heavy couples of $SU(2)_L$ triplets given in section 4.A.3.

3. At M_C

   At the scale where the extended colour group of the Pati–Salam theory breaks the colour scalars originating by $\Delta_R \oplus \overline{\Delta}_R$, ρ and $\Delta_L \oplus \overline{\Delta}_L$ become massive. These are

   - the $SU(2)_L$ singlets given in section 4.A.1,
   - the $SU(2)_L$ doublets given in section 4.A.2,
   - the $SU(2)_L$ triplets given in section 4.A.3.

4. At M_R

   At the scale where the righthanded $SU(2)$ is broken, the singlet ξ_0 becomes massive;

5. At M_T

   At the scale M_T of the type-II seesaw, the light couple of $SU(2)_L$ triplets given in section 4.A.3 obtains a mass.

6. At M_{susy}, the supersymmetry scale, next to the familiar sparticles, we find

   - the scalar singlets δ^{++} and $\overline{\delta}^{++}$ given in section 4.A.1 – these are well known low-energy remnants of models with Pati–Salam unification,
   - the $SU(2)_L$ light doublets given in section 4.A.2.

With the Higgs field content given in tables 4.4 and 4.6 and the scalar spectrum so far sketched we can calculate the running of the gauge couplings and see if the conditions given in (4.60) or those in (4.61) can be satisfied. Furthermore, in the study of this running (see appendix 4.C for details) from the M_{GUT} to the EW scale we have to impose the following constraints.

- We should recover the EW values for α_3, α_2 and α_1, related to the gauge couplings of the SM gauge group ;
- At $M_R \leq M_C$ the hypercharge $U(1)_Y$ is obtained by the $SU(2)_R \times U(1)_{B-L}$ breaking;
- We impose $\alpha_{B-L} = \alpha_C$ at M_C ;
- The 'GUT scale' is defined as the scale at which the largest $\alpha_i = 1$. In this way we are sure to be in a perturbative regime up to the GUT scale and thus we are allowed to adopt the one-loop renormalization group equations (RGEs).

Even using all these constraints we are left with two more free parameters, the value of the $SU(4)_C$ and $SU(2)_R$ breaking scales, i.e. M_C and M_R respectively.

We adopt two distinct approaches, that we indicate as the *more constraining* and the *less constraining* ones. In the first case we define M_C to be the scale at which the largest α_i is equal or smaller than $1/4\pi$. In this way all the gauge coupling g_i are smaller than 1 at M_C . In the second case we allow the largest α_i to correspond to a gauge coupling in the range $1 < g_i < 3$, so $1/4\pi < \alpha_R < 9/4\pi$. Then M_R should satisfies equation (4.60) or (4.61), but its exact value is not fixed yet.

A few general comments are in place. The non-minimal PS field content affects the running of the gauge couplings in a non-negligible way. In particular the presence of the charged singlets δ^{++} and $\overline{\delta}^{++}$ down to M_{susy} deeply modifies the $U(1)_Y$ and $SU(2)_R$ gauge coupling evolution. It turns out that the largest α_i above the M_R scale is always α_R. Therefore the two approaches we described can be formulated as follows:

- More constraining approach $\Longleftrightarrow \alpha_R < 1/4\pi$, at M_C
- Less constraining approach $\Longleftrightarrow 1/4\pi < \alpha_R < 9/4\pi$, at M_C .

4.9.1 More constraining approach

In this case there are no solutions neither for the ranges of values of M_T and M_R given in equation (4.60) nor for those in (4.61). Indeed we find that $M_R \leq 10^{12}$ GeV, as can be seen in fig. 4.7. In other words if we adopt this constraining approach to fix the value of M_C, the type-I and type-II seesaw scales require Yukawa parameters which are at least two orders of magnitude far from their natural values to reproduce the correct neutrino mass scale. This solution is not satisfactory: in this case the type-II seesaw dominance is obtained by increasing the Yukawa couplings in the right neutrino sector and at the same time reducing the coupling of the left-handed neutrinos with the scalar triplet. Even if this may be considered a solution, the challenge was to provide a justification of type-II seesaw dominance through the analysis of the Higgs scalar potential and not by tuning the Yukawa parameters. Moreover we introduced a FN Abelian symmetry to explain the small ($\leq 10^{-2}$) Yukawa parameters necessary in the charged fermion sector to reproduce the correct mass hierarchies. The presence of Yukawa parameters of this order in the purely left-handed neutrino sector makes the introduction of the FN symmetry questionable.

4.9.2 Less constraining approach

In this case there are solutions only for the second range of values of M_T and M_R given in equation (4.61). As can be seen in fig. 4.8, M_R can now reach the value of 10^{13} GeV. The three scales M_R, M_C and M_{GUT} are compressed in a narrow region around 10^{13} GeV and therefore our model is described by an extended MSSM model almost up to the GUT scale, defined as the scale where one of the couplings – in practice g_R – becomes non-perturbative [11], i.e. $\alpha_i > 1$. Nevertheless, the PS origin is reflected in the non-trivial relations between the Yukawa couplings. In conclusion, by admitting the Yukawa parameters span in a range 0.1–10. The scales M_R, M_C and M_{GUT} are driven to be very close to each other; we have found a narrow region of the parameter space where our model could still give a realistic description of fermion masses and mixings and in which type-II seesaw dominance is not imposed by hand.

To finally consider our model viable, we should study the stability of the flavour structure of the mass matrices under the RGEs from the GUT scale down to the EW one. The study of the full set of the

[11] Above this energy scale an other gauge structure could be active. We do not take in consideration an high-energy completion of the model, but it is reasonable that larger gauge groups or particular constructions could be present at these energies: for example an $SO(10)$ inspired approach in which fermions do not belong to a unique representation.

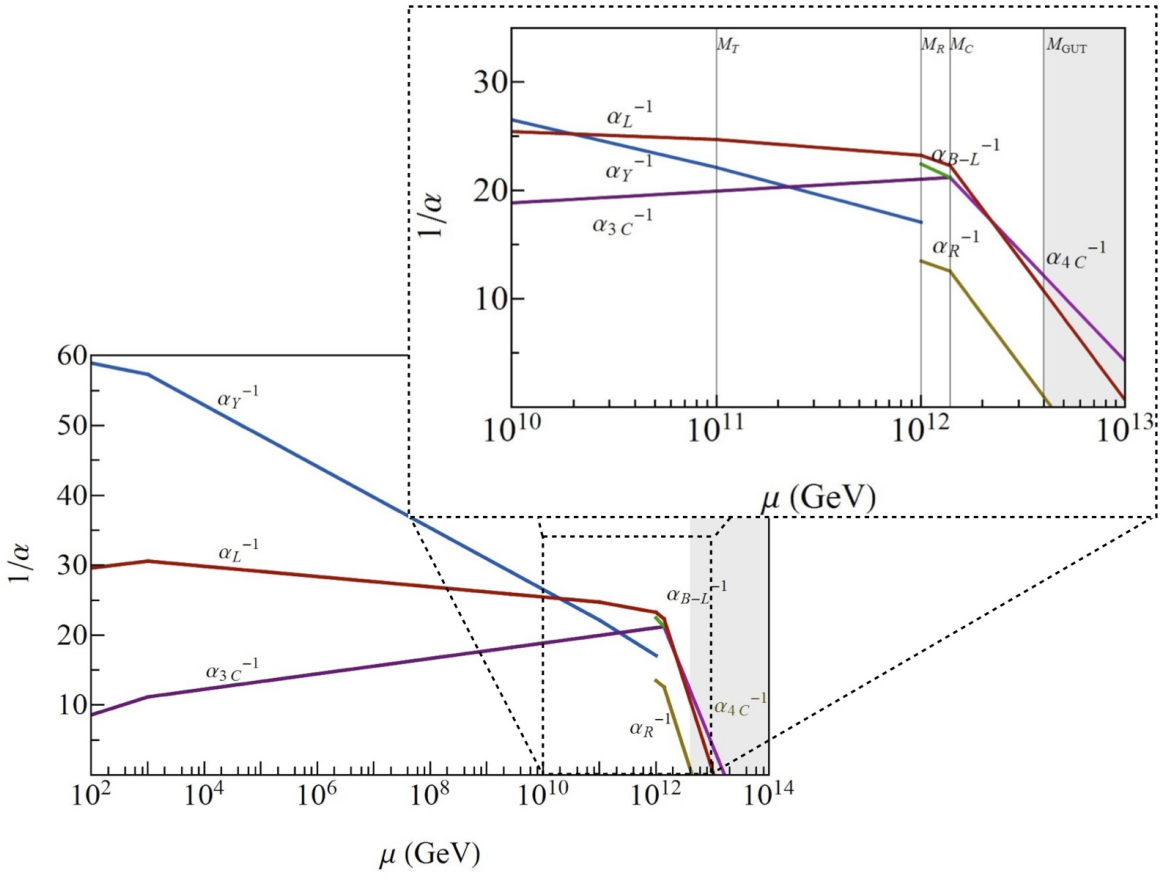

Figure 4.7: *The running of the gauge coupling constants in the more constraining approach.* $M_T = 10^{11}$ *GeV,* $M_R = 10^{12}$ *GeV,* $M_C = 1.4 \times 10^{12}$ *GeV (where* $\alpha_R = 1/4\pi$*) and* $M_{gut} = 4.0 \times 10^{12}$ *GeV (where* $\alpha_R = 1$*). In the dotted figure, we show a detail of the full plot, restricting the energy scale inside the range* $10^{10} \div 10^{13}$ *GeV.*

RGEs of the model presented is beyond the purpose of this work. For this reason we neither run the parameters of the scalar superpotential nor include and run the parameters of the soft SUSY breaking potential. Under these approximations the EW vacuum expectation values do not change from the GUT scale down to the EW one. However this does not affect our conclusions for what concerns the stability of the mass matrix structures since the EW vev shifts due to the running factorize out and leave the Yukawa flavour structure unchanged. The study of the Yukawa matrix running is done in the next section.

4.10 Running of the Yukawa couplings

In the previous section we analyzed the constraints on the scalar Higgs sector coming from the requirement of type-II seesaw dominance and from the presence of the flavour symmetry under which the Higgs fields non-trivially transform. We found that the model is viable only in a small region of the parameter space for which M_R, M_C and $M_{GUT} \sim 10^{13}$ GeV are very close to each other. At the same time M_T lies at only one order of magnitude below M_R. For these reasons to study the stability of the flavour structure of the fermion mass matrices at low scale we can consider only the running from M_T onwards, thus neglecting the running from higher energies. Furthermore we also neglect the running from $M_{\rm susy}$ to the EW scale, which would introduce only minor corrections. We work under the assumption that type-II seesaw is dominating over type-I and moreover that the

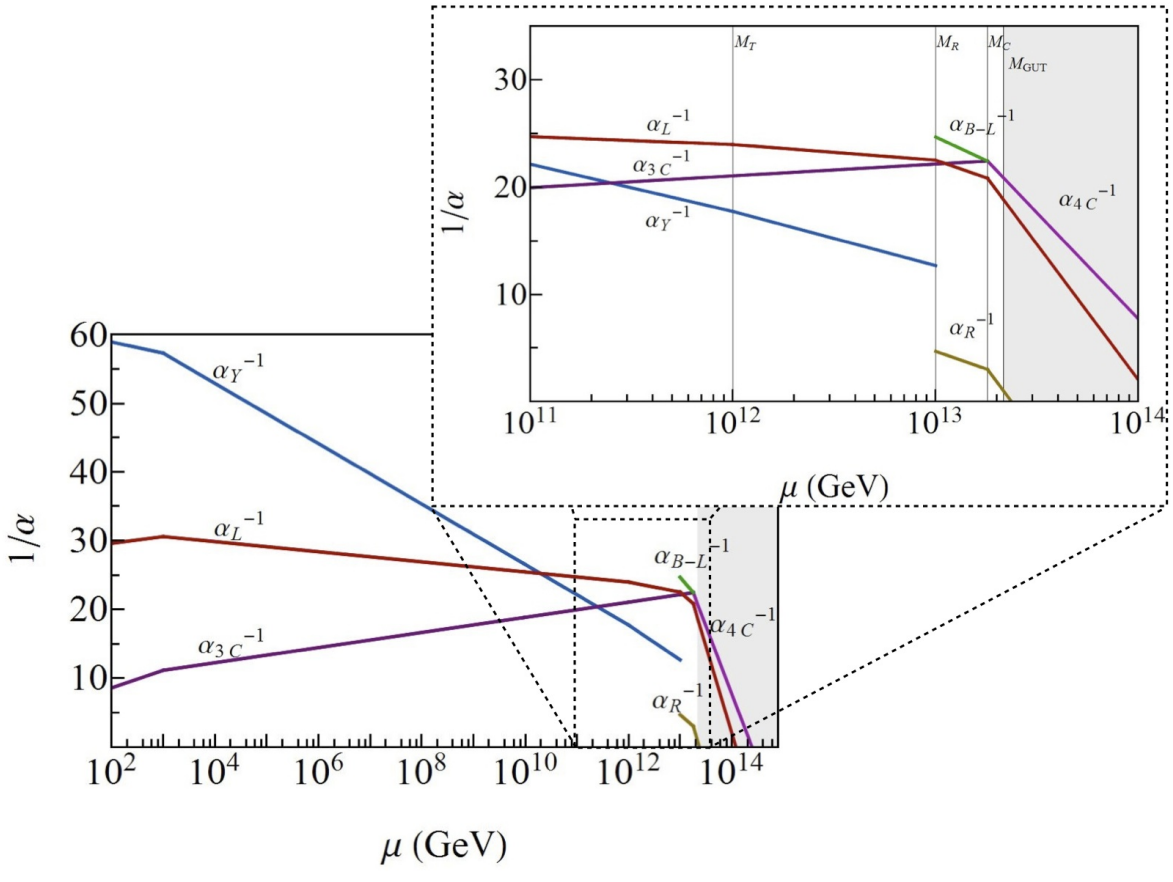

Figure 4.8: *The running of the gauge coupling constants in the less constraining approach.* $M_T = 10^{12}$ *GeV,* $M_R = 10^{13}$ *GeV,* $M_C = 1.8 \times 10^{13}$ *GeV (where* $\alpha_R = 1/3$*) and* $M_{gut} = 2.2 \times 10^{13}$ *GeV (where* $\alpha_R = 1$*). In the dotted figure, we show a detail of the full plot, restricting the energy scale inside the range* $10^{11} \div 10^{14}$ *GeV.*

effects from the type-I terms under the RGEs are negligible. Therefore, when studying the running of the Yukawa couplings, we do not take into account the Weinberg operator originating by integrating out the right-handed neutrinos. The error we introduce in this way is less than λ^2 and we will see in a while that these contributions do not modify our results. Furthermore, we study the stability under the Renormalization Group (RG) running in the approximation corresponding to the NLO, i.e. considering the mass matrices introduced in equations (4.46)–(4.48).

4.10.1 Yukawa matrices at M_T

We start the renormalization group running at M_T; at this scale we integrate out the $SU(2)_L$ scalar triplet T obtaining an effective Weinberg operator responsible of the type-II seesaw contribution. The origin of this effective operator is in the Majorana parts of the matter superpotential given in (4.31) and (4.51), that contain terms with the coupling

$$F_L F_L \Delta_L \ . \tag{4.77}$$

The scalar part of the superpotential (4.74) contains the terms

$$\begin{aligned}&\frac{1}{2}\lambda_{\phi\Sigma}\phi\phi\Sigma+\frac{1}{2}\lambda_{\phi'\Sigma}\phi'\phi'\Sigma+\lambda_{\phi\phi\Sigma}\phi'\phi\Sigma+\frac{1}{2}\lambda_{\rho\Sigma}\rho\rho\Sigma+\\&+\lambda_{\Delta\Sigma'}\Delta_L\overline{\Delta}_R\Sigma'+\overline{\lambda}_{\Delta\Sigma'}\Delta_R\overline{\Delta}_L\Sigma'+\frac{1}{3}\lambda_{\Sigma}\Sigma\Sigma\Sigma+\frac{1}{2}\lambda_{\Sigma'}\Sigma'\Sigma'\Sigma\,.\end{aligned}\tag{4.78}$$

These terms ensure the mixing between the (1,3,1) ((1,3,-1)) components of Δ_L ($\overline{\Delta}_L$), Σ and Σ', whose lighter combination is identified with T ($\overline{T}$), and provides the coupling of T ($\overline{T}$) with the light doublets h_d and h'_d (h_u and h'_u). The effective Weinberg operator at M_T is given by

$$\alpha_{ij}Y_{L_{rs}}\,\frac{L_rL_sh_{u_i}h_{u_j}}{M_T}\,.\tag{4.79}$$

Here L_i represents the $SU(2)_L$ lepton doublets; $h_{u_1}=h_u$, $h_{u_2}=h'_u$ and α_{ij} are coefficients arising by the scalar potential whilst Y_L is given by 4.53 without terms of order λ^3, that we neglect because they are irrelevant for the following analysis.

$$Y_L=\begin{pmatrix}k'_0 & k'_1\lambda & 0\\ k'_1\lambda & k'_0 & 0\\ 0 & 0 & k'_0+k'_2\lambda^2\end{pmatrix}\,.\tag{4.80}$$

The Dirac part of the superpotential at M_T is written as a function of the charged fermion Yukawa matrices and the low energy Higgs fields $h_{u,d}$ and $h'_{u,d}$.

$$Y_uQ\,U^ch_u+Y'_uQ\,U^ch'_u+Y_dQ\,D^ch_d+Y'_dQ\,D^ch'_d+Y_eL\,E^ch_d+Y'_eL\,E^ch'_d\,.\tag{4.81}$$

These matrices have the same textures as their counterparts (4.46) –(4.48), but we absorb a factor of λ

$$\begin{aligned}Y_u&=\frac{1}{\beta}Y'_u=\begin{pmatrix}0 & \tilde{y}_8\lambda^5 & \tilde{y}_6\lambda\\ \tilde{y}_5\lambda^6 & \tilde{y}_3\lambda^4 & \tilde{y}_1\\ \tilde{y}_{10}\lambda^6 & -\tilde{y}_3\lambda^4 & \tilde{y}_1\end{pmatrix}\,,\\ Y_d&=U_{13}\begin{pmatrix}0 & \tilde{y}_7\lambda & 0\\ \tilde{y}_4\lambda^2 & \tilde{y}_2 & 0\\ \tilde{y}_9\lambda^2 & -\tilde{y}_2 & 0\end{pmatrix}\lambda^2+\begin{pmatrix}0 & 0 & \tilde{y}_6\lambda\\ 0 & 0 & \tilde{y}_1\\ 0 & 0 & \tilde{y}_1\end{pmatrix}\,,\\ Y'_d&=U_{23}\begin{pmatrix}0 & \tilde{y}_7\lambda & 0\\ \tilde{y}_4\lambda^2 & \tilde{y}_2 & 0\\ \tilde{y}_9\lambda^2 & -\tilde{y}_2 & 0\end{pmatrix}\lambda^2+\beta\begin{pmatrix}0 & 0 & \tilde{y}_6\lambda\\ 0 & 0 & \tilde{y}_1\\ 0 & 0 & \tilde{y}_1\end{pmatrix}\,,\\ Y_e&=-3U_{13}\begin{pmatrix}0 & \tilde{y}_7\lambda & 0\\ \tilde{y}_4\lambda^2 & \tilde{y}_2 & 0\\ \tilde{y}_9\lambda^2 & -\tilde{y}_2 & 0\end{pmatrix}\lambda^2+\begin{pmatrix}0 & 0 & \tilde{y}_6\lambda\\ 0 & 0 & \tilde{y}_1\\ 0 & 0 & \tilde{y}_1\end{pmatrix}\,,\\ Y'_e&=-3U_{23}\begin{pmatrix}0 & \tilde{y}_7\lambda & 0\\ \tilde{y}_4\lambda^2 & \tilde{y}_2 & 0\\ \tilde{y}_9\lambda^2 & -\tilde{y}_2 & 0\end{pmatrix}\lambda^2+\beta\begin{pmatrix}0 & 0 & \tilde{y}_6\lambda\\ 0 & 0 & \tilde{y}_1\\ 0 & 0 & \tilde{y}_1\end{pmatrix}\,.\end{aligned}\tag{4.82}$$

The U matrix defines the light $SU(2)_L$ Higgses in term of the PS Higgs field components, as explicitly written in appendix 4.A while $\tilde{y}_i$ has to be read as $U_{11}\tilde{y}_i^{(1)}+U_{12}\tilde{y}_i^{(2)}$ and $\beta\tilde{y}_i$ as $U_{21}\tilde{y}_i^{(1)}+U_{22}\tilde{y}_i^{(2)}$.

4.10.2 Analytical approximations

In the appendix 4.D, we report all the RGEs for the Yukawa matrices, while here we discuss the results. The RGEs present the general compact expressions

$$\begin{aligned}
\frac{dY_L}{dt'} &= \mathcal{F}_L\left[Y_{f'}Y_{f'}^\dagger\right]Y_L + Y_L\mathcal{F}_L^T\left[Y_{f'}Y_{f'}^\dagger\right] + \left[\mathcal{G}_\mathcal{L}\left[\mathrm{Tr}(Y_{f'}Y_{f'}^\dagger)\right] - \sum_i c_i^\nu g_i^2\right]Y_L\,, \\
\frac{dY_f}{dt'} &= \mathcal{F}_f\left[Y_{f'}Y_{f'}^\dagger\right]Y_f + \left[\mathcal{G}_f\left[\mathrm{Tr}(Y_{f'}Y_{f'}^\dagger)\right] - \sum c_i^f g_i^2\right]Y_f\,.
\end{aligned} \tag{4.83}$$

In these equations the index f runs over $\{e,u,d\}$; the parameter t' is defined as $t' \equiv t/(16\pi^2) \equiv \log\mu/(16\pi^2)$; $\mathcal{F}_X\left[\ldots\right]$ is a matrix written in terms of the fermion Yukawa matrices $Y_{f'}$; $\mathcal{G}_X\left[\ldots\right]$ is function of the trace in the flavour space over the Yukawa matrices $Y_{f'}$ and c_i^f are the Casimir coefficients related to the group representations (see appendix 4.D for the details). The generic solutions are given by

$$\begin{aligned}
Y_L(\mu) \sim \prod_i e^{-c_i^\nu\mathcal{I}_i} &\times \exp\left[\int_{t'(\mu_0)}^{t'(\mu)}\mathcal{G}_L\left[\mathrm{Tr}(Y_{f'}Y_{f'}^\dagger)\right]dt'\right]\times\exp\left[\int_{t'(\mu_0)}^{t'(\mu)}\mathcal{F}_L\left[Y_{f'}Y_{f'}^\dagger\right]dt'\right] \\
&\times Y_L(\mu_0)\times\exp\left[\int_{t'(\mu_0)}^{t'(\mu)}\mathcal{F}_L^T\left[Y_{f'}Y_{f'}^\dagger\right]dt'\right]\,, \\
Y_f(\mu) = \prod_i e^{-c_i^f\mathcal{I}_i} &\times \exp\left[\int_{t'(\mu_0)}^{t'(\mu)}\mathcal{G}_f\left[\mathrm{Tr}(Y_{f'}Y_{f'}^\dagger)\right]dt'\right]\times\exp\left[\int_{t'(\mu_0)}^{t'(\mu)}\mathcal{F}_f\left[Y_{f'}Y_{f'}^\dagger\right]dt'\right] \\
&\times Y_f(\mu_0)\,.
\end{aligned} \tag{4.84}$$

Here $\mathcal{I}_i = \int_{t'(\mu_0)}^{t'(\mu)} g_i(t')^2 dt'$. When we fix $\mu_0 \sim M_T$ and $\mu \sim M_{\rm susy}$ these formulas can be approximated as functions of $\Delta t' = 1/16\pi^2\log(M_{\rm susy}/M_T) \approx 0.13$

$$\begin{aligned}
Y_L(M_{\rm susy}) &\simeq \left(1 + \mathcal{G}_L\left[\mathrm{Tr}(Y_{f'}Y_{f'}^\dagger)\right]\Delta t' - \sum_i c_i^\nu\mathcal{I}_i\right)Y_L(M_T) + \\
&+ \left(\mathcal{F}_L\left[Y_{f'}Y_{f'}^\dagger\right]Y_L(M_T) + Y_L(M_T)\mathcal{F}_L^T\left[Y_{f'}Y_{f'}^\dagger\right]\right)\Delta t'\,, \\
Y_f(M_{\rm susy}) &\simeq \left(1 + \mathcal{G}_f\left[\mathrm{Tr}(Y_{f'}Y_{f'}^\dagger)\right]\Delta t' - \sum_i c_i^f\mathcal{I}_i\right)Y_f(M_T) + \mathcal{F}_f\left[Y_{f'}Y_{f'}^\dagger\right]Y_f(M_T)\,\Delta t'\,.
\end{aligned} \tag{4.85}$$

In the quark sector we find the following approximate expressions for the masses of the last two families and the Cabibbo angle

$$\begin{aligned}
m_t^2(M_{\rm susy}) &\sim m_t^2\left(1 - 2\textstyle\sum_i c_i^u\,\mathcal{I}_i + 14\,\gamma\,\Delta t'\right)\,, \\
m_c^2(M_{\rm susy}) &\sim m_c^2\left(1 - 2\textstyle\sum_i c_i^u\,\mathcal{I}_i + 6\,\gamma\,\Delta t'\right)\,, \\
m_b^2(M_{\rm susy}) &\sim m_b^2\left(1 - 2\textstyle\sum_i c_i^d\,\mathcal{I}_i + 16\,\gamma\,\Delta t'\right)\,, \\
m_s^2(M_{\rm susy}) &\sim m_s^2\left(1 - 2\textstyle\sum_i c_i^d\,\mathcal{I}_i + 8\,\gamma\,\Delta t'\right)\,, \\
\theta_{12}^q(M_{\rm susy}) &\sim \theta_{12}^q + \frac{1}{6\sqrt{2}}U_{13}^2\,\lambda\,\Delta t'\,.
\end{aligned} \tag{4.86}$$

Here $\gamma = m_t^2/(v_1^u + \beta v_2^u)^2$ and the masses and the Cabibbo angle on the right of the previous expressions are intended at the M_T scale. Note that the demand that m_b^2 is still positive at $M_{\rm susy}$ gives a lower bound on γ of 0.7. The charged lepton masses are very similar to the down-quark masses and indeed we have

$$\begin{aligned}
m_\tau^2(M_{\rm susy}) &\sim m_\tau^2\left(1 - 2\textstyle\sum_i c_i^e\,\mathcal{I}_i + 16\,\gamma\,\Delta t'\right)\,, \\
m_\mu^2(M_{\rm susy}) &\sim m_\mu^2\left(1 - 2\textstyle\sum_i c_i^e\,\mathcal{I}_i + 8\,\gamma\,\Delta t'\right)\,.
\end{aligned} \tag{4.87}$$

We now consider the neutrino sector (see [112–119] for a general approach to RGEs with or without flavour symmetries) and the modification due to the RG running. We recall that our model at the GUT scale naturally predicts the quasi degenerate (QD) spectrum, with both normal and inverse ordering, while choosing a less natural range of the parameters space we may have both the normal hierarchy (NH) and the inverted hierarchy (IH). To simplify the analysis of the effect of the RGEs on the neutrino mass matrix M_ν, we rotate M_ν by a maximal rotation in the $(1\ 2)$ sector. Then, at the high scale, M_ν is diagonal and reads as

$$M_\nu = \begin{pmatrix} k'_0 - \lambda k'_1 & 0 & 0 \\ 0 & k'_0 + \lambda k'_1 & 0 \\ 0 & 0 & k'_0 + \lambda^2 k'_2 \end{pmatrix} v_L \,. \tag{4.88}$$

Without loss of generality k'_0 can be taken real, by a redefinition on the phases. After the running at M_{susy} equation (4.88) gets a correction ΔM_ν. The form of this correction depends on the neutrino hierarchy. For the quasi-degenerate hierarchy and the inverse hierarchy (when $k'_2 \sim \mathcal{O}(1)$, it reads as follows (with $w_\pm = (\pm\gamma/\sqrt{2} + \sqrt{2}\lambda)$)

$$\begin{aligned} \frac{\Delta M_\nu}{v_L} \sim & \left(-k'_0 \sum_i c_i^\nu \mathcal{I}_i + \frac{13}{2} k'_0 \gamma\, \Delta t' \right) \mathbb{1} + \sum_i c_i^\nu \mathcal{I}_i \begin{pmatrix} \lambda k'_1 & 0 & 0 \\ 0 & -\lambda k'_1 & 0 \\ 0 & 0 & 0 \end{pmatrix} + \\ & + \Delta t' \begin{pmatrix} -2\lambda k'_0 - 13\lambda k'_1 \gamma/2 & -k'_0\gamma/2 & k'_0 w_- + k'_1 \lambda\gamma/2\sqrt{2} \\ -k'_0\gamma/2 & 2\lambda k'_0 + 13\lambda k'_1\gamma/2 & k'_0 w_+ + k'_1\lambda\gamma/2\sqrt{2} \\ k'_0 w_- + k'_1\lambda\gamma/2\sqrt{2} & k'_0 w_+ + k'_1\lambda\gamma/2\sqrt{2} & 7\gamma k'_0 \end{pmatrix} . \end{aligned} \tag{4.89}$$

For the normal hierarchy case characterized by $k'_2 \sim \lambda^{-2}$, ΔM_ν assumes the following form

$$\begin{aligned} \frac{\Delta M_\nu}{v_L} \sim & \left(-k'_0 \sum_i c_i^\nu \mathcal{I}_i + \frac{13}{2} k'_0 \gamma\, \Delta t' \right) \mathbb{1} + \sum_i c_i^\nu \mathcal{I}_i \begin{pmatrix} \lambda k'_1 & 0 & 0 \\ 0 & -\lambda k'_1 & 0 \\ 0 & 0 & -\lambda^2 k'_2 \end{pmatrix} + \\ & + \Delta t' \begin{pmatrix} -2\lambda k'_0 - 13\lambda k'_1 \gamma/2 & -k'_0\gamma/2 & k'_0 w_- + k'_-\gamma/2\sqrt{2} \\ -k'_0\gamma/2 & 2\lambda k'_0 + 13\lambda k'_1\gamma/2 & k'_0 w_+ + k'_+\gamma/2\sqrt{2} \\ k'_0 w_- + k'_-\gamma/2\sqrt{2} & k'_0 w_+ + k'_+\gamma/2\sqrt{2} & 7\gamma(k'_0 + k'_2\lambda^2) \end{pmatrix} . \end{aligned} \tag{4.90}$$

Here $k'_\pm$ is given by $(k'_1\lambda \pm k'_2\lambda^2)$.

We can now consider the three different cases QD, NH and IH, which the model accounts for at the GUT scale.

- QD case $\Longrightarrow k'_0, k'_1, k'_2 \sim \mathcal{O}(1)$.
  The correction given by the running induces a rotation in the (23) sector characterized by

$$\tan 2\theta_{23}^\nu \sim -\frac{\sqrt{2}\Delta t'}{\lambda} \frac{k'_0}{|k'_1|}\gamma \sim -2\sqrt{2}\lambda \frac{k'_0}{|k'_1|}\gamma \,. \tag{4.91}$$

  The last equality follows from $\Delta t' \sim 2\lambda^2$. This is a large contribution, which deviates the atmospheric angle from the initial maximal value, spoiling the agreement with the experimental data at 3σ. A possible way out would be if this large correction is erased by a corresponding large correction in the charged lepton mass matrix. However this is not the case, because the maximal θ_{23}^e in the charged lepton mixing matrix is stable under the RG running. As a result, the QD case is not viable. This is an unexpected result. Obviously, the combination of flavour symmetries and grand unified symmetries puts more constraints on model building than naively expected.

- NH case $\Longrightarrow k'_0 \sim \lambda^2$, $k'_1 \sim \mathcal{O}(1)$ and $k'_2 \sim \lambda^{-2}$.
  The corrections both to the atmospheric and to the reactor angles are of order $\Delta t'\gamma/2\sqrt{2} \sim 3\lambda^3$ and can be safely neglected. Analogously, also the mass splittings receive deviations which can be neglected. On the other hand, the charged lepton mixing matrix is stable under the RG running. As a result the three mixing angles at M_{susy} can be well approximated with their initial values at M_T.

- First IH case $\Longrightarrow k'_0 \sim \lambda^2$ and $k'_1, k'_2 \sim \mathcal{O}(1)$.
  All the corrections to the neutrino mixing are of order $\gamma\Delta t'/\sqrt{2}$. While the solar mass splitting receives negligible contributions, the atmospheric mass splitting is corrected as follows

$$\Delta m^2_{atm}(M_{\text{susy}}) = \Delta m^2_{atm}\left(1 - 2\sum_i c^\nu_i \mathcal{I}_i + 13\,\gamma\,\Delta t'\right) . \tag{4.92}$$

  Corrections to the mixing angles coming from the RG running are proportional to $\Delta t'$. At this order of approximation, the corrections to $\theta^l_{12}(M_{\text{susy}})$ and $\theta^l_{13}(M_{\text{susy}})$ come from the charged lepton sector, while that one to $\theta^l_{23}(M_{\text{susy}})$ arises only by the neutrino sector. The resulting mixing angles at the susy scale are

$$\begin{aligned}
\theta^l_{12}(M_{\text{susy}}) &\sim \pi/4 - \theta^e_{12} + \theta^e_{13}\gamma/2\Delta t' , \\
\theta^l_{23}(M_{\text{susy}}) &\sim \theta^e_{23} + \gamma\Delta t' , \\
\theta^l_{13}(M_{\text{susy}}) &\sim \theta^e_{13} - \theta^e_{12}\gamma/2\Delta t' .
\end{aligned} \tag{4.93}$$

  These corrections are more significant than those of the NH case, but their magnitude is small enough to consider the mixing pattern still viable. In this scenario, we only used one 'unnatural' parameter ($k'_0 \sim \lambda^2$), while the NH case has two (one of order λ^2 and one of order λ^{-2}). We can thus conclude that after the dismissal of the QD scenario, the appearance of the inverse hierarchy with neutrino observables as above is a (weak) prediction of our model.

- Second IH case $\Longrightarrow k'_2 \sim \lambda^2$, $k'_0 \sim 1$ and $k'_1 \sim \lambda^{-1}$.
  We recover the same shifts as in the previous case for the atmospheric mass splitting and the lepton mixing angles. The difference lies in the fact that also the solar mass splitting gets a non-negligible correction

$$\Delta m^2_{sol}(M_{\text{susy}}) = \Delta m^2_{sol}\,(1 - 2\textstyle\sum_i c^\nu_i\,\mathcal{I}_i + 14\,\gamma\,\Delta t') . \tag{4.94}$$

  This scenario is thus also possible, but slightly disfavoured with respect to the previous one.

We conclude this section by re-stating the important conclusion. Due to interference between the flavour and the grand unified symmetry, the Yukawa coupling running from the GUT scale (or from the type-II seesaw scale) to a low scale has important effects. These effects are strongest in the quasi-degenerate case and we have seen that agreement with the data cannot support this shift. As a result, only the normal and inverse hierarchy are feasible, with the latter slightly preferred. In the next section we study the phenomenological consequences for the neutrino sector.

4.11 Neutrino Phenomenological Analysis

In the previous section, it was concluded that the quasi-degenerate spectrum is unstable under the RG running and becomes phenomenologically inviable due to too large corrections to the atmospheric mixing angle. Only the normal and inverse hierarchies were shown to be stable and phenomenologically viable. This is different from [64], where only the normal hierarchy and the quasi-degenerate spectrum with normal ordering were found.

In this section, we discuss neutrino phenomenology in more detail, focussing on the value of the reactor mixing angle θ^l_{13} and the possibility of neutrinoless double beta decay.

The analytical expression of the reactor mixing angle is given by equation (4.63) at NLO and it is corrected by the RG running as in equation (4.93) for the two IH scenarios studied in the previous section. We see that θ^l_{13} is typically of order $\lambda \approx 0.2$, so $\sin^2\theta^l_{13} \approx 0.04$. This is rather large: approximately at the $+2\sigma$ level according to [24], so still viable and values of θ^l_{13} just slightly smaller fit the central region very well. This is both true for the current data and for the data at the time when the model was first written down [22, 23].

Here, we complete the study of θ_{13}^l, performing a numerical analysis and comparing it with (the errors on) the data. As can be seen from equations (4.46)–(4.53), the neutrino and the charged lepton mass matrices at NLO are functions of many parameters. However the GUT nature of the model allows us to fix most parameters that occur at LO because they enter in the low energy expressions for quark and charged lepton masses, as can been seen comparing equation (4.26) with (4.86). Note that all dimensionless parameters, i.e. the $\tilde{y}_i$, can be fixed to be of order 1.

The other free parameters can be fixed as random numbers of order 1, except for the cases where we have argued in the previous section that they should have slightly larger or smaller values. Because of the use of random numbers, the predictions of our model are no longer single valued.

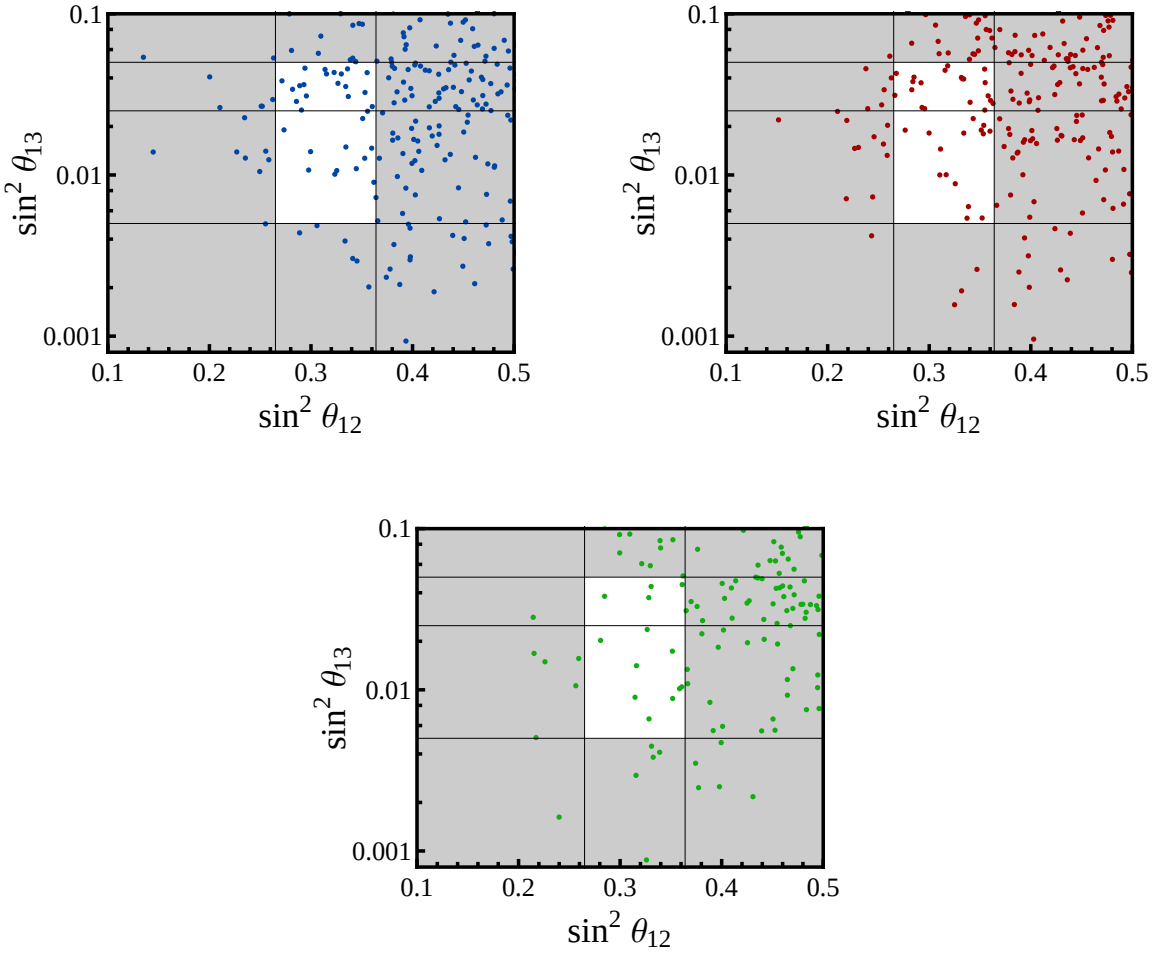

Figure 4.9: The solar angle versus the reactor angle. On the upper line the two IH cases of the previous section (on the left the first case and on the right the second one), while on the lower line the NH one. The two vertical lines are the 3σ bounds for $\sin^2\theta_{12}^l$ according to [24]. The upper horizontal line is the 3σ upper bound for $\sin^2\theta_{13}^l$ and the middle line is the best fit value and the lower line is the 3σ lower bound.

We plot the reactor angle versus the solar angle in figure 4.9. At NLO, equation (4.64), θ_{12}^l is driven away from the maximal value $\pi/4$ by a term proportional to λ (note that we take only the corrections which decrease the value of the solar angle, neglecting those which increase it). We see that this deviation is not for all values of the parameters large enough to bring it in the observed region, although this happens for a significant number of them. As explained above, larger values of $\sin^2\theta_{13}^l$ are favoured and almost all points are in the sensitive region for experiments.

To study neutrinoless double beta decay, we consider the effective $0\nu\beta\beta$ parameter m_{ee}, defined as

$$m_{ee} = [U \,\mathrm{diag}(m_1,\, m_2,\, m_3)\, U]_{11}. \tag{4.95}$$

In figure 4.10 we plot m_{ee} against the lightest neutrino mass, which is m_1 and m_3 in the NH and IH case respectively. The future experiments are expected to reach good sensitivities: 90 meV [30] (GERDA), 20 meV [31] (Majorana), 50 meV [32] (SuperNEMO), 15 meV [33] (CUORE) and 24 meV [34] (EXO). As a result, looking at figure 4.10, the whole IH band will be tested in the next future and with it the two cases of our model which allow for the IH spectrum.

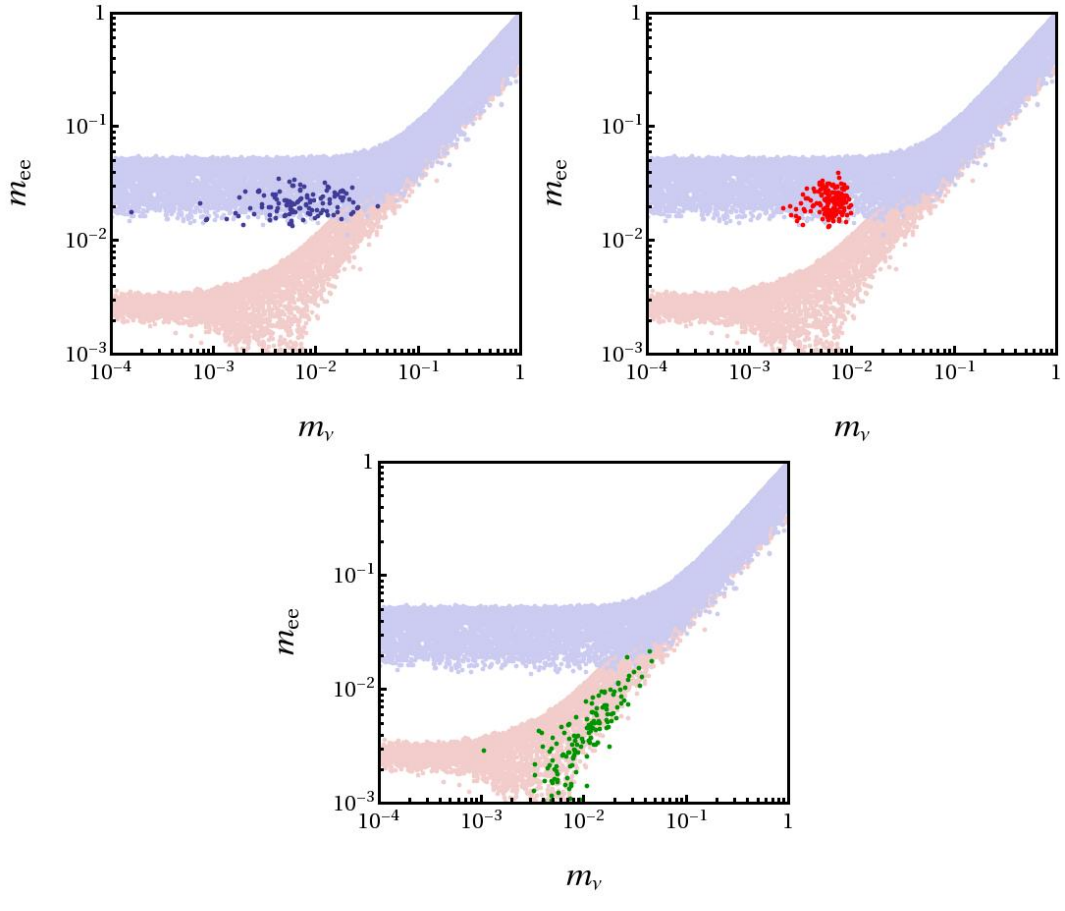

Figure 4.10: *Neutrinoless double beta decay plots. On the upper line the two IH cases of the previous section (on the left the first case and on the right the second one), while on the lower line the NH one. The background red (blue) points refer to the allowed region for the NH (IH), taking into account the lepton mixing angle values with their 3σ errors.*

4.12 Conclusions of the chapter

In this chapter we have addressed several aspects of the interplay between a GUT based model and a discrete flavour symmetry. The chapter should indeed be considered as the combination of three distinct parts: it starts with a part in which many concepts and motivations are introduced. In the second one we mainly discussed the building of the model from the flavour point of view, while in the last one we faced the problem to justify the assumptions made in the second part and to achieve the correct gauge symmetry breaking chain. We found that this gives non-trivial constraints on the model building.

More in detail, the symmetry group of our model is $PS \times G_f$, where PS stands for the GUT Pati–Salam gauge group $SU(4)_C \times SU(2)_L \times SU(2)_R$ and G_f for the flavour group $S_4 \times Z_4 \times U(1)_{FN} \times U(1)_R$. Within this GUT context one has the relationship between the down-quark and charged leptons mass matrices, $M_d \sim M_e$, which can easily be used to revise the old idea of quark-lepton complementarity. In the model this is obtained by the use of the non-Abelian discrete flavour symmetry S_4 properly broken through the vevs of a set of flavon fields, which transform as triplets under S_4. The additional Abelian symmetries, which enters in G_f, play different roles: Z_4 keeps quarks separated from leptons and neutrinos from charged leptons and prevents dangerous couplings in the superpotential of the model; $U(1)_{FN}$ helps to justify the charged fermion mass hierarchies; $U(1)_R$ is a common ingredient of supersymmetric flavour models. It contains the discrete R-parity and is useful to build a suitable flavon superpotential that allows the correct S_4 breaking pattern.

Already at the leading order, the model shows nice features: we are able to reproduce the mass hierarchy between the third and the second charged fermion families, the bottom-tau unification, the Georgi–Jarlskog [99] relation $|m_\mu| = 3|m_s|$ and, under the assumption of type-II seesaw dominance at the GUT scale, a realistic neutrino spectrum. However at this level of approximation, both the CKM and the PMNS mixing matrices are not correct: the quark mixing matrix coincides with the identity matrix, while the lepton one is given by the BM pattern. It is worth to recall here that the BM mixing corresponds to maximal solar and atmospheric angles and to a vanishing reactor angle: only the solar angle is not in agreement with the data as it deviates from the experimental central value by a quantity close to the Cabibbo angle, $\lambda \sim 0.2$.

At next-to-leading order, the wrong predictions for the fermion mixing angles are corrected: in the CKM matrix, the mixing angle θ^q_{12} receives contributions of the order of λ, fitting the value of the Cabibbo angle; analogously, in the PMNS matrix, the solar angle is corrected by the same amount and we find the nice result that $\theta^l_{12} \sim \pi/4 - \mathcal{O}(\lambda)$. At the same time, also the reactor angle receives significant contributions and indeed at this level of approximation it results $\theta^l_{13} \sim \mathcal{O}(\lambda)$: this is an interesting feature of our model, this value is close to the experimental upper bound at the time the model was constructed and indeed this prediction seems confirmed by more recent data. It will further be tested in the forthcoming neutrino experiments [42–45, 120–123].

Once we consider the higher order terms, we find the other two CKM angles of the correct order of magnitude, $\theta^q_{23} \sim \mathcal{O}(\lambda^2)$ and $\theta^q_{13} \sim \mathcal{O}(\lambda^3)$, and small corrections are introduced in the PMNS angles: in particular the atmospheric angle becomes $\theta^l_{23} \sim \pi/4 + \mathcal{O}(\lambda^2)$, justifying a small deviation from the maximality. For what concerns the masses, all the fermions are massive and the mass hierarchies fit the experimental observations.

On the other hand, the neutrino spectrum could be either quasi degenerate or normal or inverse hierarchical. Only the first case corresponds to a completely natural choice of the parameters, which, in the absence of an explanation coming form a higher energy theory, should be of order 1: in order to allow the NH and the IH, the parameters should span in a larger range of values, namely $\lambda^{-2} \div \lambda^2$. In short, the combination of flavour and GUT symmetries allow many observed patterns in the flavour sector to be reproduced. If at this moment a balance had to be made like we did at the end of sections 2.3.1 and 2.4.6, this balance is likely to be positive, or at least as positive as the balances of chapter 2. Our model is slightly larger, but it also explains much more peculiarities of the flavour sector.

In the third part of the chapter (from section 4.9) the tides turned. We have studied the Higgs scalar potential and the running of both the gauge couplings and the Yukawa mass matrices under the RGEs. With this analysis we looked for the constraints which arise to justify the Higgs field vev pattern used in the flavour section and the assumption of the type-II seesaw dominance. The presence of the flavour group G_f modifies the Higgs field content necessary to implement the classical breaking pattern of the PS gauge group and as consequence not all the results obtained by studying minimal versions of PS are recovered. In particular we need the presence of two PS multiplets $(15,1,1)$, A and B, responsible to break the unified colour symmetry $SU(4)_C$ to $SU(3)_C \times U(1)_{B-L}$. Two copies of the $(1,2,2)$ multiplet, ϕ and ϕ', and one $(15,2,2)$ field, ρ, are necessary to implement the condition $v^u_\rho = 0$. Lastly, we need the new fields $\Sigma, \Sigma' \sim (1,3,3)$ and $\xi \sim (1,1,1)$ to have a type-II seesaw contribution at tree level.

The running of the gauge couplings is affected by the large field content and in particular we found that the requirement of having type-II See-Saw dominance constrains the model in a small region of the parameter space, in which all the heavy mass scales are sandwiched between 10^{11} GeV and 10^{13} GeV. At the same time Yukawa mass matrix running shows that while the CKM Cabibbo angle is stable under the RGEs evolution, the PMNS mixing angles are stable only if neutrinos present a NH or an IH spectrum, ruling out the QD case. As already stated, the QD spectrum would be the most natural and probable case at the GUT scale, but the Yukawa RGEs analysis further reduces the allowed region of the parameter space. Whether the negative evidence of the third part of the chapter is enough to swing the balance mentioned above to the negative side (assuming it was positive to start with) is up for everybody's judgement, but it is clear that this evidence should be taken into account in order to form a fair opinion.

In section 4.11, we performed a brief phenomenological analysis of neutrino observables considering all the constraints which come from the flavour and the Higgs sectors. We have first considered the value of the reactor angle in terms of the deviations of the solar angle from the maximal value and the numerical analysis confirmed the analytical results: in our model, θ_{13}^{l} naturally acquires values that more recent data indeed point at. After this, we studied the neutrinoless double beta decay effective mass, m_{ee}, and we have seen that the next future experiments are expected to reach sufficiently good sensitivities to test our model in the IH regime.

The main conclusion of the chapter is that there is a strong tension in combining a GUT model with a (discrete non-Abelian) flavour symmetry and therefore a parallel study is not only interesting but also recommended to provide a viable model. In the second part of the chapter we produced a flavour-GUT model that is quite realistic and viable. Only the study done in the third part, regarding the Higgs sector revealed that the model is restricted into a small region of the parameter space, reducing the freedom in the choice of the parameter values. Even if our results are model dependent, our construction shares many features with other models present in literature, where often a detailed discussion of the Higgs sector is missing. In our opinion, this is a serious drawback and we would suggest to consider the interplay between GUTs and flavour symmetries in this kind of models as well.

Appendices to chapter 4

4.A Higgs scalar spectrum

In this appendix we present the scalar mass matrices for all the fields introduced in section 4.9 in terms of representations of the SM$\sim SU(3)_C \times SU(2)_L \times U(1)_Y$; we also indicate their origin with respect to the PS and the colour-broken Pati-Salam (CbPS) phase, in which the symmetry group is given by $SU(3)_C \times SU(2)_L \times SU(2)_R \times U(1)_{B-L}$. For completeness for each field we also indicate the corresponding T_{3R} value, with T_{3R} the diagonal generator of $SU(2)_R$. We use the same notation as in [124]: we write the Dirac scalar mass matrices as they could be read directly from the superpotential (4.74) at the scale M_R. We label the mass matrices with S, D and T when they refer to the singlet, doublet and triplet representations respectively of the $SU(2)_L$ gauge symmetry.

Obviously the most interesting subsection of this appendix is 4.A.2 that discusses the colour-singlet $SU(2)$-doublets, that give rise to the light electroweak breaking Higgs fields.

4.A.1 $SU(2)_L$ singlets

We first consider singlets under $SU(2)_L$. When the symmetry breaks down from the Pati-Salam symmetry group to the Standard Model, this $SU(2)_L$ is the only product group that remains unbroken. All Goldstone bosons related to the symmetry breaking chain so far are thus singlets of $SU(2)_L$. In total, the breaking from $SU(4)_C \times SU(2)_L \times SU(2)_R \to SU(3)_C \times SU(2)_L \times U(1)_Y$ should give rise to nine Goldstone bosons. In this appendix, we indeed reproduce these.

• Singlets $(1, 1, 0)$

The mass matrix for the Standard Model singlet scalar fields reads

$$M_{S1} = \begin{pmatrix} 0 & 0 & \frac{3}{\sqrt{2}}\lambda_R M_R & 0 & 0 \\ 0 & 0 & \frac{3}{\sqrt{2}}\lambda_R M_R & 0 & 0 \\ \frac{3}{\sqrt{2}}\lambda_R M_R & \frac{3}{\sqrt{2}}\lambda_R M_R & \sqrt{2}M_{C_1}\lambda_A + x & \lambda_{AB\xi}V_\xi + \frac{1}{\sqrt{2}}\lambda_B M_{C_2} & \frac{1}{\sqrt{2}}\lambda_{AB\xi}M_{C_2} \\ 0 & 0 & \lambda_{AB\xi}V_\xi + \frac{1}{\sqrt{2}}\lambda_B M_{C_2} & \frac{1}{\sqrt{2}}\lambda_{B\xi}M_{C_1} - y & \frac{1}{\sqrt{2}}\lambda_{AB\xi}M_{C_2} \\ 0 & 0 & \frac{1}{\sqrt{2}}\lambda_{AB\xi}M_{C_2} & \frac{1}{\sqrt{2}}\lambda_{AB\xi}M_{C_1} & -\frac{M_{C_1}M_{C_2}}{V_\xi\sqrt{2}}\lambda_{AB\xi} \end{pmatrix} .$$

The parameters x and y are given by

$$x = \frac{1}{2\sqrt{2}M_{C_1}}(-4\lambda_A M_{C_1}^2 - 2\sqrt{2}\lambda_{AB\xi}M_{C_2}V_\xi - 2\lambda_B M_{C_2}^2 - 8\lambda_R M_R^2) ,$$
$$y = \frac{M_{C_1}}{\sqrt{2}M_{C_2}}(\sqrt{2}\lambda_{AB\xi}V_\xi + 2\lambda_B M_{C_2}) .$$

M_{S1} has a vanishing eigenvalue that is eaten by the corresponding gauge boson. Moreover it can be checked that one of the singlets, which we call ξ_0, has a mass $\sim M_R$ while all the others masses appear as combinations of M_{C1}, M_{C2} and V_ξ and are heavier still. We present all states and their origins in the table below.

Field	Origin	PS	CbPS	T_{3R}
C_1, R_1	Δ_R	$(10,1,3)$	$(1,1,3,-2)$	1
C_2, R_2	$\overline{\Delta}_R$	$(\overline{10},1,3)$	$(1,1,3,2)$	-1
C_3, R_3	A	$(15,1,1)$	$(1,1,1,0)$	0
C_4, R_4	B	$(15,1,1)$	$(1,1,1,0)$	0
C_5, R_5	ξ	$(1,1,1)$	$(1,1,1,0)$	0

• **Singlets $(3,1,2/3) \oplus (\overline{3},1,-2/3)$**

$$M_{S2} = \begin{pmatrix} \sqrt{2}\lambda_A M_{C_1} + x & \lambda_{AB\xi} V_\xi + \frac{1}{\sqrt{2}}\lambda_B M_{C_2} & 2\lambda_R M_R \\ \lambda_{AB\xi} V_\xi + \frac{1}{\sqrt{2}}\lambda_B M_{C_2} & \frac{1}{\sqrt{2}}\lambda_B M_{C_1} - y & 0 \\ 2\lambda_R M_R & 0 & -\sqrt{2}\lambda_R M_{C_1} \end{pmatrix} .$$

M_{S2} has a vanishing eigenvalue: it corresponds to the massless GBs $(3,1,2/3) \oplus (\overline{3},1,-2/3)$ eaten by the gauge bosons.

Field	Origin	PS	CbPS	T_{3R}
C_1	A	$(15,1,1)$	$(3,1,1,4/3)$	0
C_2	B	$(15,1,1)$	$(3,1,1,4/3)$	0
C_3	Δ_R	$(10,1,3)$	$(3,1,3,-2/3)$	1
R_1	A	$(15,1,1)$	$(\overline{3},1,1,-4/3)$	0
R_2	B	$(15,1,1)$	$(\overline{3},1,1,-4/3)$	0
R_3	$\overline{\Delta}_R$	$(\overline{10},1,3)$	$(\overline{3},1,3,2/3)$	-1

• **Singlets $(8,1,0)$**

$$M_{S3} = \begin{pmatrix} -\sqrt{2}M_{C1}\lambda_A + x & V_\xi \lambda_{AB\xi} - \frac{1}{\sqrt{2}}\lambda_B M_{C2} \\ V_\xi \lambda_{AB\xi} - \frac{1}{\sqrt{2}}\lambda_B M_{C2} & -\frac{1}{\sqrt{2}}M_{C1}\lambda_B - y \end{pmatrix} .$$

In this case, there are no massless states.

Field	Origin	PS	CbPS	T_{3R}
C_1, R_1	A	$(15,1,1)$	$(8,1,1,0)$	0
C_2, R_2	B	$(15,1,1)$	$(8,1,1,0)$	0

• **Singlets $(1,1,\pm 1)$**

$$M_{S4} = 0 .$$

These states correspond to the last two massless Goldstone bosons eaten by the gauge bosons. With these two states present, the total number of GBs eaten is $1 + 2 \times 3 + 2 = 9$, exactly as required by the symmetry breaking scheme.

Field	Origin	PS	CbPS	T_{3R}
C_1	Δ_R	$(10,1,3)$	$(1,1,3,-2)$	0
R_1	$\overline{\Delta}_R$	$(\overline{10},1,3)$	$(1,1,3,2)$	0

• **Singlets $(1,1,\pm 2)$**

$$M_{S5} = 0 \ .$$

The mass matrix for the colour- and $SU(2)_L$-singlets with hypercharge (and thus electric charge) ± 2 vanishes, implying that these states remain massless until the susy scale, providing a testable prediction of the model (as well as other Pati-Salam set ups). We write these as δ^{++} and $\overline{\delta}^{++}$.

Field	Origin	PS	CbPS	T_{3R}
C_1	Δ_R	$(10,1,3)$	$(1,1,3,-2)$	-1
R_1	$\overline{\Delta}_R$	$(\overline{10},1,3)$	$(1,1,3,2)$	1

• **Singlets $(3,1,-1/3) \oplus (\overline{3},1,1/3)$**

$$M_{S6} = -\sqrt{2} M_{C1} \lambda_R \ .$$

Field	Origin	PS	CbPS	T_{3R}
C_1	Δ_R	$(10,1,3)$	$(3,1,3,-2/3)$	0
R_1	$\overline{\Delta}_R$	$(\overline{10},1,3)$	$(\overline{3},1,3,2/3)$	0

• **Singlets $(3,1,-4/3) \oplus (\overline{3},1,4/3)$**

$$M_{S7} = -\sqrt{2} M_{C1} \lambda_R \ .$$

Field	Origin	PS	CbPS	T_{3R}
C_1	Δ_R	$(10,1,3)$	$(3,1,3,-2/3)$	-1
R_1	$\overline{\Delta}_R$	$(\overline{10},1,3)$	$(\overline{3},1,3,2/3)$	1

• **Singlets $(6,1,4/3) \oplus (\overline{6},1,-4/3)$**

$$M_{S8} = -2\sqrt{2} M_{C1} \lambda_R \ .$$

Field	Origin	PS	CbPS	T_{3R}
C_1	Δ_R	$(10,1,3)$	$(6,1,3,2/3)$	1
R_1	$\overline{\Delta}_R$	$(\overline{10},1,3)$	$(\overline{6},1,3,-2/3)$	-1

• **Singlets $(6,1,1/3)\oplus(\overline{6},1-1/3)$**

$$M_{S9} = -2\sqrt{2}M_{C1}\lambda_R \ .$$

Field	Origin	PS	CbPS	T_{3R}
C_1	Δ_R	$(10,1,3)$	$(6,1,3,2/3)$	0
R_1	$\overline{\Delta}_R$	$(\overline{10},1,3)$	$(\overline{6},1,3,-2/3)$	0

• **Singlets $(6,1,-2/3)\oplus(\overline{6},1,2/3)$**

$$M_{S10} = -2\sqrt{2}M_{C1}\lambda_R \ .$$

Field	Origin	PS	CbPS	T_{3R}
C_1	Δ_R	$(10,1,3)$	$(6,1,3,2/3)$	-1
R_1	$\overline{\Delta}_R$	$(\overline{10},1,3)$	$(\overline{6},1,3,-2/3)$	1

4.A.2 $SU(2)_L$ doublets

Next we consider the $SU(2)_L$ doublets. We start with the doublets that have the right quantum numbers to break electroweak symmetry.

• **Doublets $(1,2,\pm 1/2)$**

The mass matrix relevant for the electroweak-symmetry breaking doublets is

$$M_{D1} = \begin{pmatrix} M_\phi & M_{\phi\phi'} & \frac{1}{\sqrt{2}}M_{C2}\lambda_{\phi\rho} \\ M_{\phi\phi'} & M_{\phi'} & \frac{1}{\sqrt{2}}M_{C2}\lambda_{\phi'\rho} \\ \frac{1}{\sqrt{2}}M_{C2}\lambda_{\phi\rho} & \frac{1}{\sqrt{2}}M_{C2}\lambda_{\phi'\rho} & M_\rho + \frac{1}{\sqrt{2}}\lambda_{\rho A}M_{C1} \end{pmatrix} \tag{4.A.1}$$

M_{D1}^2 is diagonalized according to

$$U^T \cdot M_{D1}^2 \cdot U = \hat{M}_{D1}\hat{M}_{D1} \ . \tag{4.A.2}$$

This gives three up-type (down-type) Higgs doublets h_u, h'_u, H_u (h_d, h'_d, H_d) .

$$\begin{pmatrix} \phi_{u,d} \\ \phi'_{u,d} \\ \rho_{u,d} \end{pmatrix} = U^T \begin{pmatrix} h_{u,d} \\ h'_{u,d} \\ H_{u,d} \end{pmatrix} \ . \tag{4.A.3}$$

Therefore for the up (down) projections we have

$$\begin{aligned} v_\phi^{u,d} &\equiv \langle\phi_{u,d}\rangle &&= U_{11}v_1^{u,d} + U_{21}v_2^{u,d} + U_{31}v_3^{u,d} \ , \\ v_{\phi'}^{u,d} &\equiv \left\langle\phi'_{u,d}\right\rangle &&= U_{12}v_1^{u,d} + U_{22}v_2^{u,d} + U_{32}v^{u,d} \ , \\ v_\rho^{u,d} &\equiv \langle\rho_{u,d}\rangle &&= U_{13}v_1^{u,d} + U_{23}v_2^{u,d} + U_{33}v_3^{u,d} \ . \end{aligned} \tag{4.A.4}$$

In general a light doublet, i.e. massless at the M_C scale, gets a mass term at M_{SUSY} and its vev, at the EW scale, is of order of the EW scale $\sim v_W$. On the contrary for a heavy doublet of mass M, its

induced vev at the EW scale is $\sim v_W^2/M$ For $M \sim M_C$ this is completely negligible with respect to v_W.

Consider now the condition $\langle \rho_u \rangle = 0$ that we imposed to get the correct fermion mass matrices. In the standard case we would have only one up- and one down-type light Higgs doublets, with all the other doublets heavy. Assume now that $h_{u,d}$ in equation (4.A.3) are the up- and down-type light doublets at M_C. Then we have $v_1^{u,d} \sim v_W$ while $v_2^{u,d} \sim v_3^{u,d} \sim 0$. From equation (4.A.4) we see that in this case it would be impossible to make the ρ projection vanish along the up-direction (that implies $U_{13} = 0$), while still maintaining a non-vanishing $\langle \rho_d \rangle$.[12] For this reason the condition $\langle \rho_u \rangle = 0$ implies a non-standard scenario and the presence of two light doublets of up-type at the M_C scale, namely h_u and h'_u. However the symmetric nature of M_{D1} ensures that as consequence we are also left with two down-type light Higgs doublets, h_d and h'_d. Nevertheless this does not imply that $\langle \rho_d \rangle$ vanishes because $v_i^{u,d}$ depend on the soft terms and we get

$$\begin{aligned} \langle \rho_u \rangle &= U_{13} v_1^u + U_{23} v_2^u = 0\,, \\ \langle \rho_d \rangle &= U_{13} v_1^d + U_{23} v_2^d \neq 0\,, \end{aligned} \tag{4.A.5}$$

In conclusion we have to impose two constraints on the free parameters that enter in M_{D1} corresponding to require that M_{D1} has two vanishing eigenvalues. Notice that the condition that M_{D_1} has rank 1 is fine-tuned but it is not more fine-tuned than imposing M_{D_1} of rank 2, which is universally accepted whenever the MSSM has to be recovered. In our case the fermion mass matrix structures impose a slightly different condition –M_{D_1} of rank 1 – but both the requirements are satisfied by fine-tuning the parameters that enter in the mass matrix.

Field	Origin	PS	CbPS	T_{3R}
C_1	ϕ	$(1,2,2)$	$(1,2,2,0)$	$1/2$
C_2	ϕ'	$(1,2,2)$	$(1,2,2,0)$	$1/2$
C_3	ρ	$(15,2,2)$	$(1,2,2,0)$	$1/2$
R_1	ϕ	$(1,2,2)$	$(1,2,2,0)$	$-1/2$
R_2	ϕ'	$(1,2,2)$	$(1,2,2,0)$	$-1/2$
R_3	ρ	$(15,2,2)$	$(1,2,2,0)$	$-1/2$

• **Doublets $(\mathbf{3,2,7/6}) \oplus (\overline{\mathbf{3}}\mathbf{,2,-7/6})$**

$$M_{D2} = M_\rho + \frac{1}{\sqrt{2}} \lambda_{\rho A} M_{C_1}\ .$$

Field	Origin	PS	CbPS	T_{3R}
C_1	ρ	$(15,2,2)$	$(3,2,2,4/3)$	$1/2$
R_1	ρ	$(15,2,2)$	$(\overline{3},2,2,-4/3)$	$-1/2$

• **Doublets $(\mathbf{3,2,1/6}) \oplus (\overline{\mathbf{3}}\mathbf{,2,-1/6})$**

$$M_{D3} = M_\rho + \frac{1}{\sqrt{2}} \lambda_{\rho A} M_{C_1}\ .$$

[12] Even the condition $U_{13} = 0$ is not natural. Therefore in the most general case with only one up-type (down-type) light doublet, the condition $\langle \rho_u \rangle = 0$ implies that all the other vevs given in equation (4.A.4) vanish.

Field	Origin	PS	CbPS	T_{3R}
C_1	ρ	$(15,2,2)$	$(3,2,2,4/3)$	$-1/2$
R_1	ρ	$(15,2,2)$	$(\overline{3},2,2,-4/3)$	$1/2$

• **Doublets $(8,2,1/2)\oplus(8,2,-1/2)$**

$$M_{D4} = M_\rho - \frac{1}{\sqrt{2}}\lambda_{\rho A} M_{C_1} \ .$$

Field	Origin	PS	CbPS	T_{3R}
C_1	ρ	$(15,2,2)$	$(8,2,2,0)$	$1/2$
R_1	ρ	$(15,2,2)$	$(8,2,2,0)$	$-1/2$

4.A.3 $SU(2)_L$ triplets

Lastly, we discuss triplets under the Standard Model's $SU(2)_L$.

• **Triplets** $(1,3,1)\oplus(1,3,-1)$

$$M_{T1} = \begin{pmatrix} M_\Sigma & \lambda_\xi V_\xi & 0 \\ \lambda_\xi V_\xi & M_{\Sigma'} & \frac{1}{\sqrt{2}}\lambda M_R \\ 0 & \frac{1}{\sqrt{2}}\overline{\lambda} M_R & M_{\Delta L} + \frac{3}{\sqrt{2}}\lambda_L M_{C_1} \end{pmatrix} .$$

with

Field	Origin	PS	CbPS	T_{3R}
C_1	Σ	$(1,3,3)$	$(1,3,3,0)$	1
C_2	Σ'	$(1,3,3)$	$(1,3,3,0)$	1
C_3	Δ_L	$(\overline{10},3,1)$	$(1,3,1,2)$	0
R_1	Σ	$(1,3,3)$	$(1,3,3,0)$	-1
R_2	Σ'	$(1,3,3)$	$(1,3,3,0)$	-1
R_3	$\overline{\Delta}_L$	$(10,3,1)$	$(1,3,1,-2)$	0

• **Triplets $(1,3,0)$**

$$M_{T2} = \begin{pmatrix} M_\Sigma & \lambda_\xi V_\xi \\ \lambda_\xi V_\xi & M_{\Sigma'} \end{pmatrix} .$$

with

Field	Origin	PS	CbPS	T_{3R}
C_1, R_1	Σ	$(1,3,3)$	$(1,3,3,0)$	0
C_2, R_2	Σ'	$(1,3,3)$	$(1,3,3,0)$	0

• **Triplets $(\mathbf{3, 3, -1/3}) \oplus (\mathbf{\overline{3}, 3, 1/3})$**

$$M_{T3} = M_{\Delta_L} + \frac{1}{\sqrt{2}}\lambda_L M_{C1} \ .$$

with

Field	Origin	PS	CbPS	T_{3R}
C_1	Δ_L	$(\overline{10}, 3, 1)$	$(3, 3, 1, 2/3)$	0
R_1	$\overline{\Delta}_L$	$(10, 3, 1)$	$(\overline{3}, 3, 1, -2/3)$	0

• **Triplets $(\mathbf{6, 3, 1/3}) \oplus (\mathbf{\overline{6}, 3, -1/3})$**

$$M_{T4} = M_{\Delta_L} - \frac{1}{\sqrt{2}}\lambda_L M_{C1}$$

with

Field	Origin	PS	CbPS	T_{3R}
C_1	Δ_L	$(\overline{10}, 3, 1)$	$(6, 3, 1, -2/3)$	0
R_1	$\overline{\Delta}_L$	$(10, 3, 1)$	$(\overline{6}, 3, 1, 2/3)$	0

4.B NLO contributions to the flavon scalar potential

The superpotential w_d of equation (4.71), linear in the driving fields D_R, φ_R, χ_R and σ_R, is modified into:

$$w_d = w_d^0 + \delta w_d \ . \tag{4.B.1}$$

The addition δw_d contains the NLO contributions, suppressed by one power of $1/\Lambda$ with respect to w_d^0; it is given by the most general quartic, $S_4 \times Z_4$-invariant polynomial linear in the driving fields, and can be obtained by inserting an additional flavon field in all the LO terms. The Z_4-charges prevent any addition of the flavons φ and φ' at NLO, while a factor of σ or χ can be added to all the LO terms. The full expression of δw_d is the following:

$$\delta w_d = \frac{1}{\Lambda}\left(\sum_{i=1}^{3} x_i I_i^{\sigma_R} + \sum_{i=1}^{5} w_i I_i^{\chi_R} + \sum_{i=1}^{6} s_i I_i^{D_R} + \sum_{i=1}^{5} v_i I_i^{\varphi_R}\right) \ . \tag{4.B.2}$$

where x_i, w_i, s_i and v_i are coefficients and $\left\{I_i^{\sigma_R},\ I_i^{\chi_R},\ I_i^{D_R},\ I_i^{\varphi_R}\right\}$ represent a basis of independent quartic invariants:

$$\begin{aligned}
&I_1^{\sigma_R} = \sigma_R\sigma\sigma\sigma && I_3^{\sigma_R} = \sigma_R\sigma(\chi\chi)_{1_1} \\
&I_2^{\sigma_R} = \sigma_R(\chi(\chi\chi)_{3_1})_{1_1} && \\
&I_1^{\chi_R} = (\chi_R\chi)_{1_1}(\chi\chi)_{1_1} && I_4^{\chi_R} = (\chi_R(\chi\chi)_{3_1})_{1_1}\,\sigma \\
&I_2^{\chi_R} = ((\chi_R\chi)_2(\chi\chi)_2)_{1_1} && I_5^{\chi_R} = (\chi_R\chi)_{1_1}\sigma\sigma \\
&I_3^{\chi_R} = ((\chi_R\chi)_{3_1}(\chi\chi)_{3_1})_{1_1} && \\
&I_1^{D_R} = ((D_R\chi)_{3_1}(\varphi\varphi')_{3_1})_{1_1} && I_4^{D_R} = (D_R(\varphi\varphi)_2)_{1_1}\,\sigma \\
&I_2^{D_R} = ((D_R\chi)_{3_2}(\varphi\varphi')_{3_2})_{1_1} && I_5^{D_R} = (D_R(\varphi'\varphi')_2)_{1_1}\,\sigma \\
&I_3^{D_R} = ((D_R\chi)_{3_1}(\varphi'\varphi')_{3_1})_{1_1} && I_6^{D_R} = (D_R(\varphi\varphi')_2)_{1_1}\,\sigma \\
&I_1^{\varphi_R} = (\varphi_R\chi)_{1_s}(\varphi\varphi')_{1_2} && I_4^{\varphi_R} = ((\varphi_R\chi)_{3_2}(\varphi\varphi')_{3_2})_{1_1} \\
&I_2^{\varphi_R} = ((\varphi_R\chi)_2(\varphi\varphi')_2)_{1_1} && I_5^{\varphi_R} = (\varphi_R(\varphi\varphi')_{3_2})_{1_1}\,\sigma \\
&I_3^{\varphi_R} = ((\varphi_R\chi)_{3_1}(\varphi\varphi')_{3_1})_{1_1} \ . &&
\end{aligned} \tag{4.B.3}$$

In these terms we indicate with $(\ldots)_R$ the representation R of S_4.

The NLO flavon vevs are obtained by imposing the vanishing of the first derivative of $w_d + \delta w_d$ with respect to the driving fields σ_R, χ_R, D_R and φ_R. We look for a solution that perturbs equations (4.16) and (4.17) to first order in the $1/\Lambda$ expansion: for all components of the flavons $\Phi = (\sigma,\ \chi,\ \varphi,\ \varphi')$, we denote the shifted vev's by

$$\langle \Phi \rangle = \langle \Phi \rangle_{LO} + \delta\Phi \ . \tag{4.B.4}$$

The original $\langle \Phi \rangle_{LO}$ here are given by equations (4.16) and (4.17).

It is straightforward to verify the following results. In the Majorana mass sector the shifts $\delta\sigma,\ \delta\chi$ turn out to be proportional to the LO vev's $\langle \Phi \rangle_{LO}$ and can be absorbed in a redefinition of the parameters v_χ and v_σ. Instead, in the Dirac mass sector, the shifts $\delta\varphi,\ \delta\varphi'$ have a non-trivial structure, so that the LO texture is modified:

$$\langle \varphi \rangle = \begin{pmatrix} \delta v_\varphi \\ v'_\varphi \\ v'_\varphi \end{pmatrix} \qquad \langle \varphi' \rangle = \begin{pmatrix} \delta v_{\varphi'} \\ v'_{\varphi'} \\ -v'_{\varphi'} \end{pmatrix} \ . \tag{4.B.5}$$

Here v'_φ and $v'_{\varphi'}$ satisfy a relation similar to that in equation (4.72) and the shifts δv_φ and $\delta v_{\varphi'}$ are suppressed by a factor λ with respect to the LO entries v'_φ and $v'_{\varphi'}$, respectively.

4.C Beta coefficients of the gauge coupling running

In this appendix, we provide the coefficients of the β–functions for the gauge coupling running in the different regimes. The complete matter fields run from the GUT scale down to the M_{SUSY} scale, where the SUSY partners decouple. We have already outlined the spectrum for the scalar fields in section 4.9, according to the different scale at which the fields decouple. As a result the computation of the β–functions is straightforward. We write μ for a generic scale and obtain in the different energy regimes

- $M_C < \mu < M_{GUT}$: all matter is in the left and right handed multiplets $(4,\ 2,\ 1)$ and $(\overline{4},\ 1\,,2)$ as mentioned in table 4.2. In the Higgs sector, we have all the fields mentioned in table 4.6. This leads to the coefficients

  $$\beta_{SU(4)_C} = 54 \ , \qquad \beta_{SU(2)_L} = 69 \ , \qquad \beta_{SU(2)_R} = 69 \ . \tag{4.C.1}$$

  Due to the large matter content these coefficients are very large and the β–functions are very steep. As consequence the theory is in the Pati-Salam regime only for a very small range of energies, as can indeed be seen in figure 4.8. Almost directly after passing the scale M_C, the $SU(2)_R$ coupling constant enters the non-perturbative regime.

- $M_R < \mu < M_C$: in this range the Pati-Salam gauge group is broken to the 'colour-broken Pati-Salam' $SU(3)_C \times SU(2)_L \times SU(2)_R \times U(1)_{B-L}$ symmetry. We find the following coefficients for the matter (left and right handed doublets of quarks and leptons characterized by different $U(1)_{B-L}$ charges) and the scalar fields

  $$\beta_{SU(3)_C} = -3 \ , \qquad \beta_{SU(2)_L} = 18 \ , \qquad \beta_{SU(2)_R} = 18 \ , \qquad \beta_{U(1)_{B-L}} = 24 \ . \tag{4.C.2}$$

- $M_T < \mu < M_R$: in this regime we have all the usual MSSM matter particles, four light higgs doublets (two up-type and two down-type), a couple of SM triplets $(1,3,1) \oplus (1,3,-1)$ and two extra charged singlets (δ^{++} and $\bar{\delta}^{++}$). The coefficients of the β–functions are

  $$\beta_{SU(3)_C} = -3 \ , \qquad \beta_{SU(2)_L} = 4 \ , \qquad \beta_{U(1)_Y} = 69/5 \ . \tag{4.C.3}$$

  The hypercharge that appears in the last term is related to $SU(2)_R$ and the $B-L$ charges in the previous regime by

  $$Y = T_{3R} + \frac{B-L}{2}.$$

- $M_{SUSY} < \mu < M_T$: in this regime we have all the usual MSSM matter particles, four light higgs doublets (two up-type and two down-type) and two extra charged singlets (δ^{++} and $\bar{\delta}^{++}$). The β–function coefficients are

$$\beta_{SU(3)_C} = -3\,, \qquad \beta_{SU(2)_L} = 2\,, \qquad \beta_{U(1)_Y} = 12\,. \tag{4.C.4}$$

  This should be compared with the (-3, 1, 33/5) coefficients of the ordinary MSSM.

- $v_W < \mu < M_{SUSY}$: we have the particle content of the standard model, with the exception that there are four Higgs doublets. We have therefore the following β–function coefficients

$$\beta_{SU(3)_C} = -7\,, \qquad \beta_{SU(2)_L} = -8/3\,, \qquad \beta_{U(1)_Y} = 22/5\,. \tag{4.C.5}$$

  This should be compared with the (-7, -19/6, 41/10) coefficients of the ordinary SM.

4.D Yukawa running

In section 2.1.1 we remarked that we can consider only the running between M_T and M_{SUSY} to provide analytical approximations for the evolution of fermion masses and mixing under the RGEs effect. This is due to the closeness of the intermediate scales between M_{GUT} and M_T. At M_T the scalar $SU(2)_L$ triplet has been already integrated out giving rise to the effective Weinberg operator for neutrino masses

$$\alpha_{ij} Y_{L_{rs}} \frac{L_r L_s h_{u_i} h_{u_j}}{M_T}\,, \tag{4.D.1}$$

For the Higgs fields we have $h_{u_1} = h_u$ and $h_{u_2} = h'_u$; the α_{ij} coefficients arise from the scalar potential and Y_L is given in equation (4.80).

For what concerns the charged fermion Yukawa, at M_T the Dirac part of the superpotential is written as

$$Y_u Q\, U^c h_u + Y'_u Q\, U^c h'_u + Y_d Q\, D^c h_d + Y'_d Q\, D^c h'_d + Y_e L\, E^c h_d + Y'_e L\, E^c h'_d\,, \tag{4.D.2}$$

with the Yukawa mass matrices given in equation (4.82).

The Yukawa matrices RGEs are therefore given by

$$\begin{aligned}
16\pi^2 \frac{dY_u}{dt} &= \left[3\,Y_u Y_u^\dagger + Y_d Y_d^\dagger + 3\,Y'_u Y'^\dagger_u + Y'_d Y'^\dagger_d + 3\,\mathrm{Tr}(Y_u Y_u^\dagger) - \Sigma_i c_i^u g_i^2\right] Y_u\,,\\
16\pi^2 \frac{dY'_u}{dt} &= \left[3\,Y_u Y_u^\dagger + Y_d Y_d^\dagger + 3\,Y'_u Y'^\dagger_u + Y'_d Y'^\dagger_d + 3\,\mathrm{Tr}(Y'_u Y'^\dagger_u) - \Sigma_i c_i^u g_i^2\right] Y'_u\,,\\
16\pi^2 \frac{dY_d}{dt} &= \left[Y_u Y_u^\dagger + 3\,Y_d Y_d^\dagger + Y'_u Y'^\dagger_u + 3\,Y'_d Y'^\dagger_d + 3\,\mathrm{Tr}(Y_d Y_d^\dagger) + \mathrm{Tr}(Y_e Y_e^\dagger) - \Sigma_i c_i^d g_i^2\right] Y_d\,,\\
16\pi^2 \frac{dY'_d}{dt} &= \left[Y_u Y_u^\dagger + 3\,Y_d Y_d^\dagger + Y'_u Y'^\dagger_u + 3\,Y'_d Y'^\dagger_d + 3\,\mathrm{Tr}(Y'_d Y'^\dagger_d) + \mathrm{Tr}(Y'_e Y'^\dagger_e) - \Sigma_i c_i^d g_i^2\right] Y'_d\,,\\
16\pi^2 \frac{dY_e}{dt} &= \left[3\,Y_e Y_e^\dagger + 3\,Y'_e Y'^\dagger_e + 3\,\mathrm{Tr}(Y_d Y_d^\dagger) + \mathrm{Tr}(Y_e Y_e^\dagger) - \Sigma_i c_i^e g_i^2\right] Y_e\,,\\
16\pi^2 \frac{dY'_e}{dt} &= \left[3\,Y_e Y_e^\dagger + 3\,Y'_e Y'^\dagger_e + 3\,\mathrm{Tr}(Y'_d Y'^\dagger_d) + \mathrm{Tr}(Y'_e Y'^\dagger_e) - \Sigma_i c_i^e g_i^2\right] Y'_e\,,\\
16\pi^2 \frac{dY_L}{dt} &= \left[(Y_e Y_e^\dagger + Y'_e Y'^\dagger_e) Y_L + Y_L (Y_e Y_e^\dagger + Y'_e Y'^\dagger_e)^T - \Sigma_i c_i^\nu g_i^2) Y_L\right] (\alpha_{11} + \alpha_{12} + \alpha_{22})\\
&\quad + \left[6\,\mathrm{Tr}(Y_u Y_u^\dagger)\alpha_{11} + 3\,\mathrm{Tr}(Y_u Y_u^\dagger)\alpha_{12} + 3\,\mathrm{Tr}(Y'_u Y'^\dagger_u)\alpha_{12} + 6\,\mathrm{Tr}(Y'_u Y'^\dagger_u)\alpha_{22}\right] Y_L\,,
\end{aligned} \tag{4.D.3}$$

The coefficients here are numerically given by

$$\begin{aligned} c_1^u &= \frac{13}{15}\,, \qquad c_2^u = 3\,, \qquad c_3^u = \frac{16}{3}\,, \qquad & c_1^d &= \frac{7}{15}\,, \qquad c_2^d = 3\,, \qquad c_3^d = \frac{16}{3}\,, \\ c_1^e &= \frac{9}{5}\,, \qquad c_2^e = 3\,, \qquad c_3^e = 0\,, \qquad & c_1^\nu &= \frac{6}{5}\,, \qquad c_2^\nu = 6\,, \qquad c_3^\nu = 0\,. \end{aligned} \tag{4.D.4}$$

Chapter 5

Flavour symmetries at the electroweak scale

For there are three that bear record in heaven,
[...]: and these three are one.

The Bible - King James Version
1 John 5:7

5.1 Introduction

When studying the Altarelli–Feruglio model in chapter 2 we found that the mass scale of flavons of flavour symmetries is typically very high. It can be as high as the assumed energy scale of grand unification. In the previous chapter, we used this to our advantage and constructed a model that contains both grand unified and family symmetries. The disadvantage is that the model is not very predictive. There is a limited effect of the physics at the very high scale on the physics at scales that the current experiments are investigating, the TeV scale for the LHC and even lower scales for neutrino experiments. There are some predictions, for instance about the rates of neutrinoless double beta decay and the presence at the SUSY scale of extra doubly charged scalars δ^{++} and $\bar{\delta}^{--}$, but these are not very many. The predictiveness of flavour models is significantly enlarged if the scale of symmetry breaking can be lowered to the electroweak scale. In this chapter we study a set up in which this is indeed the case.

The flavour model of the previous section contained flavons and pure Higgs fields. Flavons are scalar fields that are singlets of the SM gauge group, but charged under the family symmetry group, while for pure Higgs fields it is exactly the other way around. The central idea of this chapter, introduced in section 5.2, is to combine these two fields to form 'flavo-Higgses' that are in non-trivial representations of both the flavour symmetry group and the electroweak group. Naturally, breaking electroweak symmetry also implies breaking the flavour symmetry and we obtain low-energy, highly predictive models of flavour.

In particular we are interested in models where there are three Standard-Model like Higgs fields that are in the triplet representation of the family symmetry group A_4. In section 5.3 we introduce this scenario and in section 5.4 we present the corresponding potential for the flavo-Higgs fields. Section 5.5 discusses the physical Higgs fields present after breaking electroweak symmetry.

The potential of section 5.4 allows only a limited number of minima. In section 5.6 we construct a complete list of all those vacua and in section 5.7 we discuss the question whether in these cases CP is violated in the Higgs sector. The vacua are solutions of the mathematical equations that minimize the potential. The question whether they are also physically viable is a different one. In section 5.8 we develop a number of tests that are only sensitive to the Higgs sector of a model and in section 5.9

we confront the minima of section 5.6 with these tests.

To constitute a complete model, knowledge of the representation of the Higgs fields (an A_4-triplet), is not enough. Only when also the fermionic content is given a complete model arises. In section 5.10 we present four such models, three from the literature and one original work, called 'quark mixing in the discrete dark matter model'. In section 5.11 we present a number of tests for these models that are sensitive also to the fermionic content and in section 5.12 we present the results of these tests. Lastly, section 5.13 presents the conclusions.

5.2 The pros and cons of flavons

The crucial assumption of models with flavour symmetries is the existence of a horizontal gauge group. Invariance under this flavour group dictates which terms are allowed in the Lagrangian of the resulting field theory. The Lagrangian of the Standard Model, equation (2.1), is well-known

$$\mathcal{L}_{\text{SM}} = \mathcal{L}_K + \mathcal{L}_{\text{gauge}} + \mathcal{L}_Y + V_{\text{Higgs}}.$$

Typically, adding a family symmetry group does not affect the kinetic and gauge terms, as the usual choice is not to gauge the flavour group. The effect on the Yukawa terms, on the other hand, is drastic. The terms originally present in the Standard Model are not invariant under the flavour group. In chapters 2 and 4 we have seen ways to fix this deficit and we found that the way in which invariance is recovered ultimately dictates what the masses and mixing angles of the fermions look like. A crucial choice is whether the last term V_{Higgs} is to be modified as well.

In the previous chapters, the solution to make the Yukawa terms invariant, was to introduce flavons. These fields transform trivially under (vertical) gauge transformations, but are in extended representations of the flavour symmetry. The flavons acquire vacuum expectation values and the structure of the vevs translates to structures in the fermion mass matrices. The Higgs sector on the other hand, was touched as little as possible. In the Altarelli–Feruglio model the Higgs fields are singlets of the family symmetry and in the Pati-Salam inspired model of chapter 4, they transform under the auxiliary Z_4, but are still singlets of the S_4 symmetry.

Modifications of the Higgs potential in the strict sense are absent in the model of Altarelli and Feruglio. The point that they are larger than naively expected in the model of chapter 4 is one of the main messages of that chapter. Still, the modifications are relatively limited when compared to a scenario where the Higgses are not only charged under Z_4, but also under S_4.

The addition 'in the strict sense' in the previous paragraph refers to the fact that the non-modification concerns the potential of the 'traditional' Higgses, i.e. the fields that break electroweak (ew) symmetry. The flavons are also fields that break a symmetry – in this case the family symmetry. To write down a mass term for fermions, both electroweak Higgses and flavons are needed. It can thus be well defended to see the flavons as a second type of Higgs fields. From this point of view, there is a very significant modification of the Higgs potential

$$V_{\text{Higgs}} \longrightarrow V_{\text{ew Higgs}} + V_{\text{Flavons}} \,. \tag{5.1}$$

In the previous chapters, we have seen that the idea of using flavons is quite attractive. It is possible to build models that reproduce the tribimaximal or bimaximal mixing patterns, without having to tune parameters. However, four weaker points of the approach should also be stressed.

Firstly, non-renormalizable operators are ubiquitous in models with flavons. Several flavons are added to Yukawa couplings that originally exactly had dimension 4. We discussed the effective Weinberg-operator for neutrino masses and its possible origin from one of the three types of seesaw (or a combination thereof) in chapter 2 and concluded that non-renormalizable interactions are in principle no problem for a theory. Still, their appearance makes the theory significantly more complicated.

Secondly, models can be quite baroque. In the set up of chapter 4, no fewer than nine new flavon fields had to be introduced. The flavons φ and φ' are tailored to couple to charged fermions at leading order, while χ and σ couple to neutrinos. The four driving fields do not even couple to the SM fermions directly, but are needed to help the other flavons obtain the correct vevs. The Froggatt–Nielsen messenger lastly ensured the fermion hierarchy. All flavons fulfill a well-defined role and none of them is redundant. The number nine thus seems to be rather minimal for this type of models, but it is quite large. It is worth trying to see if simpler models with flavour symmetry can be constructed.

Thirdly, all the known techniques for flavon alignment in case of more than one flavon require supersymmetry or the presence of extra dimensions. These are two types of new physics that are very well-motivated. They explain one of the greatest standing puzzles in the Standard Model, the hierarchy problem of section 1.3.2 and, as a bonus, give a dark matter candidate. Supersymmetry at the TeV scale furthermore enables gauge unification as shown in section 1.3.3. There are thus good arguments to include supersymmetry or extra dimensions in flavour model building, but it would be preferable not to depend on them and to be able to write down more minimal models. This is especially true in a time where the experimental bounds on supersymmetry (or at least on the simplest implementations of it) are becoming rather tight.

Lastly, the scale of the physics of the flavons is typically very high. In the Altarelli–Feruglio model, the cut-off scale is estimated to be of the order of 10^{15} GeV; in the model of section 4 it should be the GUT scale. This can be read from figure 4.7 and 4.8 to be of the order of 10^{13} GeV. An advantage of this high scale is that it is possible to build models that combine flavour and grand unified symmetries. The downside is that the theories are hard to test and that few direct predictions can be made. An effect on neutrino parameters is present as shown in section 4.11, but direct detection of the flavons is out of the question.

In this chapter, we discuss an alternative possibility. We assume that there are no separate flavons, but that the Standard Model Higgs field takes their role. In this 'flavo-Higgs' set up, there are three copies of the SM Higgs that are in a triplet of the flavour group. Once the Higgses get their vevs, the resulting 'vector of vevs' acts as the flavons.

In this set up, the four weak points described above are ameliorated. All couplings are of the Yukawa type fermion-fermion-Higgs and are thus renormalizable. Although there is a substantial amount of new fields (two extra copies of the Higgs field), this is far less than in the other models. The alignment in flavour space is now possible in a non-supersymmetric context and without extra dimensions; all that is required is finding the vacuum expectation values of the three Higgses. The scale of new physics is obviously the electroweak scale and the set up is thus testable at the LHC by direct detection of the extra Higgs fields and verification that they have the right couplings. The indirect tests also become numerous. These can in fact be used to constrain the models significantly.

The disadvantage is that we only have one (effective) flavon. This limits the amount of structure we can impose on the fermion masses. For instance, to reproduce the exact tribimaximal mixing pattern, we need to tune one parameter. This is still much better than in the Standard Model, where the tuning of three parameters (all three neutrino mixing angles) is required.

5.3 The three Higgs doublet scenario

In this chapter we investigate a flavo-Higgs set up. The most important choice to make is that of the family symmetry group. We choose the group A_4. This group is very well-known in particular in models with flavons. The Altarelli–Feruglio model of section 2.4 used A_4 to reproduce tribimaximal mixing in the lepton sector, although in section 3.3.1 it was shown that this requires the appearance of an additional accidental Z_2 symmetry.

The fact that an accidental symmetry was required to give a specific mixing pattern is valuable information when constructing a flavo-Higgs model. In the previous section it was shown that this

set up can produce only one direction in flavour space. Residual symmetries in the neutrino and charged lepton sector (the key for finding mixing patterns in chapter 3) will necessarily be severely limited. If accidental symmetries can realize a mixing pattern even when certain directions in flavour space are not given by flavon vevs, that is good news.

Throughout this chapter, we work in the S-diagonal basis, often referred to as the Ma-Rajasekaran basis. The transformations from this basis to the T-diagonal basis of Altarelli and Feruglio as well as all other details of the group theory of A_4 is given in appendix 3.A. We recall that the group has a trivial as well as two non-trivial one-dimensional representations (1, $1'$ and $1''$) and one three-dimensional representation (3). In order to provide a non-trivial direction in flavour space, the flavo-Higgs fields should thus transform as a triplet of A_4. We adopt the standard notation to refer to these fields as Φ instead of H.

$$\vec{\Phi} = (\Phi_1,\, \Phi_2,\, \Phi_3) \tag{5.2}$$

We stress that each of the Higgs fields has the same hypercharge $+1/2$ as the fields H_d of chapter 2. Our set up is thus very different from the MSSM, that has multiple (two) Higgs doublets, but these have different hypercharges. In the language of chapter 2, the Higgs sector in this chapter is characterized by $n_u = 0$ and $n_d = 3$.

Each of these Higgs fields is written in terms of $SU(2)_L$ components and expanded around its vacuum expectation value similar to equation (2.4)

$$\Phi_a \to \frac{1}{\sqrt{2}} \begin{pmatrix} \text{Re}\, \phi_a^1 + i\, \text{Im}\, \phi_a^1 \\ v_a e^{i\omega_a} + \text{Re}\, \phi_a^0 + i\, \text{Im}\, \phi_a^0 \end{pmatrix}. \tag{5.3}$$

Here $v_a e^{i\omega_a}$ is the vacuum expectation value of the a^{th} Higgs field. One or two of the v_a can be zero, implying that the corresponding Higgs field does not develop a vev. The phases ω_a appears due to the fact that the vacuum expectation values can generally be complex. A global rotation can remove one phase, so in a one-Higgs doublet model the vev is generally chosen real. In models with more than one Higgs doublet, phases carry physical information and should be taken into account. Note that the appearance of complex vevs does not automatically imply CP violation. For a discussion of CP violation in the Higgs sector, see section 5.7.

Next to these three Higgs fields, there may be additional Higgses in one of the one-dimensional representations. We refer to models with only the A_4 triplet Higgs as minimal and to models that also have singlets as non-minimal. In this section we investigate the potential and its vacua solutions for the minimal set up. Two of the models we discuss in section 5.10 are indeed minimal, while two others are non-minimal.

In this chapter the A_4 representation for the Higgs fields is now fixed. The choice of representation for the various fermions is still free. The requirement that the SM Yukawa couplings can still be written down requires at least one of the fermion fields to be in the triplet representation. Whether this is the left- or the righthanded field and if fields in one-dimensional representations are in 1, $1'$ or $1''$ is a further choice to be made. In this chapter we perform several tests of the viability of a certain situation. Tests that only take the Higgs sector into consideration and that are thus insensitive to choices made in the fermion representations are referred to as 'model-independent' tests, while tests that involve fermions are 'model-dependent' tests.

5.4 The A_4 invariant Higgs potential

The Higgs potential of the ordinary Standard Model Higgs as given below equation (2.19) is the well-known 'Mexican hat' potential.

$$V(H) = \mu^2 H^\dagger H + \lambda (H^\dagger H)^2$$

The coefficients μ^2 and λ of the quadratic and quartic terms are respectively negative and positive. This keeps the potential bounded from below, while having a non-trivial minimum to break electroweak symmetry.

The Higgs potential in the three Higgs doublet model with A_4 symmetry is constructed in the same spirit. It contains quadratic and quartic terms in the Higgs fields. The group theory of $SU(2)$ and A_4 dictates that only one quadratic term is possible, while there are several ways to contract the indices in the quartic terms. As shown by Ma and Rajasekaran [97], the most general potential is given by

$$\begin{aligned} V[\Phi_a] =& \mu^2(\Phi_1^\dagger\Phi_1 + \Phi_2^\dagger\Phi_2 + \Phi_3^\dagger\Phi_3) + \lambda_1(\Phi_1^\dagger\Phi_1 + \Phi_2^\dagger\Phi_2 + \Phi_3^\dagger\Phi_3)^2 + \\ &+ \lambda_3(\Phi_1^\dagger\Phi_1\Phi_2^\dagger\Phi_2 + \Phi_1^\dagger\Phi_1\Phi_3^\dagger\Phi_3 + \Phi_2^\dagger\Phi_2\Phi_3^\dagger\Phi_3) + \\ &+ \lambda_4(\Phi_1^\dagger\Phi_2\Phi_2^\dagger\Phi_1 + \Phi_1^\dagger\Phi_3\Phi_3^\dagger\Phi_1 + \Phi_2^\dagger\Phi_3\Phi_3^\dagger\Phi_2) + \\ &+ \frac{\lambda_5}{2}\left[e^{i\epsilon}\left[(\Phi_2^\dagger\Phi_1)^2 + (\Phi_3^\dagger\Phi_2)^2 + (\Phi_1^\dagger\Phi_3)^2\right] + e^{-i\epsilon}\left[(\Phi_1^\dagger\Phi_2)^2 + (\Phi_2^\dagger\Phi_3)^2 + (\Phi_3^\dagger\Phi_1)^2\right]\right]. \end{aligned} \tag{5.4}$$

The parameters $\lambda_{1,3,4,5}$ and ϵ are chosen to be in accordance with the usual notation in two Higgs doublet models [125, 126]. The parameter μ^2 is typically negative in order to have a stable minimum away from the origin. All the other parameters, λ_i, are real parameters which are subject to the condition that the potential is bounded from below: this forces λ_1 and the combination $\lambda_1 + \lambda_3 + \lambda_4 + \lambda_5\cos\epsilon$ to be positive.

5.4.1 Soft A_4 breaking

When the Higgs fields develop vacuum expectation values, they break electroweak symmetry as well as the A_4 flavour symmetry. At that moment, A_4 is thus spontaneously broken. It is also possible to break A_4 explicitly, by adding terms to the potential that are not invariant. This is obviously against the spirit of introducing the symmetry in the first place and should thus only be done as a last resort. One way to break A_4 is by adding soft breaking terms to the potential (5.4) in the form

$$V_{A_4\text{soft}} = v_{\text{ew}}^2\frac{m}{2}(\Phi_1^\dagger\Phi_2 + \Phi_2^\dagger\Phi_1) + v_{\text{ew}}^2\frac{n}{2}(\Phi_2^\dagger\Phi_3 + \Phi_3^\dagger\Phi_2) + v_{\text{ew}}^2\frac{k}{2}(\Phi_1^\dagger\Phi_3 + \Phi_3^\dagger\Phi_1)\,. \tag{5.5}$$

Here m, n, k are dimensionless parameters that should presumably be smaller than one. Note that the chosen $V_{A_4\text{soft}}$ is not the most general one but it prevents an accidental extra $U(1)$ factor to appear.

The soft breaking terms are needed when we study two models [127, 128] in section 5.12. These models make use of a minimum of the potential (5.4) that gives rise to unnaturally light Higgses. The addition of the terms in (5.5) solves this problem and only after this it is meaningful to test the models on their merits.

5.5 Physical Higgs fields

After the symmetry breaking of the Higgs fields of equation (5.3) the components of the Higgs fields become the known Goldstone bosons of the Standard Model or the charged and neutral Higgs bosons. The number of expected Higgs bosons can easily be calculated. In the charged sector, we have three complex or six real degrees of freedom. Two of these relate to the Goldstone bosons that are eaten by the W^+ and W^- bosons, leaving four degrees of freedom to produce two pairs of a positively and a negatively charged boson. In the neutral sector only one of the six degrees of freedom corresponds to an eaten Goldstone boson (by the Z boson), leaving five neutral Higgses. In the case where all vevs are real, it is easy to see that three of these have a scalar and two a pseudoscalar nature. In this counting the assumption was made that only electroweak symmetry gets broken; there are no additional (global) broken symmetries. If those are present, extra Goldstone bosons appear and some of the Higgs states are massless.

The mixing of the six neutral states to five (pseudo)scalar states and a Goldstone boson can be

parameterized as in section 2.2.5[1]

$$\begin{aligned} h_\alpha &= U_{\alpha a}\text{Re}\,\phi_a^0 + U_{\alpha(a+3)}\text{Im}\,\phi_a^0\,, \\ \pi^0 &= U_{6a}\text{Re}\,\phi_a^0 + U_{6(a+3)}\text{Im}\,\phi_a^0\,. \end{aligned} \tag{5.6}$$

Here $a = 1, 2, 3$ and $\alpha = 1 - 5$, while $\alpha = 6$ refers to the Goldstone boson that we represent as π^0.

In the situation where all vevs are real the 6 by 6 scalar mass matrix reduces to a block diagonal matrix with two 3 by 3 mass matrices leading to three CP even states and 2 CP odd states and the GB π^0.

The three charged scalars mix into two new charged massive states h_α^+ and a charged Goldstone boson that we refer to as π^+ and that is eaten by the gauge bosons W^+.

$$\begin{pmatrix} h_1^+ \\ h_2^+ \\ \pi^+ \end{pmatrix} = S \begin{pmatrix} \phi_1^1 \\ \phi_2^1 \\ \phi_3^1 \end{pmatrix}\,. \tag{5.7}$$

In general, the S is a complex unitary matrix. In the special case where all vevs are real, its entries are real (and it is thus an orthogonal matrix).

It is interesting to notice that, contrary to other multi Higgs (MH) scenarios, here we cannot recover the SM limit, with one light scalar and all the others decoupled and very heavy. The flavour symmetry constrains the potential parameters in such a way that the scalar masses are never independent from each other. This can be easily understood by a parameter counting: the scalar potential (5.4) presents 6 independent parameters and the number of the physical quantities is 8, i.e. the electroweak (EW) vev and the seven masses for the massive scalar fields.

5.6 Minimum solutions of the potential

In this section we investigate the minima of the potential (5.4). We assume that electromagnetism is conserved and that thus only the neutral components of the Higgs fields develop vacuum expectation values. The fields can then be developed around their vevs as given in equation (5.3).

The tool to find minima is obviously the first derivative system

$$\frac{\partial V[\Phi]}{\partial \Phi_{\mathcal{I}}} = 0\,. \tag{5.8}$$

Here $\Phi_{\mathcal{I}}$ is one of the fields Re Φ_a^1, Re Φ_a^0, Im Φ_a^1 or Im Φ_a^0. Secondly we require non negative eigenvalues of the Hessian

$$\frac{\partial^2 V[\Phi]}{\partial \Phi_{\mathcal{I}} \partial \Phi_{\mathcal{J}}}\,. \tag{5.9}$$

This means that all the physical masses are positive except those corresponding to the Goldstone bosons (GBs) that vanish.

Some of the solutions are natural in the sense that they do not require *ad hoc* values of the potential parameters; these are only constrained by requiring the boundedness at infinity and the positivity of all the physical scalar masses. The only potential parameter constrained is the bare mass term μ^2 which is related to the physical electroweak (EW) vev, $v_{\text{ew}}^2 = v_1^2 + v_2^2 + v_3^2$. Others require specific relations between the dimensionless scalar potential parameters and may have extra Goldstone bosons.

Minima of the A_4 scalar potential are described by a vector of vevs

$$\left(v_1 e^{i\omega_1},\quad v_2 e^{i\omega_2},\quad v_3 e^{i\omega_3}\right)\,. \tag{5.10}$$

[1] As there can be no confusion, we leave the hat over the mass eigenstates h.

As already mentioned below equation (5.3) one or two of the v_i may be zero and it is always possible to choose at least one of the vevs real. In the remainder of this section, we categorize the potential solutions in two classes: those that can have all vevs real and those for which at least one vev is inherently complex.

5.6.1 Analysis of solutions with only real vacuum expectation values

When all vevs are real, the first derivative system (5.8) reads

$$\begin{aligned} v_1[2(v_1^2+v_2^2+v_3^2)\lambda_1+(v_2^2+v_3^2)(\lambda_3+\lambda_4+\lambda_5\cos\epsilon)+2\mu^2] &= 0\,,\\ v_2[2(v_1^2+v_2^2+v_3^2)\lambda_1+(v_1^2+v_3^2)(\lambda_3+\lambda_4+\lambda_5\cos\epsilon)+2\mu^2] &= 0\,,\\ v_3[2(v_1^2+v_2^2+v_3^2)\lambda_1+(v_1^2+v_2^2)(\lambda_3+\lambda_4+\lambda_5\cos\epsilon)+2\mu^2] &= 0\,,\\ v_1(v_2^2-v_3^2)\lambda_5\sin\epsilon &= 0\,,\\ v_2(v_1^2-v_3^2)\lambda_5\sin\epsilon &= 0\,,\\ v_3(v_2^2-v_1^2)\lambda_5\sin\epsilon &= 0\,. \end{aligned} \tag{5.11}$$

The first three derivatives refer to the real components of Φ_a^0 and the second ones to the imaginary parts. In the most general case, when neither ϵ nor λ_5 is zero, the last three equations allow two different solutions

1) $v_1 = v_2 = v_3 = v = v_{\rm ew}/\sqrt{3}$;

2) $v_1 \neq 0$ and $v_2 = v_3 = 0$ (and permutations of the indices).

The second case obviously implies $v_1 = v_{\rm ew}$. Both cases represent solutions of the first three equations as well, provided that

$$\begin{cases} \mu^2 = -(3\lambda_1+\lambda_3+\lambda_4+\lambda_5\cos\epsilon)v_{\rm ew}^2/3 & \text{for the first case.}\\ \mu^2 = -\lambda_1 v_{\rm ew}^2 & \text{for the second case.} \end{cases} \tag{5.12}$$

In these cases λ_5 can be chosen positive, as a sign can be absorbed in a redefinition of ϵ.

Next, we consider the case where $\sin\epsilon$ is 0. This implies $\epsilon = 0$ or π. We can absorb the minus sign corresponding to the second case in a redefinition of λ_5 that is then allowed to span over both positive and negative values.

Assuming $v_1 \neq 0$, we can solve the first equation in (5.11) with respect to μ^2. Then by substituting μ^2 in the other two equations we get

$$\begin{aligned} v_2(v_1^2-v_2^2)(\lambda_3+\lambda_4+\lambda_5) &= 0\,,\\ v_3(v_1^2-v_3^2)(\lambda_3+\lambda_4+\lambda_5) &= 0\,. \end{aligned} \tag{5.13}$$

Next to the two solutions present in the general case, this system has two further possible solutions

3) $v_3 = 0, v_2 = v_1 = v_{\rm ew}/\sqrt{2}$ and permutations. This requires

$$\mu^2 = -\left(4\lambda_1+\lambda_3+\lambda_4+\lambda_5\right)v_{\rm ew}^2/4\,. \tag{5.14}$$

4) $(\lambda_3+\lambda_4+\lambda_5) = 0$. This condition implies that in the real neutral direction there is an $O(3)$ accidental symmetry that is spontaneously broken by the vacuum configuration. Indeed in this case v_1, v_2 and v_3 are only restricted to satisfy $v_1^2+v_2^2+v_3^2 = v_{\rm ew}^2$ and the parameter μ^2 is given by $\mu^2 = -\lambda_1 v_{\rm ew}^2$. We anticipate that the spectrum of neutral Higgs states contain problematic extra Goldstone bosons.

The next four subsections are devoted to a closer look of the four minima just described. This includes a study of the masses of the physical Higgs bosons to see for which minima the spectrum is realistic. This means that all resulting masses are non-negative (no tachyons) and that the only Goldstone bosons that appear are those related to electroweak symmetry breaking. We note that the condition $\lambda_5 = 0$ allows special cases of the solutions 1) to 4), but does not give rise to new solutions. The $\lambda_5 = 0$ scenario can thus be handled in the regular subsections regarding minima 1) to 4) and does not require a separate discussion.

5.6.2 The Alignment (v, v, v) when $\epsilon \neq 0$

In the basis chosen, the vacuum alignment (v, v, v) preserves the Z_3 subgroup[2] of A_4. It is convenient to perform a basis transformation into the Z_3 eigenstate basis, $1, 1' \sim \omega, 1'' \sim \omega^2$, where ω was defined in section 2.4 as a cubic root of unity. The Z_3 eigenstates read

$$\begin{aligned} \varphi &= (\Phi_1 + \Phi_2 + \Phi_3)/\sqrt{3} \sim 1 \\ \varphi' &= (\Phi_1 + \omega\Phi_2 + \omega^2\Phi_3)/\sqrt{3} \sim \omega \\ \varphi'' &= (\Phi_1 + \omega^2\Phi_2 + \omega\Phi_3)/\sqrt{3} \sim \omega^2 \,. \end{aligned} \tag{5.15}$$

In the Z_3 basis, $\varphi \sim 1$ behaves like the standard Higgs doublet: its neutral real component develops a vacuum expectation values $\langle \varphi^{0R} \rangle = v_{\text{ew}}$ and all its other components correspond to the GBs eaten by the corresponding gauge bosons. The physical real scalar gets a mass given by

$$m_{h_1}^2 = \frac{2}{3} v_{\text{ew}}^2 (3\lambda_1 + \lambda_3 + \lambda_4 + \lambda_5 \cos\epsilon). \tag{5.16}$$

The neutral components of the other two doublets φ' and φ'' mix into two complex neutral states; their masses are given by

$$m_{n}^{\prime,\prime\prime\,2} = \frac{v_{\text{ew}}^2}{6} \left(-\lambda_3 - \lambda_4 - 4\lambda_5 \cos\epsilon \pm \sqrt{(\lambda_3 + \lambda_4)^2 + 4\lambda_5^2(1 + 2\sin^2\epsilon) - 4(\lambda_3 + \lambda_4)\lambda_5 \cos\epsilon} \right) . \tag{5.17}$$

The charged components of φ', φ'' do not mix; their masses are

$$m_{C}^{\prime,\prime\prime\,2} = -\frac{v_{\text{ew}}^2}{6} \left(3\lambda_4 + 3\lambda_5 \cos\epsilon \pm \sqrt{3}\lambda_5 \sin\epsilon \right) . \tag{5.18}$$

5.6.3 The Alignment $(v, 0, 0)$ when $\epsilon \neq 0$

In the chosen A_4 basis, the vacuum alignments $(v, 0, 0)$ preserves the Z_2 subgroup of A_4. As in the Z_3 conserving vacuum, it is useful to rewrite the scalar potential by performing the following Z_2 conserving basis transformation

$$\begin{aligned} \Phi_1 &\to \Phi_1 \,, \\ \Phi_2 &\to e^{-i\epsilon/2}\Phi_2 \,, \\ \Phi_3 &\to e^{i\epsilon/2}\Phi_3 \,. \end{aligned} \tag{5.19}$$

Φ_1 is even under Z_2 and behaves like the standard Higgs doublet, while Φ_2 and Φ_3 are odd. For what concerns the neutral states, the 6×6 mass matrix is diagonal in this basis and has some degenerated eigenvalues

$$\begin{aligned} m_{h_1}^2 &\equiv 2\lambda_1 v_{\text{ew}}^2 \,, & m_{h_2}^2 &= m_{h_3}^2 = \frac{1}{2}(\lambda_3 + \lambda_4 - \lambda_5) v_{\text{ew}}^2 \,, \\ m_{h_4}^2 &= m_{h_5}^2 = \frac{1}{2}(\lambda_3 + \lambda_4 + \lambda_5) v_{\text{ew}}^2 \,, & m_{\pi^0}^2 &= 0 \,. \end{aligned} \tag{5.20}$$

[2] In the special case where $\epsilon = 0$, the symmetry of the vacuum is enlarged to S_3 even if S_3 is not a subgroup of A_4. The reason is that setting $\epsilon = 0$ effectively enlarges the symmetry of the potential to S_4 (once also $SU(2) \times U(1)$ gauge invariance is required), which does have S_3 as a subgroup.

The charged scalar mass matrix is also diagonal with eigenvalues

$$m_{C_1}^2 = m_{C_2}^2 = \frac{1}{2}\lambda_3 v_{\text{ew}}^2\,, \qquad m_{\pi^+}^2 = 0\,. \tag{5.21}$$

The degeneracy in the mass matrices are imposed by the residual Z_2 symmetry. Contrary to the previous case the neutral scalar mass eigenstates are real and not complex.

5.6.4 The Alignment $(v, v, 0)$ when $\epsilon = 0$

This vacuum alignment does not preserve any subgroup of A_4. From the minimum equations we obtain

$$\mu^2 = -\frac{1}{4}v_{\text{ew}}^2(4\lambda_1 + \lambda_3 + \lambda_4 + \lambda_5)\,. \tag{5.22}$$

The scalar and pseudoscalar mass eigenvalues are given by

$$\begin{aligned} m_{h_1}^2 &= -\frac{v_{\text{ew}}^2}{2}(\lambda_3 + \lambda_4 + \lambda_5)\,, & m_{h_2}^2 &= \frac{v_{\text{ew}}^2}{2}(4\lambda_1 + \lambda_3 + \lambda_4 + \lambda_5)\,, \\ m_{h_3}^2 &= \frac{v_{\text{ew}}^2}{4}(\lambda_3 + \lambda_4 + \lambda_5)\,, & m_{h_4}^2 &= -\lambda_5 v_{\text{ew}}^2\,, \\ m_{h_5}^2 &= \frac{v_{\text{ew}}^2}{4}(\lambda_3 + \lambda_4 - 3\lambda_5)\,, & m_{\pi^0}^2 &= 0\,. \end{aligned} \tag{5.23}$$

In the charged sector the masses are given by

$$m_{C_1}^2 = \frac{v_{\text{ew}}^2}{4}(\lambda_3 - \lambda_4 - \lambda_5)\,, \qquad m_{C_2}^2 = -\frac{v_{\text{ew}}^2}{2}(\lambda_4 + \lambda_5)\,, \qquad m_{C_3}^2 = 0\,. \tag{5.24}$$

For $\lambda_5 \neq 0$ the alignment $(v, v, 0)$ has the correct number of GBs, while for $\lambda_5 = 0$ we have an extra massless pseudoscalar. More importantly, the conditions $m_{h_1}^2 > 0$ and $m_{h_3}^2 > 0$ can not be simultaneously satisfied. This alignment is therefore a saddle point of the A_4 scalar potential we are studying.

5.6.5 The Alignment (v_1, v_2, v_3) when $\epsilon = 0$

This vacuum alignment, as the previous one, does not preserve any subgroup of A_4. We recall that this minimum requires two constraints on the parameters of the potential: $\epsilon = 0$ and $\lambda_3 + \lambda_4 + \lambda_5 = 0$.

The mass matrix for the neutral CP-even scalar states has just one massive state

$$m{h_1}^2 = 2\lambda_1 v_{\text{ew}}^2\,. \tag{5.25}$$

There are two additional massless scalars as expected from the enlarged symmetry of the potential. There are two degenerate massive and one massless CP-odd states as well. The massless state is just the Goldstone boson π^0. The mass of the massive states is

$$m_{h_2}^2 = m_{h_3}^2 = (\lambda_3 + \lambda_4)v_{\text{ew}}^2\,. \tag{5.26}$$

Note that for the special case $\lambda_5 = 0$ even these states are massless as the original symmetry of the potential was even larger. Lastly, for the charged scalars we have

$$m_{C_1}^2 = m_{C_2}^2 = \frac{1}{2}\lambda_3 v_{\text{ew}}^2\,, \qquad m_{C_3}^2 = 0\,. \tag{5.27}$$

The total amount of GBs is 5 (7) for the case $\lambda_5 \neq 0$ ($\lambda_5 = 0$), so we have 2 (4) extra unwanted GBs. We note that the introduction of terms in the potential that softly break A_4 can ameliorate the situation with the Goldstone bosons.

5.6.6 Analysis of solutions with complex vacua

In the two subsections after this one, we study vacua that are inherently complex. We reiterate that it is always possible to remove one phase by a global rotation. Therefore, it is very easy to give an exhaustive list of vacua: there are just two possibilities.

We order the vacua by the number of zero vevs. Two zeros is not an option, as the only phase in $(v_1 e^{i\omega_1}, 0, 0)$ can always be rotated away. The first possibility is thus the configuration with one zero vacuum expectation value $(v_1 e^{i\omega_1}, v_2, 0)$. A special case occurs if the magnitudes of the two vevs are related. The second possibility reads $(v_1 e^{i\omega_1}, v_2 e^{i\omega_2}, v_3)$ and does not have any zero vevs. A number of special cases is possible, where some or all of the moduli or phases are related. In subsection 5.6.8 we see that the situation with $v_1 = v_2$ and $\omega_1 = -\omega_2$ is of special interest.

We note that the two natural vacua of the previous section (v, v, v) and $(v, 0, 0)$ obviously do not have complex analogues as they have only one phase that can be reabsorbed to make all vevs real. The two less satisfying solutions that appear under the constraint $\epsilon = 0$, given by $(v, v, 0)$ and (v_1, v_2, v_3), do have complex analogues. In the following subsections we show that these are physically more relevant than the real versions.

5.6.7 The Alignment $(v_1 e^{i\omega_1}, v_2, 0)$

The third doublet is inert if the Higgs fields appear in the vacuum $(v_1 e^{i\omega_1}, v_2 e^{i\omega_2}, 0)$. We are left only with two doublets that develop a complex vev and after the redefinition, there is only one phase ω_1. Taking the generic solution $(v_1 e^{i\omega_1}, v_2, 0)$ the minimum equations are given by

$$\begin{aligned}
&v_1 \left[\cos\omega_1 [2\mu^2 + 2\lambda_1(v_1^2 + v_2^2) + (\lambda_3 + \lambda_4)v_2^2] + \lambda_5 v_2^2 \cos(\epsilon + \omega_1)\right] = 0\,,\\
&v_2 \left[(2\mu^2 + 2\lambda_1(v_1^2 + v_2^2) + (\lambda_3 + \lambda_4)v_1^2 + \lambda_5 v_1^2 \cos(\epsilon + 2\omega_1)\right] = 0\,,\\
&v_1 \left[\sin\omega_1 [2\mu^2 + 2\lambda_1(v_1^2 + v_2^2) + (\lambda_3 + \lambda_4)v_2^2] - \lambda_5 v_2^2 \sin(\epsilon + \omega_1)\right] = 0\,,\\
&v_2 v_1^2 \sin(\epsilon + 2\omega_1) = 0\,.
\end{aligned} \tag{5.28}$$

The last equation can be solved by $\epsilon = -2\omega_1$ or $\epsilon = -2\omega_1 + \pi$. Like in section 5.6.1, we can absorb the second case by a redefinition of λ_5. The other three equations reduce to

$$\begin{aligned}
&v_1 \cos\omega_1 \left[2\mu^2 + 2\lambda_1(v_1^2 + v_2^2) + (\lambda_3 + \lambda_4)v_2^2 + \lambda_5 v_2^2\right] = 0\,,\\
&v_2 \left[2\mu^2 + 2\lambda_1(v_1^2 + v_2^2) + (\lambda_3 + \lambda_4)v_1^2 + \lambda_5 v_1^2\right] = 0\,,\\
&v_1 \sin\omega_1 \left[2\mu^2 + 2\lambda_1(v_1^2 + v_2^2) + (\lambda_3 + \lambda_4)v_2^2 + \lambda_5 v_2^2\right] = 0\,.
\end{aligned} \tag{5.29}$$

These equations are simultaneously solved for $v_1 = v_2 = v_{\text{ew}}/\sqrt{2}$ and μ^2 given by

$$\mu^2 = -\frac{v_{\text{ew}}^2}{4}(4\lambda_1 + \lambda_3 + \lambda_4 + \lambda_5)\,. \tag{5.30}$$

The neutral and charged 6×6 mass matrices can analytically be diagonalized. In the neutral sector we have

$$\begin{aligned}
m_{h_1}^2 &= \frac{1}{2}v_{\text{ew}}^2(-\lambda_3 - \lambda_4 - \lambda_5)\,, & m_{h_2}^2 &= \frac{1}{2}v_{\text{ew}}^2(4\lambda_1 + \lambda_3 + \lambda_4 + \lambda_5)\,,\\
m_{h_3}^2 &= \frac{1}{4}v_{\text{ew}}^2(\lambda_3 + \lambda_4 - \lambda_5 + 2\lambda_5\cos 3\omega_1)\,, & m_{h_4}^2 &= -\lambda_5 v_{\text{ew}}^2\,,\\
m_{h_5}^2 &= \frac{1}{4}v_{\text{ew}}^2(\lambda_3 + \lambda_4 - \lambda_5 - 2\lambda_5\cos 3\omega_1)\,, & m_{\pi^0}^2 &= 0\,.
\end{aligned} \tag{5.31}$$

The charged sector has masses

$$m_{C_1}^2 = \frac{v_{\text{ew}}^2}{4}(\lambda_3 - \lambda_4 - \lambda_5)\,, \qquad m_{C_2}^2 = \frac{v_{\text{ew}}^2}{2}(-\lambda_4 - \lambda_5)\,, \qquad m_{C_3}^2 = 0\,. \tag{5.32}$$

We see that the mass of the fourth neutral boson selects negative values for λ_5, i.e. the second solution $\epsilon = -2\omega_1 + \pi$. It is interesting to see that in the real limits $\omega_1 \to 0$ (or π), it is not possible to have both $m^2_{h_1}$ and $m^2_{h_3}$ (respectively $m^2_{h_5}$) positive. This was indeed the conclusion of subsection 5.6.4. Only in the complex situation, there are points in parameter space where all masses are positive. This is in particular clear in the region around $\cos 3\,\omega_1 = 0$. As before, $\lambda_5 = 0$ leads to two problems: an extra GB and impossibility to have all massive eigenstates positive.

5.6.8 The Alignment $(v_1 e^{i\omega_1}, v_2 e^{i\omega_2}, v_3)$

We now consider the alignment where all Higgs doublets develop a non-zero vev. This leads to two physical phases. We have the freedom to take $\omega_3 = 0$. In this case the first-derivative system is given by

$$\begin{aligned}
&v_1 \left\{\cos\omega_1[2\mu^2 + 2\lambda_1(v_1^2+v_2^2+v_3^2) + (\lambda_3+\lambda_4)(v_2^2+v_3^2)] + \right. \\
&\qquad \left. +\lambda_5[v_3^2\cos(\epsilon-\omega_1) + v_2^2\cos(\epsilon+\omega_1-2\omega_2)]\right\} = 0\,, \\
&v_2 \left\{\cos\omega_2(2\mu^2 + 2\lambda_1(v_1^2+v_2^2+v_3^2) + (\lambda_3+\lambda_4)(v_1^2+v_3^2) + \right. \\
&\qquad \left. +\lambda_5[v_3^2\cos(\epsilon+\omega_2) + v_1^2\cos(\epsilon-\omega_2+2\omega_1)]\right\} = 0\,, \\
&v_3 \left\{2\mu^2 + 2\lambda_1(v_1^2+v_2^2+v_3^2) + (\lambda_3+\lambda_4)(v_1^2+v_2^2) + \right. \\
&\qquad \left. +\lambda_5[v_1^2\cos(\epsilon-2\omega_1) + v_2^2\cos(\epsilon+2\omega_2)]\right\} = 0\,, \\
&v_1 \left\{\sin\omega_1[2\mu^2 + 2\lambda_1(v_1^2+v_2^2+v_3^2) + (\lambda_3+\lambda_4)(v_2^2+v_3^2)] + \right. \\
&\qquad \left. +\lambda_5[v_3^2\sin(\epsilon-\omega_1) - v_2^2\sin(\epsilon+\omega_1-2\omega_2)]\right\} = 0\,, \\
&v_2 \left\{\sin\omega_2(2\mu^2 + 2\lambda_1(v_1^2+v_2^2+v_3^2) + (\lambda_3+\lambda_4)(v_1^2+v_3^2)) + \right. \\
&\qquad \left. +\lambda_5[-v_3^2\sin(\epsilon+\omega_2) + v_1^2\sin(\epsilon-\omega_2+2\omega_1)]\right\} = 0\,, \\
&v_3 \left[\lambda_5(-v_1^2\sin(\epsilon-2\omega_1) + v_2^2\sin(\epsilon+2\omega_2))\right] = 0\,.
\end{aligned} \tag{5.33}$$

The last equation is solved for $\omega_2 = -\omega_1$ and $v_2 = v_1 = v$. We have checked explicitly that this is the only solution for the last equation that is compatible with the other equations. Defining $v_3 = rv$ and $v_1^2 + v_2^2 + v_3^2 = v_{\text{ew}}^2$ the previous system reduces to three equations

$$\begin{aligned}
&\mu^2 + \frac{v_{\text{ew}}^2}{2(2+r^2)}\left[(4+2r^2)\lambda_1 + (1+r^2)(\lambda_3+\lambda_4) + \frac{\lambda_5}{\cos\omega_1}(r^2\cos(\epsilon-\omega_1) + \cos(\epsilon+3\omega_1))\right] = 0\,, \\
&\mu^2 + \frac{v_{\text{ew}}^2}{2(2+r^2)}\left[(4+2r^2)\lambda_1 + (1+r^2)(\lambda_3+\lambda_4) + \frac{\lambda_5}{\sin\omega_1}(r^2\sin(\epsilon-\omega_1) + \sin(\epsilon+3\omega_1))\right] = 0\,, \\
&\mu^2 + \frac{v_{\text{ew}}^2}{(2+r^2)}\Big[(2+r^2)\lambda_1 + \lambda_3 + \lambda_4 + \lambda_5\cos(\epsilon-2\omega_1)\Big] = 0\,.
\end{aligned} \tag{5.34}$$

We can solve the third equation in (5.34) in terms of μ^2. Thereafter, the second equation can be solved in terms of λ_5.

$$\begin{aligned}
\mu^2 &= -\tfrac{v_{\text{ew}}^2}{2+r^2}[(2+r^2)\lambda_1 + \lambda_3 + \lambda_4 + \lambda_5\cos(\epsilon-2\omega_1)]\,, \\
\lambda_5 &= \frac{(r^2-1)(\lambda_3+\lambda_4)\sin\omega_1}{(r^2-1)\sin(\epsilon-\omega_1) - 2\cos\epsilon\sin(3\omega_1)}\,.
\end{aligned} \tag{5.35}$$

Then the first equation in (5.34) has two possible solutions, for λ_4 and ϵ respectively

$$\begin{aligned}
&i) \quad \lambda_4 = -\lambda_3\,, \\
&ii) \quad \tan\epsilon = \frac{r^2\sin 2\omega_1 + \sin 4\omega_1}{r^2\cos 2\omega_1 - \cos 4\omega_1}\,.
\end{aligned} \tag{5.36}$$

The solutions (5.35) and (5.36) seem to constrain the potential severely, fixing three of the potential parameters in a non-trivial way. This is indeed true for solution i) in (5.36), but in the other case the potential is still completely general; we have just expressed three of its parameters (μ^2, λ_5 and ϵ) in terms of parameters of the vev system (v_{ew}, r and ω_1).

To test the validity of the solution so far sketched it is necessary to check whether this is a true minimum of the potential and furthermore if there are extra GBs apart from three corresponding to electroweak symmetry breaking. Unfortunately the relations given in (5.35) and (5.36) do not allow

to get analytical solutions for the scalar masses in case $ii)$. For this reason we consider only three special limits in this case : $r \sim 0$, $r \sim 1$ and r very large. We think that these limit situations could be the most interesting ones in model building realizations. Indeed two of the models [127,128] that we discuss in section 5.10 and test in section 5.12 use this vacuum with a large value of r, respectively 43 and 240.

Case $i)$

In this case the constrains $\lambda_4 = -\lambda_3$ puts λ_5 to zero and this substantially enlarges the symmetries of the potential. There is an accidental $O(3)$ in the neutral real direction and two accidental $U(1)$s due to $\lambda_5 = 0$. For this reason the neutral spectrum has 5 massless particles, the GB π^0 and 4 other GBs, and only one massive state

$$m_{h_1}^2 = 2\lambda_1 v_{\rm ew}^2 \,. \tag{5.37}$$

The charged scalars are

$$m_{C_1}^2 = m_{C_2}^2 = \frac{1}{2}\lambda_3 v_{\rm ew}^2 \,, \qquad\qquad m_{C3}^2 = 0 \tag{5.38}$$

Case $ii)$

In this case, it is unfortunately not possible to find analytical solutions. Instead we consider three situations where r takes special values: $r \ll 1$ (in numerical examples $r \sim 0.05$); $r \sim 1$ and $r \gg 1$ (where we take r in the range $50 \div 200$ in numerical studies). See also figure 5.1.

In all these three cases, we find the appearance of very light states. This does obviously not prove that light states are a necessary consequence of case ii) of the $(ve^{i\omega_1},\ ve^{-i\omega_1},\ rv)$ vacuum, but it is a rather strong hint that the vacuum is, at least to some degree, pathological. The problem of the light states can be alleviated by introducing soft A_4 breaking terms. Indeed we opt to add these terms to the models studied in section 5.10.

Figure 5.1: *The three ranges of r studied in this subsection.*

- $r \sim 0$

In this case we assume that r is small and that we can thus neglect terms of order r^2. Equation (5.36) is easily solved for ϵ

$$\epsilon \sim -4\omega_1 + N\pi \,. \tag{5.39}$$

Inserting these values in the equations of (5.35) we find

$$\begin{aligned} \mu^2 &= -\lambda_1 v_{\rm ew}^2 - (\lambda_3 + \lambda_4)\frac{1 - \cos 6\omega_1}{2 - 4\cos 6\omega_1} \,, \\ \lambda_5 &= \frac{\lambda_3 + \lambda_4}{1 - 2\cos 6\omega_1} \,. \end{aligned} \tag{5.40}$$

Under these approximations the 6 x 6 neutral scalar mass matrix gives one massless state, $m_{\pi^0}^2 = 0$,

corresponding to the GB. The other five eigenvalues are at leading order in r given by

$$\begin{aligned}
m_{h_1}^2 &\sim f[\lambda_i]\mathcal{O}(r^2)v_{\rm ew}^2 \\
m_{h_2}^2 &\sim -(\lambda_3+\lambda_4)/(1-2\cos 6\omega_1)v_{\rm ew}^2 \\
m_{h_3}^2 &\sim [-2\lambda_1+(4\lambda_1+\lambda_3+\lambda_4)(1-\cos 6\omega_1)/(1-2\cos 6\omega_1)]\, v_{\rm ew}^2 \\
m_{h_4}^2 &\sim -\left[(\lambda_3+\lambda_4)\cos 6\omega_1 v_w^2/(1-2\cos 6\omega_1)\right] v_{\rm ew}^2\,, \\
m_{h_5}^2 &\sim -\left[2(\lambda_3+\lambda_4)\sin^2 3\omega_1/(1-2\cos 6\omega_1)\right] v_{\rm ew}^2\,.
\end{aligned} \tag{5.41}$$

Here $f[\lambda_i]$ stands for a linear combination of the dimensionless λ parameters of the potential. The lightest state in (5.41) may be too light to be phenomenologically acceptable. We estimate its mass by choosing $f[\lambda_i]$ in the range $0.1 \div 10$ (natural values for a function of dimensionless parameters) or $10^{-2} \div 10^2$ (slightly unnatural). Reference values for r^2 are $10^{-3} \div 10^{-2}$. Under these conditions, we find upper bounds

$$\begin{aligned}
m_{h_1}^2 &\leq 200\,{\rm GeV}^2 \qquad \text{for} \quad \lambda_i \sim 100, r^2 \sim 10^{-2}\,, \\
m_{h_1}^2 &\leq 25\,{\rm GeV}^2 \qquad \text{for} \quad \lambda_i \sim 10, r^2 \sim 10^{-3}\,.
\end{aligned} \tag{5.42}$$

This indicates that for small value of r the spectrum is likely to contain very light neutral states. On the contrary, in the charged sector we have the two GBs eaten by the corresponding gauge bosons, $m_{C_3}^2 = 0$, and two states that are not very light.

$$\begin{aligned}
m_{C_1}^2 &\sim -[\lambda_4 + (\lambda_3+\lambda_4\cos 6\omega_1)/(1-2\cos 6\omega_1)]v_{\rm ew}^2/2 \\
m_{C_2}^2 &\sim -[2\lambda_4 + (\lambda_3+2\lambda_4\cos 6\omega_1)/(1-2\cos 6\omega_1)]v_{\rm ew}^2/2\,.
\end{aligned} \tag{5.43}$$

- $r \sim 1$

If r is close to 1, we write $r \sim 1+\delta$ and make an expansion in terms of δ, neglecting terms of order δ^2. This gives for ϵ

$$\epsilon \sim \pi/2 - \omega_1 - \delta\cot 3\omega_1 + N\pi\,. \tag{5.44}$$

Equations (5.35) for μ^2 and λ_5 become

$$\begin{aligned}
\mu^2 &= -(3\lambda_1+\lambda_3+\lambda_4)/3v_{\rm ew}^2 - \delta/9(\lambda_3+\lambda_4)v_{\rm ew}^2\,, \\
\lambda_5 &= \delta(\lambda_3+\lambda_4)\csc 3\omega_1\,.
\end{aligned} \tag{5.45}$$

Under these approximations the 6 x 6 neutral scalar mass matrix gives the usual null mass state, $m_{\pi^0}^2 = 0$, corresponding to the GB and the following five eigenvalues

$$\begin{aligned}
m_{h_1}^2 &\sim m_{h_2}^2 \sim f[\lambda_i]\mathcal{O}(\delta^2)v_{\rm ew}^2\,, \\
m_{h_3}^2 &\sim m_{h_4}^2 \sim -(\lambda_3+\lambda_4)/3v_{\rm ew}^2\,, \\
m_{h_5}^2 &\sim 2(3\lambda_1+\lambda_3+\lambda_4)/3v_{\rm ew}^2\,,
\end{aligned} \tag{5.46}$$

Again $f[\lambda_i]$ stays for a linear combination of the λs. An analysis similar to the one for the case with $r \sim 0$ shows that the neutral spectrum typically has very light states.

In the charged sector we have the GBs eaten by the gauge bosons and two degenerate massive states

$$m_{C_1}^2 \sim m_{C_2}^2 \sim -\lambda_4/2v_{\rm ew}^2\,. \tag{5.47}$$

- $r \gg 1$

In the situation where r is large, we perform an expansion in term of $1/r$ and neglect terms of order $1/r^2$. From equation (5.36) we find

$$\epsilon \sim 2\omega_1 + N\pi\,. \tag{5.48}$$

After this, equation (5.35) reduces to

$$\mu^2 \sim -\lambda_1 v_{\text{ew}}^2 \,, \tag{5.49}$$
$$\lambda_5 \sim -(\lambda_3+\lambda_4)\,. \tag{5.50}$$

Under these approximations we find a massless neutral scalar state, $m_{\pi^0}^2 = 0$. The other 5 neutral masses are given at leading order by

$$\begin{aligned} m_{h_1}^2 &\sim m_{h_2}^2 \sim f[\lambda_i]\mathcal{O}(1/r^2) v_{\text{ew}}^2 \,, \\ m_{h_3}^2 &\sim 2\lambda_1 v_{\text{ew}}^2 \,, \\ m_{h_4}^2 &\sim m_{h_5}^2 \sim (\lambda_3+\lambda_4) v_{\text{ew}}^2 \,. \end{aligned} \tag{5.51}$$

The charged scalar mass matrix is diagonal up to terms of order $\mathcal{O}(1/r^2)$ with the correct number of GBs and two massive degenerate states

$$m_{C_1}^2 = m_{C_2}^2 = \lambda_3 v_{\text{ew}}^2/2\,. \tag{5.52}$$

From equation (5.51) it follows that again there are two very light neutral scalars. Using reference values for r in the range $50 \div 200$ we find

$$m_{h_{1,2}}^2 \sim \sqrt{f[\lambda_i]}\,5\,\text{GeV}^2(1\,\text{GeV}^2)\,. \tag{5.53}$$

For 'small' values of $f[\lambda_i]$ as defined above, the minimal masses that this expression can reproduce are

$$\begin{aligned} m_{1,2}^2 &\leq 50^2 \quad \text{GeV}^2 \quad \text{for} \quad r \sim 50\,, \\ m_{1,2}^2 &\leq 10^2 \quad \text{GeV}^2 \quad \text{for} \quad r \sim 200\,. \end{aligned} \tag{5.54}$$

Again we find that naturally very light scalars appear. In conclusion the solution $(e^{i\omega_1}, e^{-i\omega_1}, r)v_{\text{ew}}/\sqrt{2+r^2}$ gives very light states in each of the domains for r investigated, at least under the assumption that the functions $f[\lambda_i]$ obtained somewhat natural values. We reiterate that this is no formal proof that there exist light states for all values of r.

5.6.9 List of the available minima

In this section we have scanned the possible solutions of the first derivative system (5.8) of the A_4-invariant Higgs potential (5.4). Three candidate-vacua seemed to be under control.

- The vacuum $(v,\, v,\, v)$ of section 5.6.2.
- The vacuum $(v,\, 0,\, 0)$ of section 5.6.3.
- The vacuum $(ve^{i\omega_1}, v, 0)$ of section 5.6.7. We note that the global rotation used to get rid of the second phase could equally well be used to give the first two elements equal but opposite phases: $(ve^{i\omega_1/2}, ve^{-i\omega_1/2}, 0)$

These configurations have the right number of Goldstone bosons and in a large part of parameter space all masses are positive and in a reasonable range.

Two vacua were more problematic

- The alignment $(v_1,\, v_2,\, v_3)$ of section 5.6.5.
- The alignment $(v\, e^{i\omega_1},\, v\, e^{-i\omega_1},\, r\, v)$ of section 5.6.8.

The first vacuum here was derived under the assumption of non-trivial relations of parameters in the potential. As a result, obtaining this vacuum implies breaking extra symmetries next to electroweak symmetry. The second vacuum has two realizations, case i) and case ii). The first case suffers from the same handicaps as the previous vacuum: the potential parameters are related and extra symmetries gets broken when the Higgses develop vacuum expectation values. The second case technically gives a correct vacuum. However, for all values of $f[\lambda_i]$ and r studied, very light states appeared. In all situations, a solution is to add soft A_4 breaking terms to the potential, although that significantly reduces the appeal of the method. Lastly, one of the solutions, the candidate-vacuum $(v,\, v,\, 0)$ of section 5.6.4 turned out to be always a saddle point and is not discussed further.

5.7 Discussion on CP violation

The A_4-invariant Higgs potential 5.4 central in this chapter has an explicit complex phase ϵ. Furthermore, the solutions studied in sections 5.6.7 and 5.6.8 had an explicit complex phase ω_1 in some of the vacuum expectation values. One might thus wonder whether the Higgs sector in A_4 models gives rise to extra sources of CP violation. This CP violation can be either explicit if it appears directly at the level of the Higgs potential or implicit if it occurs due to the vacuum expectation values of the scalars. In this section we investigate explicit and implicit CP violation in the A_4 Higgs scenario. The conclusion is that neither is present. This section owes to [129] in which the question of CP violation in our class of models was first discussed in detail.

We first investigate if the potential 5.4 exhibits explicit CP violation. We find that the potential is not invariant under a 'naive' CP transformation

$$\Phi_i \xrightarrow{\text{CP}} \Phi_i^* \,, \qquad \text{i.e. } \Phi_i \xrightarrow{\text{CP}} \delta_{ij}\Phi_j^* \,. \tag{5.55}$$

Under this transformation ϵ and $-\epsilon$ get interchanged in the potential (5.4). Equation (5.55) does not describe the most general CP transformation however. A more general CP transformation follows when the 'pure' CP transformation (5.55) is combined with a Higgs basis transformation

$$\Phi_i \xrightarrow{\text{CP}} U_{ij}\Phi_j^* \,. \tag{5.56}$$

Here U is a unitary matrix in the space of the three Higgs fields. It was shown in [130] that the Higgs potential conserves CP explicitly if a matrix U exists such that the 'new' CP transformation (5.56) leaves the potential invariant. For the potential (5.4) it is not hard to find such a matrix. An example is the matrix that parameterizes the interchange of the first and second Higgs field

$$U = \begin{pmatrix} 0 & 1 & 0 \\ 1 & 0 & 0 \\ 0 & 0 & 1 \end{pmatrix} \,. \tag{5.57}$$

In this case, the CP transformation is defined according to

$$\Phi_1 \xrightarrow{\text{CP}} \Phi_2^*, \quad \Phi_2 \xrightarrow{\text{CP}} \Phi_1^*, \quad \Phi_3 \xrightarrow{\text{CP}} \Phi_3^* \,. \tag{5.58}$$

We conclude that the A_4 invariant Higgs potential does not violate CP explicitly. There is still the possibility of spontaneous CP violation through the complex vacua discussed in the previous section. In [130] and [131] it is shown that a vacuum does not give rise to spontaneous CP violation if there is a matrix U such that the CP transformation (5.56) also leaves the vacuum invariant. In that case, the vacuum thus satisfies

$$(vac) = U\ (vac)^* \,. \tag{5.59}$$

In other words, each component $v_i e^{i\omega_i}$ of the vector of vevs should be written as a linear combination of the complex conjugates of the vevs $v_j e^{i\omega_j}$ with the coefficients given by U_{ij}

$$v_i e^{i\omega_i} = U_{ij} v_j\ e^{-i\omega_j} \,. \tag{5.60}$$

In the specific case under investigation, where U has the form (5.57), this is represented by

$$v_1 e^{i\omega_1} = v_2 e^{-i\omega_2}, \quad v_2 e^{i\omega_2} = v_1 e^{-i\omega_1}, \quad v_3 e^{i\omega_3} = v_3 e^{-i\omega_3} \ . \tag{5.61}$$

The first two equations are dependent; they require v_1 and v_2 to be each others complex conjugate. The third equation requires the third vev to be real. The two candidate-CP-violating vacua, $(ve^{i\omega_1/2},\ ve^{-i\omega_1/2},\ 0)$ and $(v\,e^{i\omega_1},\, v\,e^{-i\omega_1},\, r\,v)$ both satisfy the conditions (5.61). They do thus not break CP spontaneously, notwithstanding the fact that they are inherently complex[3].

The criterium of conserving or violating CP depending on whether the transformation matrix U exists, is not always a very practical one. Even if such a transformation exists, it may not be easy to find. A more solid test is in the calculation of CP-odd basis invariants that vanish if CP is conserved and that are non-zero if CP is violated (or, at least one of them is). Invariants for the potential (5.4) and the vacua of the previous subsection were calculated in [129]. As expected, they are all zero.

5.8 Description of model-independent tests of the viability of vacua

The most direct tests for the scenario of this chapter, is obviously the direct detection of the extended Higgs sector. In each of the vacua of section 5.6 we mentioned the appearance of multiple Higgs bosons with specific relations between their masses. The LHC recently cut deep into the parameter space available to the Standard Model Higgs boson, excluding much of its mass range and finding hints for a Higgs around 125 GeV, see for instance [132,133]. Bounds for non-Standard Model Higgses have also been obtained. We have not yet applied these bounds to our model. The fact that the data are not sufficient to exclude slightly similar multi-Higgs scenarios, in particular the MSSM, however hints to the statement that more data will be needed to test our model via direct detection of the Higgs fields involved.

In this section we analyze three more indirect tests for the vacuum configurations derived in section 5.6. These tests only require pre-LHC data and involve phenomenology of the Higgs sector only. As such they are model independent according to the definition of section 5.3 as the A_4 representations of the various fermions in the theory need not be fixed.

The three tests are unitarity; Z and $W^\pm$ decays and oblique parameters. In the next section we use these three tests to examine the viability of the vacua of section 5.6 and to restrict their parameter space.

5.8.1 Unitarity

A first test for multi-Higgs models comes from the tree level unitarity constraints due to the additional scalars present in the theory. In this subsection, we examine the partial wave unitarity for the neutral two-particle amplitudes for $s \gg M_W^2, M_Z^2$. We can use the equivalence theorem, so that we can compute the amplitudes using only the scalar potential given in (5.4). In the regime of large energies, the only relevant contributions are the quartic couplings in the scalar potential [134–137] and we can write the $J = 0$ partial wave amplitude a_0 in terms of the tree level amplitude T as

$$a_0(s) \equiv \frac{1}{32\pi} \int_{-1}^{1} \mathrm{d}\cos\theta \; T(s) = \frac{1}{16\pi} F[\lambda_i] \, . \tag{5.62}$$

[3]We recall that via a global rotation the first complex vacuum can also be written as $(ve^{i\omega_1},\ v,\ 0)$ and it was indeed derived in this form in section 5.6.7. In this case, U should contain a phase as well and is written as $e^{i\omega_1}$ times the matrix in equation (5.57).

Here F represents a function of the λ_i couplings. For simplicity we use the notation

$$\Phi_a = \begin{pmatrix} w_a^+ \\ \dfrac{v_a e^{i\omega_a} + h_a^0 + i z_a}{\sqrt{2}} \end{pmatrix} . \tag{5.63}$$

Now we can write the 30 neutral two-particle channels as follows:

$$w_a^+ w_b^- \,,\ \frac{z_a z_b}{\sqrt{2}} \,,\ \frac{h_a^0 h_b^0}{\sqrt{2}} \,,\ h_a^0 z_b \,. \tag{5.64}$$

The full scattering matrix a_0 can be cast in a block diagonal structure. The first 12×12 block concerns the channels

$$w_1^+ w_1^- \,,\ w_2^+ w_2^- \,,\ w_3^+ w_3^- \,,\ \frac{z_1 z_1}{\sqrt{2}} \,,\ \frac{z_2 z_2}{\sqrt{2}} \,,\ \frac{z_3 z_3}{\sqrt{2}} \,,\ \frac{h_1^0 h_1^0}{\sqrt{2}} \,,\ \frac{h_2^0, h_2^0}{\sqrt{2}} \,,\ \frac{h_3^0, h_3^0}{\sqrt{2}} \,,\ h_1^0 z_1 \,,\ h_2^0 z_2 \,,\ h_3^0 z_3 \,.$$

The other three 6×6 blocks are related to six channels parameterized by the labels $(a,\, b)$ that take values $(1,\, 2)$, $(1,\, 3)$ and $(2,\, 3)$:

$$w_a^+ w_b^- \,,\ w_b^+ w_a^- \,,\ h_a^0 z_b \,,\ h_b^0 z_a \,,\ z_a z_b \,,\ h_a^0 h_b^0 \,,$$

Note that up this point the analysis is completely general and is valid for all the vacua presented. When testing a vacuum configuration, we express the quartic couplings λ_i in terms of the masses of the scalars. Afterwards, we can use the constraint that the largest eigenvalues of the scattering matrix a_0 has modulus less than 1. This gives upper bounds on the scalar masses that we can use in a numerical analysis.

5.8.2 Z And $W^\pm$ Decays

The next test we perform is related to the decay of Z and W gauge bosons. From an experimental point of view the decay of gauge bosons into scalar particles is detected by looking at fermionic channels, such as $Z \to hA \to 4f$ in the 2HDM, or Z decays into partial or total missing energy in a generic new physics scenario. From this point of view gauge bosons decays bound the Higgs sector in an extremely model dependent way as they are highly sensitive to the fermion content of the theory.

On the other hand, in the SM the Z and the $W^\pm$ decays have precisely been calculated and measured not only for decay into 2 or 4 fermions, but also for the sum of all decays. We can thus focus on the decays $Z, W^\pm \to all$. Doing this we overestimate the allowed regions in the parameter space, but we have a first and model-independent cut arising from the decay of the gauge bosons. Once we pass to a model dependent analysis the region can only be restricted, not enlarged. Actually, we expect the error to be quite small, given that the contribution from new physics $\Delta\Gamma$ satisfies

$$\Delta\Gamma^{2f}_{Z,W^\pm} \sim \Delta\Gamma^{4f}_{Z,W^\pm} \sim \Delta\Gamma^{all}_{Z,W^\pm} \ll \Gamma_{Z,W^\pm} \,. \tag{5.65}$$

LEP data give an estimate for the width that can be assigned to new physics effects

$$\Gamma^{\text{exp}}_{Z,W^\pm} = \Gamma^{\text{SM}}_{Z,W^\pm} + \Delta\Gamma_{Z,W^\pm} \,. \tag{5.66}$$

Experimentally $\Delta\Gamma_Z \sim 0.0023$ GeV and $\Delta\Gamma_{W^\pm} \sim 0.042$ GeV [6]. This can be used to calculate the width of Z and W decay to respectively two neutral Higgs states and to one neutral and one charged state.

$$\begin{aligned} Z &\to h_i h_j \,, \\ W^+ &\to h_i^+ h_j \,. \end{aligned} \tag{5.67}$$

In the final step we select the points for which the the widths of the Z and W bosons due to the multi-Higgs set up are allowed by the LEP data.

$$\Gamma^{\rm MH}_{Z,W^\pm} \leq \Delta\Gamma_{Z,W^\pm} \,. \tag{5.68}$$

In the vacuum analysis of section 5.6 we have seen that in a few situations there are extra massless or very light particles. Even if we assume that these do not directly rule out the related configurations (some light scalars may indeed be hard to find directly), the gauge-boson decays put very strong bounds on their existence. Bound on Z decay translate to the following inequalities

$$\begin{cases} k_Z \leq \Delta\Gamma_Z \dfrac{16\pi}{m_Z}\dfrac{4c_W^2}{g^2} & \text{if both particles } h_i \text{ and } h_j \text{ are massless}\,. \\ k_Z \left(1-\dfrac{m_{h_i}^2}{m_Z^2}\right)^3 \leq \Delta\Gamma_Z \dfrac{16\pi}{m_Z}\dfrac{4c_W^2}{g^2} & \text{if } h_j \text{ is massless and } 0<m_{h_i}^2<m_Z^2\,. \\ k_Z \left(1-\dfrac{m_{h_i}^2+m_{h_j}^2}{m_Z^2}\right)^3 \leq \Delta\Gamma_Z \dfrac{16\pi}{m_Z}\dfrac{4c_W^2}{g^2} & \text{if } h_i,h_j\neq 0 \text{ and } 0<m_{h_i}^2+m_{h_j}^2<m_Z^2\,. \end{cases} \tag{5.69}$$

In these equations, g is the $SU(2)$ gauge coupling, c_W the cosine of the Weinberg angle θ_W and the parameter k_Z is expressed in terms of the matrix U defined in equation (5.6)

$$k_Z = \left(-U^T_{ab}U^T_{(a+3)c} + U^T_{(a+3)b}U^T_{ac}\right)^2 \,. \tag{5.70}$$

A similar equation exist for $W^\pm$ decay in the situation where h_j is massless and $m_{C_i}^2 < m_W^2$

$$k_W \left(1-\frac{m_{C_i}^2}{m_W^2}\right)^3 \leq \Delta\Gamma_W \frac{16\pi}{m_W}\frac{4c_W}{g^2} \,. \tag{5.71}$$

Analogous to k_Z, the parameter k_W is given in terms of the matrix S defined in equation (5.7).

$$k_W = \left|S^\dagger_{ab}U^T_{ac}\right|^2 + \left|S^\dagger_{(a+3)b}U^T_{(a+3)c}\right|^2 \,. \tag{5.72}$$

Large Mass Higgs Decay

Electroweak data analysis considering the data from LEP2 [138] and Tevatron [139] put an upper bound on the mass of the SM Higgs of 194 GeV at 99% CL [6]. In a MH scenario this bound can be roughly translated in the upper bound for the lightest scalar mass, m_{h_1}. For large values of the SM Higgs mass, $m_h \geq 2m_W$, the main decay is $h \to W^+W^-$ and the upper bound is completely 'model independent' in the sense that it does not depend on the fermionic content of the model.

In a MH model the lightest Higgs boson coupling to the gauge bosons is given in terms of a parameter $\beta \leq 1$

$$\begin{aligned} g_{h_1ZZ} &= \beta\, g^{SM}_{hZZ}\,, \\ g_{h_1WW} &= \beta\, g^{SM}_{hWW}\,. \end{aligned} \tag{5.73}$$

In the three-Higgs model, β is given by

$$\beta = \frac{v_a}{v_{\rm ew}} f_a(\cos\omega_a\, U^T_{a1} + \sin\omega_j\, U^T_{(a+3)1})\,. \tag{5.74}$$

In these models, the lightest Higgs h_1 is less copiously produced than the SM Higgs of the same mass, which in turn is always less than the SM Higgs production at the highest allowed mass of 194 GeV

$$\Gamma^{MH}_{WW}(m_{h_1}) \sim |\beta|^4 \Gamma^{SM}_{WW}(m_{h_1}) \leq \Gamma^{SM}_{WW}(194)\,. \tag{5.75}$$

We use this to obtain an upper bound for m_{h_1} of 194 GeV.

5.8.3 Constraints By Oblique Corrections

Lastly, the consistency of a MH model with the current experimental data has to be checked also by means of the oblique corrections. These corrections can be classified [140–145] by means of three parameters, S T and U, that maybe written in terms of the physical gauge-boson vacuum polarizations

$$\begin{aligned} T &= \frac{4\pi}{e^2 c_W^2 m_Z^2}\left[A_{WW}(0) - c_W^2 A_{ZZ}(0)\right] , \\ S &= 16\pi \frac{s_W^2 c_W^2}{e^2}\left[\frac{A_{ZZ}(m_Z^2) - A_{ZZ}(0)}{m_Z^2} - A'_{\gamma\gamma}(0) - \frac{(c_W^2 - s_W^2)}{c_W s_W} A'_{\gamma Z}(0)\right] , \\ U &= -16\pi \frac{s_W^2}{e^2}\left[\frac{A_{WW}(m_W^2) - A_{WW}(0)}{m_W^2} - c_W^2 \frac{A_{ZZ}(m_Z^2) - A_{ZZ}(0)}{m_Z^2} - s_W^2 A'_{\gamma\gamma}(0) - 2 s_W c_W A'_{\gamma Z}(0)\right] . \end{aligned} \tag{5.76}$$

As in equation (5.69), c_W is the cosine of θ_W and s_W is its sine; e is the electric charge. EW precision measurements severely constrain the possible values of the three parameters T, S and U. In the SM assuming $m_h^2 > m_Z^2$ the oblique parameters are given by

$$\begin{aligned} T_h^{SM} &\sim -\frac{3}{16\pi c_W^2}\log\frac{m_h^2}{m_Z^2} , \\ S_h^{SM} &\sim \frac{1}{12\pi}\log\frac{m_h^2}{m_Z^2} , \\ U_h^{SM} &\sim 0 . \end{aligned} \tag{5.77}$$

For a Higgs boson mass of $m_h = 117$ GeV (and in brackets the difference assuming instead $m_h = 300$ GeV), the data allow [6]

$$\begin{aligned} S^{exp} &= 0.10 \pm 0.10(-0.08) \\ T^{exp} &= 0.03 \pm 0.11(+0.09) \\ U^{exp} &= 0.06 \pm 0.10(+0.01) . \end{aligned} \tag{5.78}$$

A detailed analysis on the S, T and U parameters in a MH model has been presented in [146, 147] where all details are carefully explained. However the resulting formulas are valid only for scalar masses larger or comparable to m_Z. This is not the case for a generic MH model. In particular in some of the configurations studied in the previous section there are massless and extremely light particles. We modify their results, getting full formulas valid for any value of the scalar masses in appendix 5.A.

5.9 Results of the model-independent tests

In this section we report on numerical analyses for all vacuum configurations summarized in section 5.6.9. The aim of the analysis is to find, for each configuration, whether a region in parameter space exists, where all the Higgs constraints are satisfied. Points in parameter space are generated and then tested through subsequent constraints, from the weaker one to the strongest. Points that 'pass' a certain test and then 'fail' the next one are classified as points Y, B and G. Points that 'pass' all tests are referred to as R.

- Points Y. These points are true minima: all the squared masses are positive, but the unitarity test fails (yellow points in the figures);
- Points B. These points are true minima and the unitarity bounds are passed, but Z and $W^\pm$ decays are not (blue points);

- Points G. Here also the Z and $W^{\pm}$ decays are according to data, but the oblique parameters are not (green points);
- Points R. These points pass all tests we performed, including being in accordance with the T, S and U parameters (red points).

The ratios B/Y, G/B, R/G can be used to indicate which is the stronger constraint for each of the allowed minima. Whenever possible, we plot the mass of the lightest neutral state m_1 to the mass of the second lightest neutral state m_2 and of the lightest charged one m_{ch_1}. For all green points that pass the unitarity and W/Z constraints, i.e. the green and the red points, we plot the T and S oblique parameters. It turns out that for all cases considered that T is the most constraining one. For this reason we have not inserted the plots concerning U.

5.9.1 The Alignment (v, v, v)

We first consider the minimum (v, v, v). We showed in section 5.6.2 that this conserves a Z_3 symmetry. There we have also redefined the initial 3 doublets in terms of the surviving Z_3 symmetry representations: 1, $1'$ and $1''$. One combination corresponds to a Z_3 singlet doublet, that behaves like the SM Higgs: it develops a non-vanishing vev, gives rise to a CP even state which we call h_1 and to the three GBs eaten by the gauge bosons. The others two doublets, φ' and φ'', are inert. Depending on which Higgs is the lightest, we can describe the allowed decay patterns and describe what is expect from a numerical scan. The results of this scan are given in figure 5.2.

1) When h_1 is the lightest state, the usual SM mass upper bound applies. On the contrary as long as we do not consider its coupling with the fermions we do not have a model-independent lower mass bound. This is due to a combined effect of the CP and Z_3 symmetries: h_1 is CP even and a singlet under Z_3. This forbids couplings like Zh_1h_1, $Zh_1\varphi'^0$ and $Zh_1\varphi''^0$. Gauge boson decays can therefore not constrain the lower mass of h_1.
2) When φ'^0 or φ''^0 is the lightest state, we do not have an upper bound on this state by the heavy Higgs decays because the couplings $\varphi'^0W^+W^-$ ($\varphi''^0W^+W^-$) are absent. On the contrary we can have a lower bound by W and Z decay because couplings like $Z\varphi'^0\varphi''^0$ and $W^-\varphi'^0\varphi''^-$ are allowed.

5.9.2 The Alignment $(v, 0, 0)$

The second minimum we consider is $(v, 0, 0)$ that is Z_2 conserving. In this minimum, there is only one Z_2 even Higgs boson. We refer to this as h_1, although, again, it is not necessary the lightest one. There are also four Z_2 odd states: a degenerate pair of CP even bosons, labeled $h_{2,3}$ and a degenerate pair that is CP odd, labeled $h_{4,5}$. As in the previous subsection we sketch the expectations for a numerical analysis.

1) When h_1, the Z_2-even SM-like Higgs, is the lightest boson, we expect the SM Higgs upper bound to apply, but there should be no lower bound because the interactions $Zh_1h_{4,5}$ are forbidden by the Z_2 symmetry;
2) When the two lightest bosons are the Z_2 odd degenerate states $h_{2,3}$ (CP even) or $h_{4,5}$ (CP odd) we expect no upper bound. Moreover since they are degenerate we do not expect a lower bound either. On the contrary we expect that Z and W decays constrain the third lightest neutral Higgs mass and that of the charged ones.

In figure 5.3 we see a large number of points on the diagonal. This means that the lightest mass m_1 is identical to the second-lightest mass m_2, with values up to 700 GeV. Having one of the degenerate

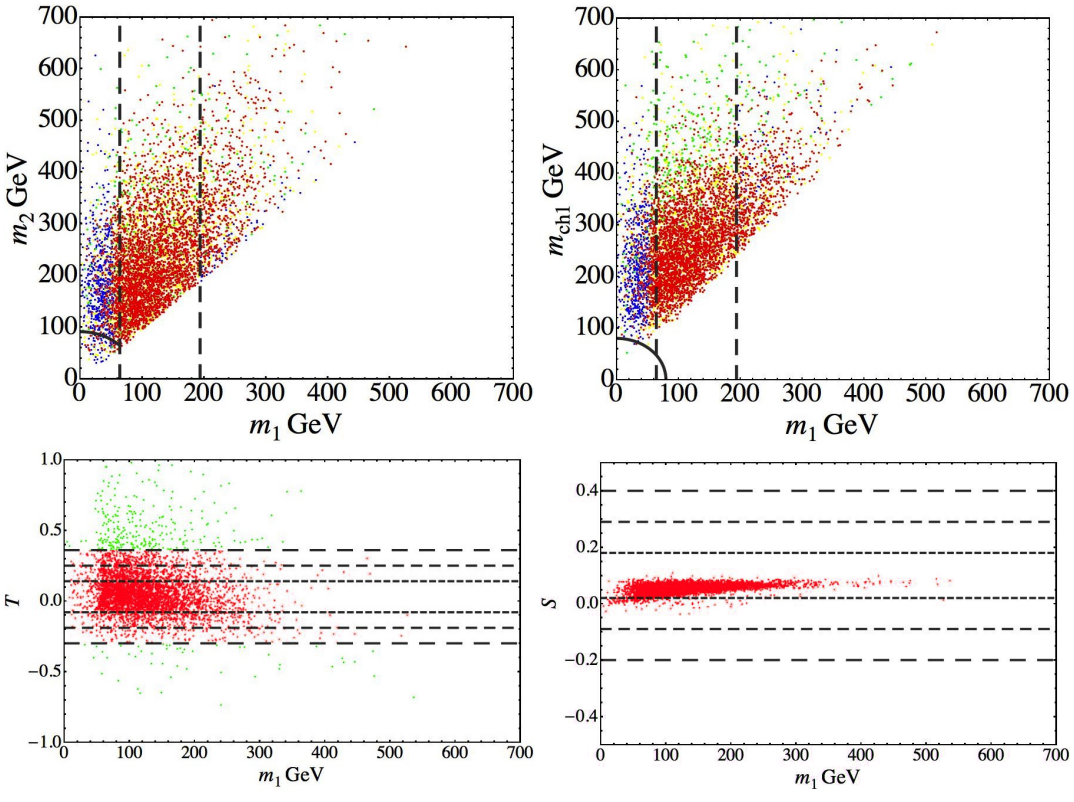

Figure 5.2: *The Z_3 conserving alignment (v, v, v): the upper panels show the lightest neutral mass m_1 versus the second lightest neutral mass m_2 and versus the lightest charged one m_{ch_1} respectively. The gray arc delimits the region below which the Z (W) decay channel opens. On the left plot the arc is only $45°$ because $m_2 \geq m_1$. For points below the arc the Z (W) decay can happen. The points allowed stretch in the region close to the border because of the conditions (5.69). The dashed vertical lines indicates the approximate cuts that occur at $m_1 \sim m_Z/\sqrt{2}$ and $m_1 \sim 194$ GeV according to case 2) and case 1) respectively as explained in the text. The lower panels show the contributions to T and S for the green and red points. The gray dashed lines indicate the experimental values at 3, 2, 1σ level with long, normal and short dashing respectively. T turns out to be the most constraining oblique parameter.*

pairs as the lightest states reflects case 2). The points corresponding to case 1) have a sharp cut at $m_1 = 194$ GeV. This cut rejects many blue points, i.e. those that satisfy the unitarity constraint but not the decay constraint. We have also reported m_1 versus m_3 to check that indeed, when $m_1 \to 0$, m_3 is bounded by m_Z as we expected. Our intuitions are also confirmed by the plot $m_1 - m_{ch_1}$, where m_{ch_1} stands for the lightest charged Higgs. As in the Z_3 preserving case the most constraining oblique parameter is T.

5.9.3 The Alignment (v_1, v_2, v_3) with $\epsilon = 0, \lambda_3 + \lambda_4 + \lambda_5 = 0$

In this case we do not have any surviving symmetry that forbids specific couplings as was the case in the previous two subsections. However from subsection 5.6.4 we know that the conditions $\epsilon = 0$, $\lambda_3 + \lambda_4 + \lambda_5 = 0$ give rise to two extra massless CP even particles. This justifies two expectations.

1) When the lightest massive state is CP odd, then its mass is bounded by the Z decay through equation (5.69);

2) When the lightest massive state is CP even, then its mass could reach smaller values since the Z decay bound would constrain the combination of its mass with the lightest CP odd state mass.

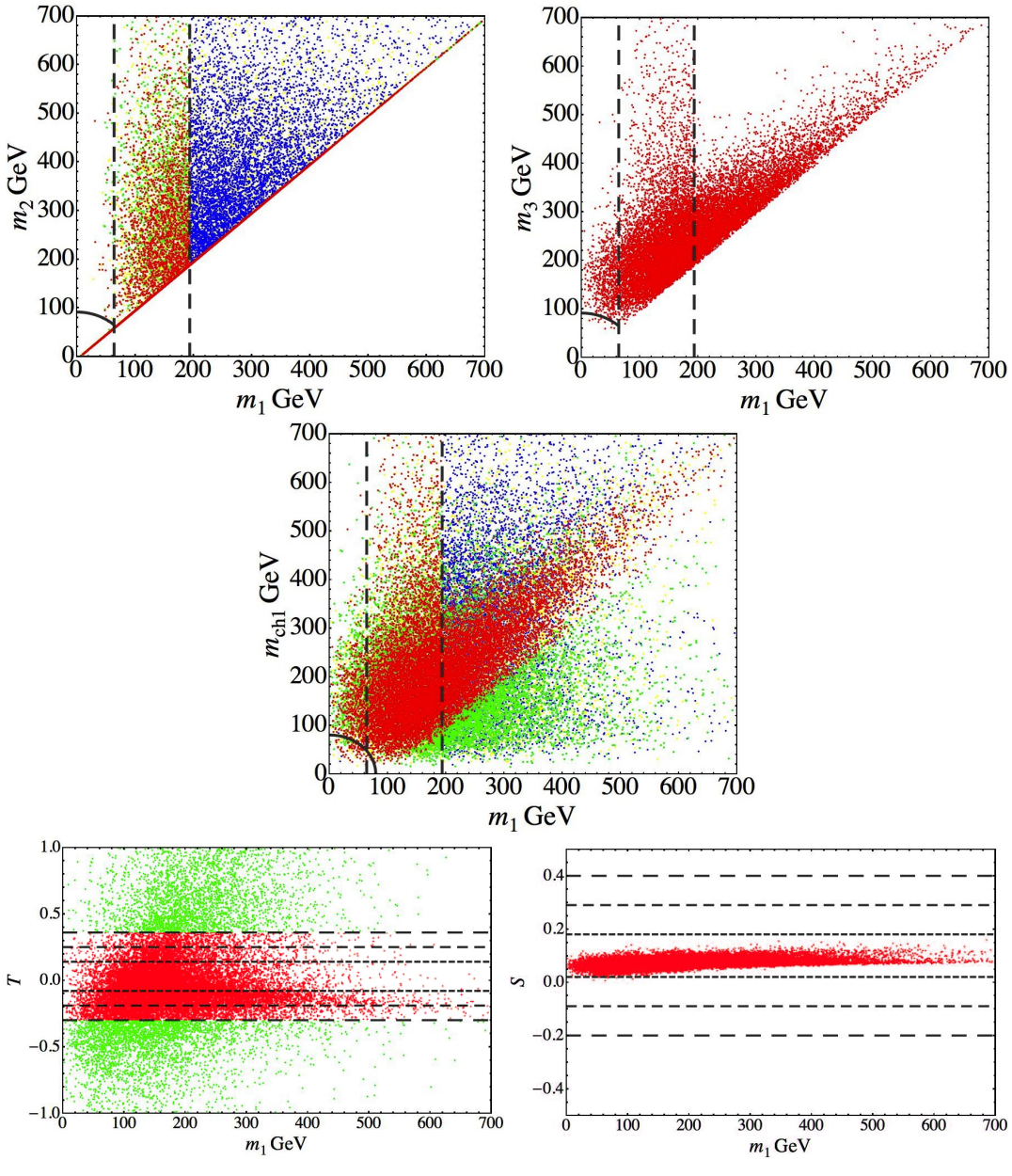

Figure 5.3: *The alignment* $(v, 0, 0)$*: the upper panels show* m_1 *versus* m_2 *(on the left) and third lightest* m_3 *(on the right). For the latter we reported only the R points. The central panel shows* m_1 *versus* m_{ch_1}*. The gray arc delimits the region below which the Z (W) decay channel opens while the second dashed vertical line indicates the SM-Higgs mass upper bound at* 194 *GeV. The first dashed vertical line at* $m_1 = m_Z/\sqrt{2}$ *is given to help a comparison with the* Z_3 *preserving case. On the first two plots the arc is only 45 degrees because* $m_{2,3} \geq m_1$*. The lower panels show the contributions to T and S. Again, the T parameter turns out to be the most constraining one.*

Moreover in both cases we expect the mass of the lightest charged scalar bounded by W decay, according to equation (5.71), due to its coupling with W and the massless particles.

Figure 5.4 shows that case 2) happens very rarely as there are very few red points below the Z cut. As for the Z_3 and Z_2 preserving minima the T parameter is the most constraining one. In general, we mention that it is remarkable that there are many red points in the figures. Even with extra massless particles present, it is quite possible to pass all electroweak tests.

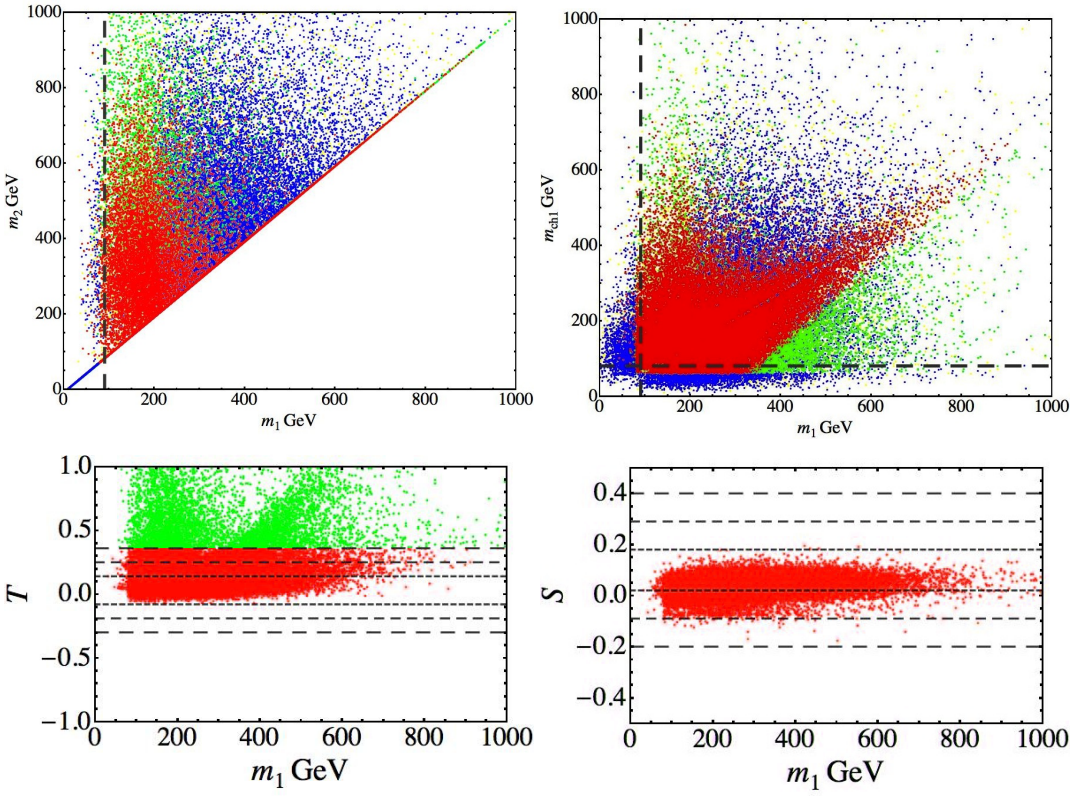

Figure 5.4: *The alignment (v_1, v_2, v_3) with extra Goldstone bosons: the upper panels show m_1 versus m_2 and m_{ch_1} respectively. The dashed lines at $m_1 = m_Z$ (vertical) and $m_{ch1} = m_W$ (horizontal) delimit the region below which the Z and W decay channels open respectively. The allowed points concentrate close to the borders according to equations 5.69-5.71. The lower panels show the contributions to T and S. Again, the T parameter turns out to be the most constraining one.*

5.9.4 The Alignment $(ve^{i\omega_1}, v, 0)$

The alignment $(ve^{i\omega_1}, v, 0)$ does not preserve any A_4 subgroup, just like the vacuum alignment (v_1, v_2, v_3) discussed above. We expect that Z decay does not give a lower bound on m_1 and m_2 in figure 5.5 as the two lightest Higgs might have the same CP eigenvalue, preventing the Z to decay into them. W decay on the other hand gives a lower bound on the quantity $m_1^2 + m_{ch_1}^2$. Regarding the upper bound on the lightest neutral mass state we do not expect any clear cut because we may not identify a SM-like Higgs.

5.9.5 The Alignment $(ve^{i\omega_1}, ve^{-i\omega_1}, rv)$ case $i)$

In section 5.6.8 we have seen that the alignment $(ve^{i\omega_1}, ve^{-i\omega_1}, rv)$ with the constrains $\lambda_5 = 0$, $\lambda_4 = -\lambda_3$, gives rise to 4 extra GBs and only to one neutral state. The expressions for the three non-vanishing masses (5.37) and (5.38) show that λ_1 and λ_3 should be positive in this case.

The positivity constraint is therefore easily met. Also the test of unitarity can be passed if the parameters are centred around 1. We expect that the most stringent bound is given by the decay constrains and not by the T, S and U parameters: massless particles give a small contribution to the oblique parameters and due to the limited number of new massive particles (two charged degenerate scalars) T, S and U should not deviate too much from the SM values. Indeed in figure 5.6 it is shown that the oblique parameters are not constraining at all at 3σ level. For this reason we only report the

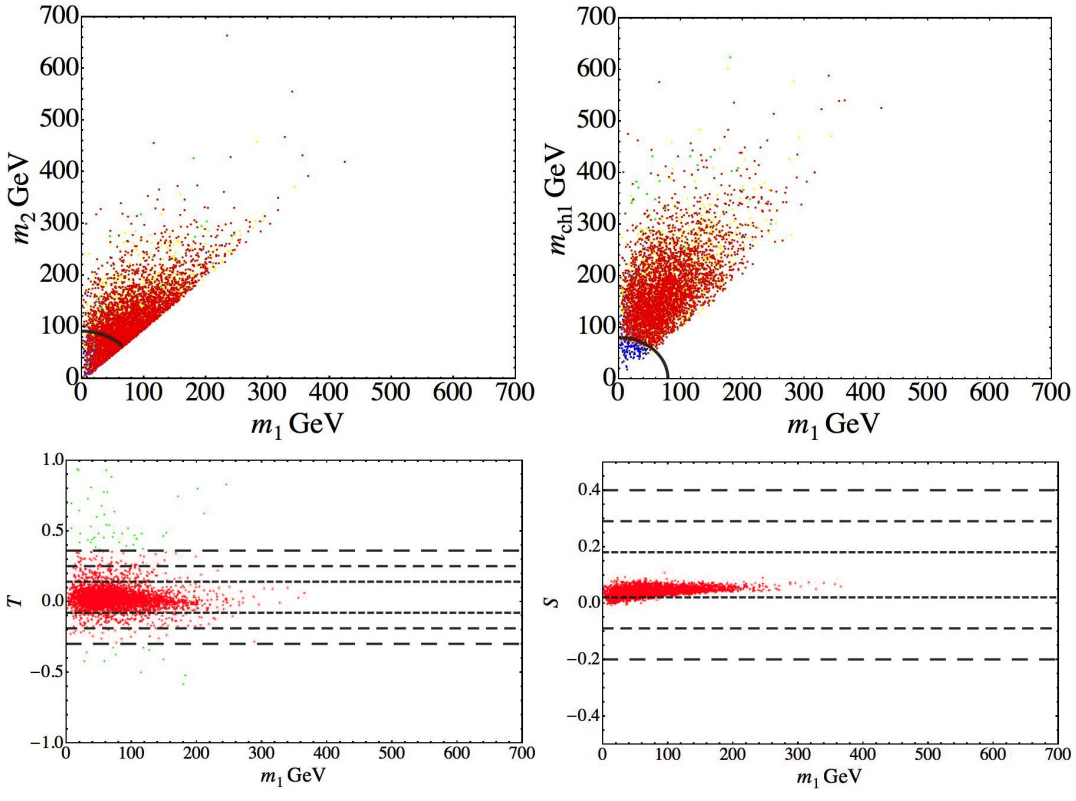

Figure 5.5: *The complex alignment* $(ve^{i\omega_1}, v, 0)$*: as in the previous figure the upper panels show* m_1 *versus* m_2 *and* m_{ch_1} *respectively. In the plot on the right, the effect of the* W *decay constraint on* $m_1^2 + m_{ch_1}^2$ *is clear by looking at the B points. The lower panels show the contributions to* T *and* S*. Again, the* T *parameter turns out to be the most constraining one.*

points R in the upper panel of figure 5.6. In the $m_1 - m_{ch_1}$ plot (obviously, the absence of a second neutral state prohibits a $(m_1 - m_2)$–plot), we see that with respect to the minima so far analyzed there are much fewer points and that as expected there are cuts in correspondence to m_Z and m_W.

In conclusion, the solutions for the alignment $(ve^{i\omega_1}, ve^{-i\omega_1}, rv)$ with $\lambda_5 = 0$, $\lambda_4 = -\lambda_3$ are not easy to find, but the Higgs phenomenology does not completely rule out this vacuum configuration. We could introduce a weight to estimate the degree to which a solution is stable or fine-tuned, but this goes beyond the purposes of this work. We note however that this situation with four extra massless particles should be very problematic when considering the model dependent constraints. Indeed the two models with this vacuum studied in section 5.10 are of the second type, where there are no extra Goldstone bosons, although light states might be problematic.

5.9.6 $(ve^{i\omega_1}, ve^{-i\omega_1}, rv)$ case $ii)$

In section 5.6.8 we showed that at least in the three special limits $r \sim 0$, $r \sim 1$ and $r >> 1$, there are one or two very light particles.

It turns out that finding actual minima (i.e. solutions of equation (5.8) that are not saddle points) is very hard. Scanning over 100.000 points in parameter space with variable r, we only found a handful of minima (yellow or otherwise coloured points). This is sketched in figure 5.7. The other relevant information in this diagram is that for any value of r the two lightest states are always very light, thus confirming our rough analytical approximations. Indeed both m_1 and m_2 are lighter then expected. This holds in particular for m_2 in case $r \sim 0$, where equation (5.41) just predicts one very light state. This indicates that some cancelations have to occur in order to make all masses greater than 0. This

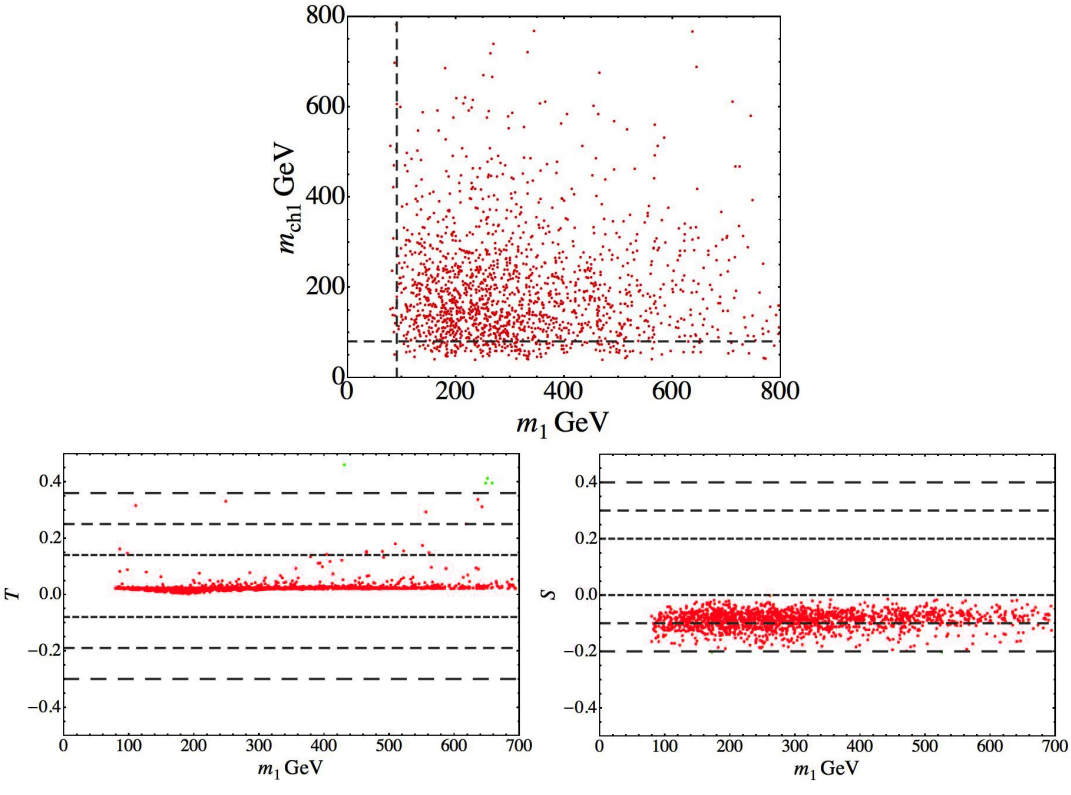

Figure 5.6: *Case i) of the alignment $(ve^{i\omega_1}, ve^{-i\omega_1}, rv)$ case i): the upper panel show m_1 versus m_{ch_1}. Only the R points are reported. The lower panels show the contributions to T and S for the G points. For this specific case the oblique parameter constraint is irrelevant compared to the decay one.*

might explain the difficulty to find solutions; this cannot to be ascribed to any constraint imposed, because even in presence of 4 additional Goldstone bosons as in section 5.9.5 there is a significant larger number of solutions.

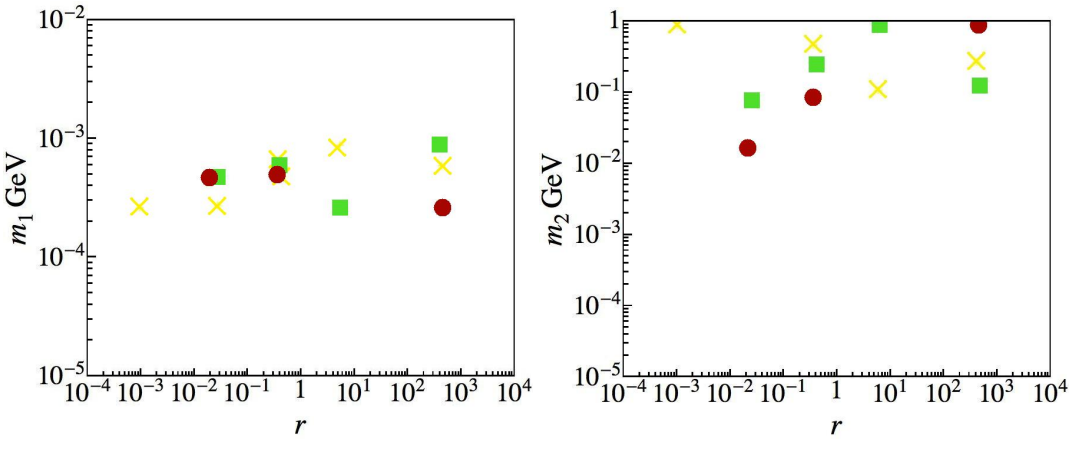

Figure 5.7: *Case ii) of the alignment $(ve^{i\omega_1}, ve^{-i\omega_1}, rv)$, the panels show m_1 (on the left) and m_2 (on the right) versus r. The number of points is small, but the most interesting information is the order of magnitude of the masses.*

It is possible to add soft A_4 breaking terms as given in equation (5.5) to the potential. All five neutral and all four charged Higgses can be in the LHC sensitive range between 100 GeV and 1 TeV if the

dimensionless parameters m, n, k are approximately 0.05, corresponding to effective parameters of a few GeV after multiplying $n_{\text{soft,eff}} = \sqrt{m^2 + n^2 + k^2}$ by v_{ew}. It is interesting to underline that such large Higgs masses have been recovered by using soft terms at most of order of 5% of the EW vev. This underlines a non-linear dependence, as can be seen in figure 5.8. In this figure r is fixed to the large value of 240, in accordance with model 2 of the next section.

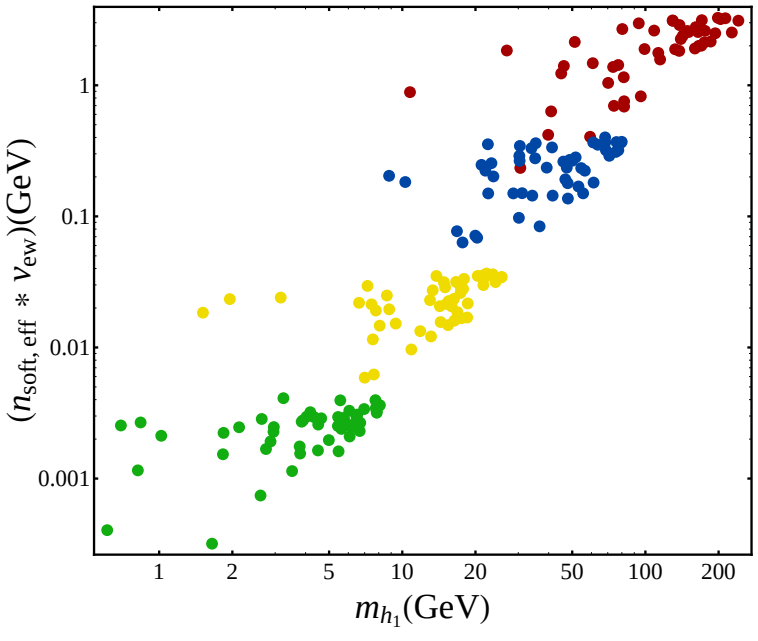

Figure 5.8: *Correlation among the lightest Higgs mass and the soft breaking parameter. The different colours correspond to the ranges that the individual parameters m, n and k are in, respectively $(0 - 10^{-4})$, $(0 - 10^{-3})$, $(0 - 10^{-2})$ and $(0 - 10^{-1})$*

5.10 Four models of flavour symmetries at the electroweak scale

In this section we describe four concrete models that contain a triplet of Higgses. In these models the A_4 representations of not only the Higgs sector are chosen, but also of the various Standard Model fermions. The model of Ma and Rajasekaran [97] (model 1) and the model of Morisi and Peinado [128] (model 2) focus on the lepton sector. The model of Lavoura and Kühböck [148] (model 3) describes the quark sector. In 'quark mixing in the discrete dark matter model' (model 4), we consider both sectors, but specifically focus on quarks.

Models 1 and 4 are non-minimal in the definition of section 5.3; models 2 and 3 are minimal. These two models use exactly the minimum we found to be the most problematic in the previous section. When analyzing the phenomenology in section 5.12 therefore, we allow for the presence of soft A_4 breaking terms.

5.10.1 Model 1

Model 1 [97] is an extension of a simpler model by one of the authors [149] that generates neutrino masses via a TeV-scale seesaw of type-I. In both models several Higgs fields occur, one of which carries lepton number. In [97] the choice is made to make the Higgs $SU(2)$-doublet that does not carry lepton number a triplet of A_4. The most general potential for this triplet of Higgses 5.4 is written down for the first time there. The triplet Φ_a couples only to charged leptons and the chosen

vacuum alignment falls in the class (v, v, v), with v real. In the original work, the constraint that the ϵ phase of the potential should be zero is assumed to make this alignment possible, but as shown in section 5.6.2 this is in fact not necessary.

All the time there is also a fourth Higgs doublet. This is a singlet η of A_4 and, as mentioned above, it carries a single unit of lepton number. The appearance of a singlet next to the triplet makes this model clearly a non-minimal one. Two new terms are added to the scalar potential (5.4)

$$\begin{aligned} V_\eta &= \mu_\eta^2(\eta^\dagger\eta) + \lambda_\eta(\eta^\dagger\eta)^2 + \lambda_{\eta\Phi}(\eta^\dagger\eta)(\phi_1^\dagger\phi_1 + \phi_2^\dagger\phi_2 + \phi_3^\dagger\phi_3) \\ V_{\eta\,soft} &= \mu_{\eta\Phi}^2\left[\eta^\dagger(\phi_1+\phi_2+\phi_3) + (\phi_1^\dagger+\phi_2^\dagger+\phi_3^\dagger)\eta\right], \end{aligned} \tag{5.79}$$

where the A_4 soft breaking part $V_{\eta\,soft}$ is needed in order to avoid additional GBs. $V_{\eta\,soft}$ breaks A_4 as well as lepton number, but preserves its Z_3 subgroup thus the full potential may naturally realize the vacuum configuration

$$\langle\Phi\rangle \sim (v, v, v), \qquad \langle\eta\rangle \sim v_\eta \propto \mu_{\eta\Phi}^2 v. \tag{5.80}$$

The vacuum expectation value of the field η is much smaller than that of Φ. This relates to the relative smallness of $\mu_{\eta\Phi}^2$ that is natural in the sense that if it goes to zero the model's symmetry is increased because lepton number is unbroken. This makes v_η very fit to generate the (small) neutrino masses.

The fermion content of the model is much like the (later constructed) Altarelli–Feruglio model of section 2.4: the lepton doublet is a triplet of A_4 and the righthanded charged fermions are singlets of respectively type 1, $1'$ and $1''$. A righthanded neutrino is present as A_4-triplet – which is indeed also Altarelli and Feruglio's choice in the seesaw version of their model. It is interesting to note that this righthanded neutrino has zero lepton number. The complete fermion and Higgs content of the model is given in table 5.1.

Field	L_L	e_R	μ_R	τ_R	ν_R	Φ	η
A_4	3	1	$1'$	$1''$	3	3	1
lepton number	1	1	1	1	0	0	-1

Table 5.1: The lepton and Higgs content of model 1.

Lepton number constrains the triplet Φ to couple only to charged leptons and the singlet η to participate only in the neutrino Dirac terms:

$$\mathcal{L} = \frac{1}{2}M\nu_{Ri}^2 + f\bar{\nu}_{Ri}L_{Li}\eta + Y_{ijk}\bar{L}_{Li}l_{Rj}\Phi_k + \text{h.c.} \tag{5.81}$$

In this formula, l_R is general notation for the three righthanded charged leptons. The Yukawa matrices in the charged lepton sector are

$$Y_{ij1} = \begin{pmatrix} y_1 & y_2 & y_3 \\ 0 & 0 & 0 \\ 0 & 0 & 0 \end{pmatrix}, \quad Y_{ij2} = \begin{pmatrix} 0 & 0 & 0 \\ y_1 & \omega y_2 & \omega^2 y_3 \\ 0 & 0 & 0 \end{pmatrix}, \quad Y_{ij3} = \begin{pmatrix} 0 & 0 & 0 \\ 0 & 0 & 0 \\ y_1 & \omega^2 y_2 & \omega y_3 \end{pmatrix} \tag{5.82}$$

After the diagonalization of the charged lepton mass matrix, it is straightforward to relate the coefficient y_i to the mass eigenvalues:

$$y_1 = \frac{m_e}{\sqrt{3}v}, \quad y_2 = \frac{m_\mu}{\sqrt{3}v}, \quad y_3 = \frac{m_\tau}{\sqrt{3}v}. \tag{5.83}$$

Since the vevs of the scalar potential are real, the U matrix that rotates the Higgs fields into the mass basis (2.54) is block diagonal. Neutrino masses are given through the type I See-Saw and have magnitude f^2u^2/M. Due to the smallness of v_η, the righthanded neutrino masses can be at a (relatively) low scale around a TeV. Maximal mixing in the $(\mu\ \tau)$ sector is obtained and depending on soft A_4 breaking terms for the righthanded neutrinos, specific mixing patterns like the bimaximal or the tribimaximal are possible.

5.10.2 Model 2

The second model we discuss is the one by Morisi and Peinado [128]. Like model 1, this model focuses on the lepton sector, but four important choices are different with respect to the work of Ma and Rajasekaran. The first is that this model does not employ an A_4-singlet Higgs; all the Higgs fields present are in the triplet Φ.

The second difference is in the vacuum of the Φ field. This is a permutation of the complex vacuum introduced in section 5.6.8 – in particular of case $ii)$ of that section, as the potential parameters are not constrained.

$$\langle \Phi \rangle = \frac{v_{ew}}{\sqrt{2+r^2}} \left(r, \quad e^{i\omega_1}, \quad e^{-i\omega_1} \right) . \tag{5.84}$$

As shown below, r needs to be very large in order to incorporate the charged lepton masses: $r \simeq 240$. This case was studied in detail in sections 5.6.8 and 5.9.6, where it was concluded that in order for this minimum to be viable, the potential needs a contribution from soft breaking terms. When we study the fermion-dependent processes in section 5.12, we indeed assume these terms to be present.

Thirdly, models 1 and 2 differ in the choice of fermion representations. In model 2, the choice is made to put all relevant fields in the triplet representation of A_4. Table 5.2 that shows the content of the model is therefore very simple

Field	L_L	l_R	Φ
A_4	3	3	3

Table 5.2: The lepton and Higgs content of model 2.

The Yukawa Lagrangian for the charged leptons is also very simple. It contains the two possible ways to contract three A_4 triplets to a singlet.

$$\mathcal{L} = y_1 \Big(\bar{L}_{L1} \Phi_3 l_{R2} + \bar{L}_{L2} \Phi_1 l_{R3} + \bar{L}_{L3} \Phi_2 l_{R1} \Big) + y_2 \Big(\bar{L}_{L1} \Phi_2 l_{R3} + \bar{L}_{L2} \Phi_3 l_{R1} + \bar{L}_{L3} \Phi_1 l_{R2} \Big) . \tag{5.85}$$

When the three Higgs fields obtain their vevs as in equation 5.84, this results in a charged lepton mass matrix without diagonal components:

$$M_l = \begin{pmatrix} 0 & a & b \\ b & 0 & ar \\ a & br & 0 \end{pmatrix} . \tag{5.86}$$

Here $a = y_1 v_{ew}/\sqrt{2+r^2} = 0.43$ MeV; $b = y_2 v_{ew}/\sqrt{2+r^2} = 7.3$ MeV and, as mentioned before, $r = 242$. The mass matrix is real because all phases can be absorbed in the fields.

The fourth and last important difference between model 1 and 2 is that in the latter neutrino masses originate from effective dimension-5 operators. To a good approximation the neutrino mass matrix is

$$M_\nu = \begin{pmatrix} x r^2 & \kappa r e^{-i\omega_1} & \kappa r e^{i\omega_1} \\ \kappa r e^{-i\omega_1} & z r^2 & \kappa \\ \kappa r e^{i\omega_1} & \kappa & y r^2 \end{pmatrix} . \tag{5.87}$$

In this matrix x, y, z and κ are linear combinations of the parameters that occur in the effective Lagrangian. In the limit where $\omega_1 \to 0$ and $y \to z$, the neutrino mass matrix is $(\mu\ \tau)$-invariant, implying maximal atmospheric and zero reactor mixing angle. The solar mixing angle, however, is undetermined.

5.10.3 Model 3

In model 3, constructed by Lavoura and Kühböck [127], the quark sector is central. The minimum configuration of the Higgs fields is, up to permutations, the same as in model 2 (with model 3 having the priority), although the value of r used is smaller, $r \simeq 43$, bringing the model less deep into the $r \gg 1$ limit. The presence of soft A_4-breaking terms is thus also mandatory for this model. Figure 5.8 that shows the behaviour of the lightest Higgs as a function of the soft breaking terms, was constructed for the parameters of model 2; for those of model 3, it looks very similar.

The fermion representation chosen are the triplet for the lefthanded doublets and three different singlets 1, $1'$ and $1''$ for both types of righthanded quarks; see also table 5.3.

Field	Q_L	u_R	c_R	t_R	d_R	s_R	b_R	Φ
A_4	3	1	$1'$	$1''$	1	$1'$	$1''$	3

Table 5.3: The lepton and Higgs content of model 3.

This fermion assignment is much like that of model 1, with quarks replacing charged leptons and indeed the Yukawa Lagrangian and matrices have the same structure. The relevant Lagrangian reads

$$\mathcal{L} = Y^d_{ijk}\bar{Q}_{Li}d_{Rj}\Phi_k + Y^u_{ijk}\bar{Q}_{Li}u_{Rj}\tilde{\Phi}_k + \text{h.c.} \tag{5.88}$$

Here $\tilde{\Phi} = i\sigma_2\Phi^*$ to provide up-type Higgs bosons. This Lagrangian corresponds to the mass matrices for the down quarks (cf. equation (5.82))

$$M^d = \begin{pmatrix} y_1 & y_2 & y_3 \\ 0 & 0 & 0 \\ 0 & 0 & 0 \end{pmatrix} \frac{v_{ew}}{\sqrt{2+r^2}} e^{i\omega_1} + \begin{pmatrix} 0 & 0 & 0 \\ y_1 & \omega y_2 & \omega^2 y_3 \\ 0 & 0 & 0 \end{pmatrix} \frac{v_{ew}}{\sqrt{2+r^2}} e^{-i\omega_1} + \begin{pmatrix} 0 & 0 & 0 \\ 0 & 0 & 0 \\ y_1 & \omega^2 y_2 & \omega y_3 \end{pmatrix} \frac{r v_{ew}}{\sqrt{2+r^2}} . \tag{5.89}$$

The up Yukawa matrices have the same structure, but with y_4, y_5 and y_6 as parameters and the phases reversed (due to the complex conjugation in equation (5.88). The eight parameters of the model $y_1 - y_6$, r and ω_1 can now be fit against nine observables in the quark sector (the six quark masses and the three CKM angles). This fit has a minimum corresponding to $\chi^2 = 0.057$ and parameters given by

$$\begin{array}{rclrclrcl} y_1 &=& 0.010, & y_2 &=& 0.022, & y_3 &=& 0.00058, \\ y_4 &=& 0.97, & y_5 &=& 0.127, & y_6 &=& 0.00026, \\ r &=& 43, & \omega_1 &=& 0.23 \text{ rad.} & & & \end{array} \tag{5.90}$$

All three angles of the CKM matrix are fit very well by the parameters given above, but the phase is not. The CKM matrix that is the result of the construction of model 3 is completely real, providing no source of CP violation.

5.10.4 Model 4 - Quark mixing in the discrete dark matter model

In model 4 we present an extension of a number of studies [150–152] in which the concept of discrete dark matter (DDM) is developed. In these works, the focus is on the scalar sector, but also charged leptons are discussed, although quarks are not. In our work, we add quarks to the set up and allow for quark mixing in a way that is much like the one described in chapter 4.

At a number of places in this thesis we have seen the connection between symmetries and the presence of a dark matter candidate in a theory. Examples were the axion of section 1.3.1 and the 'lightest supersymmetric particle' (LSP) of section 1.3.2. The key to the relation between symmetry and dark matter is that a symmetry can prevent the decay of a particle, thus making it stable and letting it exist in the cosmos. It is a very natural question to ask whether flavour symmetries can

provide a dark matter candidate. Note that this question is less relevant in models where flavour symmetries are combined with supersymmetry or extra dimensions, as those on themselves already provide a dark matter candidate. In the models of this section on the other hand, where flavour symmetry is the only relevant symmetry beyond the Standard Model, the question becomes more interesting.

The naive answer to the question of the previous paragraph is 'no'. Flavour symmetries cannot provide a dark matter candidate, because flavour symmetries are always broken when flavons (or Higgs fields in non-trivial representations of the flavour group) develop vacuum expectation values. In some cases, however, there is a residual symmetry after a flavour symmetry is broken. In this chapter we have seen that there is a residual symmetry Z_3 when the three Higgses have their vevs as (v, v, v) and Z_2 when the vev alignment is $(v, 0, 0)$. Those residual symmetries can well be the symmetries that make a dark matter candidate stable.

In [150] the vacuum $(v, 0, 0)$ is selected, while also a A_4-singlet Higgs is present. The inert fields Φ_2 and Φ_3 give rise to four neutral Higgs bosons: two scalars h_2 and h_3 and two pseudo scalars A_2 and A_3. The lightest of these cannot decay and is a dark matter candidate. Note that even if the dark matter candidate cannot decay, a pair of two candidates can annihilate. In [152] it is shown that the correct relic abundance can still be obtained for a dark matter mass M_{DM} in the large range 1 - 100 GeV. In our set up, additional annihilation channels to quarks are added and the relic density is a crucial test of the viability of the extension as discussed in section 5.12.

The matter content of the model is given in table 5.4. We see that in this model all charged fermion fields, both left- and righthanded are in the various singlet representations of A_4. Note that all these A_4 singlets transform under the Z_3 subgroup of A_4, but not under the Z_2 subgroup, making them even under the residual symmetry. There are four righthanded neutrinos originating from a A_4 triplet and a singlet. The second and third component of the neutrino triplet are odd under the residual Z_2 just like the corresponding components of the Higgs triplet.

Field	Φ	η	Q_{L_1}	Q_{L_2}	Q_{L_3}	q_{R_1}	q_{R_2}	q_{R_3}
A_4	3	1	1	$1'$	$1''$	1	$1'$	$1''$
Field	L_{L_e}	L_{L_μ}	L_{L_τ}	l_{R_e}	l_{R_μ}	l_{R_τ}	ν_{R_T}	ν_{R_4}
A_4	1	$1'$	$1''$	1	$1'$	$1''$	3	1

Table 5.4: *The A_4 representations of the fields in model 4; $q = u, d$.*

The resulting Yukawa Lagrangian for the quarks reads

$$\begin{aligned}\mathcal{L}_{\rm q} = &y_u\overline{Q}_1\tilde{\eta}u_{1R} + y_c\overline{Q}_2\tilde{\eta}u_{2R} + y_t\overline{Q}_3\tilde{\eta}u_{3R}+\\ &y_d\overline{Q}_1\eta d_{1R} + y_s\overline{Q}_2\eta d_{2R} + y_b\overline{Q}_3\eta d_{3R} + \text{h.c.},\end{aligned} \tag{5.91}$$

Here the up-type Higgs $\tilde{\eta}$ is defined analogously to $\tilde{\Phi}$ as given below equation (5.88).

At the renormalisable level, both up- and down-quark matrices are diagonal with all masses given by $m_i = y_i v_\eta/\sqrt{2}$, with $v_\eta/\sqrt{2}$ the vacuum expectation value of the A_4-singlet Higgs field. Obviously, at this level, the CKM matrix is the identity matrix.

For the leptons, the Lagrangian is the same as in [150]

$$\begin{aligned}\mathcal{L}_{\rm l} = &y_e\overline{L}_e l_{Re}\eta + y_\mu\overline{L}_\mu l^c_{R\mu}\eta + y_\tau\overline{L}_\tau l^c_{R\tau}\eta+\\ &y_1^\nu\overline{L}_e(\nu_{R_T}\tilde{\Phi})_1 + y_2^\nu\overline{L}_\mu(\nu_{R_T}\tilde{\Phi})_{1'} + y_3^\nu\overline{L}_\tau(\nu_{R_T}\tilde{\Phi})_{1''}+\\ &y_4^\nu\overline{L}_e\nu_{R_4}\eta + M_1N_TN_T + M_2N_4N_4 + \text{h.c.}\end{aligned} \tag{5.92}$$

This leads to charged lepton masses similar to the quark masses and a light neutrino mass matrix of

the form

$$M_\nu = \frac{v_\Phi^2}{2M_1}\begin{pmatrix} (y_1^\nu)^2 + (y_4^\nu)^2\frac{M_1}{M_2}\frac{v_\eta}{v_\Phi} & y_1^\nu\, y_2^\nu & y_1^\nu\, y_3^\nu \\ y_1^\nu\, y_2^\nu & (y_2^\nu)^2 & y_2^\nu\, y_3^\nu \\ y_1^\nu\, y_3^\nu & y_2^\nu\, y_3^\nu & (y_3^\nu)^2 \end{pmatrix} . \tag{5.93}$$

The neutrino mass matrix has one zero eigenvalue, so a prediction of the model is one massless neutrino. The (1 3) mixing angle is zero at the renormalizable level. The other two angles are not determined and a simple tuning can reproduce the tribimaximal mixing pattern.

Quark mixing (and additional lepton mixing) can be generated by dimension six operators that contain extra insertions of the Higgs fields. There are three ways to contract the $SU(2)$ indices, represented by brackets in the equation below

$$\frac{f_{ij}}{\Lambda^2}(\overline{Q}_i\hat{H})d_j(\eta^\dagger\eta) + \frac{f'_{ij}}{\Lambda^2}(\overline{Q}_i\eta)d_j(\eta^\dagger\hat{H}) + \frac{f''_{ij}}{\Lambda^2}(\overline{Q}_i\eta)d_j(\hat{H}^\dagger\eta)\,. \tag{5.94}$$

The contraction of A_4 indices between the two $\eta^{(\dagger)}$ triplets is such that it generates the right type of singlet (1, 1′ or 1″) to match the charges for $\overline{Q}_i$ and d_j. It is important to note that this is possible for any combination of i and j due to the product rules of A_4, giving non-zero entries at all elements of the mass matrix. Λ is the cut-off scale, up to which we accept the theory to be valid and the f couplings are dimensionless. Analogous dimension-6 operators can obviously be constructed for up-type quarks and charged leptons.

The mass term Lagrangian (5.91) and the effective couplings (5.94) generate the effective mass matrix for down-type quarks

$$M_d = \begin{pmatrix} m_d & 0 & 0 \\ 0 & m_s & 0 \\ 0 & 0 & m_b \end{pmatrix} + \frac{v_H v_\eta^2}{\Lambda^2}\begin{pmatrix} h_{dd} & h_{ds} & h_{db} \\ h_{sd} & h_{ss} & h_{sb} \\ h_{bd} & h_{bs} & h_{bb} \end{pmatrix} + \mathcal{O}(\frac{1}{\Lambda^4})\,, \tag{5.95}$$

where $h_{ij} = (f_{ij} + f'_{ij} + f''_{ij})/2\sqrt{2}$. Analogous expressions again hold for up-type quarks and charged leptons.

The crucial question is how large the cut-off scale Λ is. In principle, this is a scale we are free to set. Only using 'naturalness' and 'finetuning' arguments, we can find a range for it. We give two arguments, both pointing to a scale of 1 to 10 TeV.

In the first argument, we demand that there should not be more than 10 to 100% corrections to the Higgs from one-loop corrections to the Higgs propagator with the fermions and the (new) scalars of the theory. These corrections are typically of the order $\Lambda^2/(4\pi)^2$ and requiring them to be not too large with respect to $v_{ew}^2 = (246\text{GeV})^2$ indeed gives $\Lambda \lesssim (1 \text{ to } 10)$ TeV.

Interestingly, we find the same scale from an argument where we require the dimensionless parameters h, in particular h_{ds}, to be of order 1. The off-diagonal terms in equation (5.95) are responsible for generating the quark mixing as parameterized by the CKM matrix. As we do not have information about the size of the dimensionless parameters h, we assume them to be of order 1, which can be seen as the most natural assumption for dimensionless parameters.

Under this assumption, the absolute values of the corrections to the leading order elements of the mass matrix are of the same order for the up-type quark matrix and the down-type quark matrix. However, due to the much larger elements of the leading order up-type quark mass matrix, the effects on quark mixing are dominated by the down-type quark contributions. This allows us to estimate the order of magnitude of the cut-off scale.

Now the (1 2) element of equation (5.95) should be of order $\lambda_C\, m_s$ in order to reproduce the Cabibbo angle.

$$h_{ds}\frac{v_H v_\eta^2}{\Lambda^2} = \lambda_C m_s. \tag{5.96}$$

We define a parameter $\tan\tilde{\beta}$ as the ratio between the vev of η and Φ in the same spirit as in 'normal' models where two Higgs doublet acquire a vev. With this definition, we can solve the previous equation for Λ^2

$$\Lambda^2 = h_{ds}\frac{v_H v_\eta^2}{\lambda_C m_s} = h_{bd}\frac{v_{ew}^3}{(\tan^2\tilde{\beta})(1+\frac{1}{\tan^2\tilde{\beta}})^{3/2}\lambda_C m_s} = [(1 \text{ to } 10)\text{ TeV}]^2. \tag{5.97}$$

The exact value depends on the exact values of h_{ds} and $\tan\tilde{\beta}$; to obtain the range, we have taken them between 0.1 and 1 and between 0.1 and 10 respectively. The mass of the bottom quark is rather large and therefore the effect of h_{db} and h_{sb} θ_{13} and θ_{23} is relatively minor even if these parameters are of the same size as h_{ds}. This naturally keeps these angles smaller than the Cabibbo angle. Indeed in a large part of parameter space, we can fit them to their measured values.

The analogue of the dimension 6 operator (5.94) affects the lepton mixing. The fact that the down-type quark and charged lepton mass matrices are alike (at least at leading order) suggests that the matrices that diagonalize them, V_L^d and V_L^e are also similar. We thus expect a large angle (of the order of the Cabibbo angle) in the (1 2) sector of V_L^e. In the lepton mixing matrix $V_{\rm PMNS} = (V_L^e)^\dagger V_L^\nu$, this affects all three angles. In particular, we predict a Cabibbo-sized correction to the θ_{13}-angle, bringing it in the range of the current fits given in table 2.4.

The cut-off scale Λ may coincide with the scale M_1 that appears in the neutrino mass matrix (5.93). In that case, the seesaw mechanism indeed takes place at a low energy scale, 1 TeV, as compared to 10^{12} GeV as in chapter 4. In this case, the parameters y_i^ν should not be too small, $y_\nu = 10^{-(4\div 5)}$.

5.11 Description of model dependent tests of flavour symmetries at the electroweak scale

The interaction of fermions with the Higgs particles induces flavour violating processes in the lepton and quark sectors. In the first one, rare decays of muon and tau particles into three leptons are allowed at tree-level, while processes as $l_i \to l_j\gamma$ take place through one-loop graphs. For the quarks the possibility of $\Delta F = 2$ meson-antimeson oscillations is considered.

In this section we study these processes and obtain formulas that give the contribution of the new physics processes. We rely heavily on the equations obtained in section 2.2.5 where we have described the interactions of different fermions with multiple Higgs bosons. The formulas derived in this section are used in the next one, where we discuss to what degree they constrain the four models of the previous section.

5.11.1 The Processes $\mu^- \to e^-e^-e^+$ and $\tau^- \to \mu^-\mu^-e^+$

We consider the decay of a muon into a positron and two electrons as given in figure 5.9 on the left. In the approximation of massless final states, the decay amplitude is written as

$$\Gamma(\mu \to ee\overline{e}) = \frac{m_\mu^5}{(4\pi)^3\times 24} I_{\mu eee}\,. \tag{5.98}$$

The coefficient $I_{\mu eee}$ is a combination of I_{ij} and J_{ij}, that were defined in section 2.2.5.

$$I_{\mu eee} = \left|\sum_\alpha \frac{I_{\mu e}^\alpha I_{ee}^\alpha}{m_H^{\alpha\,2}}\right|^2 + \left|\sum_\alpha \frac{J_{\mu e}^\alpha J_{ee}^\alpha}{m_H^{\alpha\,2}}\right|^2 + \left|\sum_\alpha \frac{I_{\mu e}^\alpha J_{ee}^\alpha}{m_H^{\alpha\,2}}\right|^2 + \left|\sum_\alpha \frac{J_{\mu e}^\alpha I_{ee}^\alpha}{m_H^{\alpha\,2}}\right|^2. \tag{5.99}$$

The prediction for the corresponding branching ratio is

$$\text{Br}(\mu \to ee\overline{e}) \approx \frac{\Gamma(\mu \to ee\overline{e})}{\Gamma(\mu \to e\overline{\nu}_e\nu_\mu)} = \frac{I_{\mu eee}}{8G_F^2}\,. \tag{5.100}$$

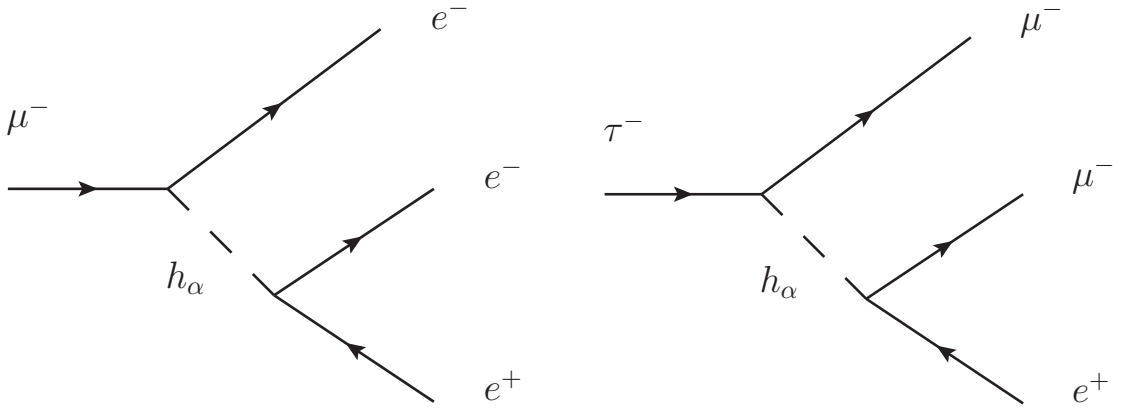

Figure 5.9: *The decays $\mu^- \to e^+e^-e^-$ (left) and $\tau^- \to e^+\mu^-\mu^-$ (right) can occur at tree level in our models.*

This is to be compared with the experimental limit [6] of $\text{Br}(\mu \to ee\overline{e})_{exp} \leq 1.0 \times 10^{-12}$.

The decay of a τ into two muons and a positron (figure 5.9 on the right) is generally less constrained that the decay of the muon in two electrons and a positron, but it is of interest in models where the latter process is prohibited by the symmetries. The calculation proceeds in an analogous way. The decay amplitude is now

$$\Gamma(\tau \to \overline{e}\mu\mu) = \frac{m_\tau^5}{(4\pi)^3 \times 24} I_{\tau\mu\mu e} \ . \tag{5.101}$$

The coefficient $I_{\tau\mu\mu e}$ is now given by the following expression:

$$I_{\tau\mu\mu e} = \left| \sum_\alpha \frac{I^\alpha_{\tau\mu} I^\alpha_{e\mu}}{{m^\alpha_H}^2} \right|^2 + \left| \sum_\alpha \frac{J^\alpha_{\tau\mu} J^\alpha_{e\mu}}{{m^\alpha_H}^2} \right|^2 + \left| \sum_\alpha \frac{I^\alpha_{\tau\mu} J^\alpha_{e\mu}}{{m^\alpha_H}^2} \right|^2 + \left| \sum_\alpha \frac{J^\alpha_{\tau\mu} I^\alpha_{e\mu}}{{m^\alpha_H}^2} \right|^2 . \tag{5.102}$$

The branching ratio becomes

$$\text{Br}(\tau \to \overline{e}\mu\mu) = 0.17 \times \frac{\Gamma(\tau \to \overline{e}\mu\mu)}{\Gamma(\tau \to \mu\overline{\nu}_\mu\nu_\tau)} = 0.17 \times \frac{I_{\tau\mu\mu e}}{8G_F^2}, \tag{5.103}$$

This branching ratio should be compared with the experimental limit [6] $\text{Br}(\tau \to \overline{e}\mu\mu)_{exp} \leq 2.3 \times 10^{-8}$.

5.11.2 The process $\mu^- \to e^-\gamma$

The relevant diagram for the decay of the muon to an electron and a photon has one loop with a charged fermion and a neutral Higgs (see figure 5.10). We consider the limit in which the Higgs is much heavier than the virtual fermion and the final electron is massless. Under this assumption the decay amplitude becomes [153]

$$\Gamma(\mu \to e\gamma) = \frac{e^2 m_\mu^5}{6 \times (16)^3 \pi^5} \left| \sum_{\alpha,f} \frac{(R^\alpha_{fe})^* R^\alpha_{f\mu}}{{m^\alpha_H}^2} \right|^2 \tag{5.104}$$

This uses the coupling tensor R defined in section 2.2.5. The branching ratio is

$$\text{Br}(\mu \to e\gamma) = \frac{\Gamma(\mu \to e\gamma)}{\Gamma(\mu \to e\nu\overline{\nu})} = \frac{\alpha_{em}}{32\pi G_F^2} \left| \sum_{\alpha,f} \frac{(R^\alpha_{fe})^* R^\alpha_{f\mu}}{{m^\alpha_H}^2} \right|^2 \tag{5.105}$$

This should be compared with the current experimental bound from MEGA [154] of 10^{-11} and the future experimental bound from MEG [155] of (10^{-13}).

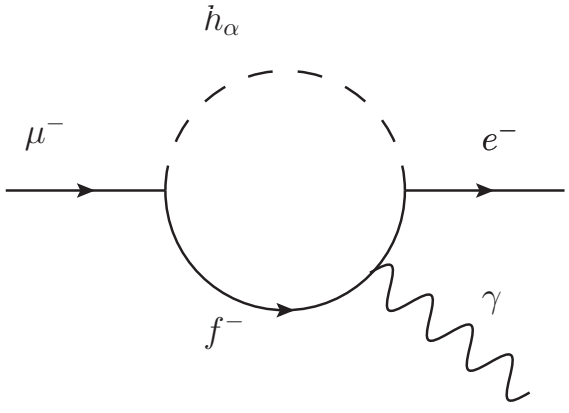

Figure 5.10: *The decays $\mu^- \to e^-\gamma$ proceeds at one loop in our models, but can be much larger than in the Standard Model, where a GIM-like cancellation occurs.*

5.11.3 Meson oscillations

Meson-antimeson oscillations are constrained to be generated by box processes in the SM (figure 5.11 on the left), but in the presence of flavour violating Higgs couplings, they can also proceed via tree-level Higgs exchange. Note that there is a large difference with the lepton processes. Those practically have zero background from the Standard Model and experimentally there are only upper bounds. Meson oscillations have been measured and fit fairly well to the Standard Model calculations. It is preferred that the new physics contributions are much smaller than the Standard Model, although in principle they can be of comparable magnitude if there is cancellation at the amplitude level.

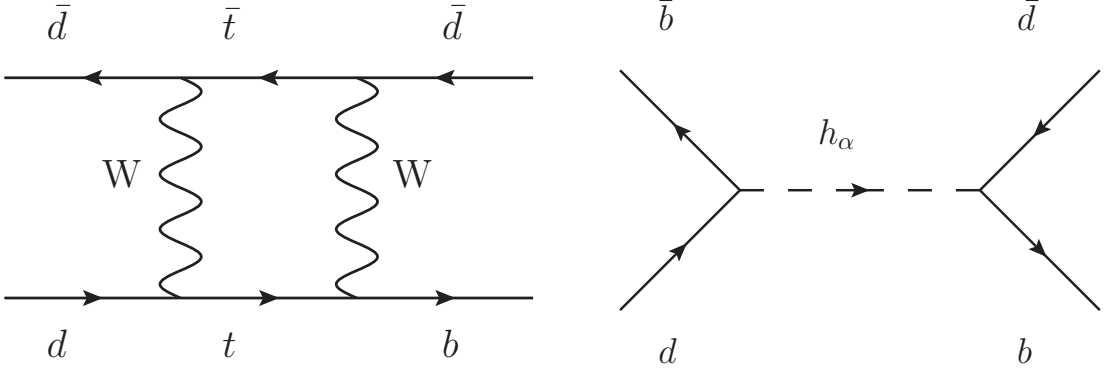

Figure 5.11: *B_d-$\overline{B}_d$ oscillations take place via box diagrams in the Standard Model, but can proceed via tree-level Higgs exchange in multi-Higgs models.*

For the mass splitting connected to $F^0 - \overline{F}^0$ oscillations [156, 157], we find

$$\Delta M_F = B_F^2\, f_F^2\, M_F \sum_\alpha \left[\frac{1}{{m_H^\alpha}^2}\Big(|I_{rs}^\alpha|^2\Big(\frac{1}{6}+\frac{1}{6}\frac{M_F^2}{(m_r+m_s)^2}\Big)+|J_{rs}^\alpha|^2\Big(\frac{1}{6}+\frac{11}{6}\frac{M_F^2}{(m_r+m_s)^2}\Big)\Big)\right]. \quad (5.106)$$

Here, M_F is the mass of the meson, f_F is its decay constant and B_F are recalibration constants of order 1, related to vacuum insertion formalism. Lastly, m_r and m_s are the masses of the quarks of which the meson is build, i.e. $rs = bd, bs, ds$ stands for B_d, B_s and K^0 respectively. Recent experimental values for the meson parameters, including ΔM_F that should be reproduced by the model, are given in table 5.11.3

Meson	M_F (GeV)	f_F (GeV)	B_F	ΔM_F (GeV)
B_d ($\bar{b}d$)	5.2795	0.1928 ± 0.0099	1.26 ± 0.11	$(3.337 \pm 0.006) \times 10^{-13}$
B_s ($\bar{b}s$)	5.3664	0.2388 ± 0.0095	1.33 ± 0.06	$(1.170 \pm 0.008) \times 10^{-11}$
K ($\bar{s}d$)	0.497614	0.1558 ± 0.0017	0.725 ± 0.026	$(3.500 \pm 0.006) \times 10^{-15}$
D ($\bar{u}c$)	1.8648	0.165	0.82	$(0.95 \pm 0.37) \times 10^{-14}$

Table 5.5: *Properties of neutral mesons (from [158] for B_d, B_s and K and from [157] for D).*

We stress that the tests developed in this section do not constitute a complete list. Many other other processes can be thought of. The ones considered in this section already prove to be very constraining as shown in the next section when we apply them to the models described in the previous section.

5.12 Results of the model dependent tests

The tests developed in the previous section can be applied to the four models described in section 5.10. Of course we apply the lepton tests to models 1 and 2 and the meson oscillation tests to model 3. For model 4 we focus on the addition of quarks to the model and we apply the meson oscillation tests also here. Furthermore we study the effect of the new dimension-6 operators on the relic density of the dark matter candidate.

5.12.1 Model 1

Discussion of the flavour violating processes in model 1 is best done in terms of the fields φ, φ' and φ'' in the Z_3 eigenstate basis of section 5.6.2. In the context of lepton triality, this was discussed before in [159]. Furthermore, the transformation properties of the additional scalar η allow a mixing between φ^0 (φ^1) and η^0 (η^1), both behaving as the SM-Higgs. However, this mixing interaction, $iZ\eta^0\varphi^0 + h.c.$, that was not present in section 5.6.2, is irrelevant for the scalar spectrum discussion, because the coupling, being suppressed by v_η, is extremely small .

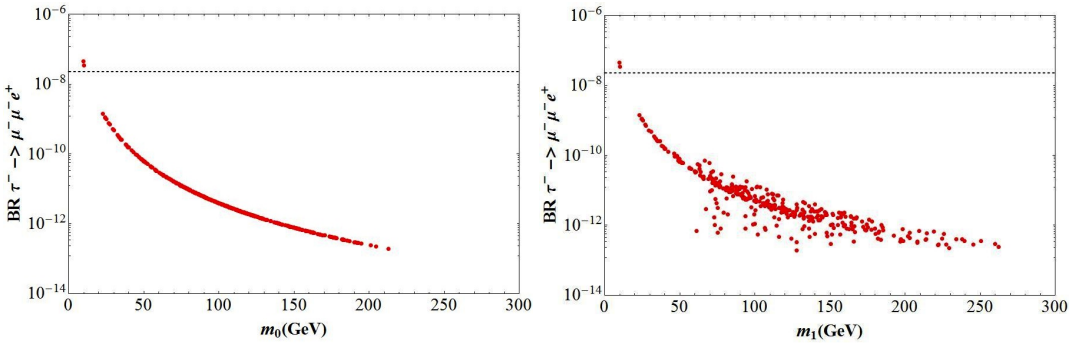

Figure 5.12: *The branching ratio for the decay $\tau^- \to \mu^-\mu^-e^+$ in model 1 as a function of the effective mass m_0 (left) and the smallest mass m_1 (right) in the situation where the parameter ϵ is zero. The horizontal line corresponds to the experimental upper bound.*

The coupling of the Higgses φ'^0, φ''^0 to fermions is purely flavour violating. This setup has striking effects on the lepton processes. In fact it was shown in [160] that, when the A_4 symmetry is unbroken, only a limited number of processes is allowed and these either conserve flavour or satisfy the

constraint $\Delta L_e \times \Delta L_\mu \times \Delta L_\tau = \pm 2$. The only source of symmetry breaking is the vev of the SM-like Higgs φ^0, which is flavour-conserving and thus not involved in the processes we are looking at. We conclude that all flavour violating processes should satisfy the selection rule. In particular this implies that the decays $\mu^- \to e^- e^- e^+$ and $\mu \to e\gamma$ are not allowed, in the latter case in contrast with what was reported in [97], but in agreement with the more recent [161].

Of the allowed processes, $\tau^- \to \mu^- \mu^- e^+$ is least suppressed, since its branching ratio is proportional to $m_\tau^2 m_\mu^2$. However, even this decay is very rare and below the experimental limit for most values of the Higgs masses. In the upper part of figure 5.12, we plot the branching ratio for the decay against an effective mass defined as $m_0^{-2} = m_{h_A}^{-2} + m_{h_B}^{-2}$, where A and B are the two pairs of degenerate bosons. In the lower part, the same branching ratio against the mass of the lightest state, m_1. In both the plots, the parameter ϵ is set to zero, corresponding to the real Higgs potential discussed in [97]. For the first picture, we reproduce the result of [97] that the branching ratio is proportional to m_0^{-4}. In the second one, this dependence is lost, even if we can see a similar behaviour. Once we take ϵ over the full range $[0, 2\pi]$, we verified that the points cover a larger parameter space, but still concentrating around the previous points with $\epsilon = 0$.

In figure 5.13, we show the masses of the SM-Higgs φ^0, m_{h_1}, against the mass of the lightest state m_1. A plot with the mass of the SM-Higgs η^0 against m_1 looks very similar to figure 5.13. All the points are above the diagonal and this corresponds to the fact that the SM-Higgses are always heavier than the lightest state. As already mentioned in section 5.9.1, there is no upper bound on the mass of the SM-like Higgs mass. In particular the standard upper bound of 194 GeV at 99% CL [6] does not apply, due to the combined effect of the CP and Z_3 symmetries and the smallness of the $iZ\eta^0\varphi^0 + h.c.$ coupling.

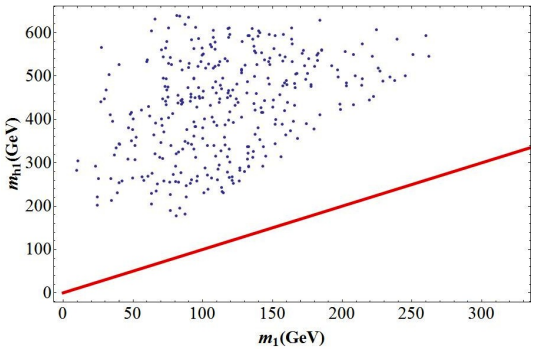

Figure 5.13: *The mass of the SM-like Higgs m_{h_1} against the smallest Higgs mass m_1 in model 1.*

5.12.2 Model 2

In contrast with the Model 1, A_4 is completely broken by the vev of the Higgs triplet. As there is no residual symmetry, there are no special selection rules that forbid flavour changing interactions. In particular the processes $\mu^- \to e^- e^- e^+$ and $\mu^- \to e^- \gamma$ are allowed. The first process, figure 5.14 occurs at tree level and produces a strong bounds on the Higgs sector, where the lightest Higgs mass is expected to be above about 300 GeV. On the other hand, the radiative muon decay to an electron, figure 5.14, is loop suppressed and the new physics leads to a branching ratio below the observed experimental bound.

5.12.3 Model 3

Experimentally, in the quark sector two features have been explored: flavour changing interactions and CP violation. Remarkably, the CKM matrix obtained in the model under inspection is completely

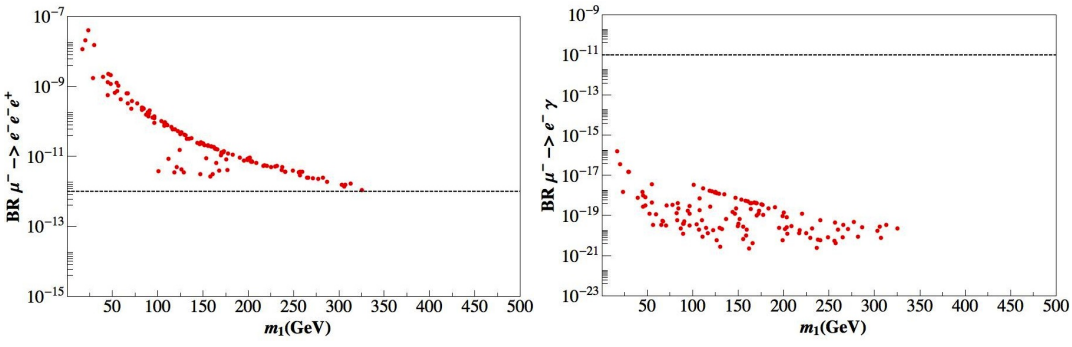

Figure 5.14: *The branching ratio of the decay of $\mu^- \to e^- e^- e^+$ (left) and $\mu^- \to e^- \gamma$ (right) in model 2 versus the lightest Higgs mass. The horizontal band is the experimental limit [6].*

real. It seems then of scarce value to explore CP violating effects coming from the complex vevs of the Higgs triplet, not having the dominant contribution from the Standard Model CKM matrix to compare them with. Consequently we only focus on flavour changing processes. As discussed in section 5.11.3 meson oscillations are in these models mediated by tree level diagrams instead of box diagrams. We therefore expect strong bounds from the mass splittings in the neutral B-meson and Kaon systems. In figure 5.15, we plot ΔM_F versus the lightest Higgs mass for these systems. Indeed ΔM_F is large, up to several orders of magnitude above the experimental value for the B_d meson and the Kaon.

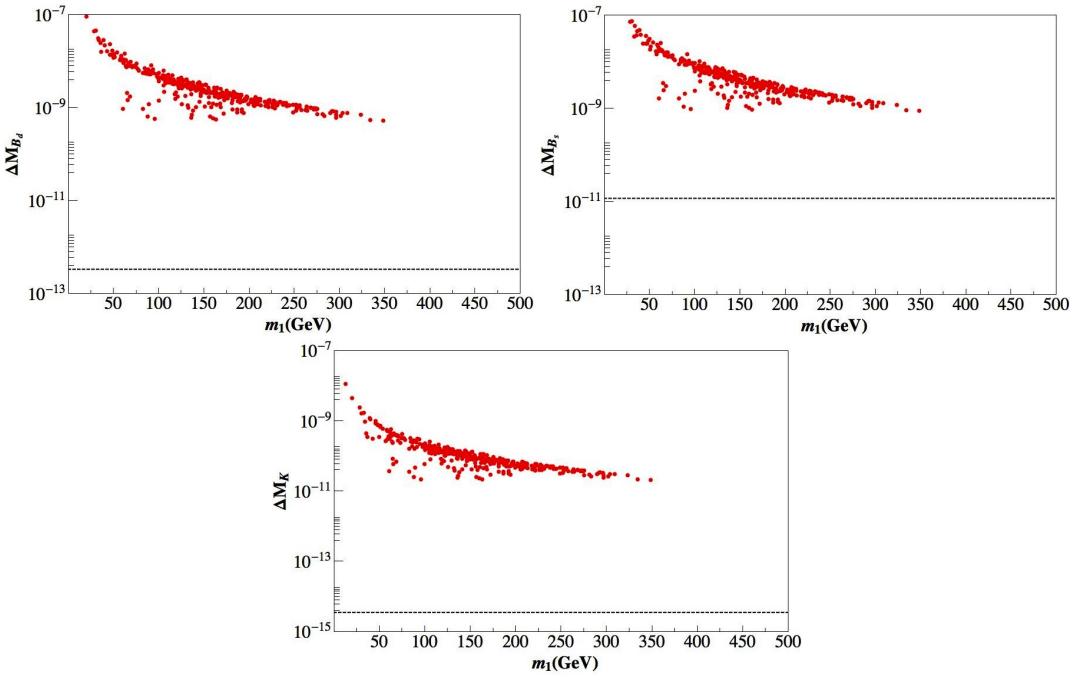

Figure 5.15: *ΔM_F for B_d, B_s and K mass splittings versus the lightest Higgs mass in model 3. The horizontal lines correspond to the experimental values as reported in [158].*

5.12.4 Model 4 - Quark mixing in the discrete dark matter model

In section 5.10.4 we discussed how adding effective dimension-6 operators to the original discrete dark matter model allowed the quarks to mix according to the CKM matrix. These operators also

allow flavour changing neutral currents and in particular meson-antimeson oscillations, that occur through diagrams given in figure 5.16, challenge the validity of our extension of the model.

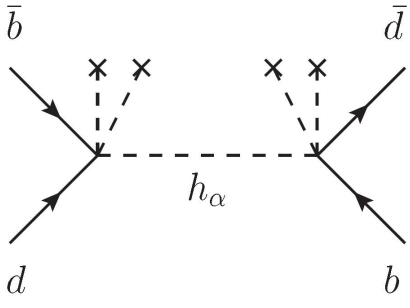

Figure 5.16: *In model 4, B_d and other meson oscillations can occur through a special version of the diagram on the right of figure 5.11.*

As mentioned in the section 5.10.4, the CKM matrix can dominantly originate from corrections to the up-type quark mass matrices or the down-type quark mass matrices and we mentioned that dominance of the latter is more natural. Indeed we find that if corrections of the former type dominate or even if there is no dominance of one of the two, the contribution to ΔM_D of D meson oscillations given only by the new diagrams is much larger than the experimental value [157] and this scenario should be excluded as shown in figure 5.17.

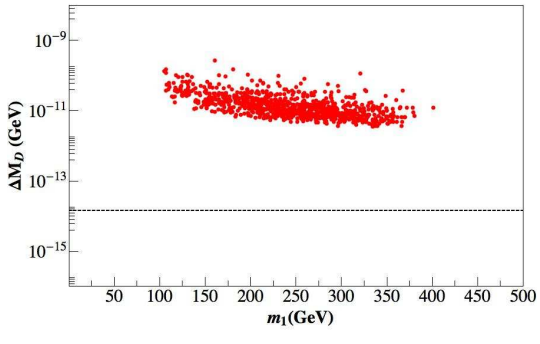

Figure 5.17: *D meson oscillations in model 4 in a scenario where the CKM matrix is generated dominantly by corrections to the up-type quark mass matrix.*

In case the CKM matrix mostly originates from corrections to the down-type quark mass matrix, we find that the bounds from meson mixing are rather strong. In figure 5.18, we show the contribution of the new diagrams to ΔM_{B_d}, ΔM_{B_s} and ΔM_K as function of the lightest Higgs mass. We see that in almost all of parameter space the points are near or even above the short-dashed line, which indicates the current experimental value [158] that is rather well described by the Standard Model box diagrams [6, 162]. Naively, this is interpreted as an exclusion of the model, which is true in most of parameter space, but not in points where the Standard Model and new physics contributions partially cancel. To see this, we write the mixing amplitude for B_d mixing as [163]

$$\left[M_{12}^d\right]_{\rm NP} = (1 - \frac{1}{1 + h_d^2 e^{2i\sigma_d}})\left[M_{12}^d\right]_{\rm full} \tag{5.107}$$

and analogously for B_s. We have verified that our expression for the NP contribution carries enough phases to generate a flat distribution for σ_d and σ_s. We check that the points in $(h_d^2 = 0.41, \sigma_d = 100^\circ)$ and $(h_s^2 = 1.6, \sigma_s = 90^\circ)$ are allowed by the data [163, 164] and give a nett contribution of NP with respect to the full result of respectively 0.65 and 2.67 times the observed value. For B_d mesons, NP effects are thus forced to be less than the observed value, while for B_s mesons, it can even be slightly more. These values (and a corresponding estimate in case of the kaons) correspond to the dot-dashed

lines in 5.18. We see that a small, but significant number of points is allowed by the data under the assumption of partial cancellation.

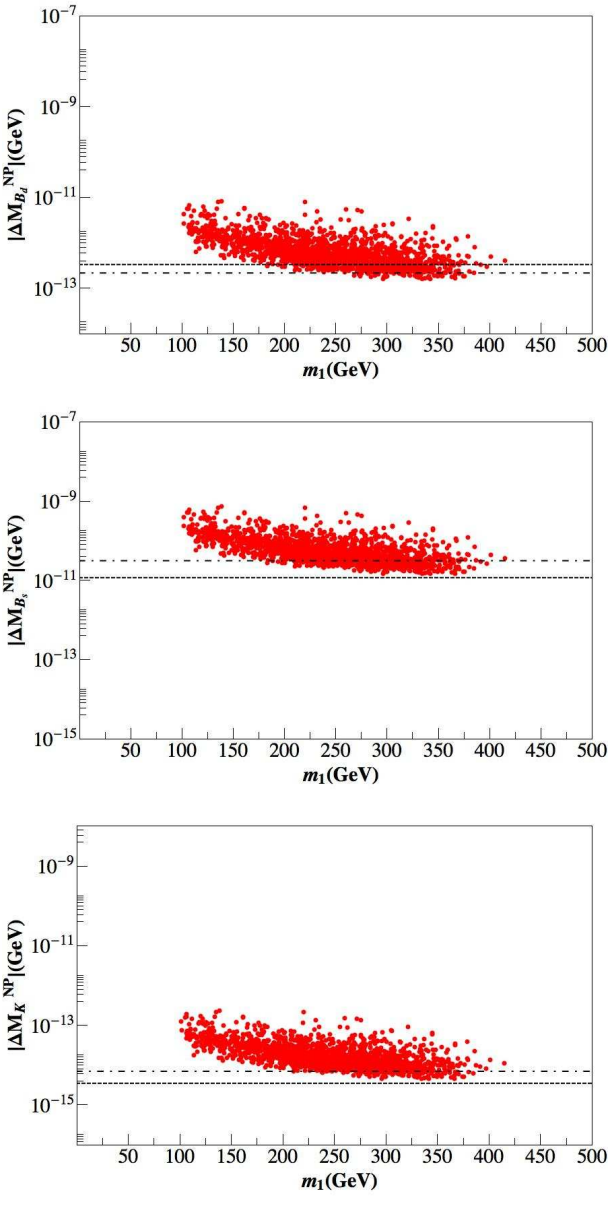

Figure 5.18: *B and K mesons oscillations. The horizontal lines are as explained in the text.*

The naturalness of this cancellation, that requires finetuning between the phase and amplitude of the new and the Standard Model contribution, can be a matter of debate. The need for cancellation diminishes for larger Higgs masses, although there are still no points below the lower line for B_s and K. Indeed, requiring that the new diagrams contribute less than the experimental bound, as is customarily done, the model would be excluded. On the other hand allowing a strong negative interference between the SM and the DDM contributions does not further constrain the scalar spectrum with respect to the analysis done in [152]. Indeed figure 5.19 shows that there is no correlation between the bound imposed and the mass of the lightest Z_2-even scalar state, even if the number of points allowed is significantly reduced with respect to the earlier analysis.

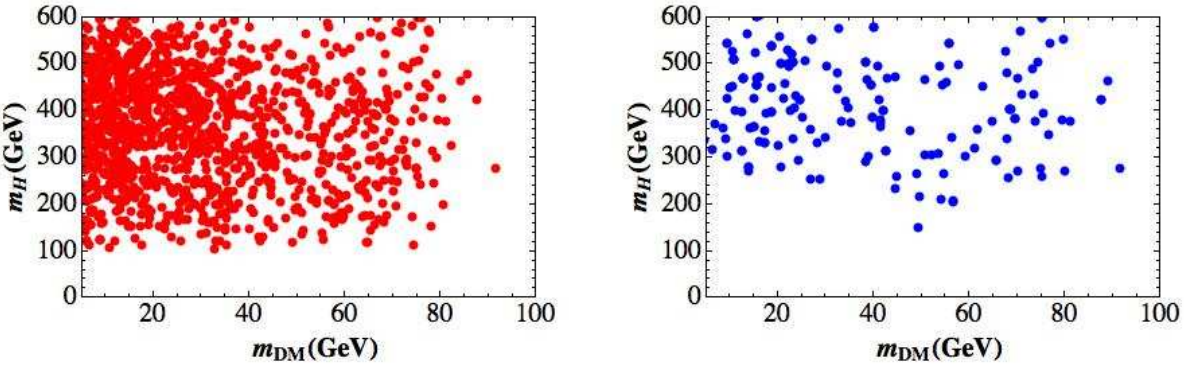

Figure 5.19: *The mass of the lightest Z_2-even state of model 4 versus the mass of the DM candidate without (red) and with (blue) meson oscillation constraints.*

Dark matter relic density and direct detection

Here we consider the effect of the inclusion of the dimension-six terms of equation (5.94) to the relic density. The operators (5.94) give an effective quartic coupling of the dark matter with quarks. This enhances the annihilation of the dark matter candidate into quark pairs that in the original model is only possible via SM Higgs exchange in the s-channel. We only study the decay into down quarks; decay to up quarks is barely affected as we have seen that D-meson constraints force the off-diagonal elements in the up-type quark mass matrix to be very small.

We define the λ^q_{eff} as the parameter of the four points interaction $\chi\chi d_i\bar{d}_j$ - i.e. the result of the three couplings in (5.94) when H but not the two ηs obtain their vevs. We can use equation (5.96) to estimate its size. The assumption is that all hs are of the same natural order of magnitude as the h_{ds} of equation (5.96). An important exception may be h_{dd} that needs to be small in order not to inflate the down mass. For all other couplings, we find

$$\lambda^d_{eff} \sim h^d_{ij}\frac{v_H}{\Lambda^2} \sim \frac{m_s\lambda_C}{v_\eta^2}\,. \tag{5.108}$$

We compare the effect of this operator on the σv_{rel} of the process $\chi\chi \to d_i\bar{d}_i$ to the effect of s-channel exchange of the SM-like lightest CP-even scalar. The SM-like Higgs couples to fermions proportionally to $y_q \sim m_q/v_H$. The new contribution is negligible if

$$\frac{m_s\lambda_C}{v_\eta^2} < \frac{m_q A_H}{v_H m_h^2}\,. \tag{5.109}$$

In this equation m_h is the mass of the lightest CP-even neutral scalar and $A_H \sim v_{\rm ew}$ is the dimensional coupling that controls the interaction of the dark matter with the Higgs doublet $H\chi\chi$. Since

$v_\eta \sim v_H \sim m_h \sim A_H \sim v_{\rm ew}$ the new contribution is naturally subleading for the second and third generation. For the first generation, on the contrary the new contribution to $\chi\chi \to d\bar{d}$ is of the same order as the old one. We can (conservatively) estimate that this channel is negligible only for values $M_{DM} \geq 1\,\text{GeV}$. This is basically satisfied for all values of the dark matter mass, that we reported to be in the range 1 - 100 GeV in section 5.10.4.

Direct detection is not affected at all by the NLO terms: the quark flavour diagonal scattering contribution are subdominant with respect to those mediated by the scalar H while the off-diagonal one could only give rise to processes that are not kinematically allowed such as $\chi + \mathcal{N} \to \chi + \mathcal{N} + \pi^+ + e^- + \bar{\nu}$, with $\mathcal{N}$ a nucleus in the detector bulk.

This concludes the discussion of the quark extension of the discrete dark matter model. Relic density and direct detection calculations do not constrain its viability. Meson oscillations do. D meson oscillations exclude any significant off-diagonal elements in the up-quark mass matrix. Kaon and B_s meson oscillations also produce very tight constraints. These do not immediately rule out the set up, but the model can only be in accordance with the experimental data if there is significant finetuning between Standard Model and new physics contributions. All together, honesty forces us to say that this 'natural extension' is less natural then we hoped.

5.13 Conclusions of the chapter

Flavour models based on non-Abelian discrete symmetries under which the SM scalar doublet (and its replicates) transforms non trivially are quite appealing for many reasons. First of all there are no new physics scales, since the flavour and the EW symmetries are simultaneously broken. Furthermore this kind of models are typically more minimal with respect to the ones in which the flavour scale is higher than the EW one: in particular the vacuum configuration is simpler and the number of parameters is lower. We then expect a high predictive power and clear phenomenological signatures in processes involving both fermions and scalars.

In this chapter we focussed on the A_4 discrete group, but this analysis can be safely generalized for any non-Abelian discrete symmetry. We consider three copies of the SM Higgs fields, that transform as a triplet of A_4. This setting has already been chosen in several papers [97, 127, 128, 150–152, 159] due to the simple vacuum alignment mechanism. In each of these works, a certain configuration has been assumed for the vacuum expectation values of the three Higgs bosons.

In this chapter we have considered all the possible vacuum configurations allowed by the $A_4 \times SM$ scalar potential. These obviously contain the vacua studied in earlier models. We showed furthermore that the total list is rather small. The potential allows only the five minima mentioned in section 5.6.9 and permutations of their components.

The fact that a certain vev combination is a true minimum of the Higgs potential does not automatically imply that a model that uses three Higgs fields with these vacuum expectation values is physically viable. In this chapter we described two groups of tests to check if a model is in accordance with the current (pre-LHC) data. The first group of tests only considers the Higgs sector. It is not influenced by the choice of A_4 representations for the fermions, only by the representation choice for the Higgs fields, that are fixed to be in the triplet representation of A_4. We considered constraints by unitarity, by W and Z decays, and by the oblique parameters S, T and U. For all but one vacua considered, a significant number of points passed all three tests. The exception is one of the complex vacua. This can only be realistic if the A_4-invariant Higgs potential is extended with some terms that break the family symmetry softly. This makes models that use this vacuum significantly less attractive.

The second group of tests consists of processes in which the fermions participate and for which it is thus needed to know the A_4 representations of these fields. We developed a very general formalism to describe the interaction of charged and neutral Higgs and of fermions. In the mass basis of both Higgs bosons and fermions the interaction depends on the Yukawa matrices that appear in the

Lagrangian and the unitary matrices that rotate the flavour basis into the mass basis. When these matrices are given, a number of flavour violating processes can be calculated and these calculations can be used to test the viability of models in the literature.

We showed that for three of the four models considered in detail in this chapter, flavour violating processes significantly reduce the viability of the set up. It is not a coincidence that he only model for which the flavour changing neutral currents do not pose a large problem, assumes the Higgs fields to be in the configuration with the maximal residual symmetry.

In conclusion, we showed that for flavour models with the family symmetry implemented at the electroweak scale, it is possible to test their phenomenology beyond the prediction of the mixing patterns. This is a powerful tool to discriminate among them. Indeed, many Higgs vacuum configurations and concrete models considered in this chapter can be strongly constrained or almost ruled out. The fact that this falsification is possible is most important advantage of the set up of flavour symmetries at the electroweak scale.

Appendix to chapter 5

5.A Analytical formulæ for the oblique parameters

In this appendix we provide a dictionary from the notation in the original papers introducing the oblique parameters [141, 144] to ours.

In the notation of Peskin and Takeuchi, we are in the case in which $n_d = 3$ and $n_n, n_c = 0$; this implies that the matrices $\mathcal{T}$ and $\mathcal{R}$ are vanishing. The quantities that need to be translated are

$$\begin{aligned} \mathcal{U} &\rightarrow S \\ \mathrm{Re}\mathcal{V}_{ki} &\rightarrow U_{ki}\,, \\ \mathrm{Im}\mathcal{V}_{ki} &\rightarrow U_{k+3i}\,, \\ \omega_k &\rightarrow f_k e^{i\omega_k}\,. \end{aligned} \tag{5.A.1}$$

Moreover they put the GBs as first mass eigenstates while we put them as the last ones and contrary to them we use the standard definition for the photon.

We have rewritten the expression for

$$\frac{A(I,J,Q)-A(I,J,0)}{Q} = \begin{cases} dA(I,J) & \text{for } I \neq 0 \text{ and/or } J \neq 0\,, \\ \dfrac{QF(Q)}{Q} \sim \dfrac{1}{48\pi^2}\log Q & \text{for } I = J = 0 \text{ since } A(0,0,0) = 0\,. \end{cases} \tag{5.A.2}$$

In the first row of equation(5.A.2) we used

$$A(I,J,Q) \simeq A(I,J,0) + Q\frac{\partial A(I,J,Q)}{\partial Q}\bigg|_{Q=0} = A(I,J,0) + Q\,dA(I,J)\,. \tag{5.A.3}$$

In this expression $dA(I,J)$ is given by

$$dA(I,J) = \begin{cases} \dfrac{1}{288(I-J)^3\pi^2}\left[I^3 + 9JI^2 + 6(I-3J)\log(I)I^2 - 9J^2I - J^3 + 6(3I-J)J^2\log(J)\right] \\ \qquad\qquad \text{for } I, J \neq 0, I \neq J\,, \\ \dfrac{1}{288\pi^2}(1 + 6Log[I]) \qquad \text{for } J = 0\,, \\ \dfrac{1}{48\pi^2}(1 + \log[I]) \qquad \text{for } I = J\,. \end{cases} \tag{5.A.4}$$

The function $\bar{A}(I,J,Q)$ enters only in the loops in which a gauge boson and a scalar run, so we have always $J = Q$ when computing the quantity

$$\frac{\bar{A}(I,J,Q)-\bar{A}(I,J,0)}{Q} = \bar{dA}(I,J)\,. \tag{5.A.5}$$

As a result, for this function, it does not make sense to consider the case $I = J = 0$ where $J = Q = m_V^2$ the gauge boson mass. Eventually we find

$$d\bar{A}(I,Q) = \begin{cases} \frac{1}{8(I-Q)^3\pi^2}\left[Q\left(-I^2 + 2Q\log(I)I - 2Q\log(Q)I + Q^2\right)\right] & \text{for } I \neq Q, I \neq 0\,, \\ \sim 0 \qquad\qquad\qquad\quad \text{for } I = 0\,, \\ \sim 0 \qquad\qquad\qquad\quad \text{for } I = Q\,. \end{cases} \tag{5.A.6}$$

Chapter 6

Summary, conclusions and outlook

> La science, mon garçon, est faite d'erreurs, mais d'erreurs qu'il est bon de commettre, car elles mènent peu à peu à la vérité.
>
> Science, my boy, is built upon errors; but upon errors that are good to be made, as step by step they lead to the truth.
>
> *Jules Verne [165], Voyage au centre de la Terre*

One of the oldest and most important questions humanity has asked itself is "What is it made of?" Every time this question seemed answered in a particular field, people started looking for structures in the answer. When structures were found, the next challenge was to understand them from a deeper principle. Particle physics and in particular its flavour branch is no exception to this rule.

Our current world view is that all normal matter is made of atoms. Atoms consist of a shell of electrons surrounding a nucleus. The electrons are thought to be elementary particles; the nucleus is not, but digging deep enough, one finds supposedly-elementary up and down quarks. This is not the whole story; exotic matter can be observed in the cosmic rays and at particle colliders. This gives two new leptons and a whole zoo of new mesons and baryons, but the quark model structures this in terms of just four new quarks. Together with three neutrinos, this is the complete matter content of the Standard Model as recapitulated in figure 6.1.

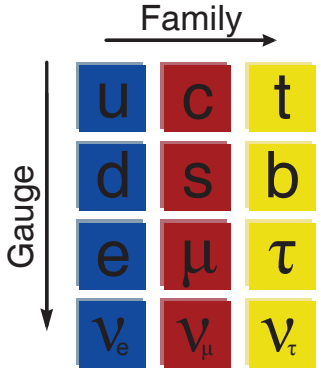

Figure 6.1: *The matter particles of the Standard Model and two arrows that might suggest symmetry relations.*

Structure in similarity

The vertical arrow in figure 6.1 generically depicts the three gauge interactions of the Standard Model. These structure the allowed interactions between the elementary particles. In a sense, their representation structure even dictates which particles are to appear in the figure. The weak nuclear force for instance has a doublet as fundamental representation and indeed the electron and the electron neutrino as well as the up and down quark come in pairs in figure 6.1.

The horizontal arrow in the figure corresponds to the fact that particles that are standing next to each other are very similar. The up, charm and top quark have exactly the same quantum numbers of colour, weak isospin and hypercharge and the same holds for all other rows. This is a structure that is easily observed in the answer to the question what matter is made of, but an explanation for the structure is lacking in the conventional Standard Model. The existence of three families is considered an experimental fact, but not connected to a deeper symmetry principle to explain it.

The fundamental assumption of this thesis is that this is unsatisfactory. A theory in which the family structure can be explained is to be preferred over one in which it cannot. A suggestion to the explanation is already given in figure 6.1. There might be a force – or, more general, a symmetry relation – working not in the vertical, but in the horizontal direction. If a horizontal symmetry group with a three-dimensional irreducible representation is assumed, the three-family structure of the Standard Model results.

Structure in difference 1: the masses

A horizontal symmetry, often also referred to as a flavour or family symmetry, can thus provide and explain structure in the similarities of the particles of the three generations. The particles are indeed identical in their coupling to the gauge sector, but the mass sector is very different. It is an interesting question if there are also structures here. The answer is that there might, both in the masses of the fermions and in the mixings between flavour and mass eigenstates.

Firstly, we observe that the masses of the quarks and (charged) leptons are very hierarchical, with the mass gaps between particles of the same type of comparable order on a logarithmic scale. In section 2.3.1 we observed that the mass ratios of the muon to the tau lepton and of the electron to the muon are respectively λ^2 and λ^3, with λ numerically equal to 0.2 and possibly related to the Cabibbo angle. According to Froggatt and Nielsen, this may not be a numerical coincidence, but related to the charges of the different generations under the Frogatt-Nielsen family symmetry. Again, we see that family symmetries can be used to motivate observed structures.

Structure in difference 2: the mixings

The second part where one can looks for structures in the fermion masses is in the mixing of flavour eigenstates to mass eigenstates. The data shown in figure 6.2 give rise to several models constructed in the main body of this thesis. These models invoke some new physics, at least containing a horizontal symmetry, to reproduce the pie charts of figure 6.2, either by predicting exactly these values or by producing a probability distribution for the mixing angles peaked at or close to the values corresponding to those in the figure. The fact that the models correctly 'postdict' the mixing angles obviously isn't enough to immediately declare them the new Standard Model. All models also make a number of predictions that can be tested by experiments in the near or more distinct future and lastly, there is the difficult issue of the 'aesthetical value' of models. We try to make a final balance in the remainder of this chapter.

Figure 6.2: *Pie charts showing the flavour content of the three quark mass eigenstates (left) and neutrino mass eigenstates (right). Quark data taken from [6] and the errors on these data are very small. neutrino data correspond to average values of the elements of the mixing matrix from [7]. The errors here are large, corresponding to tens of percents in some cases.*

The beauty and the beast

The astuicle that chapter 4 of this thesis is based on, was originally called 'Discrete Flavour Symmetries in GUTs: the Beauty and the Beast'. After a rightful comment of the referee that he or she did not consider this a very appropriate title for a scientific publication, the title was changed. Still, the concept of beauties and beasts, positive and negative messages about beyond-the-Standard-Model models, is an important theme in the article as well as in the articles on which the other chapters of this thesis are based. In that fashion, this summarizing and concluding chapter can continue in a 'beauty-like' or a 'beast-like' way.

The beauty

The beautiful conclusion of the thesis would be that the field of flavour model building is very rich. There are many ideas around, making the field very versatile and flexible.

The application of family symmetries to flavour mixing was first popularized approximately ten years ago when the mixing deferred from neutrino oscillations seemed to be in accordance with the bimaximal mixing pattern, although there were large experimental errors.

$$\theta_{12}^l = \theta_{23}^l = \pi/4;\ \theta_{13}^l = 0\ , \qquad \text{or}$$
$$\sin^2\theta_{12}^l = \sin^2\theta_{23}^l = 1/2;\ \sin^2\theta_{13}^l = 0\ .$$

This pattern is probably the third simplest mixing pattern one can think of. Only 'no mixing' and 'maximal mixing in just one sector' are simpler. It is indeed a very remarkable fact that the data were in accordance with such a simple pattern and it was worth researching if there is a deeper reason for this. This turned out not to be the case; the agreement between early data and the bimaximal pattern was accidental.

A larger data set allowed a more precise determination of the solar mixing angle θ_{12}^l and it was found that it is in fact not 'maximal', but seems to settle near another special value; the one corresponding to $\sin^2\theta_{12}^l = 1/3$. The focus on bimaximal mixing pattern was swiftly changed for this tribimaximal one. One way to realize tribimaximal mixing is using A_4 as a horizontal symmetry group as discussed in section 2.4. A_4 is one of the simplest groups available in the mathematical literature. It only has 12 elements, which makes it the smallest group to have a three-dimensional representation. The ability of A_4 to generate tribimaximal mixing is another elegant example of the force of group theory in physics. As elaborated upon in chapter 3, an accidental symmetry is necessary when A_4 reproduces tribimaximal mixing. The group S_4 on the other hand, is almost as simple as A_4; it can reproduce tribimaximal mixing as well as bimaximal mixing without resort to accidental symmetries.

The bimaximal and the tribimaximal mixing differ in the values of the solar mixing angle, but they agree on the two other mixing angles. The atmospheric angle θ_{23}^l should be 45° and the reactor angle 0°. The first prediction has so far stood the test of time and is in accordance with the current best fits at 1σ or less. It is interesting to note that the two different global fits given in chapter 2 present central values that deviate from this value in opposite directions.

The prediction $\theta_{13}^l = 0^\circ$ for the reactor mixing angle seems not to have held. Over the last years,

non-zero θ_{13}^l was first presented as a hint in global fits of all neutrino oscillation observables. For a long time the best-fit value of the angle was positive, although a vanishing angle was still allowed at the 2 to 3σ level. In the summer of 2011, observations of the T2K collaboration have finally swung the balance to $\theta_{13}^l > 0^\circ$. The next big step from an experimental point of view will be the independent confirmation or refutation of this measurement. As mentioned in the start of chapter 3, the falsification of the hypothesis of exact tribimaximal mixing opens up a number of directions in the space of model building. We investigated many of these ways in the different chapters of this thesis.

In chapter 3 itself we systematically scanned a large number of mixing patterns that naturally arise when horizontal symmetry groups and residual symmetries are selected. We found that the bimaximal and tribimaximal patterns are elements of a large, but finite, list of naturally obtained mixing structures. Four of these structures, $\mathtt{M}_1$ - $\mathtt{M}_4$, are particularly appealing, as they naturally predict non-zero reactor mixing angle, while the other two neutrino angles are also close to the current best fits on the data. They are different from the predictions of tribimaximal mixing. There are thus three unique predictions that will be tested when more precise fits of the mixing angles become available.

Chapter 4 discusses a set up in which the mixing angles are significantly different at leading order in the number of flavons present in the Lagrangian from the eventual all-order result. In this set up, indeed one of the predictions is a non-zero reactor mixing angle. The main message of the chapter is that the combination of the S_4 family symmetry (with bimaximal mixing at leading order) and the Pati–Salam grand unified theory (with quark-lepton complementarity) is indeed feasible. The combination of flavour and GUT symmetry enabled a double stroke of unification, making the model attractive from a aesthetical point of view. A number of predictions is made by the model; these include the observation of neutrinoless double beta decay in a particular range and the existence of doubly charged scalars at a few TeV. In a more distinct future, new experimental techniques might be able to scan the complete gauge structure, but at the moment the related energy scales are still very far out of sight.

From the point of view of predicting neutrino mixing angles, chapter 5 presents a less ambitious set up. In this chapter, we discuss a situation in which there are no separate flavons and correspondingly there is no separate scale of the flavour symmetry breaking. The flavour symmetry is realized via non-trivially transforming Higgs bosons and all the flavour symmetry processes take place at the electroweak scale. The fact that these Higgses provide only one direction in flavour space ('just one flavon') means that the mixing angles in quark and lepton sector cannot be uniquely determined. Patterns such as the tribimaximal mixing are obtained by finetuning some parameters, although significantly less than in the Standard Model. When the tuning is not exact, a pattern close to, but not identical to tribimaximal naturally comes out and this is indeed what the current data seem to point at. The strongest point of the set up of chapter 5 is that the predictions are testable at the LHC. We have given elaborate lists of the Higgs bosons and their masses in each of the vacua considered. Furthermore, pre-LHC data can be used to significantly reduce the parameters space available in each of the vacua as well as to test specific models in which details of the fermionic content are given.

The beast

On the other hand, a beasty conclusion is possible. This focusses on the point that application of the 'hierarchy-problem argument' might not be very fit in the context of flavour symmetries.

We recall that in chapter 1 the reasons to go beyond the Standard Model were separated into two groups. There is observational evidence that the Standard Model is incomplete and there are theoretical or aesthetical reasons to expand it. The first reasons pose a strong obligation to the theorists to extend the Standard Model. As shown by e.g. Shaposhnikov and alluded to in section 1.2.4, this does not need much new physics. Just the addition of three righthanded neutrinos with finetuned masses does the job. The crucial point is that this finetuning is much disliked in the

theoretical physics community. New physics can be assumed in order to prevent a theory from being finetuned. Axions to fight the strong-CP problem and supersymmetry to fight the Higgs-mass hierarchy problem are examples given in section 1.3. The motivation for flavour symmetries falls into the same category.

Finetuning in the fermion sector can appear in the masses or the mixings of the particles. The hierarchy in the fermion masses was already discussed above as well as the potentially related Froggatt–Nielsen symmetry. The crucial point is that the fermion mass hierarchy provides a rather clear signal. This is less the case in the fermion mixings. The three pie-charts on the right hand side of figure 6.2 were calculated with the central values of the allowed ranges for each of the nine mixing matrix elements. These figures show the suggestion of near-tribimaximal mixing with small θ_{13}^l effects. The assumption is that if the data favour such a special mixing pattern, we should see the appearance of this pattern as a finetuning and try to explain it.

The problem with this reasoning is that the data do not point at the patterns as strongly as perhaps suggested by figure 6.2. Indeed, the central values may provide an interesting signal, but those central values are surrounded by large error bands. This already revealed itself in the fact that in the past years there were 'phase transitions' between different paradigms, going from the bimaximal to the tribimaximal to the 'near-tribimaximal with non-zero reactor angle' paradigm. All those patterns were allowed within the 2 or 3σ bounds at the time of their popularity. Within those bounds, also other mixing schemes exist that do not show any pattern and thus do not call for a symmetry explanation. This is graphically illustrated in figure 6.3.

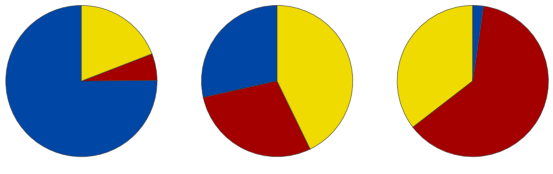

Figure 6.3: *Pie charts showing a possibility for the flavour content of the three neutrino mass eigenstates. Instead of taking the average values given in [7] we have taken other values in the 3σ intervals. The figures resemble neither the tribimaximal nor any other simple pattern much.*

With this in mind, flavour symmetric model building can be seen as preemptive model building. In the last few years, the tribimaximal mixing pattern was allowed by the data, but not firmly pointed at. The models were constructed to anticipate that the data might settle at exact tribimaximal mixing that is in need of an explanation of the apparent fine-tuning.

The data did not settle at exact tribimaximal mixing. Instead evidence for non-zero reactor mixing angle was found. 'Vanilla' tribimaximal mixing models cannot explain this and in this thesis, suggestions for more elaborate flavours are given. These however, are all still in the framework of flavour symmetries. The question is how well one can still defend this framework.

Let us imagine a world that has never been through the 'tribimaximal paradigm' era. In this world, one day after the establishment of neutrino oscillations, an ingenious experimentalist builds a machine that immediately measures all three mixing angles with a precision that in our world was only reached in the summer of 2011. She sends this information to her theorist colleagues and asks if they see anything in the data. The theorists will not come up with tribimaximal mixing: it is already excluded by the data; it is also unlikely that they will go in one step from nothing to '(tri-) bimaximal mixing with significant corrections', as in the model of chapter 4. The motivation to defend this from a finetuning perspective is simply lacking.

It is interesting to ask whether the hypothetical theorists would come up with groups such as $\Delta(96)$ and $\Delta(384)$ of chapter 3 to address the mixing patterns. Indeed, in our world, where we have been through the 'tribimaximal paradigm' phase, it can be defended that these groups are not much more

complicated than A_4 and S_4 and indeed are generated by the same basic principles. In the other world, assuming a very complicated group to explain a mixing pattern that on first sight looks quite innocent might be a step too far. The same holds for the assumption of an A_4-triplet of Higgs fields as discussed in chapter 5.

If the beasty conclusion is true, flavour symmetries may not be 'the truth', but in discussing them, we may step by step have moved closer to understanding Majorana neutrinos, dark matter, multi-Higgs models and many other aspects of the physics of the exciting times we live in.

Samenvatting

Lieve hart mijn boek is af, mijn boek is af!

Multatuli, 1859
en
In memoriam *Sjoerd Hardeman [166], proefschrift 2011*

Twee vragen die de mens van oorsprong heeft beziggehouden zijn 'Waar is dat van gemaakt?' en 'Zit daar structuur in?'. Als die vragen beantwoord zijn, volgen vaak nieuwe vragen van het type 'Is daar een reden voor?' en 'Kan ik dat verklaren vanuit een onderliggend principe?'

Sinds ongeveer een eeuw hebben we een redelijk beeld van de bouwstoffen van alledaagse materie. Materie komt in veel verschijningsvormen; zo lijken lucht, water, stenen en gras niet echt veel op elkaar. Als je maar diep genoeg inzoomt, blijken ze echter toch allemaal dezelfde bouwstoffen te hebben. Uiteindelijk is alles opgebouwd uit atomen, die op hun beurt weer uit een kern en een aantal elektronen bestaan, zoals weergegeven in figuur 1.

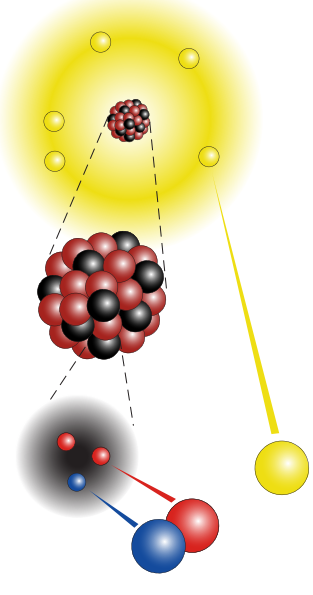

Figuur 1: *Materie is opgebouwd uit atomen. Een atoom heeft een elecronenwolk (geel) en een kern. In de kern zitten protonen (zwart) en neutronen (donkerrood), die op hun beurt weer uit zogeheten quarks (rood en blauw) bestaat [Schematische voorstelling – niet op schaal].*

Elektronen lijken elementaire deeltjes te zijn: hoe hard je ook je best doet, je kunt ze niet splitsen

in kleinere bouwstenen. Dat blijkt niet zo te zijn voor de atoomkern die in veel gevallen gesplitst kan worden, bijvoorbeeld in een kernreactor. Een atoomkern blijkt opgebouwd uit protonen en neutronen, waarin op hun beurt weer zogeheten up en down quarks[1] blijken te zitten, altijd drie in totaal. Daarnaast blijkt er nog een deeltje, het neutrino, te bestaan, dat zich in zekere zin verhoudt tot het elektron zoals het up en down quark zich tot elkaar verhouden.

Deze beschrijving beantwoordt de eerste twee vragen. Alles is gemaakt uit de vier deeltjes elektron, neutrino, up quark en down quark en het feit dat dit voor alle materie geldt en dat er numerieke relaties zijn tussen de aantallen van verschillende deeltjes in een atoom, geeft aan dat er structuur in zit. Het antwoord op de vraag of dit deze via een onderliggend principe verklaard kunnen worden, moest wachten tot de jaren '60 van de vorige eeuw. Toen is het standaardmodel van de deeltjesfysica opgesteld, waarin gesteld wordt dat er een diepe relatie is tussen materie, krachten en een tak van wiskunde genaamd groepentheorie.

De vraag waarom er drie quarks in een proton of neutron zitten, wordt bijvoorbeeld beantwoord door te stellen dat quarks een extra eigenschap 'kleur' hebben en dat alleen kleurneutrale of 'witte' objecten stabiel kunnen zijn. Zoals wit licht verkregen kan worden door rood, groen en blauw licht te mengen, kan een kleurneutraal proton of neutron gevormd worden uit drie quarks, elk met één van de kleuren. De details volgen bij het bestuderen van de $SU(3)$-groepentheorie van kwantumchromodynamica, de theorie van de sterke kernkracht

Daarnaast wordt het feit dat het elektron en het neutrino alsmede het up en down quark als paren voorkomen, verklaard als een eigenschap van de $SU(2)$-groepentheorie van de zwakke kernkracht, die ook zorgt voor radioactief verval.

Bovenstaande is een algemene beschrijving van de elementaire-deeltjesfysica zoals we die nu kennen. Het daadwerkelijke onderwerp van dit proefschrift komt naar voren in de waarneming dat weliswaar alle *stabiele* materie uit de vier bovenstaande deeltjes bestaat, maar dat er daarnaast twee 'broertjes' lijken te bestaan voor elk van deze deeltjes. Het up quark lijkt op zijn broertjes charm en top die beiden ook weer in drie 'kleuren' voorkomen; het down quark wordt vergezeld door quarks met de namen strange en bottom en naast het elektron bestaan er een muon en een tau lepton en er zijn ook in totaal drie neutrinos. Dit is nog eens samengevat in figuur 2. De enige eigenschap waarin de broertjes (meestal aangeduidt als tweede en derde familie) verschillen van de stabiele-materie deeltjes (de eerste familie) is hun massa.

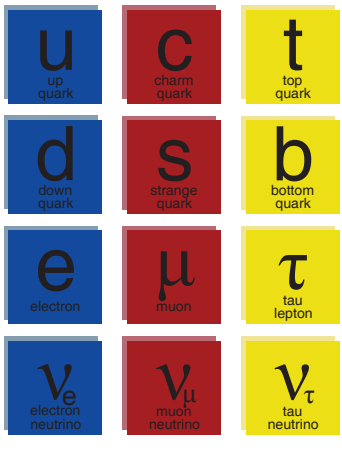

Figuur 2: *De materiedeeltjes die samen het standaardmodel vormen.*

De vraag of er structuur in de families van deeltjes in het standaardmodel zit, wordt duidelijk beantwoord door figuur 2. De vraag of daar ook een onderliggende reden achter zit, is echter

[1] We gebruiken hier de Engelse namen voor de quarks. Nederlandse namen bestaan: op-, neer-, vreemde, tover-, bodem- en top-quark in volgorde van toenemende massa, maar deze zijn zeer ongebruikelijk.

nog open. In de traditionele theorie wordt deze vraag met 'nee' beantwoord. Het bestaan van drie families wordt als een experimenteel feit gezien, maar niet verklaard.

De fundamentele stellingname van dit proefschrift is dat dit onbevredigend is, en er een onderliggende reden moet zijn achter het bestaan van de drie families. Een hint naar de oplossing is hierboven al gegeven, toen gevonden werd dat de groepentheorie van de kernkrachten uit wees dat deeltjes soms in paren (up en down quark; elektron en neutrino) of in drievoud (rood, groen en blauw quark) voorkomen. Wellicht kan hetzelfde principe gelden voor de drie families. Als er een kracht – of, meer algemeen, een symmetriegroep – bestaat tussen de drie families, kan de groepentheorie hiervan *verklaren* dat ieder van de stabiele-materie deeltjes twee zwaardere broertjes heeft.

Een familiesymmetrie kan dus de gelijkenis tussen de drie families verklaren. Zoals boven aangegeven, lijken de deeltjes in de drie families inderdaad heel erg op elkaar, maar verschillen ze ook op een belangrijk punt: in hun massa. Nu is het interessante dat ook in die massa's weer structuren lijken te zitten. Zo zijn de deeltjes van de derde familie typisch ongeveer 100x zwaarder dan die van de tweede familie, die op hun beurt weer zo'n 100x zwaarder zijn dan de deeltjes van de eerste familie[2]. In de theorie van Froggatt en Nielsen, beschreven in sectie 2.3.1, kan de massahierarchie inderdaad verklaard worden middels een familiesymmetrie.

Hier blijft het niet bij. Het geoefend oog van de theoretisch natuurkundige denkt méér patronen te kunnen waarnemen. Één hiervan is gerelateerd aan de 'menging' van neutrinos. Aangezien er drie neutrinos zijn, kunnen we drie massa's toeschrijven aan de neutrinos. Maar in bepaalde interacties, blijken het niet precies de toestanden met een zekere massa ('massa-eigentoestanden') te zijn die reageren, maar bepaalde combinaties daarvan ('interactie-eigentoestanden') – en wel heel specifieke combinaties. Zo is één van de massa-eigentoestanden voor zover we kunnen meten een precies gelijke combinatie van elk van de drie interactie-eigentoestanden en is een andere massa-eigentoestand een gelijke combinatie van twee van de drie interactie-eigentoestanden en bijna niks van de derde. Dit heet tri-bi-maximale mixing in de deeltjesfysicaliteratuur en sinds enige jaren zijn er modellen die het vanuit onderliggende principes kunnen reproducere, mits er een familiesymmetrie gebruikt mag worden. Een voorbeeld wordt gegeven in sectie 2.4.

De kern van dit proefschrift – de hoofdstukken 3 tot en met 5 – zijn in zekere zin allemaal geinsprireerd door het onderstreepte woordje bijna in de vorige alinea. Sinds de zomer van 2011 is er duidelijk experimenteel bewijs dat tri-bi-maximale mixing niet perfect kan zijn. Moeten familiesymmetrieën hiermee verworpen worden, of kunnen ze op een simpele manier aangepast worden?

Hoofdstuk 3 begint met een schets van een aantal mogelijke richtingen in de ruimte van theorieën waar deze waarneming naar kan wijzen. In de rest van het hoofdstuk bekijken we de groepentheoretische achtergrond van tri-bi-maximale mixing en de wiskundige groep die dit mogelijk maakt. We zien dat dit principe te generaliseren is en vinden een groot – maar eindig – aantal andere mixingspatronen die door de wiskunde naar voren worden geschoven. Een aantal hiervan komt heel erg dicht bij de meest recente data en ze hebben met elkaar gemeen dat ze op een natuurlijke manier een inmenging vinden van de derde interactie-eigentoestand in de massa-eigentoestand die voornamelijk uit gelijke delen van de andere twee bestaat, $\theta_{13}^{l} \neq 0$ in formules.

In hoofdstuk 4 gooien we het over een andere boeg en construeren een vrij uitgebreid – volgens critici wellicht barok – model. Dit model bevat naast een familiesymmetrie ook een zogeheten *grand unified* symmetrie. Deze unificeert de bekende krachten van het standaardmodel en vereenvoudigt daarnaast de beschrijving van de elementaire deeltjes. We kiezen er opzettelijk voor om de menging van zowel neutrinos als quarks in eerste benadering niet heel erg goed te laten overeenstemmen met de data. We kunnen dan een tweede-benaderingsschema invoeren waarin in één klap beide de data een stuk beter beschrijven en bovendien $\theta_{13}^{l} \neq 0$ gegenereerd wordt.

De kern van de argumentatie van het hoofdstuk ligt in de onverwachte complicaties die het com-

[2]De constante waarde 100 is lichtelijk overgesimpliceerd. In werkelijkheid verschilt de factor per deeltjestype. Zie sectie 4.2 voor een meer gedetailleerde beschrijving.

bineren van *grand unified* en familiesymmetrie geven. Hoewel de combinatie van de twee symmetrieën vanuit esthetisch oogpunt zeer wenselijk is – beide staan een compactere formulering van de theorie toe – blijkt het aantal benodigde hulpvelden onverwacht sterk toe te nemen. Daarnaast blijkt dat voorspellingen gedaan op een zekere hoge energieschaal zich minder makkelijk laten vertalen naar een lagere energieschaal dan naïef wellicht verwacht zou kunnen worden[3]. Met de toepassing van de juiste methoden kan het model toch op beide schalen geëvalueerd worden.

In hoofdstuk 5 beschouwen we juist modellen waar de energieschaal van de familiesymmetrie vrij laag is. Familiesymmetrie manifesteert zich in deze modellen op dezelfde schaal als de zwakke kernkracht waarnaar hierboven al gerefereerd is. De Large Hadron Collider (LHC) deeltjesversneller van CERN bij Genève is specifiek gebouwd om de geheimen van de zwakke kernkracht beter te doorgronden. Als de schaal van familiesymmetrie inderdaad dezelfde is als die van de zwakke kernkracht, zal de LHC ook voor familiesymmetrieën een boel waarnemingen kunnen doen. We beschouwen de voorspellingen van deze modellen voor de LHC en laten zien dat via precisiewaarnemingen van eerdere, minder energierijke versnellers veel modellen al sterk beperkt kunnen worden. Een bijkomend voordeel van deze set-up is dat deze modellen typisch θ_{13}^l ongelijk aan 0 hebben, zij het zonder een specifieke waarde te voorspellen.

Hoofdstuk 6 presenteert de conclusies van dit proefschrrift. Geïnsprireerd op de oorspronkelijke titel van één van de artikelen kan deze op een *the beauty* en een *the beast* manier gelezen worden. De goede boodschap is dat het veld van familiesymmetrieën erg veelzijdig is en dat veel interessante modellen opgesteld kunnen worden. De slechte boodschap is dat de structuur die familiemodellen inspireert, misschien toch minder overtuigend is dan eerst gedacht werd, zeker nu een waarde voor θ_{13}^l ongelijk aan 0 gevonden is. Wellicht is de structuur dan onvoldoende om de gecompliceerdheid van de modellen te rechtvaardigen.

In ieder geval kunnen we stellen dat de elementaire-deeltjesfysica de vraag 'Waar is dat van gemaakt?' beantwoord denkt te hebben. De vraag 'Zit daar structuur in?' wordt sowieso bevestigend beantwoord, maar de hoeveelheid structuur is nog onderwerp van debat. Aan de hand daarvan zijn er veel antwoorden mogelijk voor de vragen 'Is daar een reden voor?' en 'Kan ik dat verklaren vanuit een onderliggend principe?' En zodra er nieuwe antwoorden komen op de *eerste* vraag – bijvoorbeeld als de LHC nieuwe, onverwachte deeltjes vindt – kunnen alle kaarten weer anders liggen.

[3]De waarde van veel observabelen in de hoge-energiefysica blijkt van de energieschaal afhankelijk te zijn waarop een waarnemer er naar kijkt. Intuïtief kan dit als volgt verklaard worden: waarnemen vindt meestal plaats door een lichtdeeltje (foton) op een object af te schieten en te kijken hoe het terug komt. Als dit een energierijker foton is, kan het dieper in het object doordringen en ziet het dus iets anders dan een energiearmer foton, dat minder diep door dringt.

Curriculum Vitæ

Le mot impossible n'est pas français.

The word impossible is not in my dictionary.

(attributed to) Napoleon Bonaparte

Reinier de Adelhart Toorop was born in Amsterdam on the 10th of August 1984. The first written evidence of his fascination for science – astronomy in particular – stems from when he was six years old. During his education at the Dr. E. Boekmanschool (elementary school) and the Barlaeus Gymnasium (grammar school) physics and biology could be added to this list. In 2002, just after graduating from high school, he participated in the International Biology Olympiad in Latvia, winning a silver medal.

Later that year Reinier started studying Physics and Astronomy at the University of Amsterdam. In 2003, he was awarded the Physica prize of the 'Koninklijke Nederlandse Academie van Wetenschappen' (Royal Dutch Academy of Sciences) for the grades he received during his propedeuse (first year). After obtaining a kandidaatsdiploma (degree comparable to Bachelor) cum laude in 2005, Reinier continued his studies at the University of Amsterdam with a Master's study in Theoretical Physics. For his research project, he moved to the theory group of Nikhef, the Dutch national institute for subatomic physics. His Master's thesis 'Leptogenesis and the sigmamodel on $SU(8)/(SU(5) \times SU(3) \times U(1))$', written under supervision of Prof. dr. Jan-Willem van Holten, was awarded the biennial Pieter Zeemanprijs for best physics thesis at the University of Amsterdam.

During his university studies, Reinier became interested in competitive debate. In 2008 he won the World Universities Debating Championships in Thailand in the category English as a second language.

After his graduation (M.Sc., cum laude, 2007), Reinier continued his research at the Nikhef theory group as a PhD student under supervision of Prof. dr. Jan-Willem van Holten and, later, Dr. Federica Bazzocchi. Part of the research was conducted at the university of Padova. On the 21st of Februari 2012 he will defend his PhD thesis entitled 'A flavour of family symmetries in a family of flavour models' at Leiden University.

Acknowledgements

It's nice to be important,
but it's more important to be nice.

H. P. Baxxter [167], Scooter

This thesis has only one name on its cover. That does not mean that I did everything all by myself. My thesis is the result of the input of many people that I am very grateful to and that I would like to say 'thank you' to in these acknowledgements.

First and foremost I would like to thank my promotor Jan-Willem van Holten. We worked together on my master's thesis and I think the fact that I continued as your PhD student signals the fact that we were both happy with the result. Due to nature not providing the vacuum we hoped for, we did not write an article together during my PhD research, but you were still a constant source of advise for which I am very thankful.

Next, I'd like to thank Federica Bazzocchi. I am happy to have you as my copromotor and collaborator in many of my projects. I thoroughly enjoyed working together, both at the Free University and in Italy when the little Massimiliano called you home. Federica, you also introduced me to the Italian world that flavour symmetries seems to be. *Grazie* Luca Merlo, Alessio Paris and Stefano Morisi for being great people to work with! Ferruccio Feruglio, you were a great source of guidance in my research during my various stays in Padua, first as the supervisor of Luca and Alessio and later during our project on the modular subgroups. Thanks also, Claudia Hagendorn for preventing that my complete list of co-authors is Italian, and for your very critical eye that certainly improved our papers a lot.

Another person that contributed much to this thesis is Rozan Vroman. Thanks for helping me with the many illustrations in this thesis and for designing a beautiful cover. I am looking forward to see the artwork of your own thesis in neuroscience soon. *Gambatte Kudasai* with your experiments.

At Nikhef, I enjoyed the warmth of the theory group, where everyone, from bachelor student to staff member, is treated as equal. Thanks Rob, Sander, Lisa, Kristof, Giuseppe, Domenico, Michele, Gideon, Gerben, Patrick, Mert, Damien, Jan, Pierre, Thomas, Jens, Nikolas, Michel, Florian, Chris, Shannon, Robbert, Jory, Phillipp, Ioannis, Hans, Meike, Ori, Maciej, Daan, Robin, Catalin, Bart, Rik, Dana, Marieke, Robert, Eric, Jos, Justus and Bert for creating this atmosphere! I also enjoyed the regular meetings with the other Dutch phenomenologists. This community suffered a great loss in the summer of 2011, when Sjoerd Hardeman passed away. I remember Sjoerd as a great physicist and a great friend.

When not among physicists, I spend much of my spare time surrounded by debaters. I think Bonaparte is a wonderful society and I made many, many friends there as well as elsewhere in the debating world. Particular thanks go to my various debate partners and my co-organizers of the European Universities Debating Championships 2011.

Lastly, of course, I thank my family. Thanks opa, Freek, Els, Roos and Laura for being the best family one can wish.

Bibliography

[1] P. Ovidius Naso, *Metamorphoses*. 8 A.D. Translation F.H.A. Jonkers.

[2] M. Shaposhnikov, *Is there a new physics between electroweak and Planck scales?*, arXiv:0708.3550.

[3] G. Altarelli and M. W. Grunewald, *Precision electroweak tests of the standard model*, *Phys.Rept.* **403-404** (2004) 189–201, [hep-ph/0404165]. To appear in a special issue of Physics Reports dedicated to CERN on the occasion of the laboratory's 50th anniversary.

[4] **Atlas** Collaboration, "Public results of supersymmetry searches.." https://twiki.cern.ch/twiki/bin/view/AtlasPublic/SupersymmetryPublicResults.

[5] **CMS** Collaboration, "Public results of supersymmetry searches.." https://twiki.cern.ch/twiki/bin/view/CMSPublic/PhysicsResultsSUS.

[6] **Particle Data Group** Collaboration, K. Nakamura *et. al.*, *Review of particle physics*, *J.Phys.G* **G37** (2010) 075021.

[7] M. Gonzalez-Garcia, *Neutrino Physics*, *Nucl.Phys.* **A827** (2009) 5C–14C, [arXiv:0901.2505].

[8] P. F. Harrison, D. H. Perkins, and W. G. Scott, *Tri-bimaximal mixing and the neutrino oscillation data*, *Phys. Lett.* **B530** (2002) 167, [hep-ph/0202074].

[9] C. D. Froggatt and H. B. Nielsen, *Hierarchy of Quark Masses, Cabibbo Angles and CP Violation*, *Nucl. Phys.* **B147** (1979) 277.

[10] G. Altarelli and F. Feruglio, *Tri-bimaximal neutrino mixing from discrete symmetry in extra dimensions*, *Nucl. Phys.* **B720** (2005) 64–88, [hep-ph/0504165].

[11] G. Altarelli and F. Feruglio, *Tri-Bimaximal Neutrino Mixing, A4 and the Modular Symmetry*, *Nucl. Phys.* **B741** (2006) 215–235, [hep-ph/0512103].

[12] C. Darwin, *The descent of man, and selection in relation to sex.* John Murray, London, 1870.

[13] S. Mooij, *Supersymmetric Grand Unification*, *M.Sc. Thesis - University of Amsterdam* (2008). Available on http://www.science.uva.nl/onderwijs/thesis/centraal/files/f733143855.pdf.

[14] M. Drees, R. Godbole, and P. Roy, *Theory and phenomenology of sparticles: An account of four-dimensional N=1 supersymmetry in high energy physics*. World Scientific publishing, Singapore, 2004.

[15] G. 't Hooft, *Symmetry Breaking Through Bell-Jackiw Anomalies*, *Phys.Rev.Lett.* **37** (1976) 8–11.

[16] F. R. Klinkhamer and N. Manton, *A Saddle Point Solution in the Weinberg-Salam Theory*, *Phys.Rev.* **D30** (1984) 2212.

[17] R. Mohapatra, S. Antusch, K. Babu, G. Barenboim, M.-C. Chen, *et. al.*, *Theory of neutrinos: A White paper*, *Rept.Prog.Phys.* **70** (2007) 1757–1867, [hep-ph/0510213].

[18] M. Kobayashi and T. Maskawa, *CP Violation in the Renormalizable Theory of Weak Interaction*, *Prog.Theor.Phys.* **49** (1973) 652–657.

[19] L.-L. Chau and W.-Y. Keung, *Comments on the Parametrization of the Kobayashi-Maskawa Matrix*, *Phys.Rev.Lett.* **53** (1984) 1802.

[20] C. Jarlskog, *Commutator of the Quark Mass Matrices in the Standard Electroweak Model and a Measure of Maximal CP Violation*, *Phys.Rev.Lett.* **55** (1985) 1039.

[21] L. Wolfenstein, *Parametrization of the Kobayashi-Maskawa Matrix*, *Phys.Rev.Lett.* **51** (1983) 1945.

[22] G. L. Fogli, E. Lisi, A. Marrone, A. Palazzo, and A. M. Rotunno, *What we (would like to) know about the neutrino mass*, arXiv:0809.2936.

[23] G. L. Fogli, E. Lisi, A. Marrone, A. Palazzo, and A. M. Rotunno, *Hints of theta_13> 0 from global neutrino data analysis*, *Phys. Rev. Lett.* **101** (2008) 141801, [arXiv:0806.2649].

[24] G. L. Fogli, E. Lisi, A. Marrone, A. Palazzo, and A. M. Rotunno, *Evidence of theta(13)> 0 from global neutrino data analysis*, arXiv:1106.6028.

[25] T. Schwetz, M. A. Tortola, and J. W. F. Valle, *Three-flavour neutrino oscillation update*, *New J. Phys.* **10** (2008) 113011, [arXiv:0808.2016].

[26] M. Maltoni and T. Schwetz, *Three-flavour neutrino oscillation update and comments on possible hints for a non-zero theta13*, *PoS* **IDM2008** (2008) 072, [arXiv:0812.3161].

[27] T. Schwetz, M. Tortola, and J. Valle, *Global neutrino data and recent reactor fluxes: status of three-flavour oscillation parameters*, *New J.Phys.* **13** (2011) 063004, [arXiv:1103.0734].

[28] T. Schwetz, M. Tortola, and J. Valle, *Where we are on θ_{13}: addendum to 'Global neutrino data and recent reactor fluxes: status of three-flavour oscillation parameters'*, arXiv:1108.1376.

[29] **KATRIN** Collaboration, A. Osipowicz *et. al.*, *KATRIN: A Next generation tritium beta decay experiment with sub-eV sensitivity for the electron neutrino mass. Letter of intent*, hep-ex/0109033.

[30] **GERDA** Collaboration, A. A. Smolnikov, *Status of the GERDA experiment aimed to search for neutrinoless double beta decay of 76Ge*, arXiv:0812.4194.

[31] **Majorana** Collaboration, V. E. Guiseppe *et. al.*, *The Majorana Neutrinoless Double-Beta Decay Experiment*, *IEEE Nucl. Sci. Symp. Conf. Rec.* **2008** (2008) 1793–1798, [arXiv:0811.2446].

[32] **NEMO and SuperNEMO** Collaboration, H. Ohsumi, *SuperNEMO project*, *J.Phys.Conf.Ser.* **120** (2008) 052054.

[33] **CUORE** Collaboration, A. Giuliani, *From Cuoricino to CUORE: Investigating the inverted hierarchy region of neutrino mass*, *J.Phys.Conf.Ser.* **120** (2008) 052051.

[34] M. Danilov *et. al.*, *Detection of very small neutrino masses in double-beta decay using laser tagging*, *Phys. Lett.* **B480** (2000) 12–18, [hep-ex/0002003].

[35] P. F. Harrison and W. G. Scott, *Symmetries and generalisations of tri-bimaximal neutrino mixing*, *Phys. Lett.* **B535** (2002) 163–169, [hep-ph/0203209].

[36] Z.-z. Xing, *Nearly tri-bimaximal neutrino mixing and CP violation*, *Phys. Lett.* **B533** (2002) 85–93, [hep-ph/0204049].

[37] P. F. Harrison and W. G. Scott, *mu - tau reflection symmetry in lepton mixing and neutrino oscillations*, *Phys. Lett.* **B547** (2002) 219–228, [hep-ph/0210197].

[38] P. F. Harrison and W. G. Scott, *Permutation symmetry, tri-bimaximal neutrino mixing and the S3 group characters*, *Phys. Lett.* **B557** (2003) 76, [hep-ph/0302025]. [Phys.Lett.B557:76-86,2003].

[39] P. F. Harrison and W. G. Scott, *Status of tri- / bi-maximal neutrino mixing*, hep-ph/0402006.

[40] P. F. Harrison and W. G. Scott, *The simplest neutrino mass matrix*, *Phys. Lett.* **B594** (2004) 324–332, [hep-ph/0403278].

[41] **T2K** Collaboration, K. Abe *et. al.*, *Indication of Electron Neutrino Appearance from an Accelerator-produced Off-axis Muon Neutrino Beam*, *Phys.Rev.Lett.* **107** (2011) 041801, [arXiv:1106.2822].

[42] F. Ardellier *et. al.*, *Letter of intent for double-CHOOZ: A search for the mixing angle theta(13)*, hep-ex/0405032.

[43] **Double Chooz** Collaboration, F. Ardellier *et. al.*, *Double Chooz: A search for the neutrino mixing angle theta(13)*, hep-ex/0606025.

[44] Y.-f. Wang, *Measuring sin**2(2theta(13)) with the Daya Bay nuclear reactors*, hep-ex/0610024.

[45] **Daya-Bay** Collaboration, X. Guo *et. al.*, *A precision measurement of the neutrino mixing angle theta(13) using reactor antineutrinos at Daya Bay*, hep-ex/0701029.

[46] I. de Medeiros Varzielas, *Family symmetries and the origin of fermion masses and mixings*, arXiv:0801.2775.

[47] G. Altarelli and F. Feruglio, *Discrete Flavor Symmetries and Models of Neutrino Mixing*, *Rev. Mod. Phys.* **82** (2010) 2701–2729, [arXiv:1002.0211].

[48] C. I. Low and R. R. Volkas, *Tri-bimaximal mixing, discrete family symmetries, and a conjecture connecting the quark and lepton mixing matrices*, *Phys. Rev.* **D68** (2003) 033007, [hep-ph/0305243].

[49] F. Feruglio, *Models of neutrino masses and mixings*, *Nucl. Phys. Proc. Suppl.* **143** (2005) 184–193, [hep-ph/0410131]. [Nucl.Phys.Proc.Suppl.145:225-230,2005].

[50] G. G. Ross and O. Vives, *Yukawa structure, flavour and CP violation in supergravity*, *Phys. Rev.* **D67** (2003) 095013, [hep-ph/0211279].

[51] G. G. Ross, L. Velasco-Sevilla, and O. Vives, *Spontaneous CP violation and non-Abelian family symmetry in SUSY*, *Nucl. Phys.* **B692** (2004) 50–82, [hep-ph/0401064].

[52] F. Feruglio, C. Hagedorn, and L. Merlo, *Vacuum Alignment in SUSY A4 Models*, *JHEP* **03** (2010) 084, [arXiv:0910.4058].

[53] F. Feruglio, C. Hagedorn, Y. Lin, and L. Merlo, *Lepton Flavour Violation in Models with A4 Flavour Symmetry*, *Nucl. Phys.* **B809** (2009) 218–243, [arXiv:0807.3160].

[54] H. Ishimori, T. Kobayashi, Y. Omura, and M. Tanimoto, *Soft supersymmetry breaking terms from A4 lepton flavor symmetry*, *JHEP* **12** (2008) 082, [arXiv:0807.4625].

[55] A. Hayakawa, H. Ishimori, Y. Shimizu, and M. Tanimoto, *Deviation from tri-bimaximal mixing and flavor symmetry breaking in a seesaw type A4 model*, *Phys. Lett.* **B680** (2009) 334–342, [arXiv:0904.3820].

[56] C. Hagedorn, E. Molinaro, and S. T. Petcov, *Charged Lepton Flavour Violating Radiative Decays $\ell_i \to \ell_j + \gamma$ in See-Saw Models with A_4 Symmetry*, *JHEP* **02** (2010) 047, [arXiv:0911.3605].

[57] F. Feruglio, C. Hagedorn, Y. Lin, and L. Merlo, *Lepton Flavour Violation in a Supersymmetric Model with A4 Flavour Symmetry*, *Nucl. Phys.* **B832** (2010) 251–288, [arXiv:0911.3874].

[58] F. Feruglio and A. Paris, *The Golden Ratio Prediction for the Solar Angle from a Natural Model with A5 Flavour Symmetry*, *JHEP* **1103** (2011) 101, [arXiv:1101.0393].

[59] V. D. Barger, S. Pakvasa, T. J. Weiler, and K. Whisnant, *Bi-maximal mixing of three neutrinos*, *Phys. Lett.* **B437** (1998) 107–116, [hep-ph/9806387].

[60] Y. Nomura and T. Yanagida, *Bi-maximal neutrino mixing in SO(10)(GUT)*, *Phys. Rev.* **D59** (1999) 017303, [hep-ph/9807325].

[61] G. Altarelli and F. Feruglio, *Neutrino mass textures from oscillations with maximal mixing*, *Phys. Lett.* **B439** (1998) 112–118, [hep-ph/9807353].

[62] H. Ishimori, T. Kobayashi, H. Ohki, Y. Shimizu, H. Okada, *et. al.*, *Non-Abelian Discrete Symmetries in Particle Physics*, *Prog.Theor.Phys.Suppl.* **183** (2010) 1–163, [arXiv:1003.3552].

[63] **Double Chooz** Collaboration, H. de Kerret, "First results from the double chooz experiment." Talk at LowNu11 Conference, available on http://www.dchooz.org/DocDB/0033/003393/003/DCAtLowNu11_Kerret111109_Official.pdf.

[64] G. Altarelli, F. Feruglio, and L. Merlo, *Revisiting Bimaximal Neutrino Mixing in a Model with S4 Discrete Symmetry*, *JHEP* **05** (2009) 020, [arXiv:0903.1940].

[65] P. O. Ludl, *On the finite subgroups of U(3) of order smaller than 512*, *J.Phys.A* **A43** (2010) 395204, [arXiv:1006.1479].

[66] W. Grimus and P. O. Ludl, *Finite flavour groups of fermions*, arXiv:1110.6376.

[67] C. Luhn, *Spontaneous breaking of SU(3) to finite family symmetries: a pedestrian's approach*, *JHEP* **1103** (2011) 108, [arXiv:1101.2417].

[68] H. Coxeter and W. Moser, *Generators and Relations for Discrete Groups*. Springer- Verlag, Ergebnisse der Mathematik und ihrer Grenzgebiete: Band 14 3rd edition, 1972.

[69] W. Eholzer, *Fusion algebras and characters of rational conformal field theories*, hep-th/9502160.

[70] R. Gunning, *Lectures on Modular Forms*. Princeton University Press, 1962.

[71] B. Shoeneberg, *Elliptic Modular Functions - An Introduction*. Springer-Verlag, 1974.

[72] A. Nobs, *Die irreduziblen Darstellungen der Gruppen $SL_2(Z_p)$, insebondere $SL_2(Z_2)$ I*, *Comm. Math. Helv.* **51** (1976) 456–489.

[73] A. Nobs and J. Wolfart, *Die irreduziblen Darstellungen der Gruppen $SL_2(Z_p)$, insebondere $SL_2(Z_2)$ II*, *Comm. Math. Helv.* **51** (1976) 491–526.

[74] W. Eholzer, *On The Classification Of Modular Fusion Algebras*, *Commun. Math. Phys.* **172** (1995) 623, [hep-th/9408160].

[75] W. Fairbairn, T. Fulton, and J. Klink, *Finite and Disconnected Subgroups of SU3 and their Application to the Elementary-Particle Spectrum*, *J.Math.Phys.* **5** (1964) 1038.

[76] J. Escobar and C. Luhn, *The Flavor Group Delta(6n**2)*, *J.Math.Phys.* **50** (2009) 013524, [arXiv:0809.0639].

[77] A. Bovier, M. Luling, and D. Wyler, *FINITE SUBGROUPS OF SU(3)*, *J.Math.Phys.* **22** (1981) 1543.

[78] C. Lam, *Symmetry of Lepton Mixing*, *Phys.Lett.* **B656** (2007) 193–198, [arXiv:0708.3665].

[79] A. Blum, C. Hagedorn, and M. Lindner, *Fermion Masses and Mixings from Dihedral Flavor Symmetries with Preserved Subgroups*, *Phys.Rev.* **D77** (2008) 076004, [arXiv:0709.3450].

[80] C. Lam, *Group Theory and Dynamics of Neutrino Mixing*, *Phys.Rev.* **D83** (2011) 113002, [arXiv:1104.0055].

[81] N. Cabibbo, *Time Reversal Violation in Neutrino Oscillation*, *Phys.Lett.* **B72** (1978) 333–335.

[82] L. Wolfenstein, *Oscillations Among Three Neutrino Types and CP Violation*, *Phys.Rev.* **D18** (1978) 958–960.

[83] H. Minakata and A. Y. Smirnov, *Neutrino Mixing and Quark-Lepton Complementarity*, *Phys. Rev.* **D70** (2004) 073009, [hep-ph/0405088].

[84] M. Raidal, *Relation between the neutrino and quark mixing angles and grand unification*, *Phys. Rev. Lett.* **93** (2004) 161801, [hep-ph/0404046].

[85] A. Datta, L. Everett, and P. Ramond, *Cabibbo haze in lepton mixing*, *Phys. Lett.* **B620** (2005) 42–51, [hep-ph/0503222].

[86] H. Minakata, *Quark-lepton complementarity: A review*, hep-ph/0505262.

[87] F. Plentinger, G. Seidl, and W. Winter, *Systematic parameter space search of extended quark-lepton complementarity*, *Nucl. Phys.* **B791** (2008) 60–92, [hep-ph/0612169].

[88] Y. Kajiyama, M. Raidal, and A. Strumia, *The Golden ratio prediction for the solar neutrino mixing*, *Phys.Rev.* **D76** (2007) 117301, [arXiv:0705.4559].

[89] S. F. King and C. Luhn, *A New family symmetry for SO(10) GUTs*, *Nucl.Phys.* **B820** (2009) 269–289, [arXiv:0905.1686].

[90] S. F. King and C. Luhn, *A Supersymmetric Grand Unified Theory of Flavour with PSL(2)(7) x SO(10)*, *Nucl.Phys.* **B832** (2010) 414–439, [arXiv:0912.1344].

[91] X.-G. He and A. Zee, *Minimal modification to the tri-bimaximal neutrino mixing*, *Phys.Lett.* **B645** (2007) 427–431, [hep-ph/0607163].

[92] W. Grimus and L. Lavoura, *A Model for trimaximal lepton mixing*, *JHEP* **0809** (2008) 106, [arXiv:0809.0226].

[93] W. Grimus, L. Lavoura, and A. Singraber, *Trimaximal lepton mixing with a trivial Dirac phase*, *Phys.Lett.* **B686** (2010) 141–145, [arXiv:0911.5120].

[94] C. H. Albright and W. Rodejohann, *Comparing Trimaximal Mixing and Its Variants with Deviations from Tri-bimaximal Mixing*, *Eur.Phys.J.* **C62** (2009) 599–608, [arXiv:0812.0436].

[95] X.-G. He and A. Zee, *Minimal Modification to Tri-bimaximal Mixing*, *Phys.Rev.* **D84** (2011) 053004, [arXiv:1106.4359].

[96] Y. Lin, *Tri-bimaximal Neutrino Mixing from A(4) and $\theta_{13} \sim \theta_C$*, *Nucl. Phys.* **B824** (2010) 95–110, [arXiv:0905.3534].

[97] E. Ma and G. Rajasekaran, *Softly broken A(4) symmetry for nearly degenerate neutrino masses*, *Phys. Rev.* **D64** (2001) 113012, [hep-ph/0106291].

[98] A. M. J.-B. R. de Saint-Exupéry, *Terre des Hommes*. Gallimard, Paris, 1939.

[99] H. Georgi and C. Jarlskog, *A New Lepton - Quark Mass Relation in a Unified Theory*, *Phys. Lett.* **B86** (1979) 297–300.

[100] Z.-z. Xing, H. Zhang, and S. Zhou, *Updated Values of Running Quark and Lepton Masses*, *Phys. Rev.* **D77** (2008) 113016, [arXiv:0712.1419].

[101] J. C. Pati and A. Salam, *Lepton Number as the Fourth Color*, *Phys. Rev.* **D10** (1974) 275–289. [Erratum-ibid.D11:703-703,1975].

[102] H. Georgi and S. L. Glashow, *Unity of All Elementary Particle Forces*, *Phys. Rev. Lett.* **32** (1974) 438–441.

[103] A. S. Joshipura, B. P. Kodrani, and K. M. Patel, *Fermion Masses and Mixings in a μ-τ symmetric SO(10)*, *Phys. Rev.* **D79** (2009) 115017, [arXiv:0903.2161].

[104] B. Dutta, Y. Mimura, and R. N. Mohapatra, *Origin of Quark-Lepton Flavor in SO(10) with Type II Seesaw*, *Phys. Rev.* **D80** (2009) 095021, [arXiv:0910.1043].

[105] B. Dutta, Y. Mimura, and R. N. Mohapatra, *An SO(10) Grand Unified Theory of Flavor*, *JHEP* **05** (2010) 034, [arXiv:0911.2242].

[106] S. Bertolini, T. Schwetz, and M. Malinsky, *Fermion masses and mixings in SO(10) models and the neutrino challenge to SUSY GUTs*, *Phys. Rev.* **D73** (2006) 115012, [hep-ph/0605006].

[107] A. Melfo and G. Senjanovic, *Minimal supersymmetric Pati-Salam theory: Determination of physical scales*, *Phys. Rev.* **D68** (2003) 035013, [hep-ph/0302216].

[108] Z. Chacko and R. N. Mohapatra, *Supersymmetric left-right models and light doubly charged Higgs bosons and Higgsinos*, *Phys. Rev.* **D58** (1998) 015003, [hep-ph/9712359].

[109] M. Frank, K. Huitu, and S. K. Rai, *Single Production of Doubly Charged Higgsinos at linear e- e- colliders*, *Phys. Rev.* **D77** (2008) 015006, [arXiv:0710.2415].

[110] D. A. Demir, M. Frank, K. Huitu, S. K. Rai, and I. Turan, *Signals of Doubly-Charged Higgsinos at the CERN Large Hadron Collider*, *Phys. Rev.* **D78** (2008) 035013, [arXiv:0805.4202].

[111] D. A. Demir *et. al.*, *Doubly Charged Higgsinos at Tevatron*, *Phys. Rev.* **D79** (2009) 095006, [arXiv:0903.3955].

[112] S. Antusch, J. Kersten, M. Lindner, and M. Ratz, *The LMA solution from bimaximal lepton mixing at the GUT scale by renormalization group running*, *Phys. Lett.* **B544** (2002) 1–10, [hep-ph/0206078].

[113] S. Antusch, J. Kersten, M. Lindner, and M. Ratz, *Running neutrino masses, mixings and CP phases: Analytical results and phenomenological consequences*, *Nucl. Phys.* **B674** (2003) 401–433, [hep-ph/0305273].

[114] S. Antusch, J. Kersten, M. Lindner, M. Ratz, and M. A. Schmidt, *Running neutrino mass parameters in see-saw scenarios*, *JHEP* **03** (2005) 024, [hep-ph/0501272].

[115] J.-w. Mei, *Running neutrino masses, leptonic mixing angles and CP- violating phases: From M(Z) to Lambda(GUT)*, *Phys. Rev.* **D71** (2005) 073012, [hep-ph/0502015].

[116] J. R. Ellis, A. Hektor, M. Kadastik, K. Kannike, and M. Raidal, *Running of low-energy neutrino masses, mixing angles and CP violation*, *Phys. Lett.* **B631** (2005) 32–41, [hep-ph/0506122].

[117] A. Dighe, S. Goswami, and W. Rodejohann, *Corrections to Tri-bimaximal Neutrino Mixing: Renormalization and Planck Scale Effects*, *Phys. Rev.* **D75** (2007) 073023, [hep-ph/0612328].

[118] S. Boudjemaa and S. F. King, *Deviations from Tri-bimaximal Mixing: Charged Lepton Corrections and Renormalization Group Running*, *Phys. Rev.* **D79** (2009) 033001, [arXiv:0808.2782].

[119] Y. Lin, L. Merlo, and A. Paris, *Running Effects on Lepton Mixing Angles in Flavour Models with Type I Seesaw*, *Nucl. Phys.* **B835** (2010) 238–261, [arXiv:0911.3037].

[120] **MINOS Collaboration** Collaboration, P. Adamson *et. al.*, *Improved search for muon-neutrino to electron-neutrino oscillations in MINOS*, *Phys.Rev.Lett.* **107** (2011) 181802, [arXiv:1108.0015].

[121] **RENO** Collaboration, S.-B. Kim, *RENO: Reactor experiment for neutrino oscillation at Yonggwang*, *AIP Conf. Proc.* **981** (2008) 205–207. [J.Phys.Conf.Ser.120:052025,2008].

[122] **T2K** Collaboration, Y. Itow *et. al.*, *The JHF-Kamioka neutrino project*, hep-ex/0106019.

[123] **NOvA** Collaboration, D. S. Ayres *et. al.*, *NOvA proposal to build a 30-kiloton off-axis detector to study neutrino oscillations in the Fermilab NuMI beamline*, hep-ex/0503053.

[124] M. Malinsky, *Higgs sector of the next-to-minimal renormalizable SUSY SO(10)*, arXiv:0807.0591.

[125] J. F. Gunion and H. E. Haber, *Conditions for CP-violation in the general two-Higgs- doublet model*, *Phys. Rev.* **D72** (2005) 095002, [hep-ph/0506227].

[126] G. Branco, P. Ferreira, L. Lavoura, M. Rebelo, M. Sher, *et. al.*, *Theory and phenomenology of two-Higgs-doublet models*, arXiv:1106.0034.

[127] L. Lavoura and H. Kuhbock, *A4 model for the quark mass matrices*, *Eur. Phys. J.* **C55** (2008) 303–308, [arXiv:0711.0670].

[128] S. Morisi and E. Peinado, *An A4 model for lepton masses and mixings*, *Phys. Rev.* **D80** (2009) 113011, [arXiv:0910.4389].

[129] W. Dekens, *A_4 Family Symmetry*, *M.Sc. Thesis - University of Groningen* (2011). Available on http://scripties.fwn.eldoc.ub.rug.nl/scripties/Natuurkunde/Master/2011/Dekens.W.G./.

[130] G. C. Branco, M. Rebelo, and J. Silva-Marcos, *CP-odd invariants in models with several Higgs doublets*, *Phys.Lett.* **B614** (2005) 187–194, [hep-ph/0502118].

[131] L. Lavoura and J. P. Silva, *Fundamental CP violating quantities in a SU(2) x U(1) model with many Higgs doublets*, *Phys.Rev.* **D50** (1994) 4619–4624, [hep-ph/9404276].

[132] **Atlas** Collaboration, "Higgs public results." https://twiki.cern.ch/twiki/bin/view/AtlasPublic/HiggsPublicResults.

[133] **CMS** Collaboration, "Higgs physics results." https://twiki.cern.ch/twiki/bin/view/CMSPublic/PhysicsResultsHIG.

[134] M. J. G. Veltman, *Second Threshold in Weak Interactions*, *Acta Phys. Polon.* **B8** (1977) 475.

[135] B. W. Lee, C. Quigg, and H. B. Thacker, *Weak Interactions at Very High-Energies: The Role of the Higgs Boson Mass*, *Phys. Rev.* **D16** (1977) 1519.

[136] B. W. Lee, C. Quigg, and H. B. Thacker, *The Strength of Weak Interactions at Very High-Energies and the Higgs Boson Mass*, *Phys. Rev. Lett.* **38** (1977) 883–885.

[137] R. Casalbuoni, D. Dominici, F. Feruglio, and R. Gatto, *Tree level unitarity violation for large scalar mass in multi - higgs extensions of the Standard Model*, *Nucl. Phys.* **B299** (1988) 117.

[138] **LEP Working Group for Higgs boson searches** Collaboration, R. Barate *et. al.*, *Search for the standard model Higgs boson at LEP*, *Phys. Lett.* **B565** (2003) 61–75, [hep-ex/0306033].

[139] CDF and D. collaborations, *Combined CDF and DZero Upper Limits on Standard Model Higgs-Boson Production with up to 4.2 fb-1 of Data*, arXiv:0903.4001.

[140] B. Holdom and J. Terning, *Large corrections to electroweak parameters in technicolor theories*, *Phys. Lett.* **B247** (1990) 88–92.

[141] M. E. Peskin and T. Takeuchi, *A New constraint on a strongly interacting Higgs sector*, *Phys. Rev. Lett.* **65** (1990) 964–967.

[142] M. Golden and L. Randall, *Radiative corrections to electroweak parameters in technicolor theories*, *Nucl. Phys.* **B361** (1991) 3–23.

[143] A. Dobado, D. Espriu, and M. J. Herrero, *Chiral Lagrangians as a tool to probe the symmetry breaking sector of the SM at LEP*, *Phys. Lett.* **B255** (1991) 405–414.

[144] M. E. Peskin and T. Takeuchi, *Estimation of oblique electroweak corrections*, *Phys. Rev.* **D46** (1992) 381–409.

[145] I. Maksymyk, C. P. Burgess, and D. London, *Beyond S, T and U*, *Phys. Rev.* **D50** (1994) 529–535, [hep-ph/9306267].

[146] W. Grimus, L. Lavoura, O. M. Ogreid, and P. Osland, *The oblique parameters in multi-Higgs-doublet models*, *Nucl. Phys.* **B801** (2008) 81–96, [arXiv:0802.4353].

[147] W. Grimus, L. Lavoura, O. M. Ogreid, and P. Osland, *A precision constraint on multi-Higgs-doublet models*, *J. Phys.* **G35** (2008) 075001, [arXiv:0711.4022].

[148] L. Lavoura and H. Kuhbock, *Predictions of an A_4 model with a five-parameter neutrino mass matrix*, *Mod. Phys. Lett.* **A22** (2007) 181–189, [hep-ph/0610050].

[149] E. Ma, *Naturally small seesaw neutrino mass with no new physics beyond the TeV scale*, *Phys.Rev.Lett.* **86** (2001) 2502–2504, [hep-ph/0011121].

[150] M. Hirsch, S. Morisi, E. Peinado, and J. W. F. Valle, *Discrete dark matter*, *Phys. Rev.* **D82** (2010) 116003, [arXiv:1007.0871].

[151] D. Meloni, S. Morisi, and E. Peinado, *Neutrino phenomenology and stable dark matter with A4*, *Phys. Lett.* **B697** (2011) 339–342, [arXiv:1011.1371].

[152] M. S. Boucenna, M. Hirsch, S. Morisi, E. Peinado, M. Taoso, and J. Valle, *Phenomenology of Dark Matter from A4 Flavor Symmetry*, *JHEP* **05** (2011) 037, [arXiv:1101.2874].

[153] L. Lavoura, *General formulae for f1 $\to$ f2 gamma*, *Eur. Phys. J.* **C29** (2003) 191–195, [hep-ph/0302221].

[154] **MEGA** Collaboration, M. L. Brooks *et. al.*, *New Limit for the Family-Number Non-conserving Decay mu+ to e+ gamma*, *Phys. Rev. Lett.* **83** (1999) 1521–1524, [hep-ex/9905013].

[155] A. Maki, *Status of the MEG experiment*, *AIP Conf.Proc.* **981** (2008) 363–365.

[156] D. Atwood, L. Reina, and A. Soni, *Phenomenology of two Higgs doublet models with flavor changing neutral currents*, *Phys. Rev.* **D55** (1997) 3156–3176, [hep-ph/9609279].

[157] J. D. Wells, *Lectures on Higgs Boson Physics in the Standard Model and Beyond*, arXiv:0909.4541.

[158] A. J. Buras, M. V. Carlucci, S. Gori, and G. Isidori, *Higgs-mediated FCNCs: Natural Flavour Conservation vs. Minimal Flavour Violation*, *JHEP* **10** (2010) 009, [arXiv:1005.5310].

[159] E. Ma, *Quark and Lepton Flavor Triality*, *Phys. Rev.* **D82** (2010) 037301, [arXiv:1006.3524].

[160] F. Feruglio and A. Paris, *Rare muon and tau decays in A4 Models*, *Nucl.Phys.* **B840** (2010) 405–423, [arXiv:1005.5526].

[161] E. Ma, *Dark Scalar Doublets and Neutrino Tribimaximal Mixing from A_4 Symmetry*, *Phys. Lett.* **B671** (2009) 366–368, [arXiv:0808.1729].

[162] M. Dubinin and A. Sukachev, *$K^0 \to \bar{K}^0$, $B^0 \to \bar{B}^0$ mixings in the MSSM with explicit CP violation in the Higgs sector*, *Phys. Atom. Nucl.* **71** (2008) 374–387, [arXiv:0711.5023].

[163] F. J. Botella, G. C. Branco, and M. Nebot, *CP violation and limits on New Physics including recent B_s measurements*, *Nucl.Phys.* **B768** (2007) 1–20, [hep-ph/0608100].

[164] Y. Grossman, Z. Ligeti, and Y. Nir, *Future prospects of B physics*, *Prog.Theor.Phys.* **122** (2009) 125–143, [arXiv:0904.4262].

[165] J. Verne, *Voyage au centre de la Terre*. Hetzel, Paris, 1864.

[166] S. Hardeman, *Non-decoupling of heavy scalars in cosmology*. PhD thesis, Leiden University, 2011.

[167] H. P. Baxxter *et. al.*, *Scooter*. Club Tools, Scorpio Music, 1995.